Dynamic Analysis of Both On and Offshore Wind Turbines in the Frequency Domain

by

Andrew Halfpenny

A Dissertation submitted for the degree of Doctor of Philosophy in Faculty of Engineering, University of London

University College London
Department of Mechanical Engineering

February 1998.

Acknowledgements

I would like to express my sincere appreciation to my supervisor, Dr. Neil W.M. Bishop, for his advise, guidance and encouragement in carrying out this research.

I am most grateful to EPSRC and W.S. Atkins Ltd. of England and also to ECN of The Netherlands for offering me the grants and scholarships to study at University College London (UCL).

It is my pleasure to acknowledge Prof. Nigel D.P. Barltrop and Mr Ian Ward of WS Atkins and Mr. Tim Van Engelen of ECN for their help throughout this work. Also I would like to gratefully acknowledge Mr Martin Späth and Mrs Rea Späth, for accommodating me for the 9 months spent in The Netherlands, and the family of Prof. Barltrop for their kind hospitality through one of the more demanding periods in this work.

A special thanks to all faculty and staff of the Mechanical Engineering Department, UCL for all their help during my study. I would also like to express my thanks to the students of G18 with whom I have shared my time at UCL.

Finally, a special note of gratitude goes to my family and fiancée for their active support and confidence in me.

Abstract

This thesis presents several developments in analysing wind turbines in the frequency domain. Previous work in the area has developed computer-based models to predict the rotationally sampled stochastic wind speed witnessed by the blades of a wind turbine. Work has also been carried out to include rudimentary capabilities to model blade, tower and drivetrain flexibilities. These are usually limited to modelling only the first mode responses in each case. This thesis describes the development of a new frequency domain model with the ability to analyse fully flexible turbines using a Finite Element analysis approach. In addition, the analysis has a number of novel features to enhance convergence and minimise numerical errors. Comparisons are made between the theoretical and measured results for a number of commercial wind turbines.

Problems with land availability have recently prompted governments to investigate the possibility of siting wind turbines offshore. One type of concept sites turbines on floating platforms. It is necessary to develop models to predict how turbines influence the rigid body dynamics of the platform. Additionally the wave-induced motions of the platform influence dynamic loading in the turbines and this too should be analysed. A new frequency domain model has been advanced to calculate the forces induced through stochastic wave loading on floating platforms. A promising concept, based on a 'Tensioned Buoyant Platform (TBP)' has been investigated and the results presented.

Many recent developments have been made in Frequency domain fatigue analysis. An investigation into a number of methods is discussed. Recommendations are made for the practicable use of these methods for analyising wind turbine structures.

Contents

1. INTRODUCTION 27

1.1 GENERAL 27
1.2 STATEMENT OF THE PROBLEM 29
1.3 THE OBJECTIVES OF THE STUDY 30
1.4 SCOPE AND LIMITATIONS 31
1.5 ORGANISATION OF THE THESIS 32
1.6 DESCRIPTION OF COMPUTER SOFTWARE DEVELOPED IN THIS RESEARCH 33

2. FREQUENCY DOMAIN REPRESENTATION OF RANDOM PROCESSES 37

2.1 FOURIER SERIES AND THE FOURIER TRANSFORM PAIR 37
2.1.1 Representing a time signal using Fourier series 37
2.1.2 The complex Fourier series 39
2.1.3 The Fourier density coefficient 42
2.1.4 The Fourier transform pair 43
2.1.5 Fourier analysis of random time histories 44
2.1.6 Power spectral density function (PSD) 47
2.1.7 Time signal regeneration from PSDs 52
2.1.8 Summary of Fourier transformation and PSDs 55
2.2 RESPONSE OF A LINEAR SYSTEM TO A RANDOM LOADING EXPRESSED IN THE FREQUENCY DOMAIN 56
2.3 RANDOM PROCESSES 57
2.3.1 Definition of the Autocovariance function 58
2.3.2 Transformation between Autocovariance and PSD 60
2.3.3 Multiple random processes: The principle of Cross-covariance 61
2.3.4 Normalised covariance and time scales 63
2.3.5 The coherence function 63
2.3.6 Response of a linear system to multiple random loading 64
2.3.7 Matrix form of the Cross-power spectral density function 65
2.4 CONCLUSION 67

3. MODELLING THE TURBULENT WIND 69

3.1 THE NATURE OF WIND 69
3.2 ATMOSPHERIC EQUILIBRIUM AND STABILITY 71
3.3 VARIATION OF THE MEAN WIND SPEED WITH HEIGHT AND TIME 74
3.4 WIND TURBULENCE 78
3.4.1 Single point wind turbulence statistics 81

3.4.2 Variation of wind turbulence in space *86*

3.5 CONCLUSION 89

4. AERODYNAMIC MODELLING OF A WIND TURBINE 93

4.1 AIR FLOW THROUGH A WIND TURBINE ROTOR 93

4.2 THE EQUILIBRIUM WAKE MODEL 96

4.2.1 Derivation of equilibrium wake model *97*

4.2.2 Empirical modifications to the equilibrium wake model *102*

4.3 EQUILIBRIUM POWER AND LOADING CALCULATIONS 104

4.4 CALCULATING THE QUASI-STATIC AERODYNAMIC GAIN FACTORS 109

4.5 PRACTICAL CONSIDERATIONS 112

4.6 CONCLUSION 113

5. MODELLING THE WIND TURBINE LOADS 117

5.1 ROTATIONAL SAMPLING OF WIND TURBULENCE 117

5.1.1 Conceptual introduction to rotational sampling *118*

5.2 AUTO-POWER SPECTRA OF WIND SPEED AT A SINGLE POINT ON A ROTOR BLADE 120

5.2.1 Cross-power spectra of wind speed between two points on two rotor blades. *124*

5.2.2 The Cross-power spectral matrix *128*

5.3 DERIVATION OF BLADE LOADS ON A WIND TURBINE 130

5.4 DERIVATION OF ROTOR LOADS ON A WIND TURBINE 133

5.5 DERIVATION OF A ROTOR 'SUPER ELEMENT' MODEL 135

5.6 CALCULATING THE TOWER YAW AND TILT MOMENTS 138

5.6.1 Cross-power spectrum of yaw moment between two blade elements *139*

5.6.2 The rotor 'Super element' for modelling yaw moment *144*

5.7 YAW AND TILT MISALIGNMENT 145

5.8 CONCLUSION 147

6. DYNAMIC ANALYSIS OF A WIND TURBINE SUBJECTED TO TURBULENT WIND LOADS 149

6.1 OVERVIEW OF THE MODELLING PROCESS 150

6.1.1 Single degree of freedom blade model *151*

6.1.2 Multiple element blade model *153*

6.1.3 Multi-degree of freedom elements *155*

6.1.4 Natural frequency analysis and modal decomposition *156*

6.2 DERIVATION OF BLADE ELEMENT MATRICES 157

6.2.1 The blade mass matrix *157*

6.2.2 The blade stiffness matrix *159*

6.2.3 The blade damping matrix *162*
6.3 DERIVATION OF TOWER AND DRIVETRAIN MATRICES 163
6.4 ASSEMBLING THE COMBINED STRUCTURAL MATRICES 165
6.4.1 The global coordinate axis system *165*
6.4.2 Assembling the global structural matrices *168*
6.5 CALCULATION OF ELEMENT FORCES DUE TO RANDOM WIND TURBULENCE 171
6.6 CONCLUSION 171

7. FATIGUE ANALYSIS IN THE FREQUANCY DOMAIN 175

7.1 INTRODUCTION TO FATIGUE ANALYSIS 175
7.1.1 Time domain analysis, the SN method *176*
7.1.2 Frequency domain analysis *180*
7.2 COMPARISON BETWEEN FATIGUE ANALYSIS TECHNIQUES 186
7.3 DESCRIPTION OF FATIGUE ANALYSIS APPROACH ADOPTED IN THIS THESIS 187
7.4 CONCLUSION 187

8. NUMERICAL MODEL VALIDATION AND COMPARISON 191

8.1 INTRODUCTION 191
8.2 AERANA: AERODYNAMIC PRE-PROCESSOR 193
8.3 TURBANA: METEOROLOGICAL PRE-PROCESSOR 195
8.3.1 The ESDU spectra *196*
8.3.2 Rotational sampling of the turbulent wind field *199*
8.4 LINANA: STRUCTURAL FINITE ELEMENT ANALYSIS OF THE TURBINE 202
8.5 LOADANA: DERIVING THE AUTO-POWER SPECTRA OF STRUCTURAL FORCES 205
8.5.1 Non-linearity's in the aerodynamic model *211*
8.5.2 Deterministic effects which are not modelled *214*
8.5.3 Deficiencies in the structural model *215*
8.6 CONCLUSION 216

9. WIND TURBINE LOADING DUE TO STOCHASTIC BASE MOTIONS 219

9.1 PREVIOUS RELEVANT STUDIES 223
9.2 THE LOADING ON A BLADE ELEMENT AS THE TURBINE IS MOVED THROUGH SPACE 225
9.2.1 Yawing and tilting motions *225*
9.2.2 Rolling motions *228*
9.2.3 Heave and sway motions *228*
9.2.4 Surge motion *229*
9.3 DERIVATION OF TRANSFER MATRICES RELATING BLADE LOADS TO MOTIONS OF THE NACELLE ... 229
9.3.1 Aerodynamic loading *230*

9.3.2 Inertial loading *232*

9.3.3 Gyroscopic loading *233*

9.3.4 Gravity loading *233*

9.3.5 Loading brought about by a cyclic variation in in-flow angle *234*

9.3.6 The mass, damping and stiffness matrices of blade loading caused by motion of the turbine *234*

9.4 DERIVATION OF ROTOR TRANSFORMATION MATRICES RELATING ROTOR LOAD IN THE GLOBAL AXIS SYSTEM TO MOTIONS OF THE NACELLE 236

9.5 DERIVATION OF ROTOR LOADING ON A THREE BLADED TURBINE IN THE FREQUENCY DOMAIN 242

9.6 COMMENTS ON THE SOLUTION TECHNIQUE FOR ANALYSING 1 OR 2 BLADED ROTORS IN THE FREQUENCY DOMAIN 242

9.7 CONCLUSIONS 244

10. WIND TURBINE BLADE LOADS DUE TO STOCHASTIC BASE MOTIONS 247

10.1 CALCULATE THE CROSS-POWER FORCE MATRICES BETWEEN A PAIR OF BLADE ELEMENTS 247

10.1.1 Constant cross-power force matrices *248*

10.1.2 Sinusoidally varying cross-power force matrices *249*

10.1.3 Cross-power between the constant and sinusoidally varying cases. *253*

10.1.4 Summary of cross-power force matrix between elements i and j *255*

10.2 DYNAMIC ANALYSIS OF THE BLADE LOADING 255

10.3 CONCLUSION 257

11. CASE STUDY: THE ANALYSIS OF A FLOATING OFFSHORE WIND TURBINE MOUNTED ON A TENSIONED BUOYANT PLATFORM 259

11.1 INTRODUCTION 259

11.2 MOTION ANALYSIS OF THE TENSIONED BUOYANT PLATFORMS 263

11.3 ROTOR LOADS RESULTING FROM PLATFORM SURGE 266

11.4 THE AFFECT OF ROTOR DAMPING ON RIGID BODY MOTION RESPONSE 272

11.5 THE INFLUENCE OF ROTOR DAMPING ON STRUCTURAL VIBRATIONS 274

11.6 CONCLUSION 275

12. CONCLUSION 279

12.1 CONTRIBUTIONS OF THE WORK 279

12.2 SUMMARY OF EACH CHAPTER 279

12.2.1 Chapter 2: Frequency domain representation of random processes *279*

12.2.2 Chapter 3: Modelling the turbulent wind *280*

12.2.3 Chapter 4: Aerodynamic modelling of a wind turbine *280*

12.2.4 Chapter 5: Modelling the wind turbine loads *281*

12.2.5 Chapter 6: Dynamic analysis of a wind turbine subjected to turbulent wind loads *281*

12.2.6 Chapter 7: Fatigue analysis in the frequency domain *282*

12.2.7 Chapter 8: Numerical model validation and comparison *282*

12.2.8 Chapter 9: Wind turbine loading due to stochastic base motions *283*

12.2.9 Chapter 10: Wind turbine blade loads due to stochastic base motions *284*

12.2.10 Chapter 11: The analysis of a floating offshore wind turbine mounted on a tensioned buoyant platform *284*

12.3 SUGGESTIONS FOR FURTHER STUDY 285

12.3.1 Further developments necessary to the mathematical model *285*

12.3.2 Further case studies *286*

APPENDICES **289**

A: AERANA LISTING (CHAPTER 4) .....

B: TURBANA LISTING (CHAPTER 5) .....

C: LINANA LISTING (CHAPTER 6) .....

D: LOADANA LISTING (CHAPTER 6) .....

E: ROTORMAT & HYDRANA LISTINGS (CHAPTERS 9 & 10) .....

F: CALCULATION OF NORMALISED EQUIVALENT FATIGUE DAMAGE (CHAPTER 7) .....

List of Figures

FIGURE 1-1 SOME OFFSHORE TURBINE CONCEPTS 28
FIGURE 1-2 FLOW CHART OF MATHCAD MODULES USED IN THIS RESEARCH 34

FIGURE 2-1 FOURIER SERIES EXPANSION OF A TIME HISTORY 38
FIGURE 2-2 SUMMATION OF COSINE AND SINE WAVES 39
FIGURE 2-3 PLOT OF REAL AND IMAGINARY PARTS OF COMPLEX FOURIER COEFFICIENT 41
FIGURE 2-4 FOURIER DENSITY COEFFICIENTS 42
FIGURE 2-5 FREQUENCY DOMAIN REPRESENTATION OF A RANDOM TIME HISTORY 46
FIGURE 2-6 SINGLE SIDED FOURIER TRANSFORM 47
FIGURE 2-7 DOUBLE SIDED POWER SPECTRAL DENSITY (PSD) 48
FIGURE 2-8 TIME HISTORIES AND CORRESPONDING PSDS 51
FIGURE 2-9 THE FOURIER TRANSFORM BETWEEN TIME AND FREQUENCY DOMAINS 55
FIGURE 2-10 TRANSFORMATION BETWEEN TIME HISTORY AND PSD 56
FIGURE 2-11 TIME HISTORIES AND CORRESPONDING AUTOCOVARIANCE'S 59
FIGURE 2-12 MULTIPLE RANDOM PROCESSES 62
FIGURE 2-13 REACTION TO MULTIPLE RANDOM LOADING 64
FIGURE 2-14 CROSS-POWER SPECTRAL DENSITY MATRIX 66

FIGURE 3-1 ENERGY SPECTRUM OF WIND SPEED AFTER VAN DER HOVEN 69
FIGURE 3-2 WIND SPEED VARIATION WITH TIME 70
FIGURE 3-3 WIND SPEED VARIATION WITH HEIGHT 71
FIGURE 3-4 ATMOSPHERIC STABILITY 72
FIGURE 3-5 ATMOSPHERIC STABILITY CLASSIFICATION 73
FIGURE 3-6 PDF OF MEAN HOURLY WIND SPEED 77
FIGURE 3-7 VISUALISATION OF TURBULENCE 79
FIGURE 3-8 TURBULENCE CORRELATION AND CONVECTION 79
FIGURE 3-9 LENGTH SCALES OF TURBULENCE 80
FIGURE 3-10 PSD OF WIND TURBULENCE 84
FIGURE 3-11 LONGITUDINAL SEPARATION 87
FIGURE 3-12 LATERAL SEPARATION 88
FIGURE 3-13 COHERENCE 89

FIGURE 4-1 HELICAL WAKE BEHIND THE ROTOR 93
FIGURE 4-2 WIND INFLOW VELOCITY VECTOR 94
FIGURE 4-3 TURBULENT WIND SPEED SEEN BY THE ROTOR 95
FIGURE 4-4 WIND VELOCITY VECTOR ON A BLADE ELEMENT 98
FIGURE 4-5 ANNULAR STREAMTUBE 100

FIGURE 4-6 FLOW CHART SHOWING ITERATION LOOP IN AERODYNAMIC ANALYSIS 101
FIGURE 4-7 ROTOR THRUST VS AXIAL INDUCTION 102
FIGURE 4-8 CORRECTION FOR 3-D FLOW 104
FIGURE 4-9 STEADY ROTOR THRUST CURVES 105
FIGURE 4-10 STEADY ROTOR TORQUE CURVES 106
FIGURE 4-11 STEADY ROTOR POWER CURVES 107
FIGURE 4-12 STALL VISUALISATION PLOTS 108
FIGURE 4-13 LIFT AND DRAG FORCES ON AN AIRFOIL 108
FIGURE 4-14 NOTATION FOR LINEAR GAIN FACTORS 110
FIGURE 4-15 BLADE ELEMENT THRUST 111
FIGURE 4-16 THE RELATIONSHIP BETWEEN AERODYNAMIC AND STRUCTURAL DYNAMIC BLADE MESH 112
FIGURE 4-17 PERCENTAGE ERROR IN ROTOR THRUST AND TORQUE WITH DEMINISHING NUMBER OF ELEMENTS 113

FIGURE 5-1 ROTATIONAL SAMPLING OF A SINGLE EDDY 119
FIGURE 5-2 AUTO-POWER SPECTRUM FOR A BLADE ELEMENT 120
FIGURE 5-3 DOUBLE SIDED AUTO-POWER SPECTRUM OF ROTATIONALLY SAMPLED WIND 123
FIGURE 5-4 SINGLE SIDED PSD OF WIND TURBULENCE 124
FIGURE 5-5 CROSS-POWER SPECTRA BETWEEN BLADE ELEMENTS 124
FIGURE 5-6 CROSS-POWER SPECTRAL DENSITY MATRIX OF TURBINE ELEMENTS 129
FIGURE 5-7 BLADE CROSS-MATRICES 130
FIGURE 5-8 SIMPLE BLADE LOADING 131
FIGURE 5-9 MULTIPLE BLADE LOADS 132
FIGURE 5-10 PSD OF BLADE ROOT SHEAR FORCE IN THE OUT-OF-PLANE DIRECTION 133
FIGURE 5-11 ROTOR THRUST 134
FIGURE 5-12 PSD OF ROTOR THRUST AT TOWER TOP 135
FIGURE 5-13 TOWER TOP LOADING DUE TO ROTATIONAL SAMPLING OF A TURBULENT GUST 135
FIGURE 5-14 ANALOGY OF THE ROTOR SUPER ELEMENT 136
FIGURE 5-15 CROSS-POWER SPECTRA BETWEEN TWO OBSERVERS ON A 'SUPER ELEMENT' 137
FIGURE 5-16 TURBINE AXIS SYSTEM 138
FIGURE 5-17 TURBINE YAW 139
FIGURE 5-18 CROSS-POWER OF YAW MOMENTS 139
FIGURE 5-19 CROSS-POWER SPECTRA OF YAW MOMENT 143
FIGURE 5-20 SINGLE SIDED PSD OF YAW MOMENT 143
FIGURE 5-21 SINGLE SIDED PSD OF YAW MOMENT 145
FIGURE 5-22 YAW MISALIGNMENT 145
FIGURE 5-23 YAW MISALIGNMENT FORCE DUE TO ROTOR CONING 146

FIGURE 6-1 SINGLE DEGREE OF FREEDOM BLADE MODEL 151

FIGURE 6-2 MULTI-DEGREE OF FREEDOM BLADE MODEL 153
FIGURE 6-3 PRINCIPLE OF 'BACK SUBSTITUTION' 154
FIGURE 6-4 BLADE ELEMENT SIGN CONVENTION 155
FIGURE 6-5 FORMAT OF THE ELEMENT MASS MATRIX 158
FIGURE 6-6 DERIVATION OF NODAL MASSES 158
FIGURE 6-7 BLADE SHAPE FUNCTION 158
FIGURE 6-8 LATTICE TOWER SUB-SYSTEM 163
FIGURE 6-9 INCORPORATING THE DRIVETRAIN ELEMENT 165
FIGURE 6-10 TYPICAL ELEMENT MESH OF A TURBINE 165
FIGURE 6-11 THE BLADE COORDINATE TRANSFORMATION ELEMENT 166
FIGURE 6-12 TRANSFORMATION MATRIX BETWEEN TOWER AND BLADE AXES. 166
FIGURE 6-13 SUB-DIVISION OF THE STIFFNESS MATRIX 168
FIGURE 6-14 THE ELEMENT TRANSFORMATION PROCESS 168
FIGURE 6-15 AZIMUTH POSITION OF SUPER BLADE FOR MODELLING TILT AND YAW MOMENTS ON THE TOWER 170

FIGURE 7-1 RANGE MEAN HISTOGRAM DERIVED BY RAINFLOW CYCLE COUNTING 177
FIGURE 7-2 TYPICAL SN CURVE FOR A BRITISH STANDARD STEEL 179
FIGURE 7-3 THE SN EQUATION 180
FIGURE 7-4 RANGE MEAN HISTOGRAM PRODUCED BY BENDAT'S NARROW BAND SOLUTION 182
FIGURE 7-5 WHY BENDAT'S NARROW BAND APPROACH IS CONSERVATIVE 183
FIGURE 7-6 RANGE MEAN HISTOGRAM DERIVED BY DIRLIK 185
FIGURE 7-7 EXCEEDENCE PLOT COMPARING TIME AND FREQUENCY DOMAIN RANGE MEAN HISTOGRAMS 185

FIGURE 8-1 FLOW CHART OF MATHEMATICAL PROCEDURES IN THE ANALYSIS 193
FIGURE 8-2 COMPARISON BETWEEN CALCULATED AND PUBLISHED POWER CURVES FOR TURBINES A* AND B 195
FIGURE 8-3 COMPARISON BETWEEN MEASURED AND CALCULATED PSD OF WIND TURBULENCE 197
FIGURE 8-4 VALIDATAION OF TURBANA CALCULATION WITH TURBU-1 201
FIGURE 8-5 COMPARISON BETWEEN CALCULATED AND MEASURED PSDS FOR A MEAN WIND SPEED OF 10 M/SEC, AND A TURBULENCE INTENSITY OF 8.9%. 206
FIGURE 8-6 COMPARISON BETWEEN CALCULATED AND MEASURED PSDS FOR A MEAN WIND SPEED OF 20 M/SEC, AND A TURBULENCE INTENSITY OF 9.3%. 207
FIGURE 8-7 PROPAGATION OF STALL ALONG THE BLADES OF TURBINES A AND B 212
FIGURE 8-8 VARIATION IN AERODYNAMIC FORCE ON A BLADE ELEMENT 213

FIGURE 9-1 IDEALISATION OF A FLOATING WIND TURBINE 220
FIGURE 9-2 GLOBAL AND BLADE AXES SYSTEMS 221
FIGURE 9-3 NOTATION FOR LINEAR GAIN FACTORS 222

FIGURE 9-4 ROTOR TILT 225
FIGURE 9-5 LOCUS DUE TO HEAVING MOTION 228

FIGURE 10-1 CROSS-POWER SPECTRA OF LOADING 251
FIGURE 10-2 FLOW CHART SHOWING ITERATIVE CALCULATION OF EQUILIBRIUM BLADE FORCES 256

FIGURE 11-1 CATENARY MOORED SPAR BUOY PLATFORM (AFTER TONG & CANNELL) 259
FIGURE 11-2 MULTIPLE UNIT FLOATING OFFSHORE WINDFARM (MUFOW) (AFTER BARLTROP AND HALFPENNY ET AL.) 260
FIGURE 11-3 TENSIONED BUOYANT PLATFORM (TBP) CONCEPT 261
FIGURE 11-4 TYPICAL TBP CONCEPT 262
FIGURE 11-5 THE PDF OF SIGNIFICANT WAVE HEIGHT 264
FIGURE 11-6 RESPONSE AMPLITUDE OPERATORS FOR BOTH 4 AND 6 COLUMN TBPS 265
FIGURE 11-7 PSD OF SURGE RESPONSE FOR TBPS IN THE SEA STATE 4 265
FIGURE 11-8 PSD OF ROTOR THRUST CAUSED BY WAVE INDUCED MOTIONS AND THE TURBULENT WIND 267
FIGURE 11-9 FATIGUE DAMAGE V'S SEA STATE 269
FIGURE 11-10 PSD OF ROTOR TORQUE CAUSED BY WAVE INDUCED MOTION AND THE TURBULENT WIND 270
FIGURE 11-11 FATIGUE DAMAGE V'S SEA STATE 272
FIGURE 11-12 FEA MODEL OF TURBINE MOUNTED ON TBP 275

List of tables

TABLE 3-1 TYPICAL VALUES OF TERRAIN PARAMETERS ACCORDING TO ESDU 75
TABLE 3-2 CLASSIFICATION OF OFFSHORE WIND TURBINES ACCORDING TO GERMANISCHER LLOYD[10] 78

TABLE 4-1 CONFIDENCE INTERVALS FOR TURBULENT WIND SPEED RANGES 111

TABLE 5-1 SUMMARY OF FORMULAE FOR DETERMINING BLADE ROOT FORCES AND MOMENTS 132
TABLE 5-2 SUMMARY OF FORMULAE FOR CALCULATING ROTOR THRUST AND TORQUE 134

TABLE 7-1 COMPARISON BETWEEN DIFFERENT FREQUENCY DOMAIN FATIGUE ANALYSES 186

TABLE 8-1 COMPARATIVE DATA MADE AVAILABLE BY WS ATKINS 192
TABLE 8-2 SUMMARY OF STATISTICAL DATA FOR MEASURED AND CALCULATED PSDS 199
TABLE 8-3 STATISTICAL COMPARISON BETWEEN TURBANA AND TURBU-1 202
TABLE 8-4 COMPARISON OF FIRST MODE BLADE FREQUENCIES 203
TABLE 8-5 COMPARISON OF NATURAL FREQUENCIES 204
TABLE 8-6 COMPARISON OF STATISTICAL PROPERTIES OF PSDS FOR TURBINE A. 208
TABLE 8-7 COMPARISON OF STATISTICAL PROPERTIES OF PSDS FOR TURBINE B 210

TABLE 9-1 RIGID BODY DEGREES OF FREEDOM 221
TABLE 9-2 LOADING CONDITIONS DUE TO TURBINE MOTION 230
TABLE 9-3 AUTO-POWER SPECTRAL DENSITY FUNCTIONS FOR GENERAL SINUSOIDAL MOTION 243

TABLE 11-1 SUMMARY OF TBP DATA AFTER PATEL AND WITZ[4] 262
TABLE 11-2 SEA STATE PARAMETERS FOR THE PIERSON MOSKOWITZ SPECTRA 264
TABLE 11-3 COMPARABLE FATIGUE DAMAGE FOR WIND TURBULENCE 267
TABLE 11-4 STATISTICAL PROPERTIES AND FATIGUE DAMAGE IN THE ROTOR THRUST PSDS 268
TABLE 11-5 STATISTICAL PROPERTIES AND FATIGUE DAMAGE IN THE ROTOR THRUST PSDS 271
TABLE 11-6 EFFECT OF ROTOR DAMPING IN SURGE 273
TABLE 11-7 TURBINE MASS IN RELATION TO PLATFORM MASS 273

Nomenclature

CHAPTER 2

A_0, A_n, B_n, C_n	Fourier coefficients
$C_{xx}(\tau)$	Auto-covariance function
$C_{xy}(\tau)$	Cross-covariance function
$E\{\ \}$	The expectation operator defined by $E\{y(t)\} = \lim_{T\to\infty}\left\{\frac{1}{T}\cdot\int_{-T/2}^{T/2} y(t)dt\right\}$
N	Number of discrete rows in a time history
$S_{xx}(f)/G_{xx}(f)$	Double / single sided Auto-power Spectral Density Function.
$S_{xy}(f)/G_{xy}(f)$	Double / single sided Cross-power Spectral Density Function.
T	Period
f	Frequency in Hz.
g, $H(\omega)$	Linear aerodynamic and structural dynamic transfer functions respectively.
$m_n(S)$	nth spectral moment of the distribution S defined by $m_n(S) = \int_{-\infty}^{\infty} S(f)\cdot f^n df$
$y(t)$	Time history of event y expressed in the time domain t.
$\tilde{y}(f)$	Time history of event y expressed in the frequency domain f.
t	Time
$\Re\{X\}$, $\mathrm{I}\{X\}$	Real / Imaginary component of the complex number X.
$\gamma_{xy}(f)$	Coherence function defined by $\gamma_{xy}(f) = \frac{\lvert S_{xy}(f)\rvert}{\sqrt{S_{xx}(f)\cdot S_{yy}(f)}}$
$\rho_{xy}(\tau)$	Time scale parameter defined by $\rho_{xy}(\tau) = \frac{C_{xy}(\tau)}{C_{xy}(0)} = \frac{C_{xy}(\tau)}{\sigma_{xy}^{\ 2}}$
σ	Standard deviation

CHAPTER 3

$G_{uu}(f)$	Single sided auto-power spectral density function of turbulent wind speed. ($m/sec^2/Hz$)
I	Turbulence intensity defined by $I = \frac{\sigma}{V_z}$
V_z	Mean hourly wind speed at rotor hub. (m/sec)
V_{10}	Mean hourly wind speed 10m above ground level. (m/sec)
V_H	Mean hourly wind speed at reference height H above ground level. (m/sec)
$\overline{V_M}$	Annual mean wind speed recorded at hub height. (m/sec)

$\overline{V_E}$	10 minute mean of extreme wind speed with a mean probability of occurring once in 50 years measured at the hub height. (m/sec)
c	Weibull mode parameter (m/sec)
d	Effective displacement of the zero plane above ground level. (m)
f_c	Coriolis parameter. $f_c = 2\Omega \cdot \sin(\phi)$
f / ω	Frequency in Hz and rad/sec respectively.
h	Gradient height defined by $h = \frac{u_*}{6 f_c}$
k	Weibull slope parameter
u_*	Friction velocity defined by $u_* = \frac{V_{10}}{2.5 \ln\left(10/z_0\right)}$
z	Height above the ground to rotor hub (m)
z_0	Ground roughness length. (m)
${}^{x}L_u$, ${}^{y}L_v$, ${}^{z}L_w$	Longitudinal length scales of turbulence. (m)
${}^{y}L_u$, ${}^{z}L_u$, ${}^{x}L_v$ ${}^{z}L_v$, ${}^{x}L_w$, ${}^{y}L_w$	Lateral length scales of turbulence. (m)
${}^{r}L_u$	Radial length scale. (m)
ϕ	Angle of latitude of the site (deg)
$\gamma_{xy}(f)$	Coherence function.
σ	Standard deviation.
Γ	Gamma function defined by $\Gamma(z) = \int_0^\infty t^{z-1} \cdot e^{-t} dt$
Ω	Angular rotational velocity of the earth. $\Omega = 72.9 \cdot 10^{-6}$ rads/sec.

CHAPTER 4

A	Area. (m^2)
B	Number of blades
C_H / C_T	Coefficient of rotor thrust defined by $C_H = \frac{T}{\frac{1}{2} \cdot \rho \cdot A \cdot V^2}$
C_Q	Coefficient of rotor torque defined by $C_Q = \frac{Q}{\frac{1}{2} \cdot \rho \cdot A \cdot V^2 \cdot R}$
C_P	Coefficient of rotor power defined by $C_P = \frac{P}{\frac{1}{2} \cdot \rho \cdot A \cdot V^3}$
Cd	Coefficient of drag defined by $Cd = \frac{D}{\frac{1}{2} \cdot \rho \cdot A \cdot V^2}$
Cl / Cl_{2D}	Coefficient of lift defined by $Cl = \frac{L}{\frac{1}{2} \cdot \rho \cdot A \cdot V^2}$
Cl_{3D}	Modified coefficient of lift to account for post stall conditions.
D	Drag force. (N)
F	Tip loss factor after Prandtl.

I_u	Turbulence intensity factor.
L	Lift force. (N)
P	Rotor power. (W)
Q	Rotor torque. (N.m)
R	Radius of rotor (i.e. length of blade) (m)
T	Rotor thrust. (N)
V	Incident wind speed at an infinite distance upstream of the turbine measured at the hub height. (m/sec)
V_1	Incident wind speed at the rotor plane measured at the hub height. (m/sec)
V_2	Wind speed at an infinite distance downstream of the turbine measured at the hub height. (m/sec)
V_R	Resultant wind speed vector. (m/sec)
a	Axial induction factor.
$a`$	Radial induction factor.
c	Chord length. (m)
g, c, b	Linear aerodynamic gain factors.
r	Density of air. (Standard conditions of 15°C temperature, 1013mBar pressure gives density of r = 1.225 kg/m^3.)
r_i	Radius to the ith blade element. (m)
u	Axially induced wake velocity vector defined by $u_i = V \cdot a_i$ (m/sec)
w	Tangentially induced wake (swirl) velocity vector defined by $w_i = \Omega \cdot r_i \cdot a`_i$ (m/sec)
α	Angle of attack (or inflow angle). (rad)
β	Blade setting angle. (rad)
ϕ	Resultant inflow angle. (rad)
ψ	Rotor coning angle. (rad)
σ	Blade solidity ratio defined by $\sigma_i = \dfrac{B \cdot c_i}{\pi \cdot r_i}$
σ_u	Standard deviation of turbulent wind speed. (m/sec)
Δr	Length of blade element. (m)
Ω	Constant rotor frequency (rad/sec)

CHAPTER 5

B	Number of blades.
$C_{uv}(\tau)$	Cross-covariance function between two random processes u and v.
$\tilde{C}_{ij}(\tau)$	Rotationally sampled cross-covariance function witnessed by two rotating observers, i and j, sited at point along the rotor blades.
$E\{\ \}$	The expectation operator defined by $E\{y(t)\} = \lim_{T\to\infty}\left\{\frac{1}{T}\cdot\int_{-T/2}^{T/2} y(t)dt\right\}$
K_n	Fourier coefficient.
$S_{uu}(\omega)/G_{uu}(\omega)$	Double / single sided auto-power spectral density function of wind speed measured at the rotor hub. (see chapter 3) ((m/sec)^2/rad/sec)

$\tilde{S}_{ij}(\omega)/\tilde{G}(\omega)$	Double / single sided, cross-power spectral density function of rotationally sampled wind speed witnessed by two rotating observers sited along two rotor blades. ((m/sec)^2/rad/sec)
$S^F(\omega)/G^F(\omega)$	Double / single sided, auto-power spectral density function of force. (N^2/rad/sec)
V_z	Mean hourly wind speed at the rotor hub. (m/sec)
b	Average period for an eddy to pass through the rotor plane given by $b = \frac{{}^xL_u}{V_z}$. (sec)
d	Distance between two points (m)
g_i, c_i, q_i	Linear aerodynamic gain factors for the ith blade element. (N/m/sec)
p_i	Gain factor defined by $p_i = g_i \cdot r_i$. (N.m/m/sec)
r_i	Radius from the hub to the ith blade element. (m)
t, τ	Time (sec)
${}^xL_u$	Longitudinal length scale. (see chapter 3)
z	Height of rotor hub above the ground (m)
$\delta(\sigma)$	Dirac's delta function defined such that $\delta(\sigma)=1$ for $\sigma=0$, and $\delta(\sigma)=0$ for $\sigma\neq 0$.
$\gamma(\omega,d)$	Spatial coherence function given by ESDU. (see chapter 3)
$\tilde{v}_i(t)$	Instantaneous wind speed on the ith blade element. (m/sec)
φ_{ij}	Angle between two turbine blades, i & j, given by $\varphi_{ij} = \frac{2\pi}{B}\cdot(j-i)$
Ω	Constant rotor frequency (rad/sec)

CHAPTER 6

E	Young's modulus of elasticity (N/m^2)
G	Matrix of aerodynamic gain factors
$\tilde{G}(\omega)$	Single sided, cross-power spectral density function of rotationally sampled wind speed witnessed by two rotating observers sited along two rotor blades. ((m/sec)^2/rad/sec)
$G^F(\omega)$	Single sided, auto-power spectral density function of force. (N^2/rad/sec)
G_R	Gearbox ratio
$H(\omega)$	Structural transfer function. (m/N)
I	Second moment of area of an element (m^4)
I_L, I_H	Inertia on the low and high speed shafts respectively (N.m)
Le	Length of an element (m)
M^*, C^*, K^*	Mass, damping and stiffness matrices expressed in the modal coordinate system
T	Tensile force due to centripetal acceleration (N)
c_{crit}	Critical damping in the nth mode
c_s	Structural damping. (N/m/sec)
g, c	Aerodynamic gain factors. (N/m/sec)

k_s/k_c	Structural / centripetal stiffness. (N/m)
m	Mass. (kg)
me	Incremental mass along a beam element (kg/m)
$q(t)$	Modal displacement vector (m)
r_i	Radius to the i^{th} blade node. (m)
t	Time. (sec)
$u(t)$	Virtual displacement vector (1m)
$v(t)$	Wind speed at time t. (m/sec)
$x(t)$	Displacement at time t. (m)
$y(x)$	Shape function along the length of a beam element subjected to a unit virtual rotation at one node. (m/rad)
β	Blade element twist angle (rad)
ε	Matrix of augmented Eigen vectors (m)
ε_n	Eigen vector of nodal displacements in the n^{th} mode (m)
ϕ	Coordinate transformation matrix.
ω	Frequency. (rad/sec)
ω_n	Natural frequency of the n^{th} mode (rad/sec)
$\varphi(t)$	Azimuth angle of the rotor blade at time t (rad)
ξ_n	Damping coefficient for the n^{th} mode expressed as a percentage of the critical damping.
Ω	Constant rotor frequency. (rad/sec)

CHAPTER 7

$E[P]$	Expected number of peaks
N	Number of stress cycles
N_f	Number of cycles to failure
S	Stress range (N/mm^2)
S_{eq}	Equivalent stress accounting for exponential material SN curve
T	Length of time history (sec)
k	Material SN property, number of cycles to failure for a unit stress range
m	Material SN property, slope of exponential curve
m_n	n^{th} moment of area under the PSD
$p(S)$	Probability density function of stress range

CHAPTER 9

C	Rotor node damping matrix (N/m/sec)
K	Rotor node stiffness matrix (N/m)
M	Rotor node mass matrix (kg)
g, c, β	Aerodynamic gain factors (N/m/sec)
m	Element mass (kg)
$s(t)$	Displacement at time t (m)
ϕ	Blade azimuth coordinate transformation matrix
κ	Constant transfer function

γ_n	Weight of the n^{th} blade element (N)
φ	Blade azimuth angle (rad)

subscripts

φ	Term expressed in the Local coordinate system
o	Term expressed in the Global coordinate system
φo	Term expressed in the Local coordinate system resulting from motions expressed in the Global coordinate system

CHAPTER 10

C	Damping matrix
$C_{uv}(\tau)$	Cross-covariance function between two random processes u and v.
$\tilde{C}_{ij}(\tau)$	Rotationally sampled cross-covariance function witnessed by two rotating observers, i and j, sited at point along the rotor blades.
$E\{\ \}$	The expectation operator defined by $E\{y(t)\} = \lim_{T\to\infty}\left\{\frac{1}{T}\cdot\int_{-T/2}^{T/2} y(t)dt\right\}$
$H(\omega)$	Transfer function matrix
K	Stiffness matrix
M	Mass matrix
h	Transfer function
$s(t)$	Displacement at time t (m)

Superscripts

F	Matrix of force
c	Constant matrix
s	Sinusoidally varying matrix

Subscripts

o	Term expressed in the Global coordinate system
φ	Term expressed in the Local coordinate axis system
φo	Term expressed in the Local coordinate system resulting from motions expressed in the Global coordinate system

CHAPTER 11

C_{crit}	Critical damping in the n^{th} mode
$G_w(\omega)$	Single sided PSD of wave elevation (In this case the Pierson Moskowitz spectra is used) (m^2/Hz)
$G_{yy}(\omega)$	Single sided PSD of surge motion (m^2/Hz)
K	Stiffness matrix
M	Mass matrix comprising the structural mass and the hydrodynamic added mass (kg)
$RAO(\omega)$	Response amplitude operator(m/m)
T	Natural period of vibration (sec)

ξ	Damping coefficient expressed as a percentage of the critical damping
H_s	Significant wave height (m)
T_z	Wave zero crossing period (sec)
T_D	Period corresponding to the dominant wave frequency (sec)
ω	Frequency (rad/sec)

1. Introduction

1.1 General

Concern over the escalating damage to the environment and the depletion of fossil fuels has forced governments to reconsider their longterm energy generation strategies. In a world whose energy demand is for ever increasing,many countries are now looking seriously towards renewable energy resources such as tidal, solar, bio-masses, wind and wave energies.

Wind energy has proved very popular with governments and private investors owing to its relatively mature technology. A number of companies have established themselves producing reliable and cost effective wind turbines with electrical power ratings between 50kW and 1MW. The UK has seen a considerable growth in wind generation since 1992, however,further introduction of large numbers of wind turbines is likely to be hindered by local objections to the proposed sites. Conditions throughout Europe are similar. The Dutch and Danish, who have been utilising wind energy for many years, are now encountering potential 'land saturation' levels and there are growing concerns about the future of land based generation in these countries.

The wind energy community has responded to these concerns by developing larger machines which optimise available land area and by investigating the possibility of siting large turbines offshore. These schemes require sophisticated design tools to ensure that the installations are reliable and economic.

A number of studies on offshore wind energy schemes have been carried out. The earlier studies concentrated primarily on developing cost estimates and understandably started by considering a single, large scale turbine mounted on a fixed base platform. One notable exception has been the FLOAT project by Garrad Hassan and Tecnomare UK Ltd. (Tong and Cannell[1]) which deals with a single turbine mounted on a spar buoy type platform. Figure 1-1 illustrates a few of the concepts that have been investigated.

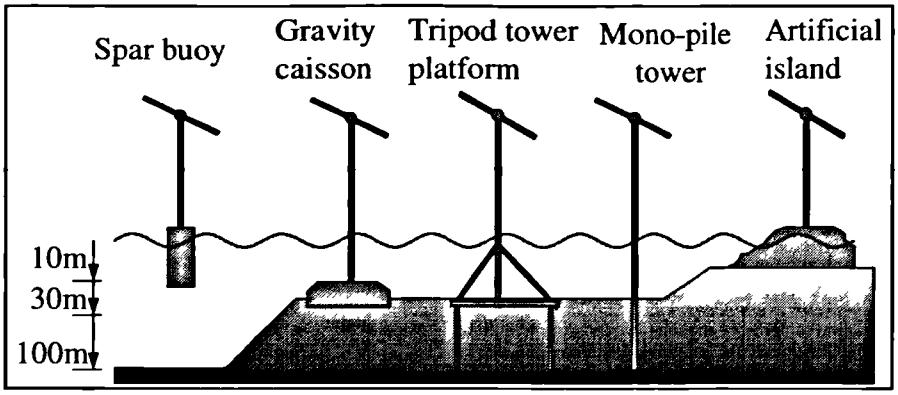

Figure 1-1 Some offshore turbine concepts

The gravity caisson scheme has been widely publicised and was employed in the famous 'Vindeby' wind farm off the coast of Denmark. (Wind Engineering[2] and Barthelmie[3]). Here the water depth is very shallow (2.1 - 5.1 m). In similar water depths the Dutch have sited a wind farm that uses a mono-pile foundation where the tower is effectively continued into the seabed and acts as a support pile. The concept adopted will depend greatly on the water depth in the chosen location. Figure 1-1 illustrates the water depths appropriate to each design. The floating concepts require water depths greater than 30m for an effective mooring system to be provided.

With the increasing size and complexity of the turbines comes a need for more flexible design tools to model the structural performance. In the case of floating turbines is the additional necessity to determine the sea keeping ability and the effect of rigid body motions on the turbine loads. There are two methods of evaluating the response to the turbulent loads:

1. Time history analysis (time domain)
2. Power spectral density analysis (PSD frequency domain)

The time domain method involves the creation of a typical time history of the fluctuating sea and wave conditions. This is then passed through a dynamic simulation computer program that evaluates the time history of the platform motions and turbine stresses. Although this is a thorough method it has a number of disadvantages, in particular the time taken to perform a representative time analysis can be quite considerable and there is also difficulty in choosing an appropriate time history to apply to the structure. A number of scenarios should be applied to cater for the many loading combinations and conditions which affect the structure. These will include the

worst sea / wind combination and the general conditions that influence the fatigue life of the structure. Each scenario will require an additional calculation and each calculation will be computationally intensive and time consuming. For these reasons the frequency domain is often more appropriate, especially for preliminary scoping and optimisation calculations.

The PSD effectively represents the energy content in the wind and waves at a particular frequency. This is based on statistical measurements. The spectral models used for the wind and wave loading are based on the ESDU[4] and Pierson Moskowitz[5] spectra respectively. The power of the frequency domain lies in its calculation speed. Assuming that the structure behaves in a near-linear way enables the engineer to calculate a structural transfer function to model the structure. Applying additional loading scenarios is then a simple matter of multiplying each loading PSD by the transfer function. This simple and rapid calculation allows the engineer more potential to optimise the structure in the early stages of design. This is particularly appealing where fatigue is an important design issue because fatigue optimisation is not possible in the time domain due to the calculation time and expense involved. Time domain calculations are typically restricted, therefore, to verification exercises carried out at the end of the design phase.

1.2 Statement of the problem

If offshore floating turbine concepts are to be fully realised it is necessary to develop mathematical models that are able to rapidly predict the dynamic loads on the various components. Floating wind turbines are subjected to numerous random loading conditions from the wind and waves. To analyse the dynamic response from these it proves much faster to use an approach based in the frequency domain in the first instance.

Design optimisation can be carried out rapidly in the frequency domain to develop a sound concept. When the engineer is happy with this then a more rigorous (and time consuming) analysis can be carried out in the time domain to verify the concepts integrity. This approach increases qualitative and quantitative understanding in

dynamic behaviour and can lead to reduced design costs and better optimised schemes.

To properly analyse the response of a floating offshore turbine it is necessary to address three questions:

1. To what extent will the platform move in the water due to the combined wind and wave loading? (Equilibrium rigid body motion analysis.)
2. What effect do these platform motions have on the structural loading of the turbine?
3. What effect does the wind turbulence have directly on the structural loading of the turbine?

Having determined platform motions and the structural loads we can carry out seakeeping analyses and fatigue life prediction.

Only question 3 has been properly addressed and only recently have people even begun to consider the effect of structural dynamics and flexibility in the frequency domain. Garrad Hassan and Tecnomare UK Ltd. (Tong & Cannell[1]) have considered Questions 1 and 2 but only for the simple case of surge motion.

This thesis derives a new analysis technique for addressing the three questions. This is an original piece of work and for the first time includes a 6-degree of freedom rigid body platform motion analysis and multi-degree of freedom structural finite element analysis.

1.3 The objectives of the study

The objectives of the study are to develop frequency domain analysis techniques for modelling wind turbine structures that are subjected to random wind loads and wave induced motions. In particular the analysis of floating offshore wind turbines.

The new analysis technique derived in this thesis is divided into two stages. The first analysis treats the turbine and platform as a rigid body and calculates the equilibrium motion response of the structure. A new approach is adopted which treats the rigid rotor as an effective 'Super Element'. Given a PSD of turbulent wind speed, this

determines the rotor loading on the structure. An analysis is then performed to evaluate mass, damping and stiffness matrices for the rigid rotor in 6 degrees of freedom. These describe the response of the rigid rotor as it is moved through the air along with the platform motion. The Super Element can be incorporated into existing analysis packages, such as AQWA[6], to perform seakeeping analyses. This takes the sea elevation spectra and the wind turbulence loading spectra calculated by the Super Element and computes the 6 degree of freedom motion response of the vessel in terms of auto- and cross-power spectral densities.

The second stage takes the PSD of the turbulent wind speed along with the auto- and cross-power spectra of platform motion and computes the loads on the flexible turbine structure. This model includes all the structural flexibilities in the blades, tower and drivetrain.

The two stage approach is valid because structural flexibilities have been found to be insignificant in affecting the platform's motion, therefore a much simpler rigid body analysis ('Super Element') is suitable for this stage which can easily be incorporated into existing commercial software packages.

At the onset of this study, little development had been carried out on modelling the structural dynamics of a turbine in the frequency domain. Software packages from ECN[7] (The Netherlands Energy Research Foundation) and Garrad Hassan Ltd. were available but these were limited in analysing only the turbulent wind loads on rigid turbine structures. It was therefore necessary to develop a new structural dynamic analysis in the frequency domain with the ability to analyse blade, tower and drivetrain flexibilities before progressing to include the rigid body motions.

1.4 Scope and limitations

The work derives mathematical models to predict the random loads on a turbine structure resulting from random wind speed and platform motion. All calculations are based in the frequency domain.

Among the significant and original aspects of the project work are:

1. The derivation of a new structural analysis procedure to model the behaviour of flexible turbines in the frequency domain. These can be used for both on and offshore turbine analysis.

2. The derivation of a new rotor 'Super element' to model the response of a rigid turbine rotor to base motions and calculate the rotor loading due to turbulent winds. This 'Super Element' is used for seakeeping analyses.

3. The derivation of a new procedure to calculate the dynamic loads on a flexible turbine blade subjected to rigid body motions and turbulent winds. This is used for structural analysis and design and for fatigue analysis using the latest frequency domain techniques.

1.5 Organisation of the Thesis

The thesis is organised as follows: chapters 2 to 4 detail the fundamental background on which the thesis is based. Chapter 2 discusses the theory of frequency domain analysis of multiple correlated random loads. It derives key relationships and formulae that are used throughout this text. Chapter 3 discusses the physical principles and theory behind the turbulent wind. It highlights the state of the art knowledge and the problems that face the offshore engineer. A thorough description of the ESDU[4] model is presented. Chapter 4 derives the state of the art aerodynamic analysis used in this project and comments on its limitations.

Chapters 5 to 8 deal with random wind loading and the general structural dynamic analysis of the turbine. This analysis is common for both on and offshore wind turbines. Chapter 5 derives the formulae for calculating the rotationally sampled turbulence. It explains the concepts involved and their effect on the fatigue life. The new rotor 'Super Element' is derived for calculating rigid rotor loads from the turbulent wind. Chapter 6 describes a new structural dynamic model based on a finite element representation of the turbine. Details are given on modelling the structure and drivetrain and the implications of transferring between stationary and rotating coordinate systems. Chapter 7 discusses the theory behind fatigue analysis in the frequency domain and comments on its application in wind turbine design. Chapter 8 concludes this section by discussing the results of case study tests comparing measured loads with those calculated using the new analysis techniques. These studies

were performed in collaboration with WS Atkins Ltd. who are currently using the techniques for analysing existing and proposed turbine concepts.

Chapters 9 to 11 deal with the analysis of floating offshore turbines. Chapter 9 derives a rigid body model of the rotor to predict the reaction loads that arise when the rotor is moved through space in 6 degrees of freedom. This new 'Super Element' can be incorporated into existing hydrodynamic analysis packages, such as AQWA[6], to perform sea keeping analyses on the platform. Chapter 10 derives a new blade model that predicts the blade forces arising when the turbine is moved through space in 6 degrees of freedom. This is complicated because of additional harmonics that occur in the loading. A description is given on how this model is incorporated in the new finite element analysis technique derived earlier. Chapter 11 introduces a simple case study using a 'Tensioned Buoyant Platform (TBP)' on which is mounted a single wind turbine. TBP's serve as very stable platforms to mount offshore turbines and are renowned for their small dynamic motion response. The simplicity of the dynamic behaviour is highlighted and design conclusions made.

Chapter 12 presents the conclusions drawn from each chapter and suggests future work to be carried out.

1.6 Description of computer programs developed in this research

Computer programs have been developed as part of this research and these are referred to throughout the thesis. The computer programs are written using Mathcad versions Plus 5 and Plus 6[†] and is in a modular format with each module performing a particular analysis related to a chapter in the thesis. An overview of the modules is shown in Figure 1-2. Several modules are currently being used by WS Atkins Ltd.

[†] The aerodynamic analysis module only works with Mathcad version Plus 5 because of errors in version 6.

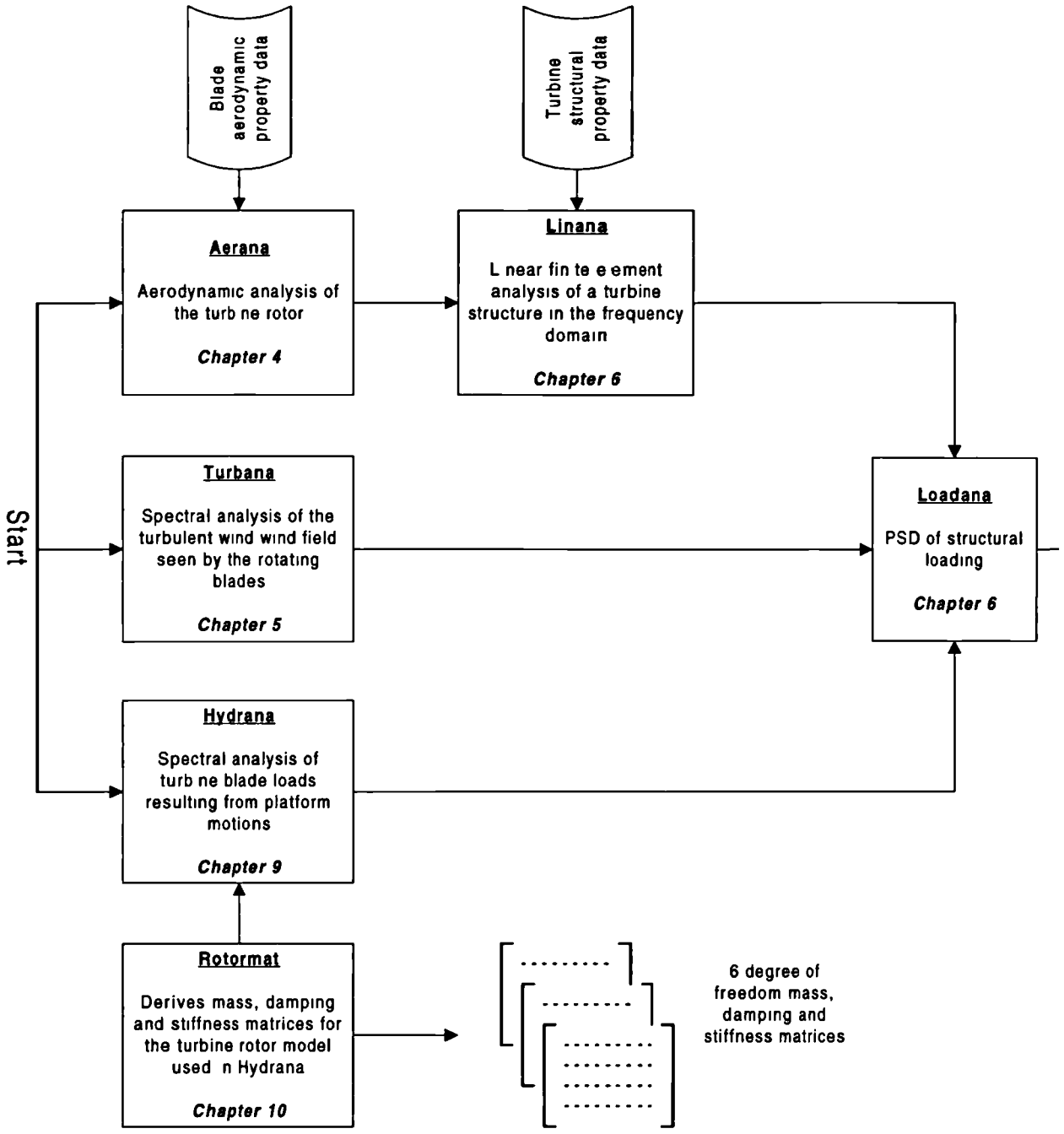

Figure 1-2 Flow chart of Mathcad modules used in this research

---

[1] Tong K and Cannell C. (1993). "Technical and economical aspects of a floating offshore windfarm." Proceedings of a BWEA/DTI seminar, Cockroft Hall, Harwell, June 1993.

[2] "Vindeby Offshore Windfarm." Wind Engineering, Volume 17 No. 3. 1993.

[3] Barthelmie R.J., Courtney M.S., Højstrup J and Sanderhoff P. (1994). "The Vindeby Project: a description." Risø report, Risø-R-741(EN),. Risø National Laboratory, Denmark.

[4] ESDU data sheets 82026 (1982), 85020 (1993) and 86010 (1991). "Strong winds in the atmospheric boundary layer. Parts I, II and III." ESDU International plc. London.

[5] Pierson W.J and Moskowitz L. (1964). "A proposed spectral form of fully developed wind seas based on the similarity theory of S.A Kitaigorodskii." Journal of Geophysics. Res., Vol. 69.

[6] Technical Manual to the AQWA-SUIT. Defraction analysis package. WS Atkins Ltd., Woodcote Grove, Ashley Road, Epsom, Surrey, England.

[7] Van Engelen T.G. (1991). "Turbu-I computer program for turbulence load analysis of horizontal axis wind turbines. Theory and program description." ECN, SU General Services, Petten, The Netherlands.

2. Frequency domain representation of random processes

2.1 Fourier series and the Fourier transform pair

2.1.1 Representing a time signal using Fourier series

Any periodic time history may be represented by the summation of a series of sinusoidal waves of various amplitude, frequency and phase. This is the basis of Fourier series expansion. A detailed explanation is given in Kreyszig[1] chapter 10. The Fourier series expansion of a time history $y(t)$ is often expressed by Equation 1.

$$y(t) = A_0 + \sum_{n=1}^{\infty}\left\{A_n \cos\left(\frac{2\pi n}{T}\cdot t\right) + B_n \sin\left(\frac{2\pi n}{T}\cdot t\right)\right\}$$

where

$$A_0 = \frac{1}{T}\int_{-T/2}^{T/2} y(t)dt$$

$$A_n = \frac{2}{T}\int_{-T/2}^{T/2} y(t)\cos\left(\frac{2\pi n}{T}\cdot t\right)dt$$

$$B_n = \frac{2}{T}\int_{-T/2}^{T/2} y(t)\sin\left(\frac{2\pi n}{T}\cdot t\right)dt$$

T = *period*

Equation 1 Fourier Series Expansion

The terms A_0, A_n and B_n are termed Fourier coefficients and provide information on the frequency content of the time history. A_0 represents the mean of the time history while A_n and B_n represent the amplitude of the various cosine and sine waves which when added together comprise the time history. Figure 2-1 shows the Fourier series expansion for a particular saw tooth time history. By the third summation the expansion is seen to give a reasonable representation of the original time history. Further summations improve the representation.

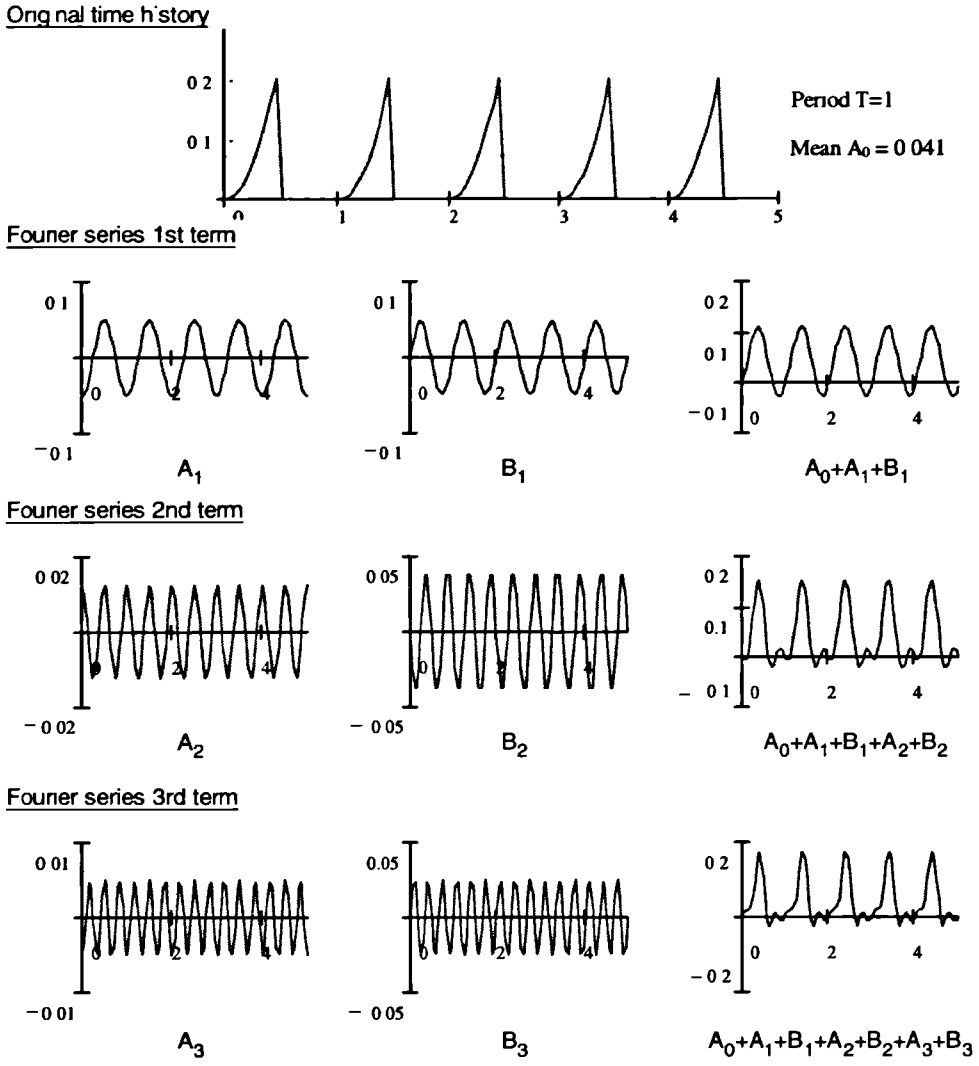

Figure 2-1 Fourier series expansion of a time history

The integrals within A_n and B_n effectively act as a filter and extract the amplitude of a cosine or sine wave of frequency n/T *Hz.* from the time history. This is accomplished using the relationships given in Equation 2.

$$\int_{-T/2}^{T/2} \cos\left(\frac{2\pi mt}{T}\right)\cos\left(\frac{2\pi nt}{T}\right)dt = \begin{cases} 0 & \text{for } m \neq n \\ T/2 & \text{for } m = n \end{cases}$$

$$\int_{-T/2}^{T/2} \sin\left(\frac{2\pi mt}{T}\right)\sin\left(\frac{2\pi nt}{t}\right)dt = \quad \Big\}$$

$$\int_{-T/2}^{T/2} \cos\left(\frac{2\pi mt}{T}\right)\sin\left(\frac{2\pi nt}{T}\right)dt = \quad \Big\} \quad 0 \text{ for all m and n}$$

Equation 2 Frequency filtering

2.1.2 The complex Fourier series

In practice the Fourier coefficients A_0, A_n and B_n prove very cumbersome to manipulate algebraically. Complex number theory helps with this aspect as all three coefficients may be replaced by one complex coefficient C_n. Many texts derive the complex Fourier series in detail, notably Kreyszig[1] chapter 10.6 and Barltrop[2] chapter 3.3.3. However since a thorough understanding of it is so crucial to the research described a short derivation is given in this chapter.

The first thing to realise is that the sum of a cosine and sine wave results in a sinusoidal wave of amplitude r and initial phase angle ϕ provided both waves have the same frequency. Figure 2-2 shows the summation of a cosine and sine wave with amplitudes A and B respectively and frequency ω.

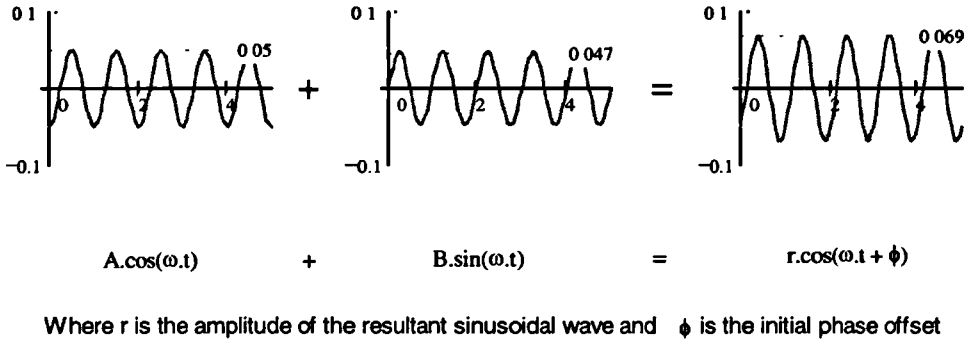

Figure 2-2 Summation of cosine and sine waves

The amplitude r and initial phase angle ϕ of the resultant sinusoidal wave can be obtained using the relationship given in Equation 3.

$$r_n = \sqrt{A_n^{\,2} + B_n^{\,2}} \qquad \phi_n = \tan^{-1}\left(\frac{B_n}{A_n}\right)$$

Equation 3

It is convenient to express the Fourier coefficients A_n and B_n in terms of the complex coefficient Λ_n where $\Lambda_n = A_n - i.B_n$. The amplitude r and phase angle ϕ can then be obtained from the 'magnitude' and 'argument' of the complex coefficient as shown in Equation 4.

$$r_n = |\Lambda_n| \quad \text{and} \quad \phi_n = \angle\Lambda_n \quad \text{where} \quad \Lambda_n = A_n - iB_n$$ **Equation 4**

Having expressed the amplitude and initial phase of the sinusoidal wave in complex terms it is now convenient to utilise the complex form of the exponential function to represent the frequency term. This technique is explained in Kreyszig[1] chapter 2.3, and follows the relationship given in Equation 5.

$$e^{\pm i\left(\frac{2\pi n}{T}t\right)} \Leftrightarrow \cos\left(\frac{2\pi n}{T}\cdot t\right) \mp \sin\left(\frac{2\pi n}{T}\cdot t\right)$$ **Equation 5**

Using these relationships the original Fourier term $A_n \cdot \cos\left(\frac{2\cdot\pi\cdot n}{T}\cdot t\right) + B_n \cdot \sin\left(\frac{2\cdot\pi\cdot n}{T}\cdot t\right)$ can be replaced with the complex number representation given in Equation 6.

$$A_n \cdot \cos\left(\frac{2\cdot\pi\cdot n}{T}\cdot t\right) + B_n \cdot \sin\left(\frac{2\cdot\pi\cdot n}{T}\cdot t\right) = \Re\left\{\Lambda_n \cdot e^{i\cdot\left(\frac{2\pi n}{T}\right)t}\right\}$$ **Equation 6**

Equation 1 may therefore be written in complex form by Equation 7.

$$y(t) = A_0 + \Re\left\{\sum_{n-1}^{\infty} \Lambda_n \cdot e^{i\left(\frac{2\pi\cdot n}{T}\right)t}\right\}$$ **Equation 7**

Where $\Lambda_n = A_n - i\cdot B_n$

The expression may be simplified further by the introduction of negative frequencies. These have the effect of cancelling the imaginary components in Equation 7 without using the $\Re\{\}$ function. Using the concept of negative frequencies Equation 7 can be expressed as Equation 8.

$$y(t) = A_0 + \tfrac{1}{2}\sum_{n=1}^{\infty} \Lambda_n e^{i\left(\frac{2\pi n}{T}\right)t} + \tfrac{1}{2}\sum_{n=-1}^{-\infty} \Lambda_n e^{i\left(\frac{2\pi n}{T}\right)t}$$

Equation 8

where $\Lambda_n = A_n - i \cdot B_n$

Changing the limits of the summation the Fourier coefficients A_0 and Λ_n can be replaced with the single complex Fourier coefficient C_n as expressed in Equation 9.

$$y(t) = \sum_{n=-\infty}^{\infty} C_n e^{i\left(\frac{2\pi \cdot n}{T}\right)t}$$

Equation 9

Double sided Fourier series

$$\text{Where } C_n = \tfrac{1}{2}\left(A_n - iB_n\right) = \frac{1}{T}\int_{-\frac{T}{2}}^{\frac{T}{2}} y(t) \cdot e^{-i\left(\frac{2\pi n}{T}\right)t} dt$$

Equation 9 is said to be double sided because it uses both positive and negative frequencies to represent the Fourier coefficients. Figure 2-3 shows a plot of the Real and Imaginary parts of the complex Fourier coefficients C_n obtained from the expansion of the saw tooth wave in Figure 2-1. These are plotted with respect to frequency *n/T Hz.*

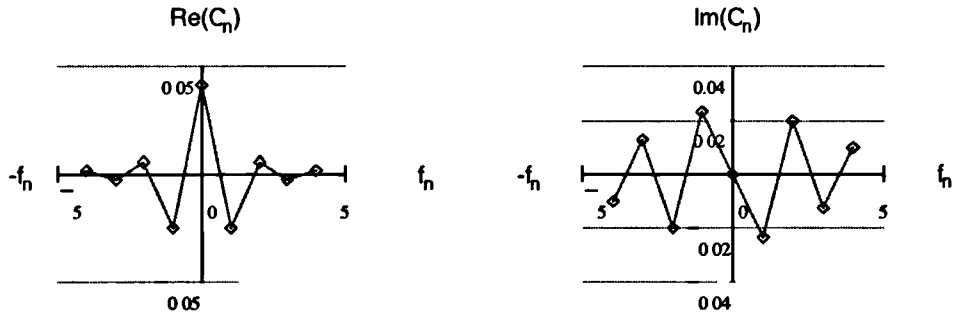

Figure 2-3 Plot of Real and Imaginary parts of complex Fourier coefficient

The complex Fourier coefficient C_n is used to obtain the amplitude and phase of the n^{th} sinusoidal wave using the formulation given in Equation 10.

$$\text{Amplitude } r_n = |C_n| + |C_{-n}| \quad \text{phase } \phi_n = \angle C_n$$

Equation 10

where $C_n = A_n + i \cdot B_n$ and $C_n = A_n - i \cdot B_n$

2.1.3 The Fourier density coefficient

Section 2.1.2 introduced the complex Fourier series expansion. For the analysis work covered in this thesis we are particularly interested in obtaining the complex Fourier coefficients. Each Fourier coefficient C_n is obtained for a frequency of *n/T Hz*. The frequency interval between each coefficient Δf is therefore *1/T Hz*. This causes problems as the frequency at which the coefficients are calculated is dependent on the period T chosen. It is common practice to normalise the coefficients to eliminate the dependence on T. The normalised coefficients take the form of a 'density function' and the Fourier coefficient is obtained from the area under the density curve for the range Δf in question. This is shown in Figure 2-1.

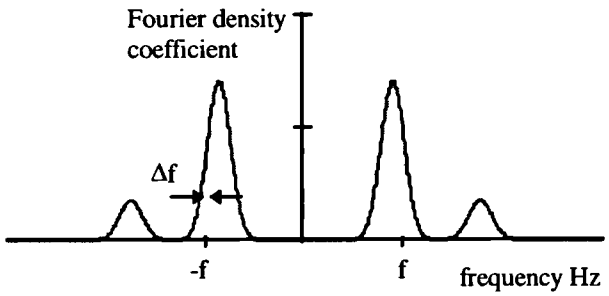

Figure 2-4 Fourier Density Coefficients

Using this normalisation the complex Fourier series expansion given in Equation 9 can be expressed by Equation 11.

Equation 11

$$y(t) = \Delta f \cdot \sum_{n=-\infty}^{\infty} c_n \cdot e^{i\left(\frac{2\pi n}{T}\right)\cdot t}$$

$$\text{where} \quad c_n = \int_{-T/2}^{T/2} y(t) \cdot e^{-i\left(\frac{2\pi n}{T}\right)\cdot t}\, dt \qquad \text{and} \qquad \Delta f = \frac{1}{T}$$

The amplitude and phase of the sinusoidal wave with frequency f is now obtained by taking the magnitude and argument of the area under the density curve in the region Δf. The function behaves much like a Probability Density Function.

If $\Delta f \rightarrow 0$ then the summation given in Equation 11 can be expressed in integral form and c_n can be written as $\tilde{y}(f)$. Changing the limits of integration between -∞ and +∞

the complex Fourier series is now expressed in integral form as Equation 12. This is known as the Fourier Transform Pair. For future reference in this thesis $\tilde{y}(f)$ shall be called the "Fourier Spectrum."

$$y(t) = \int_{-\infty}^{\infty} y(f) \cdot e^{i \cdot 2 \cdot \pi \cdot f \cdot t} df$$

Inverse Fourier Transform

where $\tilde{y}(f) = \int_{-\infty}^{\infty} y(t) \cdot e^{-i \cdot 2 \cdot \pi \cdot f \cdot t} dt$

Fourier Transform

Equation 12 Fourier Transform Pair

It is worth noting that many references use a different normalisation to that given above. A common normalisation is to use the square root of the period. In this thesis the form defined above shall be used.

2.1.4 The Fourier transform pair

The 'Fourier Transform Pair' was derived in section 2.1.3 in integral form and is expressed in Equation 12. It is now apparent that a time history *y(t)* can be completely expressed by the "Fourier Spectrum" $\tilde{y}(f)$. The Fourier spectrum can therefore be thought of as another 'frequency domain' in which a time history may be expressed. In this sense $\tilde{y}(f)$ implies a description of the time history '*y*' in the frequency domain '*f*'. The 'Fourier Transform Pair' effectively transformations between the two domains.

In addition to the integral form, the 'Fourier Transform Pair' can also be described in a discrete form. This is particularly beneficial as most measured time histories are obtained in a discrete, digitised form with values taken over equally spaced intervals in time. In these circumstances the integral form is difficult to process and it is desirable to perform some numerical routine on the measured time history to transform it into the frequency domain. This transform is known as the "Discrete

Fourier transform." The result obtained from a discrete transformation will tend to the result obtained from an integral transformation as the sample length and sampling frequency increase.

Cooley and Tukey[3] devised a very rapid discrete Fourier transform algorithm in 1965. It is known as the "Fast Fourier Transform (FFT)" and has a reverse process called the "Inverse Fourier Transform (IFFT)." There are a number of derivatives of these each using a different normalisation, it is important therefore to check software literature before implementing commercial computer routines. The normalisation proposed in this thesis is chosen to give the same result as that obtained with the integral form. The "Discrete Fourier Transform Pair" is defined in Equation 13.

$$y(t_k) = \frac{1}{T} \cdot \sum_n \tilde{y}(f_n) \cdot e^{i\left(\frac{2\pi k}{N}\right) \cdot n} \qquad \text{Inverse Fourier Transform}$$

$$\tilde{y}(f_n) = \frac{T}{N} \cdot \sum_k y(t_k) \cdot e^{-i\left(\frac{2\pi \cdot n}{N}\right) \cdot k} \qquad \text{Fourier Transform}$$

Equation 13 Discrete Fourier transform pair

The Fast Fourier Transform is only applicable for data containing exactly 2^m data points, where m is any integer number greater than 1. For this reason it is standard practice to subdivide the digitally recorded time history into buffers containing 2^m data points then evaluate the Fourier transform on each separately. As a result of the buffering then a number of issues such as windowing, overlapping and zero padding also become an issue, these are also discussed by Newland[4], chapters 10 to 11, and the author in his lecture on the frequency domain, Halfpenny[5]. We are not concerned with the discrete algorithm in this thesis and the reader is referred to the above references for more details.

2.1.5 Fourier analysis of random time histories

Under certain circumstances random time histories may be expressed in the frequency domain. By definition a random time history cannot be periodic. However, provided the time history is taken from an '*ergodic stationary Gaussian random process*' then it may be expressed in the frequency domain. A process is said to be *stationary* if its

statistics are not affected by a shift in the time origin. (i.e. the statistics of a time history $X(t)$ are the same as a time history $X(t + \tau)$ for all values of τ.) To test for stationarity we take a number of recordings of the random process at different times. The process is stationary if the probability distributions of the ensemble are the same for all points in time. If the ensemble probability density function is *Gaussian* then the process is known as a *Gaussian random process.* A stationary process is called an *ergodic process* if statistics taken from one sample are the same as those obtained for the ensemble. With an ergodic stationary random process, therefore, we can effectively take a single sampled time history from the process and safely assume that this contains all the required statistical properties of the parent process. For nonstationary processes the statistics obtained from a sampled time history would not be representative of those of the whole random process as these would be continuously changing. Priestley[6], chapter 3, and Newland[4] discuss stationarity at length and the reader is referred to these texts for more information. The analysis of nonstationary random processes is not considered in this thesis. However it does become a problem for the offshore wind farm designer because offshore wind is typically nonstationary. This is discussed later in Chapter 3.2. Further information on analysing nonstationary processes is given in Priestley[6] chapter 11.

Figure 2-5 illustrates the application of the Discrete Fourier Transform pair to a random time history taken from a stationary random process.

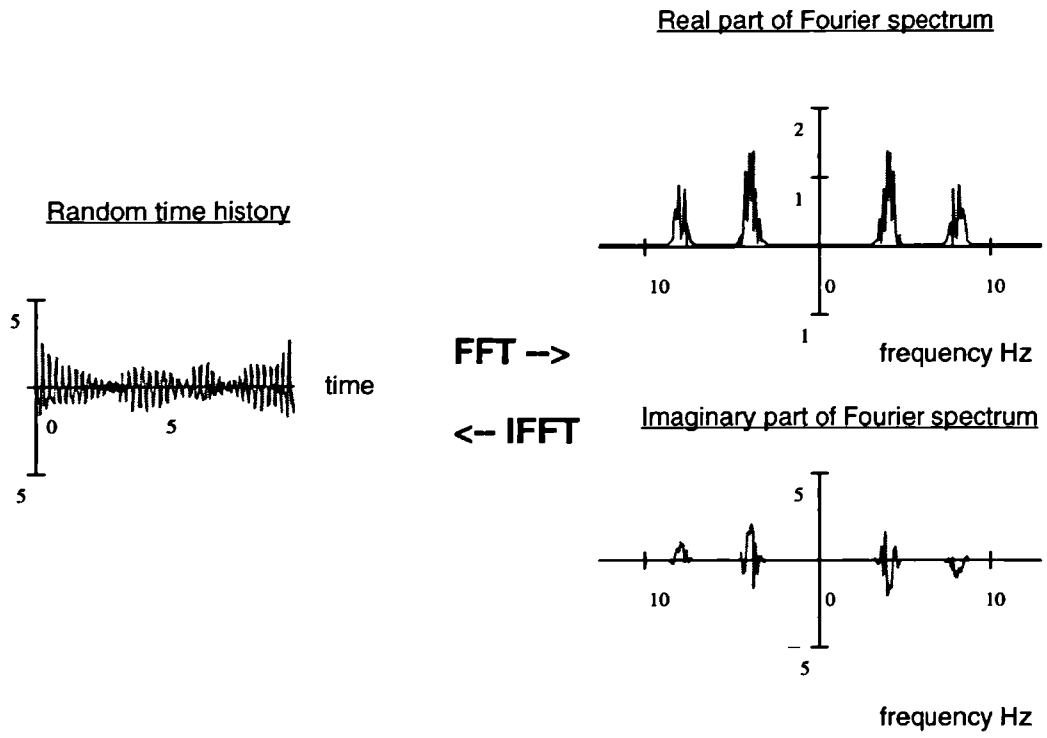

Figure 2-5 Frequency domain representation of a random time history

For real time histories the Fourier transform is symmetric about zero *Hz*. A Double Sided Spectrum is said to be symmetric if the relationships given by Equation 14 are satisfied.

$$\Re\{\tilde{y}(f)\} = \Re\{\tilde{y}(-f)\}$$
$$\mathrm{I}\{\tilde{y}(f)\} = \mathrm{I}\{-\tilde{y}(-f)\}$$

Equation 14

It is usual to express a symmetric spectrum as a "Single Sided Spectrum." The "Single Sided Spectrum" contains the same information as the "Double Sided Spectrum" but is often more convenient to use because negative frequencies are not considered. All measured time histories can be expressed as a Single Sided Spectrum. The relationship between single and double sided spectra is given by Equation 15.

$$\tilde{y}_S(f) = 2 \cdot \tilde{y}_D(f)$$

Equation 15

Figure 2-6 illustrates the Single Sided Spectrum of the random time history given above.

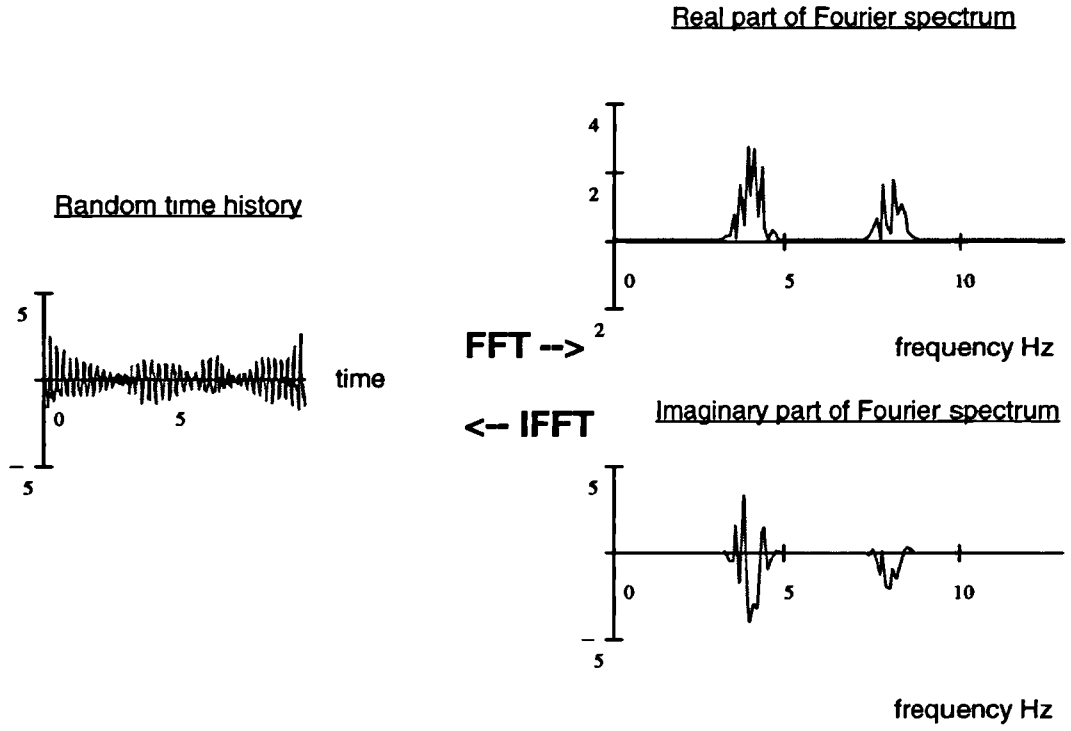

Figure 2-6 Single sided Fourier transform

2.1.6 Power spectral density function (PSD)

Previously in this thesis we have considered the representation of a time history in the frequency domain. Often it is more beneficial to have a statistical description of the time history than the *deterministic* one and for this purpose the "Power Spectral Density (PSD)" function is useful. A description is said to be *deterministic* when one can determine the actual value given by the process at any point in time. A time history is deterministic because the value can be obtained by observing the plot at the required instance in time. Likewise the Fourier spectrum is also deterministic because all the amplitude, frequency and phase information is retained and can be transformed back into the corresponding time history. The disadvantage of the Fourier spectrum is in the complex manner with which the amplitude and phases are stored. For an ergodic stationary Gaussian random process, it has been observed that the phases angles are purely random with a constant probability distribution between $-\pi$ and $+\pi$. For such cases it is therefore unnecessary to store the phase information in the frequency domain as only the amplitude information is relevant. The PSD function contains amplitude information but does not hold phase information, it is therefore real and much easier to use that the complex notation adopted in the Fourier spectrum.

Spence[7] provides a very good historical and qualitative description of history of the PSD and how to interpret its results.

The PSD gives a statistical representation of a stationary random process in the frequency domain. It is defined such that the area beneath the PSD represents the mean square amplitude of the random process. This normalisation proves very beneficial as is demonstrated later. Many design standards, such as the ESDU[8] papers on wind turbulence, express the statistical properties of random processes in terms of PSDs. Using these in conjunction with a linear structural model allows PSDs of structural stresses and deflections to be calculated and fatigue life estimates to be obtained. These subjects are covered later in the thesis. The PSD is used in the same way as the Fourier Density spectra. The mean square amplitude of a sinusoidal wave of frequency f can be obtained by taking the sum of the area under the PSD at $+f$ and $-f$ over the interval Δf as $\Delta f \rightarrow 0$. This is illustrated in Figure 2-7. The mean amplitude of the component sinusoidal waves over frequency Δf is obtained by taking the square root of twice the mean squared values.

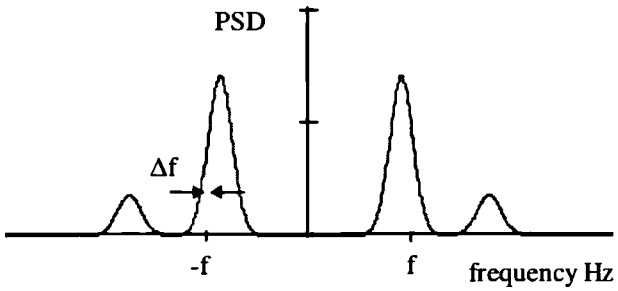

Figure 2-7 Double sided power spectral density (PSD)

PSDs may be complex and expressed as both double or single sided spectra in the same way as the Fourier density spectra. The relationships given in Equation 14 and Equation 15 hold for single and double sided PSDs. PSDs calculated from measured time histories will always be real. Complex PSDs however are encountered later in the thesis. The real part of a complex PSD $S(f)$ is known as the co-spectral density function $P(f)$ and the imaginary part as the quad-spectral density $Q(f)$.

We will now consider the transformation from a single sided Fourier Density Spectra to a single sided PSD. The mean amplitude of the component sinusoidal waves over a

frequency range Δf is obtained from the Fourier spectra by taking the modulus of the area under the curve as expressed in Equation 16.

$$Amplitude(f) = \Delta f \cdot \tilde{y}(f)$$ **Equation 16**

The area under a PSD represents the mean squared amplitude of the component sinusoidal waves where $Mean\,Square(f) = \frac{1}{2} \cdot Amplitude^2$. We can equate the mean square amplitudes calculated from the PSD and the Fourier spectra and hence determine the transformation between the two; this is derived in Equation 17.

$$\Delta f \cdot G(f) = \tfrac{1}{2} \cdot \Delta f^2 \cdot |\tilde{y}(f)|^2$$ **Equation 17**

$$\therefore G(f) = \frac{1}{2 \cdot T} \cdot |\tilde{y}(f)|^2$$

The double sided PSD is determined in a similar fashion, the results are summarised in Equation 18.

$$S(f) = \frac{1}{T} \cdot |\tilde{y}_D(f)|^2 \quad \text{or} \quad S(f) = \frac{1}{T} \cdot \left(\tilde{y}_D(f) \cdot \overline{\tilde{y}_D(f)}\right) \quad \text{for double sided PSDs or}$$

$$G(f) = \frac{1}{2 \cdot T} \cdot |\tilde{y}_S(f)|^2 \quad \text{or} \quad G(f) = \frac{1}{2 \cdot T}\left(\tilde{y}_S(f) \cdot \overline{\tilde{y}_S(f)}\right) \quad \text{for single sided PSDs}$$

Where $\overline{y_D(f)}$ is the complex conjugate of $y_D(f)$.

Equation 18

Both the modulus and complex conjugate forms of the transformations are correct however it is mathematically beneficial to use the complex conjugate form. It is also worth noting that many books adopt a different notation for the double and single sided PSDs. In this thesis the notation $S(f)$ and $G(f)$ is adopted for the double and single sided spectra respectively. In later chapters we also use radian measure and express frequency in terms of ω radians per second.

Section 2.1.3 commented on the use of different normalisations applied to the Fourier transform. It is quite common to see the $\sqrt{T}$ normalisation being used and this changes

the formulation expressed in Equation 18 to the form $S(f)=\left|\tilde{y}_D(f)\right|^2$ or $S(f)=\left(\tilde{y}_D(f)\cdot\overline{\tilde{y}_D(f)}\right)$. The normalisation chosen for the Fourier transform is not important provided that the resultant PSDs are the same.

The PSD provides considerable information about the statistics of the random process. By definition the area under the PSD represents the mean square amplitude of the time history, the root mean squared (RMS) of the time history is therefore determined as the square root of this. This is the single most important quantity in random process theory. Other statistical properties may be obtained using the spectral moments of the PSD. The nth spectral moment m_n of a PSD is defined by Equation 19.

Equation 19

$$m_n\{S(f)\}=\int_{-\infty}^{\infty}S(f)\cdot f^n df$$

The key statistical properties listed in Equation 20 were derived by S.O. Rice[9] in 1954. These properties become important when considering the fatigue life of a structure. This is explained in detail in Chapter 7.

Root Mean Square (RMS)	$\sigma=\sqrt{m_0}$
Expected number of upward zero crossings	$E[0]=\sqrt{\frac{m_2}{m_0}}$
Expected number of positive peaks	$E[p]=\sqrt{\frac{m_4}{m_2}}$
Irregularity factor	$\gamma=\frac{E[0]}{E[p]}$

Equation 20 Statistical properties of a PSD (after S.O. Rice[9])

The irregularity factor is defined as the ratio of expected number of upward zero crossings to the expected number of positive peaks. This helps classify a time history

as broad or wide band, which is introduced later. For narrow band histories $\gamma \rightarrow 1$ whereas for broader band γ reduces and tends to zero.

The appearance of the PSD plot also conveys much information. Figure 2-8 shows four types of process. The distinction between narrow and broad banded processes becomes much more apparent from the PSD plots than the time histories. This is illustrated in Figure 2-8.

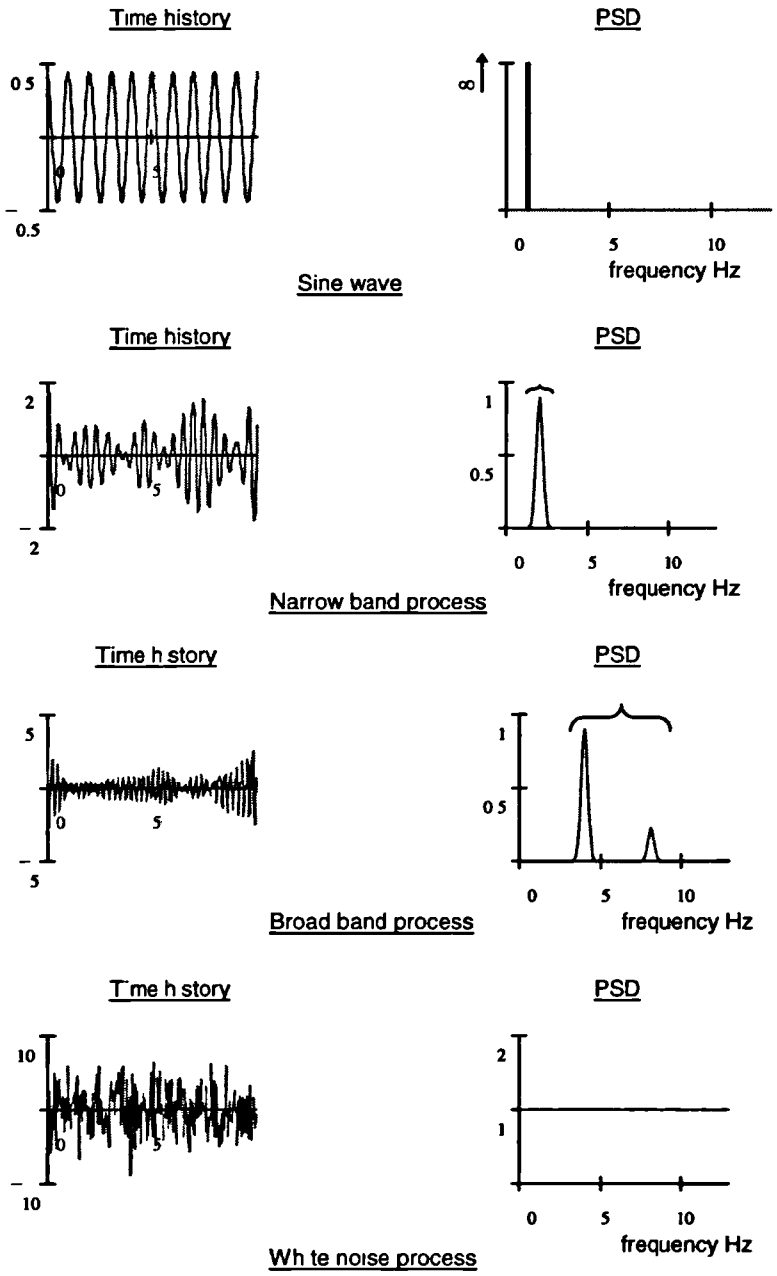

Figure 2-8 Time histories and corresponding PSDs

A sine wave of frequency f is shown in the frequency domain as a single spike centred at f. The area under the spike yields the mean squared amplitude of the sine wave and the amplitude may therefore be determined by taking the square root of twice this value. In theory the spike will be infinitely narrow as the sine wave has a single finite frequency. As the PSD is a density function, the spike will therefore have an infinite height. This situation is described by Dirac's delta function, which is described later in the thesis. In practice we usually employ a numerical solution technique for determining the PSD, such as the FFT; this will give a finite frequency resolution and so the spike will never be infinite.

The narrow band time history comprises a number of component sinusoidal waves over a narrow range of frequencies. The PSD shows this situations quite clearly. This type of time history is usually typified in the time domain by a low frequency envelope known as the 'beat effect'.

A wide band time history comprises a number of component sinusoidal waves over a wide range of frequencies. Again the PSD shows this situation quite clearly. This type of time history is usually typified in the time domain by having many valleys occurring above the mean and many peaks occurring below the mean. In contrast, the narrow band time histories demonstrate most of the peaks falling above the mean and subsequent valleys falling approximately the same distance below the mean. The irregularity factor, γ, is therefore a useful parameter for determining how 'wide banded' a signal is. For narrow band signals $\gamma \rightarrow 1$, while for wide band signals $\gamma \rightarrow 0$.

A white noise signal is formed by the summation of an infinite number of sinusoidal waves of the same amplitude and random phase. The PSD of this signal clearly shows uniform amplitude content at each frequency.

2.1.7 Time signal regeneration from PSDs

In section 2.1.2 it was shown that a stochastic or random process may be expressed in either the time or frequency domains. Transformation from one domain to the other is carried out using the Fourier transform pair. PSDs express the statistics of a random

process in the frequency domain and in many instances it is desirable to obtain a time history from a PSD.

Unlike the Fourier density spectra the PSD does not contain information about the phase relationships between the sinusoidal waves that make up the time history. It does however contain information on the Mean square amplitude of each wave. In order to regenerate a time history it is necessary to reintroduce the phase relationships between each of the waves. For many signals it has been found that the phase relationships follow a uniform random distribution between $-\pi$ and π radians and with this knowledge it is therefore possible to regenerate a time history. Time histories obeying this trend are said to be Gaussian Random processes. The regenerated time history will not be the same as the original measured time history because the phase angles are now different, however it is still statistically equivalent. There are a number of methods used for time history regeneration from PSDs. The author describes a method he employed for "nCode International[10]" that uses the PSD to calculate a digital filter by which to filter a white noise signal and hence obtain the desired frequency response. This chapter looks at the more intuitive method of evaluating the random phase angles and taking the inverse Fourier transformation.

The time history is formed by the summation of a number of sinusoidal waves of differing frequency, amplitude and phase. The n^{th} wave may be expressed in the form given in Equation 21.

$$y(t)_n = r_n \cdot \cos(\omega \cdot t + \phi_{rnd})$$

where ϕ_{rnd} is the random phase angle between 0 and π radians.

Equation 21

Using the complex relationships given in Equation 3 and Equation 4, the double sided PSD and random phase angle can be expressed in complex form as Equation 22.

$$S(f)_n = T \cdot \left(A_n^2 + B_n^2\right) \qquad \phi_{rnd_n} = \tan^{-1}\left(\frac{B_n}{A_n}\right)$$

Equation 22

Solving these two simultaneous equations yields values for the Fourier coefficients A_n and B_n defined in Equation 4. Using the normalisation described in section 2.1.1 the complex Fourier density function can be determined. Having obtained the Fourier density function the time history regeneration can be accomplished by taking the inverse Fourier transform. The formulation is given in Equation 23.

$$y(t)_n = \textit{Inverse Fourier Transform of } \tilde{y}(f)_n$$

$$\text{where} \qquad \tilde{y}(f)_n = T \cdot \left(A_n - i \cdot B_n\right)$$

$$\text{and} \qquad A_n = \sqrt{\frac{S(f_n)}{T \cdot \left(1 + \varphi_n^2\right)}} \qquad B_n = A_n \cdot \varphi_n^2 \qquad \varphi_n = \tan\left(\phi_{rnd_n}\right)$$

Equation 23 Simple time history regeneration from a double sided PSD

The method proves difficult to implement computationally however because large numeric precision errors occur when taking the tangent of a random number between 0 and π. This is not a serious problem in the context of this thesis but should be considered for other applications where time history regeneration is required. Equation 24 gives the formulation for regenerating a time history from a single sided PSD.

$$y(t)_n = \textit{Inverse Fourier Transform of } \tilde{y}(f)_n$$

$$\text{where} \qquad \tilde{y}(f)_n = 2 \cdot T \cdot \left(A_n - i \cdot B_n\right)$$

$$\text{and} \qquad A_n = \sqrt{\frac{G(f_n)}{2 \cdot T \cdot \left(1 + \varphi_n^2\right)}} \qquad B_n = A_n \cdot \varphi_n^2 \qquad \varphi_n = \tan\left(\phi_{rnd_n}\right)$$

Equation 24 Simple time history regeneration from a single sided PSD

2.1.8 Summary of Fourier transformation and PSDs

Figure 2-9 illustrates the transformation between the time and frequency domains. The frequency domain is another way of representing a time history. Transformation between the time and frequency domains is accomplished using the Fourier Transform Pair. There are two forms of transform, the integral and the discrete transform. The discrete transform is particularly useful for transforming digitally measured time histories such as those recorded using data acquisition. The "Fast Fourier Transform" is now universally used for this purpose.

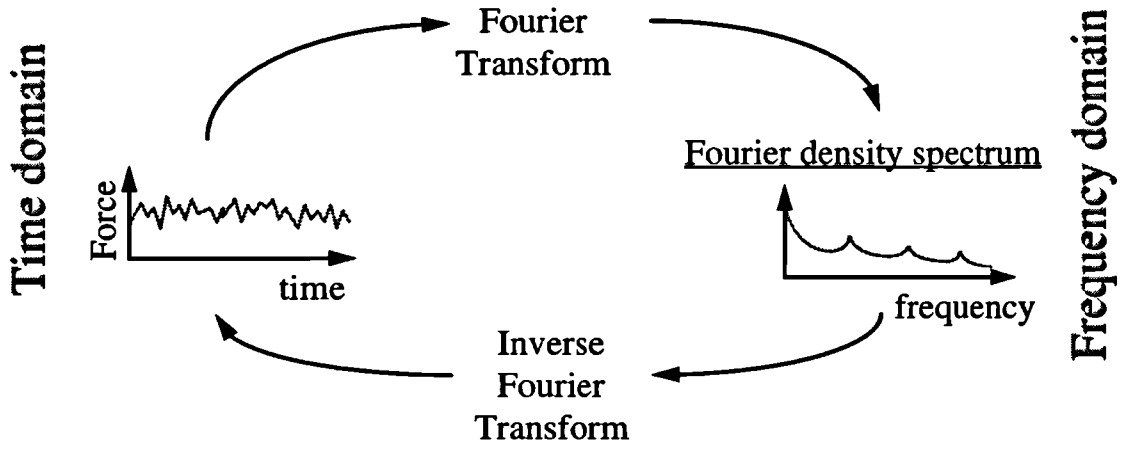

Figure 2-9 The Fourier transform between time and frequency domains

The Fourier transform gives a Fourier Density Spectrum. This is complex and may be single or double sided. Single sided spectra are a special case of the double sided spectra where the negative frequencies are the complex conjugate of the positive frequencies. This condition arises when the time history is Real. All measured time histories are real and are usually expressed as single sided spectra.

It is often more convenient to deal with the statistics of a random process than either a time or frequency domain representation of the actual signal. For this reason the Power Spectral Density (PSD) is used. The PSD represents the Mean Square amplitude of the sinusoidal waves that comprise the time history. It is often necessary to regenerate a statistically representative time history from a PSD. The PSD does not contain information on the phase relationships between the sinusoidal waves and this therefore needs adding. Provided the random process is Gaussian random then the

phase relationships will follow a uniform random distribution between $-\pi$ and π radians. Figure 2-10 illustrates the transformation between the time domain and the PSD.

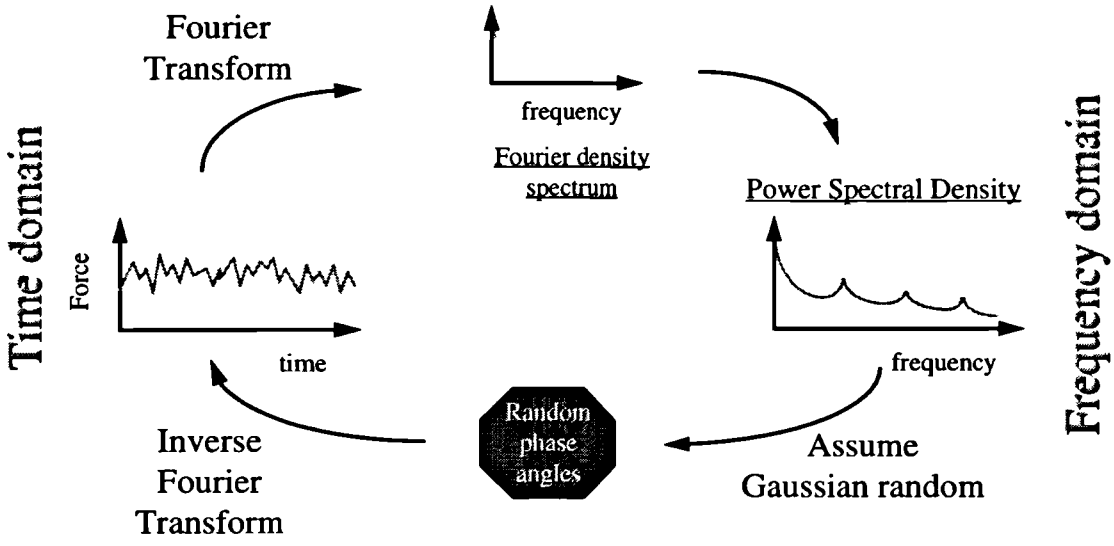

Figure 2-10 Transformation between time history and PSD

2.2 Response of a linear system to a random loading expressed in the frequency domain

The work carried out so far has enabled us to represent a measured time history in the frequency domain in the form of a PSD. This measured time history may be that of wind speed measured using anemometers or stresses in a structural component measured using strain gauges. In the case of a wind turbine the PSD is likely to be given for the turbulent wind speed witnessed near the ground. It is important to understand how a structure will react to the dynamic wind loading. We could take the PSD and regenerate a statistically representative time history and then analyse this using a dynamic analysis program in the time domain but this is very time consuming because the analysis process is complicated. For structures which behave in a linear way the analysis may be done more efficiently in the frequency domain.

A linear system is one where the output is related to the input by a linear transfer function. In the case of a wind turbine blade the load on a turbine blade could therefore be expressed as Equation 25.

$F(t) = g \cdot v(t)$ i.e. the aerodynamic force $F(t)$ on a turbine blade is given as the product of the wind speed $v(t)$ and the linear aerodynamic transfer function g.

Equation 25

If the wind speed is expressed in terms of the Fourier density function then the aerodynamic force will then be given in the frequency domain using Equation 26.

$$\tilde{F}(f) = g \cdot \tilde{v}(f) \qquad \textbf{Equation 26}$$

It is convenient to obtain the response as a PSD $S^F(f)$. From Equation 18 the double sided PSD of force can be expressed as $S^F(f) = \frac{1}{T} \cdot \left(g \cdot v(f) \cdot \bar{g} \cdot \overline{v(f)} \right)$. If the wind speed is also expressed as a double sided PSD $S^v(f)$ then the PSD of force is given by Equation 27.

$$S^F(f) = g \cdot \bar{g} \cdot S^v(f) \qquad \text{or} \qquad S^F(f) = |g|^2 \cdot S^v(f)$$

Equation 27 Linear transfer function in the frequency domain

This relationship also holds between single sided PSDs as expressed in Equation 28.

$$G^F(f) = g \cdot \bar{g} \cdot G^v(f) \text{ or} \qquad G^F(f) = |g|^2 \cdot G^F(f)$$

Equation 28

2.3 Random processes

The previous section describes the transformation of random time histories into the frequency domain using the Fourier transform pair. A simple relationship can be used to generate the Power Spectral Density function (PSD) which contains statistical properties of the random time history. In this chapter we will look at an alternative method for generating PSDs. The method uses a statistical property of the time history, namely the Autocovariance function, as a method of obtaining the PSD.

Although the Fourier transform is now universally used for obtaining PSDs, the method discussed in this chapter is important in understanding the concept of random processes. We will expand on this theory to also include multiple random events, and will define the cross-power spectral density function to represent the statistical relationships between two random events.

2.3.1 Definition of the Autocovariance function

The Autocovariance function is a statistical property that describes the frequency or periodic properties of a time history. Bartrop[2] chapter 3.2.1 gives a very good physical interpretation of the autocovariance function. The autocovariance function is defined in Equation 29.

$$C_{yy}(\tau) = E\{y(t)\cdot y(t+\tau)\} - E\{y(t)\}^2$$

where E{} is the expectation operator defined by $E\{y(t)\} = \frac{1}{T}\cdot\int_{-T/2}^{T/2} y(t)dt$

Equation 29

The notation C_{yy} indicates the autocovariance function for a single process y. The notation is introduced at this stage to distinguish between the 'cross-covariance function (C_{xy})' for two random processes x and y. This is discussed in the next chapter. For all analysis carried out in this thesis, random processes are assumed stationary and have a zero mean. Equation 29 can therefore be rewritten as the infinite time average given by Equation 30.

$$C_{yy}(\tau) = \lim_{T\to\infty}\left[\frac{1}{T}\cdot\int_{-T/2}^{T/2} y(t)\cdot y(t+\tau)dt\right]$$

Equation 30
The Autocovariance function

The autocovariance function is plotted for a number of time histories in Figure 2-11. For periodic processes with period T, the autocovariance function is also periodic with the same period. For any random process we notice that $C_{yy}(\tau)\to 0$ as $\tau\to\infty$. For stationary processes the autocovariance function is even, i.e. $C_{yy}(\tau)=C_{yy}(-\tau)$, and may be expresses as a single sided function. As stationarity is assumed for all random

processes throughout this thesis the single sided autocovariance function is usually used. (N.B. when $\tau = 0$, the autocovariance function yields the variance, or mean square value, of the time history.)

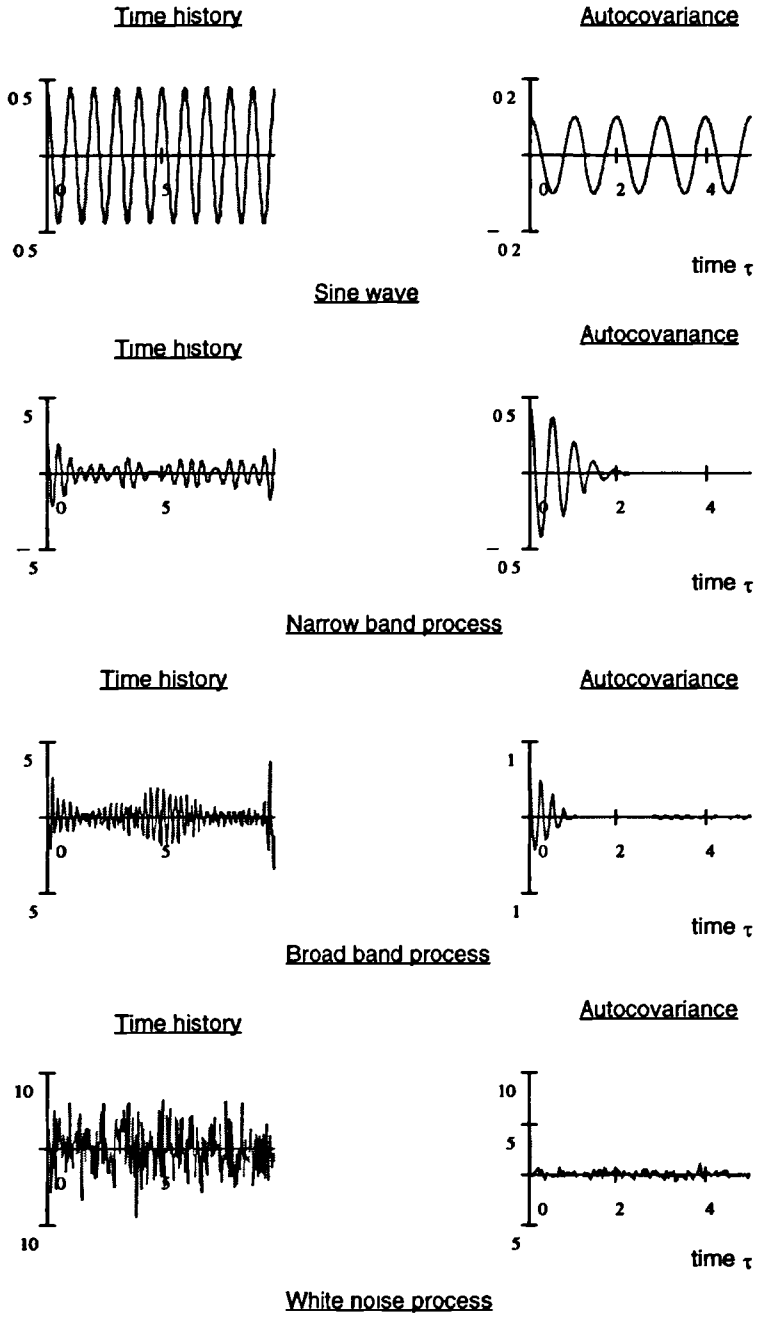

Figure 2-11 Time histories and corresponding Autocovariance

2.3.2 Transformation between Autocovariance and PSD

In this section it is shown that the Fourier transform pair can be used to transform between the autocovariance function and the PSD. In this sense the autocovariance function is similar to a time history representation of the PSD. In effect it is the time history of the mean square amplitude of the sinusoidal waves with a zero phase angle.

The autocovariance function for a zero mean, stationary random process is defined in Equation 30. From Equation 12 the term $y(t+\tau)$ may be given in terms of the Fourier transform pair as Equation 31.

Equation 31

$$y(t+\tau) = \int_{-\infty}^{\infty} \tilde{y}(f) \cdot e^{i \cdot 2 \cdot \pi \, f (t+\tau)} df$$

Substituting this into Equation 30 and simplifying yields Equation 32.

Equation 32

$$C_{yy}(\tau) = \lim_{T \to \infty} \left[\frac{1}{T} \cdot \int_{-\infty}^{\infty} \int_{-T/2}^{T/2} \tilde{y}(f) \cdot e^{i \cdot 2 \cdot \pi \cdot f \cdot \tau} dt \cdot y(t) \cdot e^{i \cdot 2 \cdot \pi \cdot f \cdot t} df \right]$$

Now from Equation 12 we know that $\lim_{T \to \infty} \left[\int_{-T/2}^{T/2} y(t) \cdot e^{i \cdot 2 \cdot \pi \, f \cdot t} dt \right] = \tilde{y}(-f) = \overline{\tilde{y}(f)}$,

therefore the autocovariance function may be expressed as Equation 33.

Equation 33

$$C_{yy}(\tau) = \frac{1}{T} \cdot \int_{-\infty}^{\infty} \tilde{y}(f) \cdot \overline{\tilde{y}(f)} \cdot e^{i \cdot 2 \cdot \pi \cdot f \cdot \tau} df$$

It is now possible to recognise the similarity with Equation 18 used to transfer from the Fourier density function to the PSD. Using this relationship the autocovariance function may be expressed in terms of the PSD as Equation 34.

$$C_{yy}(\tau) = \int_{-\infty}^{\infty} S_{yy}(f) \cdot e^{i 2 \pi f \tau} df$$

i.e. the inverse Fourier transform of the PSD $S_{yy}(f)$

Equation 34

The transformation between the autocovariance function and the PSD can therefore be accomplished using the Fourier transform pair as shown in Equation 35.

$$C_{yy}(\tau) = \int_{-\infty}^{\infty} S_{yy}(f) \cdot e^{i 2\pi f \tau} df$$ The inverse Fourier transform

$$S_{yy}(f) = \int_{-\infty}^{\infty} C_{yy}(\tau) \cdot e^{-i 2\pi f \tau} d\tau$$ The Fourier transform

Equation 35 The Fourier transform between Autocovariance and PSD

The notation S_{yy} is adopted here to describe the Auto-power spectral density function as opposed to the cross-power spectral density function (S_{xy}) between two random processes x and y. This is explained in the next section.

2.3.3 Multiple random processes: The principle of Cross-covariance

Previously in this thesis we have considered the analysis of one random process. This section introduces the analysis of multiple random processes. Figure 2-12 shows two anemometers placed side by side with separation *d*. From each anemometer a time history of the wind speed is produced. PSDs can be calculated from these and provided that the wind field is homogeneous, both PSDs will be the same. From this it is concluded that the mean square amplitudes of the sinusoidal waves which comprise the time histories are the same. The PSDs however give no information about the phase relationships between the two measured time histories.

In this chapter we are interested in the sequential relationship between the two time histories. If the two anemometers are far enough apart then the wind speed witnessed by one will be completely independent of the other, they are said to be uncorrelated. As they are moved closer together then a correlation between the two time histories will be noted. Correlation occurs because the random turbulent wind incident on anemometer x has a sufficiently large range of influence to also affect the response of anemometer y.

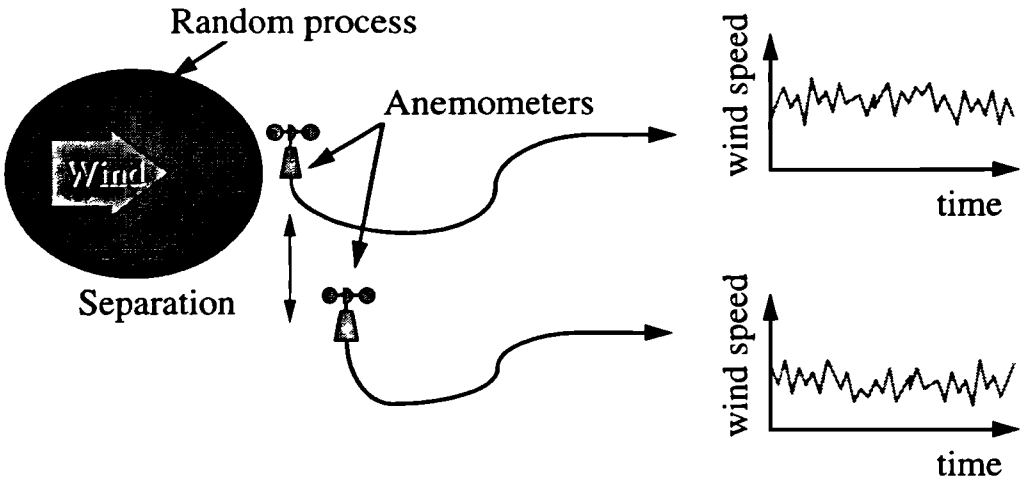

Figure 2-12 Multiple random processes

The covariance function may be used to find the sequential relationships between the two time histories in the same way as before. In this case Equation 29 is written as Equation 36. This is known as the Cross-covariance function.

$$C_{yx}(\tau) = E\{y(t) \cdot x(t+\tau)\} - E\{y(t) \cdot x(t)\} \qquad \textbf{Equation 36}$$

The notation $C_{yx}(\tau)$ is used to describe the Cross-covariance function between the two random processes x and y. It effectively tells us what the effect on y would be should a random process hit x. Assuming that the random processes are stationary and have a zero mean then the cross-covariance function may be transformed to a PSD using the Fourier transform. The resulting PSD $S_{yx}(f)$ is now termed the cross-power spectral density function. This relationship is expressed in Equation 37.

$$C_{yx}(\tau) = \int_{-\infty}^{\infty} S_{yx}(f) \cdot e^{i \cdot 2 \cdot \pi \cdot f \cdot \tau} df$$

The cross-covariance function between processes x and y.

$$S_{yx}(f) = \int_{-\infty}^{\infty} C_{yx}(\tau) \cdot e^{-i \cdot 2 \cdot \pi \cdot f \cdot \tau} d\tau$$

The cross-power spectral density function between processes x and y.

Equation 37 The Fourier transform between the Cross-covariance and Cross-power spectral density function

2.3.4 Normalised covariance and time scales

It is often convenient to normalise the covariance function in order to compare different time histories with different scales of measurement. This is achieved by dividing the covariance by the variance, or mean square value. The normalised covariance function is defined by Equation 38. It has the same shape as the covariance function except that the ordinate is scaled to have a value of 1 for $\tau=0$.

Equation 38

$$\rho_{yy}(\tau)=\frac{C_{yy}(\tau)}{C_{yy}(0)}=\frac{C_{yy}(\tau)}{\sigma_y^{\,2}}$$

The time scale is defined as the area under the normalised covariance function as Equation 39. For a random time history this roughly equates to the mean zero crossing period of the time history. For a periodic time history this is not the case however as $T_y \rightarrow 0$.

Equation 39

$$T_y=\int_0^{\infty}\rho_{yy}(\tau)\cdot d\tau$$

2.3.5 The coherence function

Another way of representing the correlation between two random processes is through the coherence function. The coherence represents the degree of correlation between two random processes. Two uncorrelated events show zero coherence where as two fully correlated events show unit coherence. The coherence function is defined in Equation 40 as a ratio of the cross-power spectral density function to the geometric mean of the two auto-power spectral density functions.

Equation 40
The coherence function

$$\gamma_{xy}(f)=\frac{S_{xy}(f)}{\sqrt{S_{xx}(f)\cdot S_{yy}(f)}}$$

Many design standards quote the auto-power spectral density function which the designer should use to verify the design. Where there are correlated multiple events it is often easier to express the correlation in terms of the coherence function than to

specify many cross-power spectral density functions. The designer may then derive his own cross-spectral density functions by rearranging Equation 40.

2.3.6 Response of a linear system to multiple random loading

Figure 2-13 illustrates the loading on a turbine blade due to two random processes. In order to calculate the reaction to this loading it is insufficient to simply sum the reactions from the two PSDs, instead we must sum the reactions from the PSDs and cross-PSDs. The cross power spectra contain information on the joint statistics of the two processes. If the two processes are correlated then the sequencing effect of the two processes may act to either increase or decrease the overall loading on the blade. Later in the thesis it is demonstrated how the cross power terms effectively reduce reaction forces at some frequencies and increase them at others. A very good mathematical explanation of this can be found in Newland[11] chapter 7.

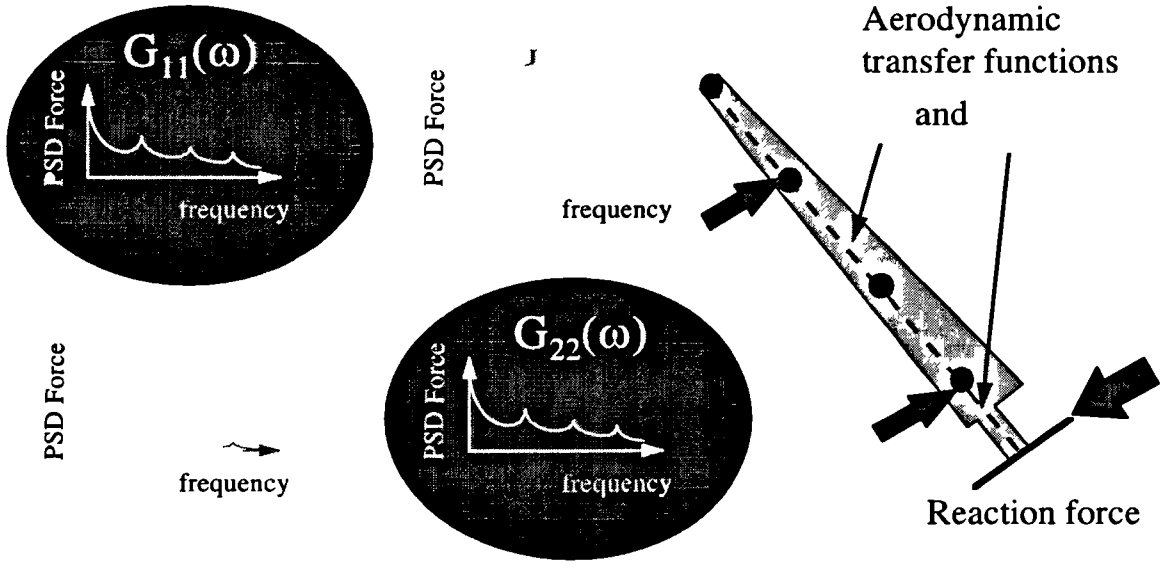

Figure 2-13 Reaction to multiple random loading

The total reaction force on the blade can be found in the time domain from Equation 41.

$$F(t) = \sum_i g_i \cdot v_i(t)$$ **Equation 41**

Where $F(t)$ is the reaction force resulting from windspeed $v(t)$ with a linear aerodynamic gain factor g on the i^{th} element of the blade.

If the wind speed is expressed in terms of the Fourier density function then the aerodynamic force will then be given in the frequency domain using Equation 42.

$$\tilde{F}(f) = \sum_i g_i \cdot \tilde{v}_i(f)$$ **Equation 42**

It is convenient to obtain the response as a PSD $S^F(f)$. From Equation 18 the double sided PSD of force can be expressed as $S^F(f) = \frac{1}{T} \cdot \left(\sum_i g_i \cdot \tilde{v}_i(f) \cdot \sum_j \overline{g_j} \cdot \overline{\tilde{v}_j(f)} \right)$. If the wind speed is also expressed as a double sided PSD, $S^v(f)$, then the PSD of force is given by Equation 43.

$$S^F(f) = \sum_i \sum_j g_i \cdot \overline{g_j} \cdot S_{ij}^v(f)$$ **Equation 43**

This relationship also holds between single sided PSDs as expressed in Equation 44.

$$G^F(f) = \sum_i \sum_j g_i \cdot \overline{g_j} \cdot G_{ij}^v(f)$$ **Equation 44**

2.3.7 Matrix form of the Cross-power spectral density function

The Auto- and cross-power spectral density functions may be expressed in matrix form. This permits the rapid calculation of responses using matrix algebra. The auto-power spectral values are located along the leading diagonal while the cross-power terms are located in the remaining cells as illustrated in Figure 2-14.

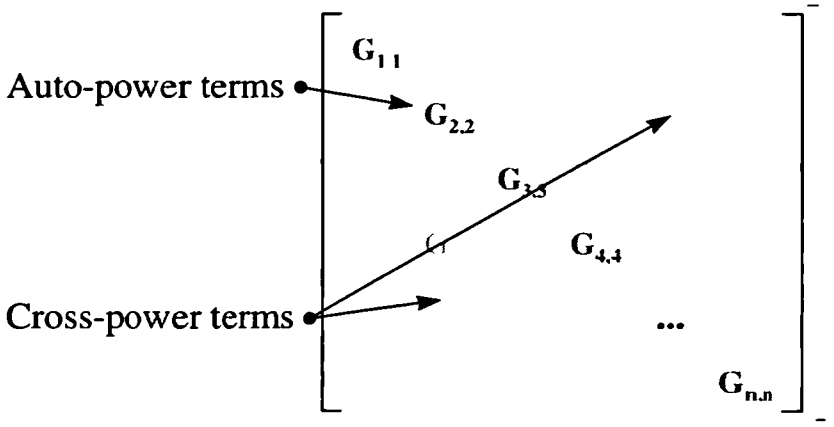

Figure 2-14 Cross-power spectral density matrix

Using matrix algebra, Equation 44 may be expressed as Equation 45.

$$G^F(f) = [g]^T \cdot [G(f)] \cdot \overline{[g]}$$

Where $[G(f)]$ is the cross-power matrix and $[g]$ is a vector of gain factors.

Equation 45 Matrix form of linear transfer function

When we are considering the dynamic analysis of a structure we often resort to a Finite Element based approach. In these analyses we calculate a matrix of linear transfer functions as opposed to the single vector [g] which is described above. Equation 45 is still valid when [g] takes the form of a matrix, however the result will also be in matrix form. The matrix $[G^F(f)]$ then gives the auto-power terms along the leading diagonal and the cross-power terms in the off-diagonal cells.

A common calculation may result in analyses which include multiple transfer functions. For example, consider the dynamic structural analysis of the rotor blade in Figure 2-13. Here we may have two transfer functions: the first, an aerodynamic transfer between wind speed and blade load; and the second, a structural dynamic transfer between blade load and element stress. In this case we must ensure that all the cross-power terms are passed through the analysis. This implies that the aerodynamic gain factors be expressed as diagonal matrices rather than vectors. This is illustrated in Equation 46.

$$\begin{bmatrix} G_{11}^F & G_{12}^F \\ G_{21}^F & G_{22}^F \end{bmatrix} = \begin{bmatrix} H_{11} & H_{12} \\ H_{21} & H_{22} \end{bmatrix}^T \cdot \begin{bmatrix} g_1 & 0 \\ 0 & g_2 \end{bmatrix}^T \cdot \begin{bmatrix} G_{11} & G_{12} \\ G_{21} & G_{22} \end{bmatrix} \cdot \overline{\begin{bmatrix} g_1 & 0 \\ 0 & g_2 \end{bmatrix}} \cdot \overline{\begin{bmatrix} H_{11} & H_{12} \\ H_{21} & H_{22} \end{bmatrix}}$$

Equation 46

In many instances we are only interested in the auto-power spectra of the responses. In the above example we are only interested in obtaining the auto-power of the element stresses, these may be used to calculate the fatigue life of the element for instance. The cross-power terms, in this case, are of no use to us and may therefore be discarded. The useful result could therefore be expressed as a vector of auto-power terms comprising the values along the leading diagonal of the matrix. i.e. $\begin{bmatrix} G_{11}^F \\ G_{22}^F \end{bmatrix}$

2.4 Conclusion

In this chapter we have discussed the principle behind the 'Fourier transform pair' and have shown how time histories may be expressed in the frequency domain. The turbulent wind and wave loads acting on an offshore turbine can be modelled as partially correlated random processes. This is derived later in the thesis. In this chapter a full description of the theory used for analysing random processes is presented. Emphasis is given to presenting a conceptual understanding of the theories involved as these are used extensively throughout the rest of the thesis. The chapter concludes by deriving an efficient matrix approach to represent the various auto- and cross-power spectra. This approach is convenient when considering structural dynamic analyses that use matrix methods.

---

[1] Kreyszig E. "Advanced Engineering Mathematics. *Seventh Edition.*" John Wiley & Sons, inc.

[2] Barltrop N.D.P and Adams A.J (1991). "Dynamics of Fixed Marine Structures." Butterworth-Heinemann Ltd. Linacre House, Jordan Hill, Oxford OX2 8DP, England.

[3] Cooley, J.W and Tukey, J.W (1965). "An algorithm for the machine calculation of complex Fourier series." Math. Comp., 19, 297-301.

[4] Newland D.E. (1993) "An introduction to Random vibrations, Spectral & Wavelet Analysis, (Third edition)." Longman Scientific & Technical.

[5] Halfpenny A. (1997) "What is the frequency domain, A practical guide to the FFT." NCode International Ltd. The Durability Institute. 230 Woodbourn Road, Sheffield, S9 3LQ. England.

[6] Priestley M.B (1981). "Spectral Analysis and Time Series." Academic Press.

[7] Spence P. "What is 'Power Spectral Density'?" The Analyst.

[8] ESDU 85020 (1993). "Characteristics of atmospheric turbulence near the ground. Part II: single point data for strong winds (neutral atmosphere)." ESDU international plc. 27 Corsham Street, London, N1 6UA, England.

[9] Rice S.O. (1954) "Mathematical analysis of random noise." Selected papers on noise and stochastic processes, Dover, New York.

[10] Halfpenny (1997) "Generating time histories from PSDs." nCode International Limited, 230 Woodbourn Road, Sheffield, S9 3LQ. England.

[11] Newland D.E. (1993) "An introduction to Random vibrations, Spectral & Wavelet Analysis, (Third edition)." Longman Scientific & Technical.

3. Modelling the turbulent wind

3.1 The nature of wind

The wind is never constant. It is characterised by many variations in its speed over many time periods. Figure 3-1 illustrates the changing nature of the wind speed close to the ground in the form of an Energy Spectrum. The peaks in the spectrum represent the periods over which most of the wind speed variations take place.

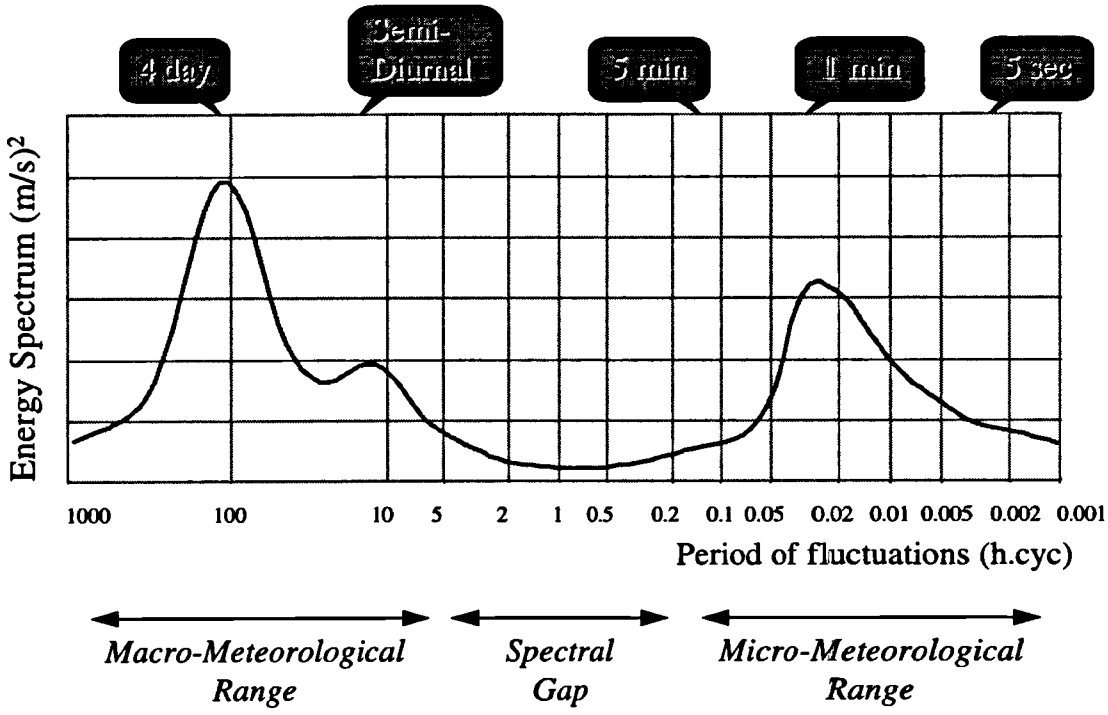

Figure 3-1 Energy Spectrum of wind speed after Van der Hoven[1]

The energy spectrum is characterised by two distinct peaks with a long trough between. The effects causing the two peaks are the macro- and micro-meteorological effects. The macro-meteorological effects are global effects caused by flow of air between pressure systems. Wind is created above the earth by differential heating of the atmosphere. Cells of high and low pressure are formed and air flows between then which causes wind. The path taken by the wind is modified by the coriolis effect of the earth's rotation. From a structural point of view these winds govern the maximum critical wind load likely to occur in the life of the turbine.

The micro-meteorological effects are turbulent gusts caused by wind blowing over obstacles in the vicinity of the turbine. These may include nearby towns, woodland

and hill ranges. It is this turbulence that presents a problem for the dynamics of the turbine. According to BS8100 (1986) "Lattice towers and masts. Part 1: Code of practice for loading."[2], wind turbulence is important if the first natural period of a structure is greater than 0.5 seconds. Rotational sampling by the rotor blades however make the effect prominent over a much wider frequency range. Turbulent wind is therefore likely to cause fatigue damage over a period of time.

The spectral gap covers the periods from 5 minutes to 5 hours. The gap is present as there are relatively few physical effects to feed energy into the system over this range. The spectral gap enables the long and short term statistics to be separated. The macro-meteorological effects will therefore appear as slow variations in the mean wind speed while the turbulence appears as rapid variations around the mean. This is shown in Figure 3-2. The mean wind speed is usually taken over a period of one hour as this period fits nicely in the region of the spectral gap. All reference to the 'mean wind speed' in this text implies a sampling period of one hour.

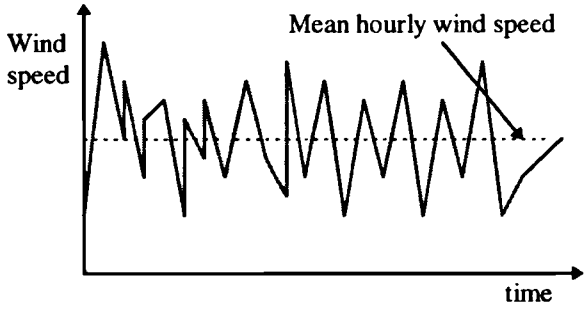

Figure 3-2 Wind speed variation with time

The turbulent gusts in the wind are caused by eddies in the wind flow. These arise from a number of contributing factors such as the presence of hills or valleys and the roughness of the terrain over which the wind is blowing. In the lower atmosphere the predominant contribution is from ground roughness. If the surface is relatively flat such as in a calm sea then there will be less turbulence than say in a plowed field with many surrounding hedges and trees. Figure 3-3 illustrates the wind speed and the turbulent gusts with respect to the height above the ground.

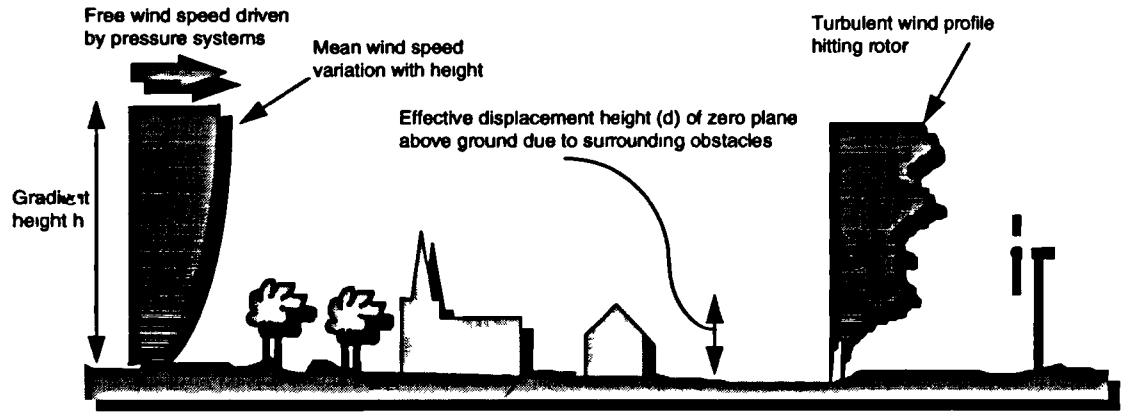

Figure 3-3 Wind speed variation with height

3.2 Atmospheric equilibrium and stability

Mathematical models are presented in this chapter to describe the turbulent wind field. Two important assumptions are made in the derivation of these which affect their use. These are:

1. Atmospheric equilibrium is present in the earth's boundary layer.
2. Neutral atmospheric stability prevails.

Atmospheric equilibrium in the earth's boundary layer is achieved when the wind blows over a homogeneous rough terrain for a considerable distance. The term 'Fetch' is given for the distance upwind of the site from the last change of surface roughness. ESDU 85020[3] suggests a minimum fetch of 30km to achieve equilibrium conditions. In practice the roughness is continually changing and so true equilibrium is seldom achieved. Research is currently underway in the wind energy industry to investigate how the turbulent wind field is affected by changes in local topography. The general title given these projects is 'micro-siting'. The certifying bodies largely circumvent the present lack of knowledge by specifying extreme turbulence parameters on which to base the turbine design. This is discussed later. Recent work published in ESDU 85020[3] however, include provisions for changes in the surface roughness. These are not discussed in this text.

The process of atmospheric stability is best described by example. Figure 3-4 illustrates the process.

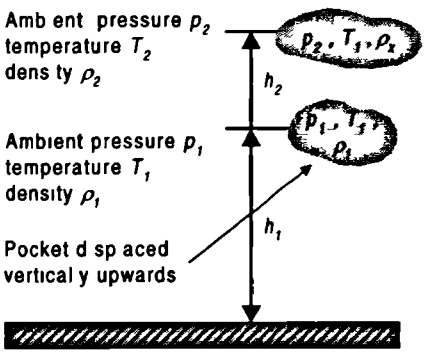

Figure 3-4 Atmospheric stability

Consider a small pocket of dry air in equilibrium at height h_1, pressure p_1, density ρ_1 and temperature T_1. The pocket is now displaced vertically upwards to height h_2 which has an ambient pressure p_2, density ρ_2 and temperature T_2. If the pocket is displaced rapidly so there is no time for it to loose or gain heat, the element will expand due to the lower ambient pressure. This expansion without change in temperature is known as adiabatic expansion. If the displaced pocket is now more dense than the ambient air it will drop back to its original position. This is known as a stable atmospheric state. If the density of the pocket is the same density as the ambient air it will remain in its displaced position and the atmosphere is then said to be in a neutrally stable state. Of course if the density of the pocket is lower than that of the ambient air it will continue to rise through buoyancy and is said to be in a unstable state.

The density of the ambient air and the pocket can be found from the unified gas law and are given by Equation 3-1.

Density of ambient air at height h_2 $\quad \rho_2 = \dfrac{p_2 \cdot T_1 \cdot \rho_1}{p_1 \cdot T_2}$ **Equation 3-1**

Density of displaced pocket x $\quad \rho_x = \dfrac{p_2 \cdot \rho_1}{p_1}$

Now in a stable atmosphere $\quad \rho_x > \rho_2 \quad \therefore T_2 > T_1$

in a neutral atmosphere $\quad \rho_x = \rho_2 \quad \therefore T_2 = T_1$

and in an unstable atmosphere $\quad \rho_x < \rho_2 \quad \therefore T_2 < T_1$

Connell[4] gives a good qualitative illustration of atmospheric stability and this is shown in Figure 3-5

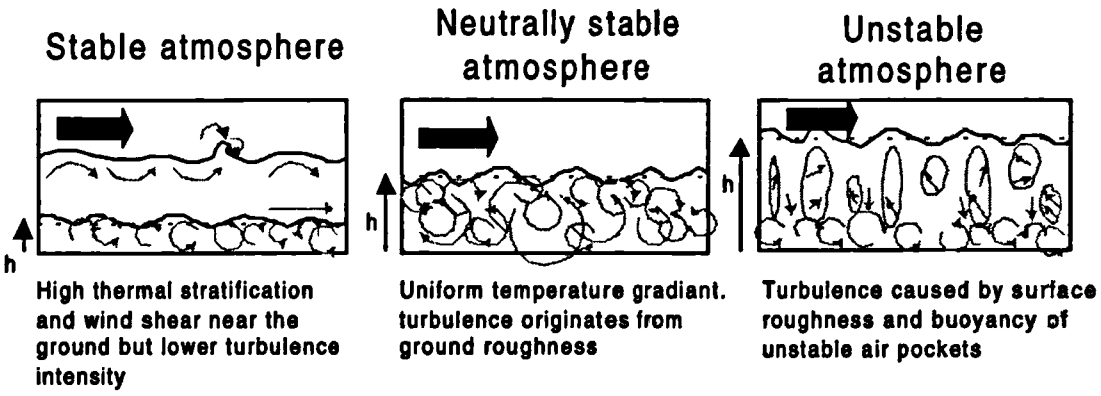

Figure 3-5 Atmospheric stability classification

Studies by Spera[5] into variations in wind shear at Clayton, New Mexico, illustrate the diurnal nature of atmospheric stability. He notes that before sunrise the air temperature increases with elevation therefore resulting in a stable atmosphere. At sunrise the ground is heated rapidly by solar radiation and the temperature profile reverses resulting in an unstable state. From about midday till one hour before sunset, neutral stability prevails. After this the earth begins to cool rapidly and a stable state takes over again until sunrise when the cycle repeats. He notes that on cloud covered days, when the earth is shielded from the sun's radiation, near-neutral stability will prevail throughout the day.

Near-neutral stability also occurs in 'strong' wind. In these conditions the energy in the wind is sufficient to cause extensive turbulent mixing resulting in a fairly even temperature profile. The turbulence is due almost entirely to mechanical mixing caused by surface roughness and will therefore be stationary.

The definition of 'strong' wind is given in ESDU 85020[3] as $V_{10}>10$ *m/s* over land. This figure is obviously influenced by the ground roughness and therefore cannot apply to offshore locations. There is little research on this but Barltrop[6] suggests values of V_{10} between *20-25 m/s* as likely. This presents problems for the offshore wind turbine designer as turbines operate in wind speeds less than this. Stability and stationarity then become a problem. For the offshore analysis in this text we shall still assume stationarity because this is a necessity for frequency domain analysis. This is common practice within the offshore industry and ESDU 85020[3] chapter 6 states that

the assumption of stationarity should lead to conservative loading on conventional structures. The problem of atmospheric stability however still remains. Because the sea has a large thermal mass, it is common to find unstable atmospheric conditions for much of the time. Measurements by Wills & Cole[7] at west sole confirm this. In general an unstable atmosphere will increase the level of turbulence due to its convective energy. It is argued however by Barltrop[6] chapter 8.4.3, that the great bulk of fatigue damage occurs in the higher wind speed range ($V_{10}>15$ *m/s*) where near neutral stability prevails. A number of design spectra have been developed for non-neutral stability conditions (Kaimal[8] and Højstrup[9]). The reader is referred to the relevant reports for more information on these.

A recent publication by Germanischer Lloyd[10] specifically addresses the problem of atmospheric stability with relation to offshore wind turbines. It concludes that most of the turbulence will occur as a result of mechanical mixing and therefore the affect of atmospheric stability may therefore be neglected.

In conclusion, the literature study conducted suggests it is reasonable to assume the atmosphere to be neutrally stable for both on and offshore climates for the purpose of dynamic analysis of the turbine structure. Furthermore it is assumed that the fetch length is sufficient to produce atmospheric equilibrium in the earth's boundary layer. If this condition is not met then the reader is referred to ESDU 85020[3] until more research is available.

3.3 Variation of the mean wind speed with height and time

The variation in mean wind speed with respect to height is known as wind shear. The ground roughness prevents air movements very close to the ground and so the wind speed tends to zero. The viscosity of the air (Reynolds's stresses) act to retard the air flow in the earth's boundary layer up to a height (h) known as the gradient height where the free wind speed will prevail. The gradient height is dictated by the ground roughness and the general height of any obstacles. ESDU 85020[3] uses the results of Deaves and Harris[11] to give the following empirical expression for calculating the gradient height. The model assumes neutral stability. It should be noted that because of thermal stratification in a stable atmosphere, the wind shear will be greater than that

given by ESDU. Conversely, in an unstable atmosphere more mixing will result in a reduced wind shear (Spera[5] chapter 8.)

$$h = \frac{u_*}{6 \cdot f_c}$$ Where u_* is the friction velocity $$u_* = \frac{V_{10}}{2.5 \cdot \ln\left(10/z_0\right)}$$ **Equation 3-2 Gradient height**

f_c is the coriolis parameter $f_c = 2 \cdot \Omega \cdot \sin(\phi)$, Ω is the angular rotation of the Earth $\Omega = 72.9 \times 10^{-6} rad/s$, ϕ is the angle of latitude of the site in degrees, V_{10} is the mean hourly wind speed recorded 10m above the ground and z_0 is the ground roughness length in metres.

The ground roughness length is used throughout the mathematical model. Table 3-1 is taken from ESDU 85020[3] and shows typical values of roughness length (z_0) and effective displacement heights (d) for various terrain. (N.B. various authors give different tables for ground roughness lengths. Germanischer Lloyd[10] specify a value of 0.002m for offshore locations.)

Terrain Description	z_0 (m)	d (m)
City centres and forests	0.7	15 to 25
Small towns, suburbs of large towns and cities and Wooded country with many trees	0.3	5 to 10
Outskirts of small towns, villages and countryside with many hedges, some trees and some buildings	0.1	0 to 2
Open level country with few trees and hedges and isolated buildings; typical farmland	0.03	0
Fairly level grass plains with isolated trees	0.01	0
Very rough sea in extreme storms (1:50 year extreme), flat areas with short grass and no obstructions, Runway areas of airports.	0.003	0
Rough sea in annual extreme storms, snow covered farmland, flat desert or arid areas and inland lakes in extreme storms.	0.001	0

Table 3-1 Typical values of terrain parameters according to ESDU

The mean wind speed varies logarithmically with height in the boundary layer. ESDU 82026[12] gives data for evaluating the mean wind speeds over a homogeneous terrain

(i.e. equilibrium state is assumed) and ESDU 84011[13] provides the same information for terrain with significant roughness changes. For this thesis we are only interested in the variation of wind speed over the height of the rotor plane. This enables the evaluation of structural loading on the turbine. For this the empirical power law shall be used as expressed in Freris[14] chapter 2.

$$\frac{V_z}{V_H} = \left(\frac{z}{H}\right)^{\alpha}$$

where V_H = mean wind speed at reference height H, z = height for which the mean speed is required and α depends on the surface roughness and the range of height being covered. Germanischer Lloyd[10] specify a value of α = 0.11 corresponding to a surface roughness length z_0 = 0.002m for offshore locations.

Equation 3-3 Mean wind speed variation with height

The mean wind speed at any point varies slowly with time. In a storm we would expect a higher mean wind speed than during a calm summer's day. It is desirable to express this variation using a probability density function (PDF). Davenport[15] considered the wind speed (U) as the resultant of two independent Gaussian variables such that $U^2=v^2+u^2$ where u = mean wind speed north-south and v = mean wind speed in the east-west direction. This assumes that the wind is isotropic, uniformly distributed and there is no prevailing wind. The resulting probability density function therefore approximates a Rayleigh distribution. Subsequent work by Mayne[16] recommended a Weibull distribution which takes the same form as the Rayleigh but has an additional parameter governing the degree of spread of the distribution. Equation 3-4 describes the Weibull distribution.

$$p(V) = \frac{k}{c} \cdot \left(\frac{V}{c}\right)^{k-1} \cdot e^{-(V/c)^k}$$ **Equation 3-4**

Where k = Weibull slope parameter and c = Weibull mode parameter

The Weibull distribution tends to the Rayleigh as $k=2$. It is now common to find Weibull c and k coefficients given by meteorological stations and standard references such as the European wind atlas[17]. Where these are unavailable it is possible to

determine the Weibull c parameter from the annual mean wind speed recorded on a site by rearranging Equation 3-5. Also research by Penwarden and Wise[18] suggests a value of k=1.85 as a good agreement for wind in the UK.

$$\overline{V} = c \cdot \Gamma\left\{1 + \left(1/k\right)\right\} \qquad \textbf{Equation 3-5}$$

Where $\overline{V}$ is the mean annual wind speed and Γ is the Gamma function.

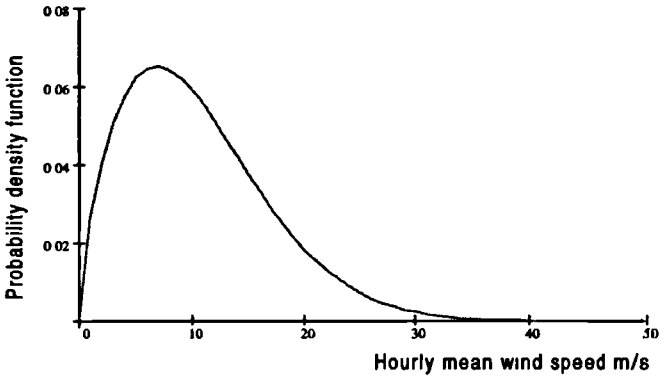

Figure 3-6 PDF of mean hourly wind speed

Figure 3-6 shows the Weibull distribution of mean hourly wind speed for an offshore location in the Rough field of the North Sea. The annual mean wind speed was recorded as V_{10}=*10.6 m/s* with Weibull c=*9.8 m/s* and k=*1.67* at 10m above mean sea level (MAREX[19]).

It is important for the engineer to design a structure to withstand the most severe wind loading. For many structures this is usually given by the most severe storm to occur during the design life. (i.e. 1:50 year storm for a structure with a 50 year design life.) Although this statistic may be obtained from the Weibull distribution described above, this in practice is erroneous as the tail of the distribution does not prove a good fit for extreme events. For distributions having an exponential form, such as Weibull and Rayleigh, the Fisher-Tippett Type-I distribution gives a better fit in this region. For further information on this topic the reader should refer to Barltrop[6] chapter 3.10. It is rare for a turbine to operate in extreme wind conditions as the control system usually shuts down. (Passive stall regulated turbines however will be operating though in deep stall.) It is unlikely therefore that this will prove to be the most severe operating condition and other scenarios should be investigated. The most onerous is likely to be through a dynamic transient load arising through a controlled shut down, etc.

Turbines are seldom designed specifically for one location. In practice a turbine manufacturer will ensure that his turbine is suitable for a number of locations. Design standards therefore give more general formulae for turbine design based on

conservative loading estimates. For offshore turbines Germanischer Lloyd[10] give the four classes of turbine shown in Table 3-2. Simplified formulae are provided to determine the mean and extreme wind speeds over differing time averaging intervals for the classifications. A simpler wind speed distribution, based on the Rayleigh distribution, is also provided. The reader is referred to Germanischer Lloyd[10] for more information.

Class	I	II	III	IV
$\overline{V}_E$ [m/s]	50	42.5	37.5	30
$\overline{V}_M$ [m/s]	10	8.5	7.5	6

Where $\overline{V}_E$ is the 10 minute mean of the extreme wind speed with a mean probability of occurring once in 50 years and $\overline{V}_M$ is the annual average wind speed over many years. Both are given at the turbine hub height.

Table 3-2 Classification of offshore wind turbines according to Germanischer Lloyd[10]

3.4 Wind turbulence

In the previous sections we have seen how the turbulent wind is produced through ground roughness in a neutrally-stable atmosphere, and through a combination of ground roughness and convection in an unstable atmosphere. The mathematical models described in this section apply to neutrally-stable atmospheric conditions. Before continuing with the mathematics it is beneficial to describe the nature of wind turbulence qualitatively. Excellent accounts are given by Connell[4] and Lawson[20].

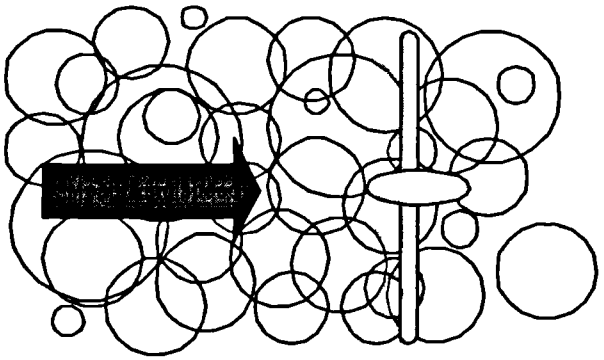

Figure 3-7 Visualisation of turbulence

Turbulent gusts are caused by eddies in the wind flow. These are blown along by the wind and travel at the mean wind speed. This is illustrated by Lawson[20] in Figure 3-7 and is based on Taylor's hypothesis. The eddies have differing frequency, amplitude and phase and may intersect one-another thus causing frequency shifts. As the eddies propagate through the air energy is lost as heat due to friction between the moving air particles, this process is known as attenuation. Eddies with higher frequencies attenuate more rapidly than those with lower frequencies. The rotor period of a wind turbine is often shorter than the time taken for an eddy to completely pass through the rotor plane. This gives rise to the periodic sampling of an eddy on numerous occasions before it has had time to pass through the rotor plane. This process has been called 'Eddy slicing' in the helicopter industry. A similar visualisation of the turbulent wind process is also given by Connell[4] and is illustrated in Figure 3-8.

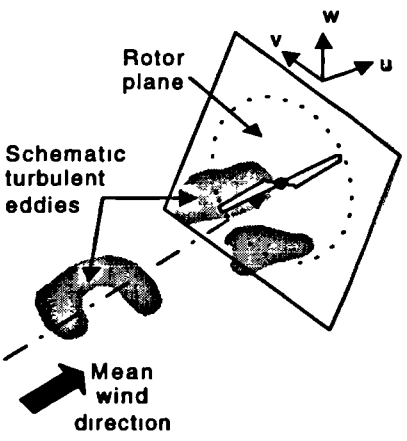

Figure 3-8 Turbulence correlation and convection

Wind turbulence is not restricted to the direction of the mean wind. In Figure 3-8 the mean wind is acting along the u axis, however lateral turbulence can also be measured in the v and w axes. The intensity of these will be smaller than that along the u axis but will still cause loading to the structure. This is likely to be small however. In this text the effect of lateral turbulence is neglected for simplicity. This is in common with all existing frequency domain analysis approaches. ECN however have proposed the inclusion of these effects in the next version of its TURBU package. The effect yields similar results to that of a turbine operating with a yaw or pitch misalignment. This is discussed later in the chapter.

The average size of a gust is given by ESDU 85020[3] and is expressed as a 'length scale.' The length scale is similar statistically to the 'time scale' discussed earlier in chapter 2.3.4. Figure 3-9 illustrates the rather complex notation used by ESDU to describe the nine principle length scales for longitudinal and lateral turbulence along the *u*, *v* and *w* axes. The length scale is defined by Equation 3-6.

$$ {}^{x}L_i = V_z \cdot \int_0^{\infty} \rho_{ii}(\tau) \cdot d\tau \quad \text{or} \quad {}^{x}L_i = V_z \cdot T_i $$

Equation 3-6

Where, ${}^{x}L_i$ is the length scale defined below, V_z is the mean hourly wind speed z metres above the ground, $\rho_{ii}(\tau)$ is the normalised covariance function and T_i is the time scale.

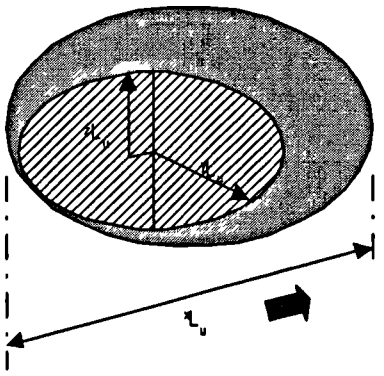

Figure 3-9 Length scales of turbulence

Figure 3-9 illustrates a turbulent gust travelling along the '*u*' axis. ${}^{x}L_u$ is known as the longitudinal length scale because it is in the direction of the gust, and ${}^{y}L_u$ and ${}^{z}L_u$ are known as the lateral length scales. This notation implies the average lengths *x*, *y* and *z* of the gust travelling in the u direction. Similarly there are two other longitudinal length scales, ${}^{y}L_v$ and ${}^{z}L_w$; and four lateral length scales ${}^{x}L_v$, ${}^{z}L_v$, ${}^{x}L_w$, and ${}^{y}L_w$. These take account of the gusts travelling along the *v* and *w* axes.

The largest length scale given in the ESDU model is ${}^{x}L_u$. The length scales increase with altitude up to approximately *h/3* and then decrease thereafter. The dependence on height is caused by the space available for the dominant eddy size. In this text we are only considering gusts in the longitudinal *u* direction which is perpendicular to the rotor plane.

The longitudinal and lateral length scales of turbulence in the *u* direction have been derived empirically and are given by ESDU 75001[21] as Equation 3-7.

$$ \text{Longitudinal length scale } {}^{x}L_u = 25 \cdot \frac{z^{0.035}}{z_0^{0.063}} $$

Equation 3-7

Lateral length scales $^{y}L_u = 10 \cdot \frac{z^{0.38}}{z_0^{0.068}}$ and $^{z}L_u = 6.3 \cdot \frac{z^{0.45}}{z_0^{0.081}}$

At large heights the turbulence becomes isotropic and the lateral length scales tend to half the value of their respective longitudinal length scale as given in Equation 3-8.

$$^{y}L_u = {}^{z}L_u = \tfrac{1}{2} \cdot {}^{x}L_u \qquad \textbf{Equation 3-8}$$

3.4.1 Single point wind turbulence statistics

In order to analyse the turbulent loading on a wind turbine it is necessary to determine the Auto-power Spectral Density function (PSD) and the Cross power Spectral Density function (CPSD) of the wind speed. This section describes the ESDU model for calculating the Auto-power spectral density function.

ESDU assumes that the wind is strong, is in equilibrium and the atmosphere is neutrally-stable. Provided these conditions are met then the level of turbulence at a particular location will vary with respect to the surface roughness and the mean wind speed. ESDU introduce a dimensionless parameter called the 'Turbulence Intensity' to represent the level of turbulence with respect to the mean wind speed. It is defined by Equation 3-9.

$$I_u = \frac{\sigma_u}{V_z} \qquad \textbf{Equation 3-9}$$

where I_u= Turbulence intensity in the u direction

σ_u= Standard deviation of wind speed in the u direction

V_z= Mean hourly wind speed z metres above the ground

According to ESDU 85020[3], the standard deviation of wind speed in the u directions is obtained from the empirical expression;

$$\sigma_u = u_* \cdot \frac{7.5\eta \cdot \left[0.538 + 0.09 \ln\left(z/z_0\right)\right]^p}{1 + 0.156 \ln\left(u_*/f_c \cdot z_0\right)} \qquad \textbf{Equation 3-10}$$

$$\text{where } \eta = 1 - \frac{z}{h} \quad \text{and} \quad p = \eta^{16}$$

u_* is defined in Equation 3-2 with respect to the mean wind speed recorded 10m above the surface. For a more accurate representation of the general case where the mean wind speed is given z metres above the surface, u_* can be obtained by the equation;

$$u_* = \frac{V_z - 86.25 \cdot f_c \cdot z}{2.5 \cdot \ln\left(z/z_0\right)} \qquad \textbf{Equation 3-11}$$

The above formulation is only suitable for equilibrium conditions. ESDU 85020[3] clarifies this by stipulating that the model is only suitable for situations where the terrain is uniform upwind of the site for at least 30km. Where there are roughness changes upwind of the site then ESDU 84030[22] provides a more appropriate calculation procedure. This is not considered in this thesis because the turbulence intensity values specified by the certifying bodies largely exceed the values obtained from the above formulation. Typical values of 15-20% are often specified for on-shore turbines, and Germanischer Lloyd[10] specify a value of 13.2%[†] for offshore locations. Specifying design turbulence intensity values eliminates the site dependency in turbine design. The ESDU model is used however in Chapter 8 to compare the theoretical and measured responses of working turbines.

The power spectral density function of the wind given by ESDU 85020[3] is based on the von Karman spectral equations. These give a good fit to measured spectra at high frequencies and fairly large heights. In order to improve their accuracy in the lower frequency band and at lower heights, ESDU have used modified length scale parameters. The inaccuracies in the model are due to limitations in the von Karman spectra and not the length scale calculations, Equation 3-7 may still be used to calculate the length scales for other models but as far as the ESDU model is concerned then the modified values should be used.

[†] Germanischer Lloyd express the turbulence intensity as a proportion of the mean wind speed measured over 10 minutes, thus a value of 12% is given in the text. This corresponds to 13.2% when considering the mean wind speed measured over 1 hour.

The theoretical computation of the power spectral density of wind speed is still an area of research and is beyond the scope of this thesis. For more information on the ESDU model the reader should consult the detailed reports issued by ESDU. The ESDU formulation given in ESDU 85020[3] is expressed in Equation 3-12.

$$G_{uu}(f) = \frac{\sigma_u^2}{f} \cdot \left[\beta_1 \cdot \frac{2.987 \cdot n_u/a}{\left[1+\left(2\pi \cdot n_u/a\right)^2\right]^{5/6}} + \beta_2 \cdot \frac{1.294 \cdot n_u/a}{\left[1+\left(\pi \cdot n_u/a\right)^2\right]^{5/6}} \cdot F_1 \right] \qquad \textbf{Equation 3-12}$$

where

$$n_u = {}^xL_u \cdot \frac{f}{V_z} \qquad F_1 = 1 + 0.455 \cdot \exp\left[-0.76 \cdot \left(n_u/a\right)^{-0.8}\right]$$

$$a = 0.535 + 2.76 \cdot (0.138 - A)^{0.68} \qquad A = 0.115 \cdot \left[1 + 0.315 \cdot \left(1 - z/h\right)^6\right]^{1/3}$$

$$\beta_1 = 2.357a - 0.761 \qquad \beta_2 = 1 - \beta_1$$

The longitudinal length scale ${}^xL_u$ referred to above should be the modified form defined by ESDU 85020[3] and given below.

$$ {}^xL_u = \frac{A^{1/2} \cdot \left(\sigma_u/u_*\right)^3 \cdot z}{2.5 K_z^{3/2} \cdot \left(1 - z/h\right)^2 \cdot \left(1 + 5.75 \cdot z/h\right)} \qquad \textbf{Equation 3-13}$$

where

$$K_z = 0.19 - \left(0.19 - K_0\right) \cdot \exp\left[-B \cdot \left(z/h\right)^n\right] \qquad K_0 = \frac{0.39}{Ro^{0.11}}$$

$$B = 24 \cdot Ro^{0.155} \qquad N = 1.24 \cdot Ro^{0.008} \qquad Ro = \frac{u_*}{f \cdot z_0}$$

The PSD may also be expressed in radian measure where ω is the frequency in *rad/sec*. This has many advantages in mathematical simplicity and is used throughout the rest of this text. Equation 3-14 gives the ESDU formulation in circular radian measure, some of the parameters have been modified, these are denoted by an asterisk in the formula.

$$G_{uu}(\omega) = \frac{\sigma_u^{\,2}}{2\pi \cdot \omega} \cdot \left[\beta_1 \cdot \frac{2.987 \cdot {}^{n_u^*}\!/_{a}}{\left[1 + \left(n_u \cdot {}^{\omega}\!/_{a}\right)^2\right]^{5/6}} + \beta_2 \cdot \frac{1.294 \cdot {}^{n_u^*}\!/_{a}}{\left[1 + \left(n_u \cdot {}^{\omega}\!/_{2a}\right)^2\right]^{5/6}} \cdot F_1^* \right] \qquad \textbf{Equation 3-14}$$

Where $n_u^* = {}^{x}L_u \cdot \dfrac{\omega}{V_z}$ $\qquad F_1^* = 1 + 0.455 \cdot \exp\left[-0.76 \cdot \left({}^{n_u^*}\!/_{a}\right)^{-0.8}\right]$

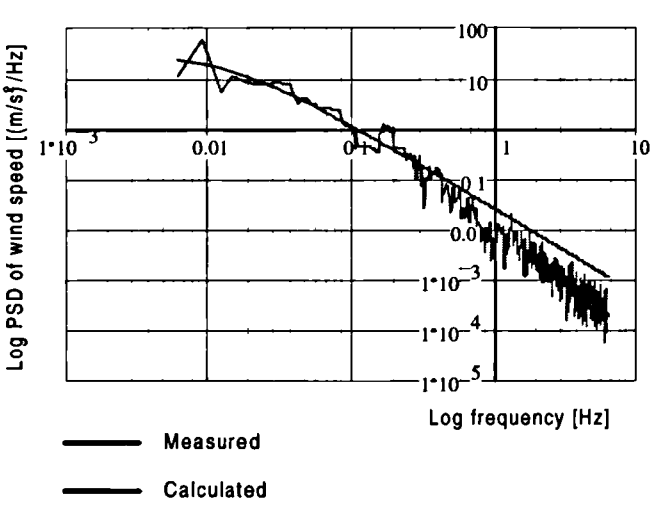

Figure 3-10 PSD of wind turbulence

Figure 3-10 shows the ESDU spectra of turbulent wind speed for a mean wind speed $V_z=10$ *m/s* at hub height $z=35$ *m* with a turbulence intensity of $I=8.9\%$[†] . The spectrum is compared with measured results from an onshore site with data provided by Ward[23]. The general obstruction height h is zero. This data is characteristic of off-sea wind in coastal areas. The comparison shows good agreement in the lower frequency range (up to 0.5Hz) after which the calculated spectrum over predicts the measured results. It will be shown later that the lower frequency band proves most

[†] The turbulence intensity was calculated from the measured data. The ground roughness length was calculated by rearranging Equation 3-10. This was found to give $z_0=0.0009$ *m* representing off-sea wind in coastal areas.

important when considering wind turbine dynamics due to the rotational sampling effects of the turbulence. This result however also shows that the calculated spectra is conservative in the higher frequency range.

3.4.2 Variation of wind turbulence in space

In the previous section we defined the formulation to find the Auto-power Spectral Density function for wind speed at a fixed point in space. In this section we shall look at the Cross-power Spectral Densities between two points in space. A full account of the derivation of the formulae in this section is given by ESDU 86010[24]. In Chapter 2.3.5 we saw how the Cross-power Spectral Density function is related to the Auto-power Spectral Density function by the Coherence function given in Equation 3-15. In this section we shall use the coherence function to determine the Cross-power Spectra. The degree of coherence between two measured processes will vary with respect to the distance between them Δr.

$$\gamma_{ij}(f,\Delta r) = \frac{\left|S_{ij}(f)\right|}{\sqrt{S_{ii}(f)\cdot S_{jj}(f)}} \qquad \textbf{Equation 3-15}$$

Where $S_{ii}(f)$ and $S_{jj}(f)$ are the double sided Auto-power Spectra measured at two locations separated by distance Δr, and $S_{ij}(f)$ is the double sided Cross-power spectrum between the two.

If we assume that the turbulence is homogeneous in the rotor plane we can see that $S_{ii}(f)=S_{jj}(f)$ and Equation 3-15 can be rearranged to determine the Cross-power spectrum with respect to the separation distance Δr as in Equation 3-16.

$$\left|S_{ij}(f,\Delta r)\right| = \gamma_{ij}(f,\Delta r)\cdot S_{ii}(f) \qquad \textbf{Equation 3-16}$$

The modulus operator implies we only get a representation of the magnitude of the Cross-power spectrum, the phase relationships will be lost. ESDU 86010[24] however comments on the usually small value of the imaginary term in the Cross-Power spectrum (quad-spectral density function). Furthermore, when used in calculating the fluctuating component of wind loading due to turbulence, the quad-coherence component together with the asymmetric component of the double sided spectrum integrate to zero over the structure. In this case the coherence tends to the co-coherence and the expression may be expressed in terms of the single sided spectra as Equation 3-17.

$$\left|G_{ij}(f,\Delta r)\right| = \gamma_{ij}(f,\Delta r)\cdot G_{u}(f) \qquad \textbf{Equation 3-17}$$

Empirical expressions to determine the coherence function are given by ESDU 86010[24]. It is noted however that these are based on mainly theoretical formulations as very few measured results exist. ESDU differentiates between longitudinal and lateral separation of the two points.

3.4.2.1 Longitudinal separation

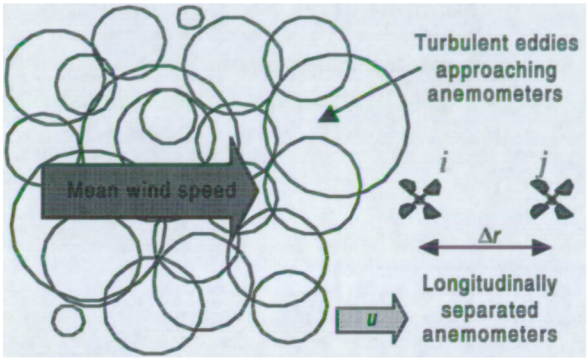

Figure 3-11 Longitudinal separation

Taylor's hypothesis postulates that the pattern of turbulence is frozen in the wind and is blown along by it as shown in Figure 3-11. If this were true then the turbulence measured at anemometers *i* and *j* would be the same but with a constant time lag between them of $T=\Delta r/V_z$. The coherence between them would therefore be unity. In practice this hypothesis is not strictly true. The eddies in the wind flow change with time due to energy transfers. ESDU 86010[24] give the following formula for calculating the coherence between the two longitudinally separated anemometers in the *u* direction.

$$\gamma_{ij}(f,\Delta r) = \exp\left(-3\cdot f\cdot {}^{\Delta r}\!/_{V_z}\right) \qquad \textbf{Equation 3-18}$$

This is expressed in circular radian measure as Equation 3-19, where ω is the frequency in rad/sec.

$$\gamma(\omega,\Delta r) = \exp\left(-3\cdot\frac{\omega}{2\pi}\cdot {}^{\Delta r}\!/_{V_z}\right) \qquad \textbf{Equation 3-19}$$

3.4.2.2 Lateral separation

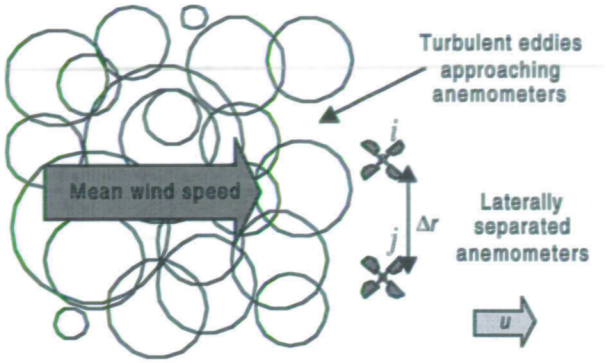

Figure 3-12 Lateral separation

The concept of lateral separation is illustrated in Figure 3-12. For *u* components with separation in the lateral or vertical directions the coherence is given by ESDU 86010[24] based on the von Karman spectral equations. The ESDU formulation is expressed in Equation 3-20.

$$\gamma_{ij}(f,\Delta r) = \exp\left(-1.15\cdot\eta_1^{1.5}\right) \qquad \textbf{Equation 3-20}$$

Where

$$\eta_1 = \sqrt{\left(0.747\cdot\tilde{r}_g\right)^2 + \left(c\cdot 2\pi\cdot f\cdot \Delta r/V_m\right)^2} \qquad \tilde{r}_g = \frac{\Delta r}{2\cdot {}^{r}L_u}$$

$$c = \frac{1.6\cdot\tilde{r}_g^{\,0.13}}{\eta^b} \text{ or 1.0 whichever is greater} \qquad b = 0.35\cdot\tilde{r}_g^{\,0.2}$$

$$\eta = \sqrt{\left(0.747\cdot\tilde{r}_g\right)^2 + \left(2\pi\cdot f\cdot \Delta r/V_m\right)^2}$$

Alternatively this may be expressed in circular radian measure in Equation 3-21 where ω is the frequency in *rad/sec*. Some of the parameters have been modified and these are denoted with an asterisk.

$$\gamma_{ij}(\omega,\Delta r) = \exp\left(-1.15\cdot\eta_1^{*1.5}\right) \qquad \textbf{Equation 3-21}$$

Where

$$\eta_1^* = \sqrt{\left(0.747\cdot\tilde{r}_g\right)^2 + \left(c\cdot\omega\cdot \Delta r/V_m\right)^2} \qquad \tilde{r}_g = \frac{\Delta r}{2\cdot {}^{r}L_u}$$

$$c = \frac{1.6\cdot\tilde{r}_g^{\,0.13}}{\eta^{*b}} \text{ or 1.0 whichever is greater} \qquad b = 0.35\cdot\tilde{r}_g^{\,0.2}$$

$$\eta^* = \sqrt{\left(0.747\cdot\tilde{r}_g\right)^2 + \left(\omega\cdot \Delta r/V_m\right)^2}$$

${}^{r}L_u$ is known as the radial length scale. For purely lateral or vertical separation it is taken as ${}^{y}L_u$ or ${}^{z}L_u$ respectively. When the separation is a combination of lateral and vertical; Δr is given by $\Delta r = \sqrt{\Delta y^2 + \Delta z^2}$ where Δy = lateral separation component and Δz = vertical separation component, and ${}^{r}L_u$ is obtained from Equation 3-22.

$$ {}^{r}L_u = \frac{\sqrt{\left({}^{y}L_u \cdot \Delta y\right)^2 + \left({}^{z}L_u \cdot \Delta z\right)^2}}{\Delta r} \qquad \textbf{Equation 3-22} $$

Where the vertical length scale $${}^{z}L_u = {}^{x}L_u \cdot \left[0.5 - 0.34 \cdot \exp\left(-35 \cdot \left(z/h\right)^{1/7}\right)\right]$$

and the lateral length scale $${}^{y}L_u = 0.16 \cdot {}^{x}L_u + 0.68 \cdot {}^{z}L_u$$

This expression proves cumbersome in our analysis and a common simplification is obtained by taking ${}^{r}L_u$ equal to the geometric mean of the lateral and vertical length scales as given by Equation 3-23. Van Engelen[25] determined that by using this assumption, the maximum error in the decay constant η_1 is about 10-15%. This error is considered satisfactory when compared with the accuracy of the model and the available data.

$$ {}^{r}L_u = \sqrt{{}^{y}L_u \cdot {}^{z}L_u} \qquad \textbf{Equation 3-23} $$

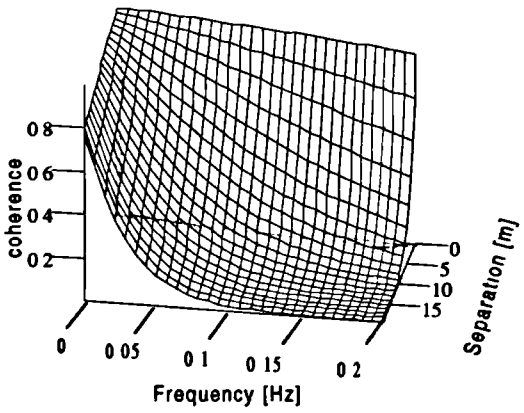

Figure 3-13 Coherence

Figure 3-13 shows the coherence with respect to frequency n and separation of the two points Δr. The function is calculated for an off-sea wind fetch using the same conditions presented in Figure 3-10.

3.5 Conclusion

In this chapter the literature review is documented discussing the mathematical model used for describing wind turbulence. The ESDU model is proposed

for modelling both the on and offshore winds. The model assumes atmospheric equilibrium, this proves a satisfactory solution for isolated turbines given an unrestricted fetch of approximately 30km. Further research is necessary, however, to improve the model's description of the real wind field over complex terrain with multiple wind turbine interactions. These conditions are typically associated with onshore windfarms.

The model also assumes a neutrally stable atmosphere which is commonly found in the case of strong winds. Since most of the fatigue damage is likely to be caused in high winds, then this assumption remains satisfactory for the onshore case. The assumption is less accurate for the offshore case where much higher wind speeds are required to achieve the mechanical mixing necessary for neutral atmospheric conditions. Recent publications (Germanischer Lloyd[10]) have concluded, however, that neutral stability is still a reasonable assumption for the purpose of offshore turbine design.

---

[1] Van Der Hoven I. (1957) "Power spectrum of horizontal wind speed in the frequency range from 0.0007 to 90 Hz." Journal of Meteorology 14, 160-164.

[2] BS8100 (1986) "Lattice towers and masts. Part 1: Code of practice for loading." British Standards Institution, London.

[3] ESDU 85020 (1993). "Characteristics of atmospheric turbulence near the ground. Part II: single point data for strong winds (neutral atmosphere)." ESDU international plc, London.

[4] Connell J.R. (1988). "A Primer of turbulence at the wind turbine rotor." Solar Energy 41, 281-293, USA

[5] Spera D.A. (1995) "Wind turbine technology." ASME press.

[6] Barltrop N.D.P and Adams A.J (1991). "Dynamics of fixed marine structures." Butterworth-Heinemann Ltd. Linacre House, Jordan Hill, Oxford OX2 8DP, England.

[7] Wills J.A.B and Cole L.R. (1989). "Wind measurement at west sole - final report." BMT Fluid mechanics Ltd.

[8] Kaimal J.C. (1978). "Horizontal velocity spectra in an unstable surface layer." Journal of Atmospheric Science, 35, 18-24.

[9] Højstrup J. (1982). "Velocity spectra in the unstable boundary layer." Journal of Atmospheric Science, 39, 2239-2248.

[10] Germanischer Lloyd, Rules for regulations 1995. "IV Non-marine technology, Part 2 - Offshore wind energy. Regulation for the certification of Offshore wind energy conversion system."

[11] Deaves D. and Harris R.I. (1978) "A mathematical model of the structure of strong winds." CIRA Report No. 76.

[12] ESDU 82026 (1982). "Strong winds in the atmospheric boundary layer. Part I: mean hourly wind speeds." ESDU International plc, London.

[13] ESDU 84011 (1984). "Wind speed profiles over terrain with roughness changes for flat or hilly sites." ESDU International plc, London.

[14] Freris L.L. (1990). "Wind energy conversion systems." Prentice Hall,

[15] Davenport A.G. (1967). "The dependence of wind loads on meteorological parameters." International research seminar on wind effects on buildings and structures, University of Toronto Press. Pages 19-82

[16] Mayne J.R. and Cook N.J. (1981). "Extreme wind analysis." Wind engineering in the eighties, CIRA conference, London

[17] "European wind atlas"

[18] Penwarden A.D. and Wise A.F.E. (1975). "Wind environment around buildings." Building Research Establishment report, HMSO, London.

[19] MAREX (1980). "Environmental study on the Rough field development." Pub. Marex, Marine Exploration Ltd. Linacre House, Jordan Hill, Oxford OX2 8DP, England.

[20] Lawson T.V. (1980) "Wind effects on buildings, Volume 2: Statistics and meteorology." Applied Science Publishers Ltd. London.

[21] ESDU 75001 (1976). "Characteristics of atmospheric turbulence near the ground. Part III: Variations in space and time for strong winds (neutral atmosphere)." ESDU International plc, London

[22] ESDU 84030 (1984). "Longitudinal turbulence intensities over terrain with roughness changes for flat or hilly sites." ESDU International plc, London.

[23] Ward I.P. (1996). "Wind turbulence data measured at a turbine test site. (Location and manufacturer are confidential)." Personal correspondence.

[24] ESDU 86010 (1991). "Characteristics of atmospheric turbulence near the ground. Part III: variations in space and time for strong winds (neutral atmosphere)." ESDU International plc, London.

[25] Van Engelen T.G. (1991). "Turbu-I computer program for turbulence load analysis of horizontal axis wind turbines. Theory and program description." ECN, SU General Services, Petten, The Netherlands.

4. Aerodynamic modelling of a wind turbine

In the previous chapter we considered the wind conditions which are seen by an operating wind turbine. In this chapter we look at how these winds influence the loading on the rotor blades and structure. The analysis described in this chapter has been performed using Mathcad worksheets.

4.1 Air flow through a wind turbine rotor

Consider the air flow through a wind turbine rotor which operates under ideal and constant wind conditions, this is illustrated in Figure 4-1. The air flow over the blade causes a lift and a drag force, these provide the force to drive the turbine. As the air flows over the blade, it is deflected as shown in the figure. This gives rise to two effects: firstly, the axial velocity behind the blade is reduced; and secondly, the air gains a tangential velocity component called 'swirl'. The net result of this is to form a helical wake behind the rotor. A good account of the physics behind the wake phenomenon is presented by Sharpe[1], Chapter 4.

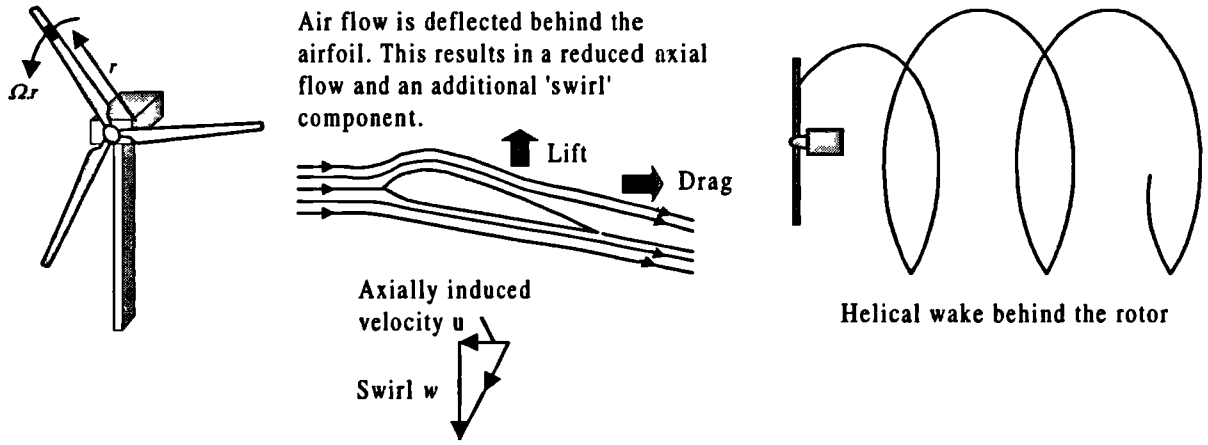

Figure 4-1 Helical wake behind the rotor

When analysing the aerodynamics, it is important to incorporate the wake effects as these influence the resultant wind speed vector V_R that represents the airflow into the rotor. The resultant wind speed vector comprises four separate vectors, these represent the following components:

1. The incident wind speed vector, V

2. The rotationally induced wind speed vector, $\Omega.r$
3. The axially induced wake velocity vector, $a.V$
4. The tangentially induced wake (swirl) velocity vector, $a`.\Omega.r$

Where a is known as the axial induction factor and $a`$ the tangential induction factor. These are illustrated in Figure 4-2.

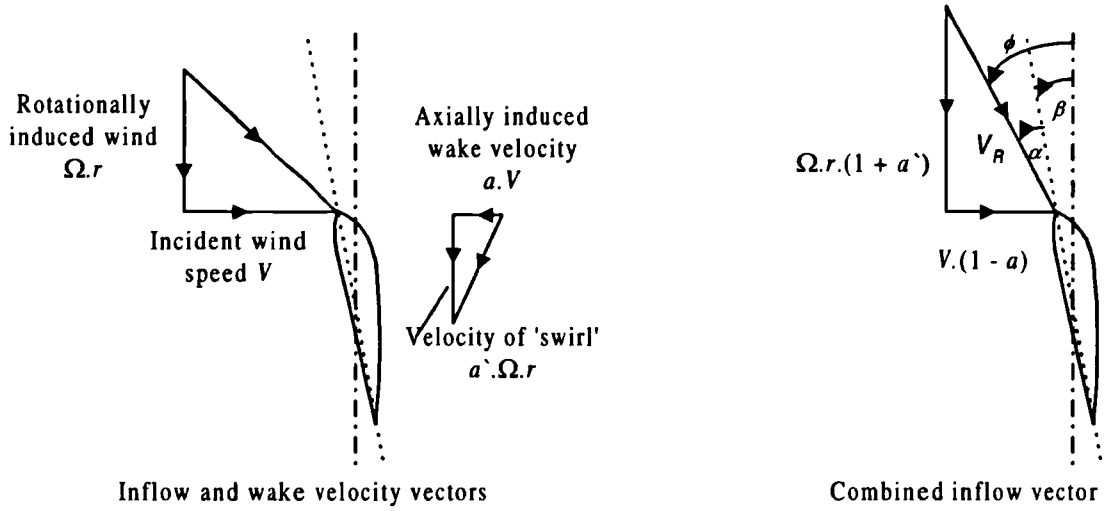

Figure 4-2 Wind inflow velocity vector

In order to evaluate the blade loads we discretise each blade into a number of elements. For each element we determine the resultant wind velocity, V_R, and the inflow angle, α relative to the blade element's chord axis. ϕ is the inflow angle relative to the rotor plane and β is the local blade setting angle. We can then use the element's lift and drag coefficients to calculate the contribution to the blade load from that element. The total blade load can then be determined by taking the sum of the loads on each element along the blade.

The question that now arises is how to determine the wake's velocity vector. Under an ideal and constant wind speed, the change in momentum of the air as it flows through the rotor must be in equilibrium with the force exerted by the blades, this gives rise to the '*equilibrium wake state*'. The equilibrium wake vector is determined using an iterative solution technique which is derived in section 4.2.

In practice we never encounter ideal conditions and in Figure 3-1 it was shown how the wind speed varies over many different time scales. It is important to understand how the wake responds to these variations in the wind.

For slow variations, such as the diurnal cycles, etc., the wake velocities change with the incident wind speed. The slow variation allows the wake to settle in an equilibrium state with the incident wind and therefore aerodynamic loads are calculated using the equilibrium wake model discussed earlier.

With more rapidly varying wind speeds, such as those occurring in the turbulent wind region, the wake velocities do not have the opportunity to reach equilibrium as the wind speed is varying too quickly. The wake is therefore seen to be oscillating dynamically around a mean position, this is said to be a dynamic wake. Mathematical modelling of the dynamic wake is still an area of active research. Already some analysis programs have models incorporated within them to calculate the dynamic wake effects [Lindenburg[2]], however these are non-linear and beyond the scope of this work.

A simplified mathematical model is often used to analyse the aerodynamic behaviour in rapidly varying wind speeds, this is known as the frozen wake model. The frozen wake model takes advantage of the high damping characteristic noticed with the dynamic wake. This implies that the wake is slow to adapt to changes in the incident wind speed. Using this characteristic we can calculate the equilibrium wake vectors for the mean wind speed and assume them to be frozen in this state when considering the rapidly varying wind speeds around this mean. This is illustrated in Figure 4-3.

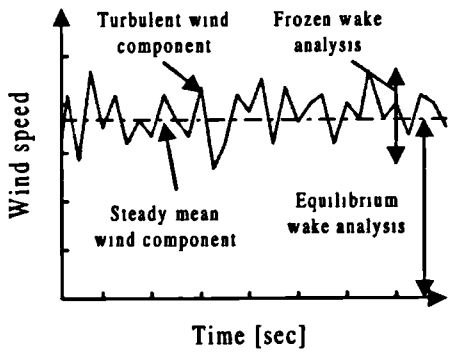

Figure 4-3 Turbulent wind speed seen by the rotor

The graph shows the turbulent wind speed seen by the rotor. The mean rotor load is evaluated using the equilibrium wake model and the turbulent variations around this using the frozen wake model. The sum of these yield the overall load.

In this chapter we first of all derive an iterative procedure for calculating the equilibrium wake velocities. Using this model we then derive

expressions for calculating the equilibrium power curves and turbine loads. We follow this by deriving the quasi-static gain factors, these give expressions for aerodynamic damping, etc. for use in a structural dynamic analysis and assume that the wake velocities are frozen. We conclude the chapter by looking at some practical considerations for analysing turbine aerodynamics.

4.2 The equilibrium wake model

In this section we derive an iterative procedure for calculating the equilibrium wake velocities. There are a number of different methods ranging in their degree of complexity. The most simple of these is the Rankine-Froude actuator disk model. This model imposes some restricting assumptions. The most significant being: a steady homogeneous wind, a uniform flow velocity over the whole rotor disk, and no wake rotation. The actuator disk model is seldom used in quantitative analysis but is still useful for computing quick approximate results.

A more advanced analysis technique, and the one employed in this research, is '*Glauert's Annulus Momentum Vortex Theory*' (also known as '*Strip Theory*'). Glauert originally developed this for analysing propellers but it has also proven to be a very reliable and rapid method for analysing wind turbines. Strictly speaking the theory is only applicable to rotors with an infinite number of blades. However, empirical modifications have been applied to the theory to improve its reliability. Where these are included in the analysis they are discussed.

This analysis method is very widely used and Stoddard[3] and Wilson[4,5] give good accounts. The derivation is given in this thesis because the author has included new state-of-the-art modification factors. In particular a factor is included to model the 3-dimensional flow past a stalled blade element. These have been obtained through various references and improve on previous models.

More advanced analysis techniques are based on wake vortex theory. These require more computational effort but yield better results for evaluating special effects, such as tip control systems, etc. that are not accurately modelled with the simpler methods. A description of these methods can be found in Abbott[6] and are beyond the scope of this thesis.

For our analysis purposes Glauert's Annulus Momentum Vortex Theory is proposed. This proves adequate for most dynamic analysis and is much easier to implement than more complex techniques. Besides, the frequency domain analysis discussed in this thesis requires a linear relationship between the turbulent wind speed variation and the structural loads. This assumption will compromise the accuracy of whatever aerodynamic analysis we choose to employ and would therefore render a more exact method pointless.

4.2.1 Derivation of equilibrium wake model

The analysis follows an iterative procedure. An overview of this procedure can be given as follows: First we determine the rotor thrust and torque due to wind on a small element of each blade. We derive these using two different techniques, firstly using blade element theory and secondly using annulus momentum theory. This results in four equations with four unknown terms that can then be solved iteratively.

Blade element theory divides the blade into a finite number of elements. The aerodynamic force is calculated for each element using the coefficients of lift and drag, *Cl* and *Cd* respectively, for the airfoil section. This theory assumes that the force on any element is independent of that on any other element. Using blade element theory, consider the combined load witnessed by the elements sited at radius r along each blade of a turbine. We assume that the turbine blades are identical and are equally spaced around the rotor. The rotor is rotating with angular velocity Ω *rad/sec* and is subjected to a uniform and constant wind speed over the rotor plane. The resulting wind velocity vector for the blade elements is illustrated in Figure 4-4.

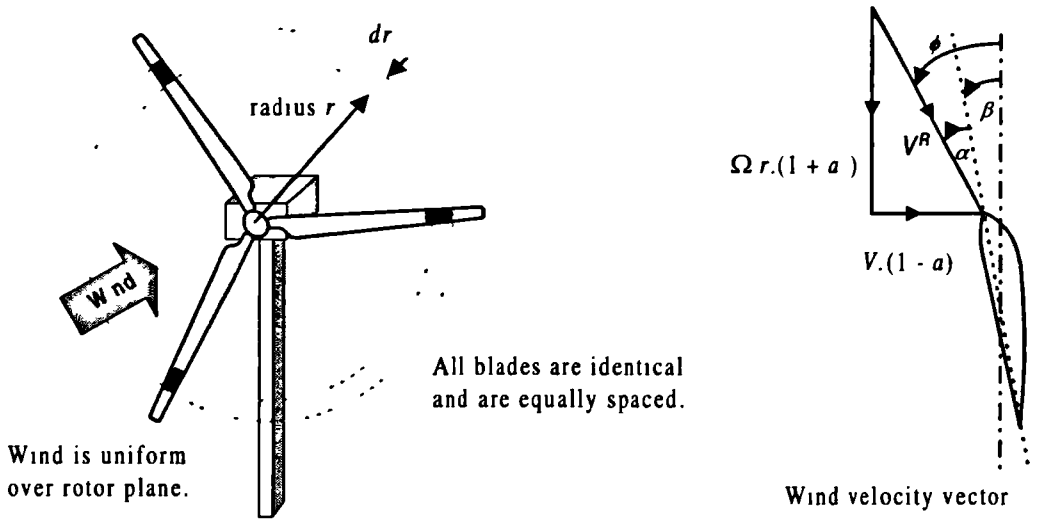

Figure 4-4 Wind velocity vector on a blade element

The resultant inflow angle ϕ and the resultant wind speed V_R can be evaluated using Equation 4-1.

$$\phi = \tan^{-1}\left(\frac{V\cdot(1-a)}{\Omega\cdot r\cdot(1+a`)}\right) \qquad V_R = \frac{V\cdot(1-a)}{\sin(\phi)} \qquad \textbf{Equation 4-1}$$

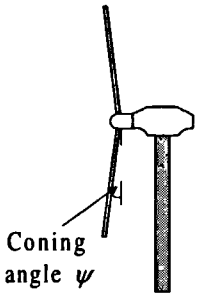

Many turbines have a pre-set 'coning' angle (ψ), this usually applies to upwind turbines to prevent tower impact. The coning angle may be incorporated in the formulae by modifying the incident wind speed seen by the blade elements. The modified wind speed can be expressed as $V\cdot\cos(\varphi)$. Equation 4-1 can be modified to include the effect of coning and is expressed as Equation 4-2.

$$\phi = \tan^{-1}\left(\frac{V\cdot(1-a)\cdot\cos(\varphi)}{\Omega\cdot r\cdot(1+a`)}\right) \qquad V_R = \frac{V\cdot(1-a)\cdot\cos(\varphi)}{\sin(\phi)} \qquad \textbf{Equation 4-2}$$

The thrust from each blade element is determined by calculating the aerodynamic forces on the blade element and resolving perpendicular to the rotor plane. The aerodynamic forces are obtained using the coefficients of lift and drag, *Cl* and *Cd* respectively, for the airfoil section. The thrust is therefore obtained using Equation 4-3.

$$T = \tfrac{1}{2}\cdot\rho\cdot V_R^2\cdot\left(Cl\cdot\cos(\phi)+Cd\cdot\sin(\phi)\right)\cdot dA \qquad \textbf{Equation 4-3}$$

For a turbine with B number of identical blades, the combined thrust is therefore given by the following expression:

$$T = \tfrac{1}{2}\cdot\rho\cdot\frac{V^2\cdot(1-a)^2\cdot\cos^2(\varphi)}{\sin^2(\phi)}\cdot\left(Cl\cdot\cos(\phi)+Cd\cdot\sin(\phi)\right)\cdot B\cdot c\cdot dr\,.$$

The coefficient of thrust C_H for the annulus is defined as $C_H = \dfrac{T}{\frac{1}{2}\cdot\rho\cdot V^2\cdot A}$, where A is the area of the annulus. C_H is therefore given by Equation 4-4.

$$C_H = \frac{\sigma}{2}\cdot\frac{(1-a)^2\cdot\cos^2(\varphi)}{\sin^2(\phi)}\cdot\left(Cl\cdot\cos(\phi)+Cd\cdot\sin(\phi)\right) \qquad \textbf{Equation 4-4}$$

Where $\sigma = \dfrac{B\cdot c}{\pi\cdot r}$

By resolving the aerodynamic forces in the plane of the rotor we can also determine the rotor torque caused by the blade elements. This is given in Equation 4-5.

$$Q = \tfrac{1}{2}\cdot\rho\cdot V_R{}^2\cdot\left(Cl\cdot\sin(\phi)-Cd\cdot\cos(\phi)\right)\cdot B\cdot c\cdot r\cdot dr \qquad \textbf{Equation 4-5}$$

At this point we have no way of determining the wake induction factors a and $a`$. These must be determined iteratively by comparing the results given above with those predicted using the annulus momentum theory. This is based on the Rankine-Froude actuator disk and is discussed at length by Wilson[4] and Stoddard[3]. As air flows through the actuator disk, in this case the rotor, some kinetic energy is removed from the flow thus reducing its velocity. The mass flow rate through the rotor must remain constant; (i.e. what flows in must flow out), implying an increased area in the wake. Figure 4-5 illustrates the annular stream tube around the rotor disk and gives formulae for the wind speeds at each stage in the flow. Stoddard[3] derives these using momentum theory and Bernoulli's equation.

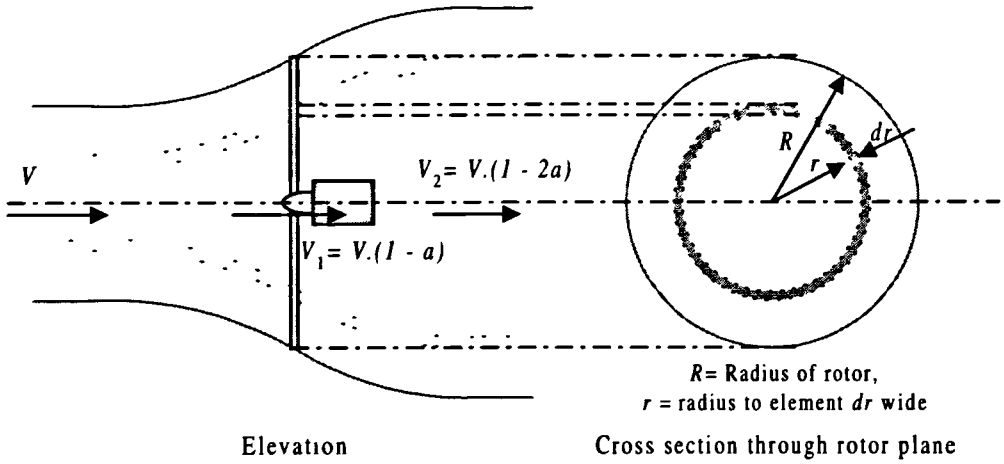

Figure 4-5 Annular streamtube

The total thrust over the annulus at radius r is determined by the change in momentum of the air and is given by the following formula:

$$T = \tfrac{1}{2} \cdot \rho \cdot A \cdot \left(V^2 - V_2^2\right) \qquad \textbf{Equation 4-6}$$

Where A is the area of the annulus and V_2 is the axial wind speed in the wake.

An important empirical correction factors is applied at this point, this allows for the tip losses from the blades and is discussed later in the text. For this derivation we shall denote the tip loss factor as F, and this is applied such that the axially induced velocity is given as $V \cdot F \cdot a$ and the swirl velocity by $\Omega \cdot r \cdot F \cdot a`$, therefore $V_1 = V \cdot \left(1 - F \cdot a\right)$ and $V_2 = V \cdot \left(1 - 2F \cdot a\right)$. Substituting this expression in Equation 4-6, we can find an expression for the coefficient of thrust C_H over the annulus. This is given by Equation 4-7[†].

$$C_H = 4 \cdot F \cdot a \cdot \left(1 - F \cdot a\right) \qquad \textbf{Equation 4-7}$$

Solving this quadratic equation, we find that the axial induction factor can be expressed as follows:

$$a = \frac{1}{2 \cdot F} \cdot \left(1 - \sqrt{1 - C_H}\right) \qquad \textbf{Equation 4-8}$$

[†] Wilson[4] states that the modification factor should be incorporated using the format, $C_H = 4F \cdot a \cdot \left(1 - a\right)$. This is in contradiction with his previous work (Wilson[5]) and also that of Stoddard[3].

An expression for the radial induction factor, $a`$, can be found in a similar manner. By considering the conservation of momentum in the annulus, the torque is given by Equation 4-9.

$$Q = 4 \cdot \rho \cdot \pi \cdot r^3 \cdot V_1 \cdot F \cdot a` \cdot \Omega \cdot dr \quad (\text{here } V_1 = V.(1 - a)) \qquad \textbf{Equation 4-9}$$

Equating Equation 4-9 with Equation 4-5 and rearranging to find the radial induction factor yields the following formula:

$$a` = \sigma \cdot \frac{Cl \cdot \sin(\phi) - Cd \cdot \cos(\phi)}{8 \cdot F \cdot \cos(\phi) \cdot \sin(\phi) - \sigma \cdot (Cl \cdot \sin(\phi) - Cd \cdot \cos(\phi))} \qquad \textbf{Equation 4-10}$$

The aerodynamic analysis is then iterative. We must first of all estimate values for a and $a`$, and then proceed through the following steps:

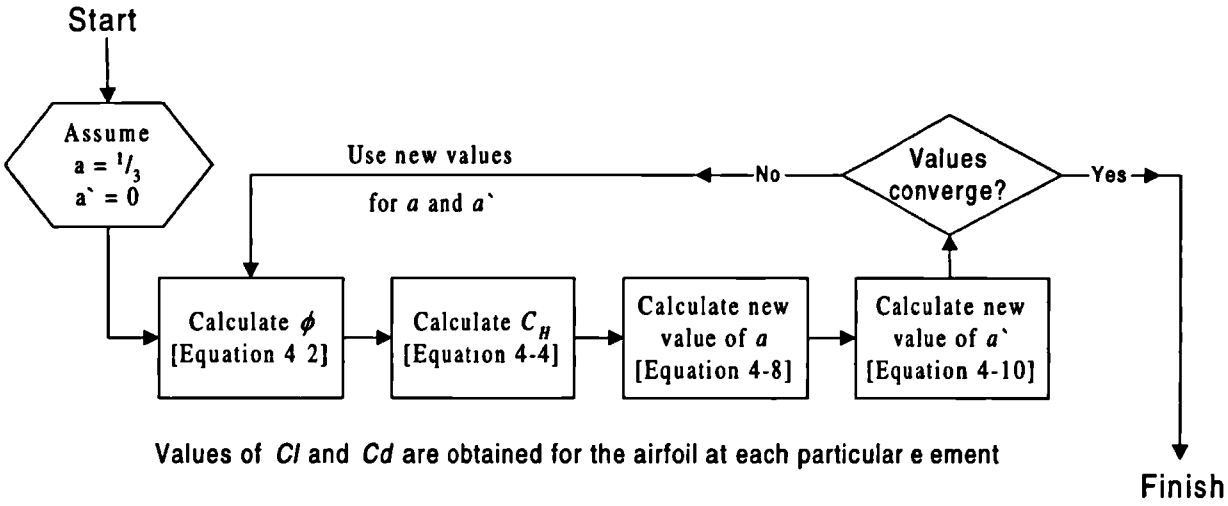

Figure 4-6 Flow chart showing iteration loop in aerodynamic analysis

Momentum theory breaks down when considering axial induction factors greater than $a = 0.5$ because $V_2 = V \cdot (1 - 2 \cdot a)$ becomes invalid. This region is associated with the turbulent wake and vortex ring states. (Stoddard[3] describes wake states.) Glauert[7] compared the results obtained by momentum theory with those typically seen by an airscrew operating in these conditions, and derived an empirical formula to represent the relationships. A similar linear model was derived by Wilson and is used by Snel[8] in the aerodynamic programs written by ECN, the 'Dutch Energy Research Foundation'. This is the method adopted in this study and is shown in Figure 4-7.

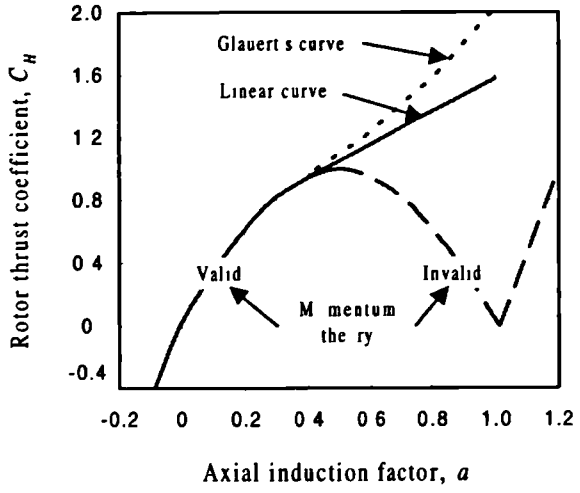

Figure 4-7 Rotor thrust Vs axial induction

The linear turbulent wake model is expressed as Equation 4-11 for values of $a > 0.38$, (i.e. $C_H > 0.9424$). These are consistent with Sharp[1].

$$C_H = 0.96 \cdot F \cdot a + 0.5776 \qquad \textbf{Equation 4-11}$$

Rearranging this formula yields an expression for the axial induction factor given in Equation 4-12.

$$a = \frac{C_H - 0.5776}{0.96 \cdot F} \qquad \textbf{Equation 4-12}$$

This can now be incorporated in Equation 4-8 and used for calculating the axial induction factor within the iterative cycle. This is determined by Equation 4-13.

For $C_H \leq 0.9424$ $\qquad a = \frac{1}{2F} \cdot \left(1 - \sqrt{1 - C_H}\right)$ **Equation 4-13**

or $C_H > 0.9424$ $\qquad a = \frac{1}{F} \cdot \left(\frac{C_H - 0.5776}{0.96}\right)$

4.2.2 Empirical modifications to the equilibrium wake model

There are a number of modifications that can be made to improve the accuracy of the model. Wilson[4] includes details of the following:

1. Tip loss correction
2. Cascade effects on lift and drag

3. Gap correction

Tip loss correction is incorporated using a modified version of Prandtl's original correction factor. Wilson[4] expresses this by the following formula:

$$F = \frac{2}{\pi} \cdot \cos^{-1}\left\{\exp\left(\frac{-B \cdot (R-r)}{2 \cdot r \cdot \sin(\phi)}\right)\right\} \qquad \textbf{Equation 4-14}$$

This correction factor accounts for the effect of vortex sheets behind the rotor tip. Wilson[5] reports a good description of the phenomenon. This correction factor is used in the analysis documented in this thesis.

Cascade effects are caused by blockage due to the blade's finite thickness. This is especially apparent at the blade root and causes the airflow to be accelerated past the blades. This affects the inflow angle to the blade and therefore the loading on the blade. No account of this is taken in the aerodynamic model reported in this thesis. It is unlikely to significantly affect the blade dynamics or the power output as the moment due to a change of force at the blade root is relatively low. In addition to this, verification studies carried out to date show a good correlation between the calculated and measured results without the inclusion of this factor.

Gap correction applies to blades employing partial span pitch control systems, etc. where spaces occur along the blade's length to accommodate the actuating mechanism. All the turbines dealt with in this study have employed full span pitch control and so the inclusion of this factor has proved unnecessary.

In addition to the above we must also consider the problem of 3 dimensional airflow over the rotor blades. The model discussed up till this point is known to yield good results for attached flow, but it becomes unreliable for separated or partially separated flow conditions. Separated flow occurs during blade stall and is therefore more apparent with stall regulated machines. This phenomenon is due to the rotation of the blades. After separation, the air stream takes on a radial flow component along the length of the blade towards the blade tip. This flow is not modelled using the conventional strip theory or vortex theories and is known to yield erroneous results. The topic of 3 dimensional flow is still under investigation and is discussed by Snel[9]. He proposes a semi-empirical formula that modifies the coefficient of lift in the post stall region. This formula is given in Equation 4-15.

$$Cl_{3D} = Cl_{2D} + \Delta Cl \cdot \tanh\left[3 \cdot \left(\frac{c}{r}\right)^2\right]$$ **Equation 4-15**

Where Cl_{2D} is the 2 dimensional coefficient of lift obtained from wind tunnel measurements, c is the chord length, r is the radius to the section and ΔCl is the departure from the linearised lift curve (Cl_{lin}) as shown in Figure 4-8. Cl_{lin} may be found by measurement or from potential flow theory by the formula, $Cl_{lin} = Cl_o + 2\pi \cdot \alpha$, where Cl_o is the lift coefficient when the inflow angle is at zero degrees.

The modified coefficient of lift is shown in Figure 4-8 for a typical wind turbine airfoil section. The post stall portion of the modified curve gives higher lift coefficients than the unmodified part.

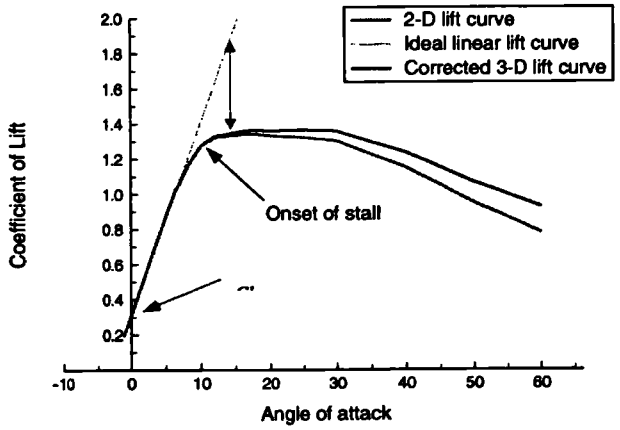

Figure 4-8 Correction for 3-D flow

4.3 Equilibrium power and loading calculations

The equilibrium wake model is used to calculate all the static or slowly varying wind speeds. In this research the equilibrium model is used for the following calculations:

1. Rotor thrust, leading to steady tower base shear and overturning
2. Rotor torque, leading to steady drivetrain loads and braking moments
3. Steady rotor power output
4. Parked loads, leading to parking brake moments

5. Visualising the propagation of stall along the blades

6. Evaluating the wake velocity vectors ready for the frozen wake analysis

Rotor thrust is determined by summing the thrust from each blade element in the discretised model. The formula for this is given in Equation 4-16.

$$T = \tfrac{1}{2} \cdot \rho \cdot B \cdot \sum_{i=1}^{N} V_R^2 \cdot \left(Cl_i \cdot \cos(\phi_i) + Cd_i \cdot \sin(\phi_i) \right) \cdot c_i \cdot \Delta r \qquad \textbf{Equation 4-16}$$

Where T is the rotor thrust in Newtons, B is the number of blades and N is the number of blade elements on each blade.

The coefficient of thrust for the whole rotor is given by Equation 4-17.

$$C_T = \frac{T}{\tfrac{1}{2} \cdot \rho \cdot V^2 \cdot A} \qquad \textbf{Equation 4-17}$$

Where A is the rotor swept area and V is the wind speed incident on the rotor.

The thrust coefficient is usually between 0 and 1. For stall regulated machines it occasionally increases beyond 1 but this is seldom. In these conditions the turbine is said to be operating in propeller brake state. Figure 4-9 shows the thrust and thrust coefficient for a typical turbine. The turbine is a stall regulated upwind machine. It has a rated capacity of $600kW$ at a wind speed of 16 m/s. It operates for wind speeds in the range 5 to 25 m/s [†].

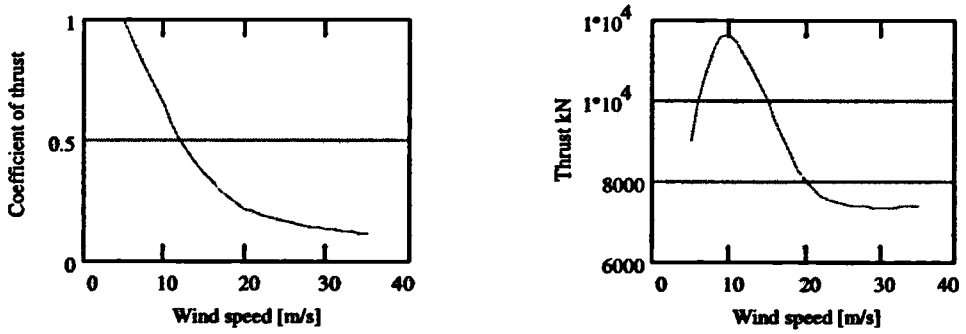

Figure 4-9 Steady rotor thrust curves

[†] Turbine manufacturer and some other details are confidential. See Chapter 8 for more information, the turbine described above is documented as Turbine B.

The rotor torque is determined by summing the in-plane moments on the blade elements. This is accomplished using the following formula:

$$Q = \tfrac{1}{2} \cdot \rho \cdot B \cdot \sum_{i=1}^{N} V_R^2 \cdot \left(Cl_i \cdot \sin(\phi_i) - Cd_i \cdot \cos(\phi_i) \right) \cdot c_i \cdot r_i \cdot \Delta r \qquad \textbf{Equation 4-18}$$

The coefficient of torque is given by Equation 4-19.

$$C_Q = \frac{Q}{\tfrac{1}{2} \cdot \rho \cdot A \cdot V^2 \cdot R} \qquad \textbf{Equation 4-19}$$

Figure 4-10 shows the torque and the coefficient of torque for the same stall regulated turbine.

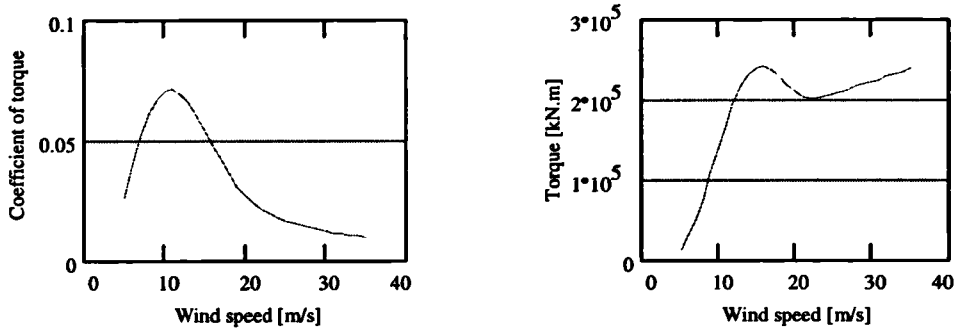

Figure 4-10 Steady rotor torque curves

The steady rotor power is determined from the following formula:

$$P = \tfrac{1}{2} \cdot \rho \cdot B \cdot \sum_{i=1}^{N} V_R^2 \cdot \left(Cl_i \cdot \sin(\phi_i) - Cd_i \cdot \cos(\phi_i) \right) \cdot c_i \cdot r_i \cdot \Omega \cdot \Delta r \qquad \textbf{Equation 4-20}$$

The coefficient of power is given by Equation 4-21.

$$C_P = \frac{P}{\tfrac{1}{2} \cdot \rho \cdot A \cdot V^3} \qquad \textbf{Equation 4-21}$$

Figure 4-11 shows the steady power and the coefficient of power for the stall-regulated turbine. The peak power coefficient, which exceeds 0.46, indicates a well optimised design. This compares well with the theoretical maximum rotor power coefficient which is found to be $Cp_{max} = 0.593$. This is know as Betz limit after Albert Betz, the German aerodynamicist. This is derived using momentum theory and is described by Sharpe[1].

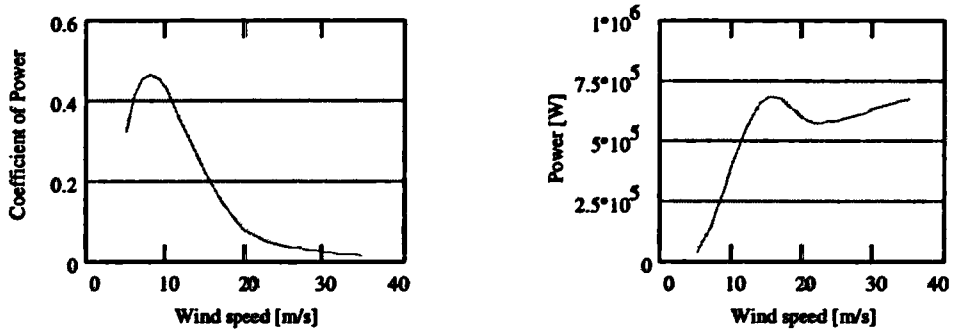

Figure 4-11 Steady rotor power curves

Parked loads are calculated using the blade lift and drag coefficients. The blades are orientated vertically or horizontally and no wake model is necessary. Predicted loads are always very low. However, in practice, turbulence loads are higher than predicted because the current model takes no account of yaw misalignment or directional variation in wind direction. These loads are still relatively small and shouldn't significantly affect the blade or tower design. However they are important when considering the parking brake, which hold the blades.

The onset and propagation of stall can be visualised by producing a surface or contour plot of the ratio of lift to drag coefficients with respect to the wind speed and radial station along the blade. The ratio of *Cl* to *Cd* is used to emphasise the onset of stall as most turbines have a fairly smooth post stall lift behaviour which is difficult to detect on its own. A rise in *Cd* also accompanies the onset of stall and therefore the event is emphasised by using the ratio of the two. A typical stall visualisation plot is shown in Figure 4-12.

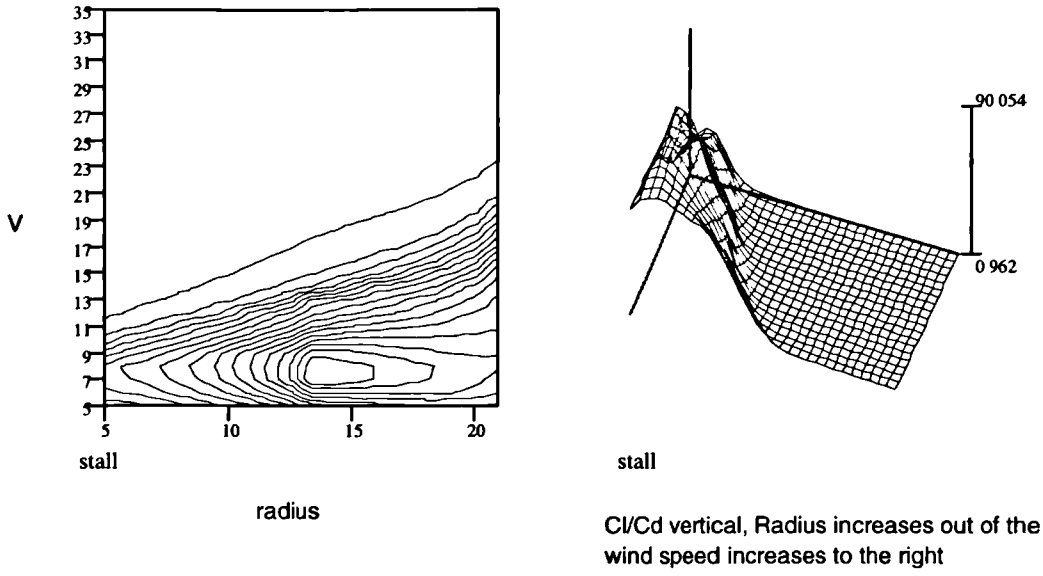

Figure 4-12 Stall visualisation plots

The plot shows the stall behaviour of the turbine blade. The low regions indicate stall. For wind speeds bellow 9.5 *m/s*, we see that the whole blade is in lift, above this stall begins. Stall starts at the blade root and gradually propagates along the length of the blade up to approximately 18 *m/s* where the whole blade is operating in stall. This gradual propagation from the root to the tip reduces the bending moment on the blade and therefore benefits the fatigue life.

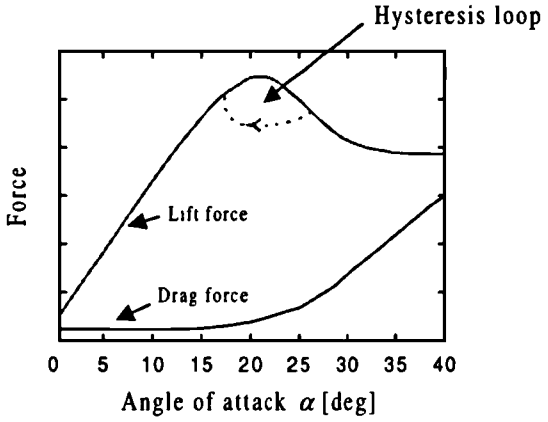

Figure 4-13 Lift and Drag forces on an airfoil

Figure 4-13 shows typical lift and drag forces on a wind turbine airfoil section as it proceeds through stall. An important difference is noticed between the behaviour of this airfoil and one typically used for aircraft production. The maximum lift is deliberately reduced in order to provide a much flatter post stall force variation. In fact in many turbines this can be flatter than the pre-stall curve. This is undertaken so stall can be used to regulate the power and speed of the turbine. Using stall regulation, and airfoils with this flat post stall curve, reduces dynamic loads and hence the fatigue damage in the structure.

The figure also illustrates a phenomenon known as stall hysteresis. As an airfoil is pitched into stall it follows the continuous line in the figure. If it is then brought back out of stall it follows the dotted line. This hysteresis causes problems with the linearisation process that is discussed later in Chapter 8.

4.4 Calculating the quasi-static aerodynamic gain factors

Quasi-static gain factors are used in the dynamic analysis of wind turbines that are subjected to rapidly varying turbulent loads. Gain factors are defined to relate variations in wind speed to variations in blade force. We are particularly interested in the in-plane (axial) and out-of-plane (tangential) blade forces which result due to the following reasons:

1. Variations in the incident wind speed
2. Variations in the tangential blade speed
3. Variations in the blade pitch angle

The notation employed is expressed in Figure 4-14. Using these gain factors allows us to calculate the blade load due to the turbulent variations in wind speed and also the aerodynamic damping due to motion of the turbine and blades.

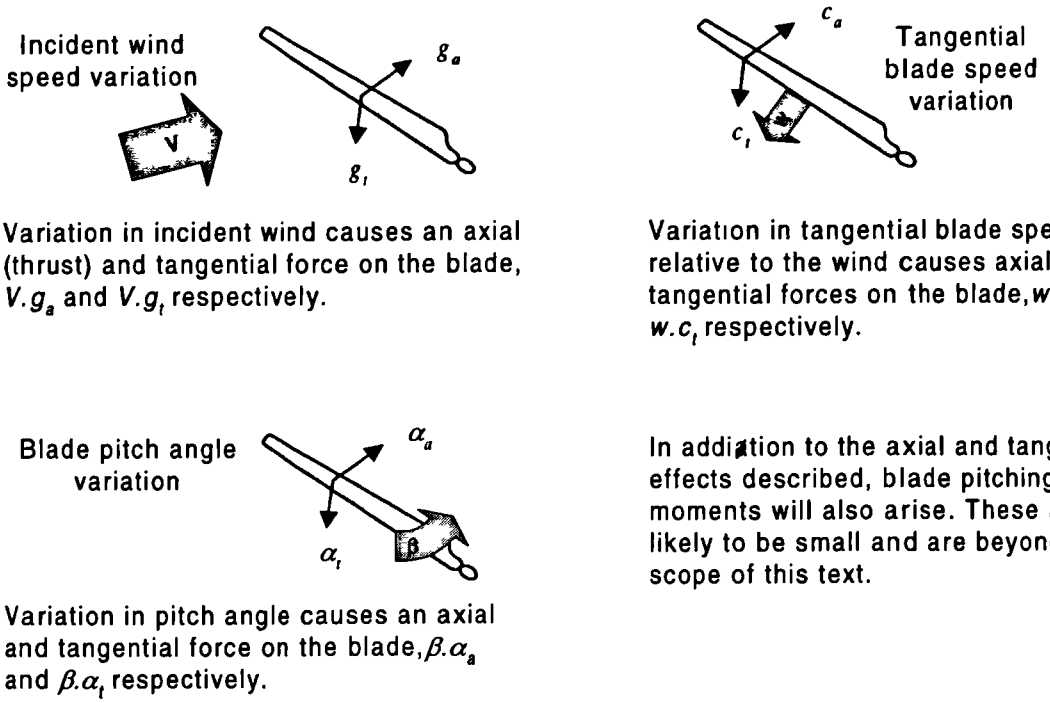

Figure 4-14 Notation for linear gain factors

The gain factors are calculated by considering how changes to the inflow vector affect the axial and tangential loads. The wake velocity vector is frozen at the mean wind speed.

This thesis is only concerned with frequency domain analysis and for this reason we are only interested in the linearised gain factors. The linearised gain factors are calculated over an interval Δu around the mean wind speed, this is illustrated in Figure 4-15 for the axial gain factor g_a. The figure shows the effect on axial load as the wind speed varies between 0 and 25 *m/s*. The equilibrium wake was calculated at a mean wind speed of 16 *m/s*.

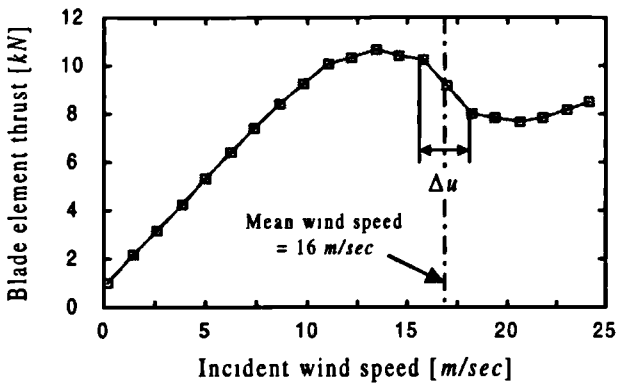

Figure 4-15 Blade element thrust

This figure clearly shows the non-linear behaviour of the actual turbine blade over the wind speed range 0 to 25 *m/sec*. In addition to this we must also consider the effect of stall hysteresis, which is not illustrated in the figure but also adds non-linearities to the response. However it should be noted that the range of the wind turbulence (Δu) is relatively small and for all pre-stall cases the turbine blade approximates very well to a linear curve. We can get a good indication of the range of the turbulent wind speed by considering the turbulence statistics. According to ESDU 85020[10], it is reasonable to assume that the probability density function (pdf) of amplitude follows a 'normal' or Gaussian distribution [†]. Using this we can therefore determine confidence intervals for the range of turbulent winds: some principal results are tabulated in Table 4-1.

Confidence	Turbulent amplitude range	
50%	$\pm 0.68\sigma_u$	
95.44%	$\pm 2\sigma_u$	Where $\sigma_u = I_u \cdot V$
99.73%	$\pm 3\sigma_u$	and I_u is the turbulence
99.9%	$\pm 3.29\sigma_u$	intensity

Table 4-1 Confidence intervals for turbulent wind speed ranges

If the pre-stall, frozen wake curves are linear in the range $V \pm 2\sigma_u$, we can be fairly certain (95.44%) that the actual wind speed will not exceed these extremes and the response will also be linear. For the post-stall case linearisation is more difficult because the blade load follows the stall hysteresis loop. This incurs high non-linearities and greatly influences the response. More information on this effect is

[†] Actually for heights below 30m it becomes slightly narrower banded than the Gaussian distribution, therefore the calculation discussed here will be more conservative at these smaller heights.

required before any serious attempt at linearisation can be carried out in this region. Stall hysteresis is neglected in the current aerodynamic model and the linear gain factor is calculated using the simple expression given in Equation 4-22.

$$g = \frac{F(V + \frac{1}{2}\Delta u) - F(V - \frac{1}{2}\Delta u)}{\Delta u} \qquad \textbf{Equation 4-22}$$

Where $F(v)$ is the force resulting from a wind speed of v *m/sec.*

An account of the accuracy of this model is given in Chapter 8.

4.5 Practical considerations

The aerodynamic calculations described in this chapter serve as a pre-processor for the structural dynamic analysis. The blade discretisation used for the aerodynamic analysis must relate to that used for the structural analysis. Effectively the aerodynamic loads will be applied to the node points in the structural mesh. Figure 4-16 Illustrates the two element meshes used to analyse a typical turbine blade.

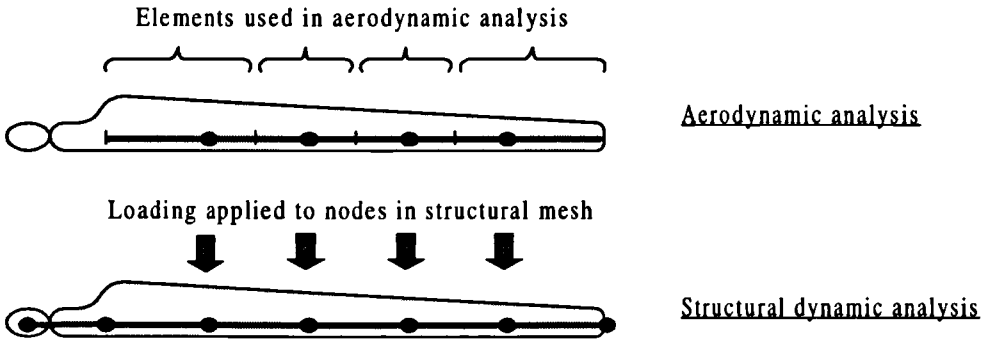

Figure 4-16 The relationship between aerodynamic and structural dynamic blade mesh

It is important that we consider how many elements to use in the mesh. From a structural dynamic perspective this is decided by the agreement between calculated and measured natural frequencies within the first few modes of vibration. In the aerodynamic case an analysis is carried out to compare the rotor thrust and torque coefficients obtained using a relatively small number of elements, with those obtained from a much denser mesh.

Using this approach it is found that an adequate representation of the blade can be made using relatively few aerodynamic elements. Figure 4-17 Illustrates the error as the number of blade elements used decrease from 20 to 1. A rapid convergence is noted.

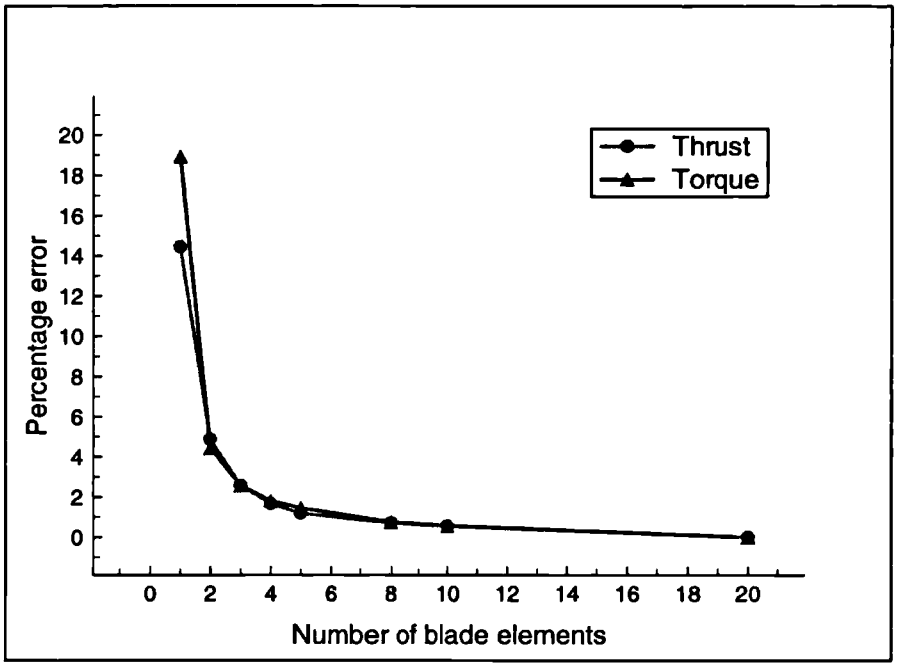

Figure 4-17 Percentage error in rotor thrust and torque with deminishing number of elements

A model validation exercise carried out by the author in conjunction with WS Atkins[11] is discussed at length in Chapter 8. This exercise highlights the accuracy of the gain factors in predicting pre-stall loads on the blades but shows discrepancies in the post-stall prediction. Blade stall commences at the root and propagates along the length of the blade towards the tip. While we have shown that only a few blade elements are required to calculate the equilibrium wake forces, more are necessary to increase the resolution of the model as stall propagates along the blade.

4.6 Conclusion

In this chapter a detailed description of the aerodynamic behaviour of wind turbines has been presented. The mathematical model chosen for the analysis is based on Glauert's annulus momentum vortex theory (strip theory) which was chosen because

of its relative simplicity and rapid calculation. To improve the model's representation, the author has included various state-of-the-art modification factors. In particular a new correction factor has been introduced to take account of the 3 dimensional flow regime in the post stall state. The model has been verified and found to give excellent agreement with measured power curves.

The post stall behaviour of wind turbines is a complicated non-linear problem and hence difficult to model in the frequency domain. A very simple linearisation method is proposed in this chapter and various aerodynamic gain factors derived which are used throughout the thesis to obtain the aerodynamic loads on the structure. Further research is still required, however, to improve the linearisation of the post stall regions since this has been found to be erroneous. (See Chapter 8 for more details.)

[1] Sharpe D.J. (1990). "Wind energy conversion systems." Edited by Freris L.L., Prentice Hall International. ISBN 0-13-960527-4

[2] Lindenburg C. Technical manual to the FATAS computer program. ECN, SU General Services, Petten, The Netherlands.

[3] Stoddard F.S and Eggleston D.M (1987). "Wind turbine engineering design." Van Nostrand Reinhold, ISBN 0-442-22195-9

[4] Wilson R.E (1995). "Wind turbine technology. Fundamental concepts of wind turbine engineering." Edited Spera D.A., ASME Press, ISBN 0-7918-1205-7

[5] Wilson R.D and Lissaman B.S (1974). "Applied aerodynamics of wind power machines." Oregon State University.

[6] Abbott I.H. and von Doenhoff A.E. (1959). "Theory of wing sections, including a summary of airfoil data." New York: Dover Publications, Inc.

[7] Glauert H (1926). "The analysis of experimental results in the windmill brake and vortex ring states of an airscrew." Reports and Memoranda, No. 1026, London: Aeronautical Research Committee.

[8] Snel. H. (1993). Personal correspondence. ECN, Petten, The Netherlands.

[9] Snel H, et al. (1993). "Sectional prediction of 3-D effects for stalled flow on rotating blades and comparison with measurements." Proceedings. European Community Wind Energy Conference, 1993.

[10] ESDU 85020 (1993). "Characteristics of atmospheric turbulence near the ground. Part II: single point data for strong winds (neutral atmosphere)." ESDU international plc, London.

[11] WS Atkins Ltd. (1996). "Summary of results for validation of wind turbine model." Personal correspondence with Ian Ward, WS Atkins Ltd. Woodcote Grove, Ashley Road. Epsom, Surrey. England.

5. Modelling the wind turbine loads

5.1 Rotational sampling of wind turbulence

The observed wind speed on a rotating blade may be substantially different from that on a fixed position derived earlier in Chapter 3. If the rotor swept area of the turbine is much smaller than the size of the eddies, ${}^{r}L_{u}$, then the observed wind speed will be the same for a rotating blade as for a fixed position. (i.e. the rotor will be engulfed by the turbulence.) However if the eddy is smaller than the rotor area then the rotor will periodically sample the eddy with each rotation until the eddy has effectively passed through the rotor plane. The average period taken for the eddy to pass through the rotor plane is given by Equation 5-1.

$$b = \frac{{}^{x}L_{u}}{V_{z}} \qquad \textbf{Equation 5-1}$$

If the rotor period is shorter than this then the eddy will be sampled many times before passing through the rotor. Later we will see the effect this has on the rotor loading.

Rosenbrock[1] first considered the rotational sampling phenomenon in 1955. However, it was not until the early 1980's that a significant interest in the subject began to develop. Connell[2] in 1982 compared measured data with that calculated from a time domain simulation of the process. Later he published his "Primer of turbulence at the wind turbine rotor" (Connell[3]) explaining the phenomenon in a qualitative way. Today many computer packages will evaluate the response of turbines to rotationally sampled turbulence. The majority of these are based on time domain simulation.

Towards the mid 1980's work was taking place on the frequency domain analysis of turbulence. At ECN, Dragt[4,5,6 & 7] discusses the phenomenon of rotationally sampled turbulence and the loading imposed on a rigid turbine.

In this chapter we look at the phenomenon in the frequency domain and derive expressions for calculating the loading on a rigid turbine. In Chapter 6 this model is extended to include structural flexibilities.

5.1.1 Conceptual introduction to rotational sampling

The principle behind rotational sampling is best demonstrated by example in the time and frequency domains. Consider the effect of a single sinusoidal eddy $\varepsilon(t)$ with frequency f *Hz* passing through the rotor plane. The eddy has unit amplitude at its centre and this decays in proportion to the coherence function as you travel away from the centre in any vertical or lateral direction. Figure 5-1 shows an observer '*i*' seated on a rotating blade revolving with frequency P *Hz*. He passes through the centre of the eddy with each revolution, the distance away from the centre $d(t)$ at any time can be calculated. The wind speed witnessed by the observer is therefore given as the product of the sinusoidal eddy $\varepsilon(t)$ and the coherence sampling function $\gamma(f,d(t))$ for any point in time t. The eddy is said to be 'amplitude modulated.'

To determine the response in the frequency domain we can now take the Fourier Transform of the time histories and calculate the PSDs as illustrated in Figure 5-1. The PSD of a single sinusoidal eddy is defined as its mean square amplitude and is therefore given as a spike with area ½ $(m/s)^2/Hz$. (In Figure 5-1 the frequency interval Δf is 1 and therefore the height of the spike is equal to its area.) The PSD of the coherence sampling function can be found algebraically and is derived later. From these two PSDs we can calculate the area of each spike in the resulting PSD by taking half the product of the PSD of the original eddy (½ $(m/s)^2/Hz$) and the PSD of the coherence sampling function at frequency mP, where m is any positive integer. The wind speed spectrum witnessed by the rotating observer is characterised by Doppler shifting. The eddy $\varepsilon(t)$ is Doppler shifted to higher frequencies each centred around harmonics of the rotor frequency P.

From this simple illustration we can see how the analysis proceeds in the frequency domain. The procedure above is repeated for each eddy that comprises the turbulent gust.

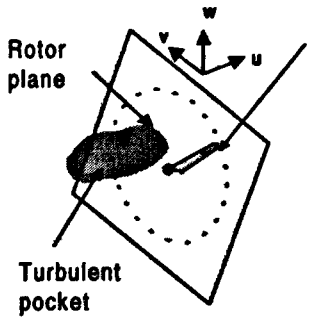

Observer seated on rotor blade witnesses the turbulence on a number of occasions before it completely passes through the rotor plane

Consider a single turbulent eddy of frequency f = 1Hz rotationally sampled by a rotor blade rotating at P = 8Hz.

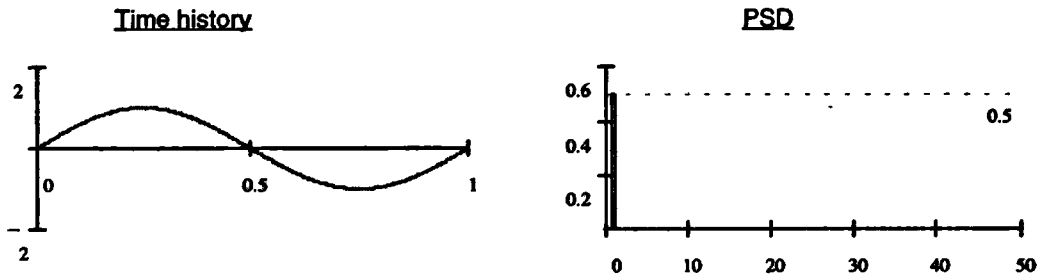

Sinusoidal eddy

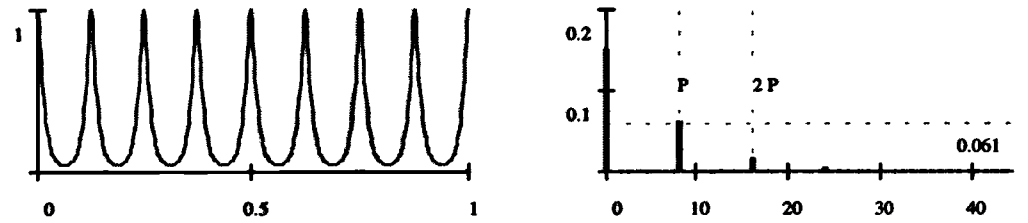

Coherence sampling function

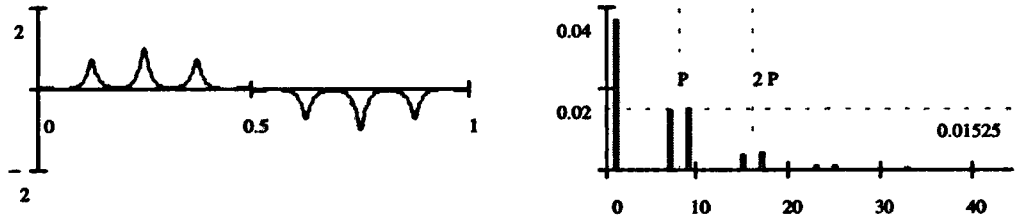

Product of eddy and sampling function

Responses are Doppler shifted by f to the left and right hand sides of the harmonics of the rotor frequency. (i.e. P , 2P , 3P . ...)

The ordinate height of the responses are found by taking half the product of the PSDs for the eddy and the sampling function.

E.g. for the first harmonic

½ x 0.5 x 0.061 = 0.015

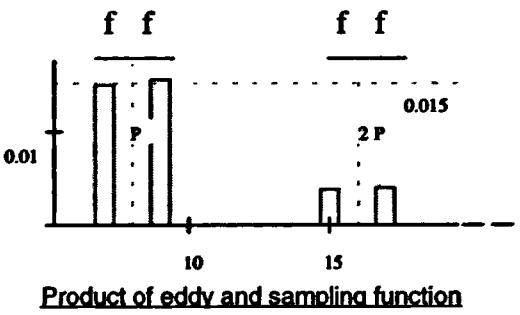

Product of eddy and sampling function

Figure 5-1 Rotational sampling of a single eddy

5.2 Auto-power spectra of wind speed at a single point on a rotor blade

For calculation purposes the blades are discretised into a number of elements. The Auto-power spectrum can be calculated for each element and the Cross-power spectrum calculated between each pair of elements. Using this information we can then determine the blade loads, this is described later in the chapter. In this section we consider the Auto-power spectrum of wind speed witnessed by a blade element *i*. All angular measurements are expressed in radian units in the following sections. Dragt[4] first derived the original theories expressed in this section.

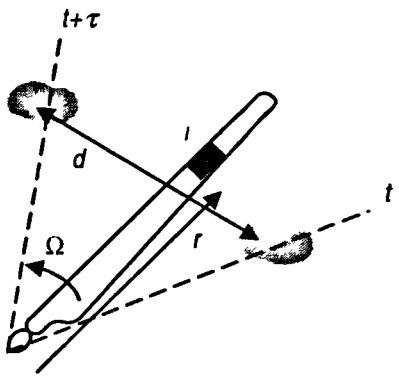

Figure 5-2 Auto-power spectrum for a blade element

Consider the wind speed witnessed by an observer situated *r* metres along a blade at element *i*. The blade is rotating with a constant frequency Ω *rad/sec*. It passes through two random processes, *u* at time *t* and *v* at time $t+\tau$. The Auto-covariance, rotationally witnessed by the blade element, is seen to be the same as the Cross-covariance between the two random processes *u* and *v*. An expression for the rotationally sampled Auto-covariance is therefore expressed in Equation 5-2.

$$\tilde{C}_{ii}(\tau) = E\{u(t)\cdot v(t+\tau)\} = C_{uv}(\tau) \qquad \textbf{Equation 5-2}$$

Where $\tilde{C}_{ii}(\tau)$ is the rotationally sampled Auto-covariance function at blade element *i*, $C_{uv}(\tau)$ is the Cross-covariance function between the two random processes *u* and *v*, and $E\{\}$ is the expectation operator defined by the expression $E\{y(t)\} = \lim_{T\to\infty}\left\{\frac{1}{T}\cdot\int_{-T/2}^{T/2} y(t)dt\right\}$. This is valid as the processes are stationary and $i(t) = u(t)$ at time *t*, and $i(t+\tau) = v(t+\tau)$ at time $t+\tau$.

If we assume that processes *u* and *v* are statistically similar and have the same Auto-power spectra (i.e. the turbulence is homogeneous across the rotor plane), the cross covariance function can be determined in terms of the coherence function. This was derived for double sided spectra in Equation 3-16, and single sided spectra in Equation 3-17. All the derivations in this chapter use double sided spectra, however

later we will prove that single sided spectra may be used for all the calculations. The rotationally sampled Auto-covariance function can therefore be found by Equation 5-3.

$$\tilde{C}_{ii}(\tau) = C_{uv}(\tau) = \int_{-\infty}^{\infty} \gamma(\omega, d(\tau)) \cdot S_{uu}(\omega) \cdot e^{i\cdot\omega\cdot\tau} d\omega \qquad \textbf{Equation 5-3}$$

Where $\gamma(\omega,d)$ is the coherence function for lateral separation given by ESDU 86010[8] as Equation 3-20. $S_{uu}(\omega)$ is the double sided Auto-power spectrum of wind speed. This can be determined from the formulation for the single sided spectrum given by ESDU 85020[9] in Equation 3-14. $d(\tau)$ is the separation distance between the two processes at time τ. This is determined by the equation $d(\tau) = \sqrt{2r^2 \cdot (1 - \cos(\Omega \cdot \tau))}$

Now the rotationally sampled Auto-power spectral density function $\tilde{S}_{ii}(\omega)$ can be obtained by taking the Fourier transform of the rotationally sampled covariance function $\tilde{C}_{ii}(\tau)$.

$$\tilde{S}_{ii}(\omega) = \int_{-\infty}^{\infty} \tilde{C}_{ii}(\tau) \cdot e^{-i\cdot\omega\cdot\tau} d\tau \qquad \textbf{Equation 5-4}$$

i.e.

$$\tilde{S}_{ii}(\omega) = \int_{-\infty}^{\infty} \left\{ \int_{-\infty}^{\infty} \gamma(\upsilon, d(\tau)) \cdot S_{uu}(\upsilon) \cdot e^{i\cdot\upsilon\cdot\tau} d\upsilon \right\} \cdot e^{-i\cdot\omega\cdot\tau} d\tau$$

Simplifying yields

$$\tilde{S}_{ii}(\omega) = \int_{-\infty}^{\infty} S_{uu}(\upsilon) \cdot \left\{ \int_{-\infty}^{\infty} \gamma(\upsilon, d(\tau)) \cdot e^{-i(\omega-\upsilon)\cdot\tau} d\tau \right\} d\upsilon$$

Now $d(\tau)$ is an even function and periodic in time τ with period $^{2\pi}/_{\Omega}$, hence the coherence function, $\gamma(\upsilon,d(\tau))$, is also even and periodic. It is beneficial to express this using a cosine Fourier series as Equation 5-5.

$$\gamma(\upsilon, d(\tau)) = \sum_{n=-\infty}^{\infty} K_n(\upsilon) \cdot e^{i\,n\,\Omega\cdot\tau} \qquad \textbf{Equation 5-5}$$

Where

$$K_n(\upsilon) = \frac{\Omega}{2\cdot\pi} \int_{-\pi/\Omega}^{\pi/\Omega} \gamma(\upsilon, d(\tau)) \cdot e^{-i\,n\,\Omega\cdot\tau} d\tau$$

This may be simplified to $$K_n(\upsilon)=\frac{1}{\pi}\int_0^{\pi}\gamma(\upsilon,d(\theta))\cdot\cos(n\cdot\theta)d\theta$$

where $d(\theta)=\sqrt{2r^2\cdot(1-\cos(\theta))}$ and n is the Fourier variable pertaining to a frequency $n\Omega$.

Now substituting Equation 5-5 into Equation 5-4 yields the following expression

$$\tilde{S}_{ii}(\omega)=\int_{-\infty}^{\infty}S_{uu}(\upsilon)\cdot\left\{\int_{-\infty}^{\infty}\sum_{n=-\infty}^{\infty}K_n(\upsilon)\cdot e^{-i\cdot\omega-\upsilon-n\Omega\ \tau}d\tau\right\}d\upsilon \qquad \textbf{Equation 5-6}$$

Noting that $\int_{-\infty}^{\infty}e^{i\sigma\cdot\tau}d\tau=\delta(\sigma)$, where $\delta(\sigma)$ is Dirac's delta function defined by the relationships $\delta(\sigma)=1$ when $\sigma=0$ and $\delta(\sigma)=0$ for all non zero values of σ, the expression reduces to Equation 5-7.

$$\tilde{S}_{ii}(\omega)=\int_{-\infty}^{\infty}S_{uu}(\upsilon)\cdot\left\{\sum_{n=-\infty}^{\infty}K_n(\upsilon)\cdot\delta(\omega-\upsilon-n\cdot\Omega)\right\}d\upsilon \qquad \textbf{Equation 5-7}$$

Integrating yields the expression: $$\tilde{S}_{ii}(\omega)=\sum_{n=-\infty}^{\infty}K_n(\omega-n\cdot\Omega)\cdot S_{uu}(\omega-n\cdot\Omega)$$

Figure 5-3 shows the Auto-power spectrum of rotationally sampled wind speed calculated for some point on a rotor blade revolving with frequency Ω *rad/sec*. Each n^{th} component is seen to be Doppler shifted by $n.\Omega$ *rad/sec*. The total response is found by summing all the individual n components, however the plot clearly demonstrates how little influence distant harmonics have on each other. For instance, if we are considering the response about the n=1 harmonic, then we observe that the contribution made by the n=-1 harmonic is so small it may be neglected. Equation 5-7 therefore may be simplified by taking the summation over a reduced number of harmonics. Sørensen[10] assumes no aliasing between neighbouring harmonics at all. This implies that for the n=1 harmonic, for example, no contribution is made by any other harmonic. This gives rise to a lower mid-harmonic dip in the spectrum. No verification of this assumption is given by Sørensen, however quantitative tests carried out by the author in the course of this work suggest typical errors of 0-7% for the area under the Auto- and Cross-power spectral density curves. The higher error

levels are observed when considering high mean wind speeds and low surface roughness values such as off-shore winds. However the errors are not significantly high. In this text the author has decided to allow aliasing between adjacent harmonics (e.g. for the n=1 harmonic, contributions are included for both the n=0 and the n=2 harmonics but no others.) This is done to minimise the error seen by Sørensen for offshore wind conditions while also saving computation time.

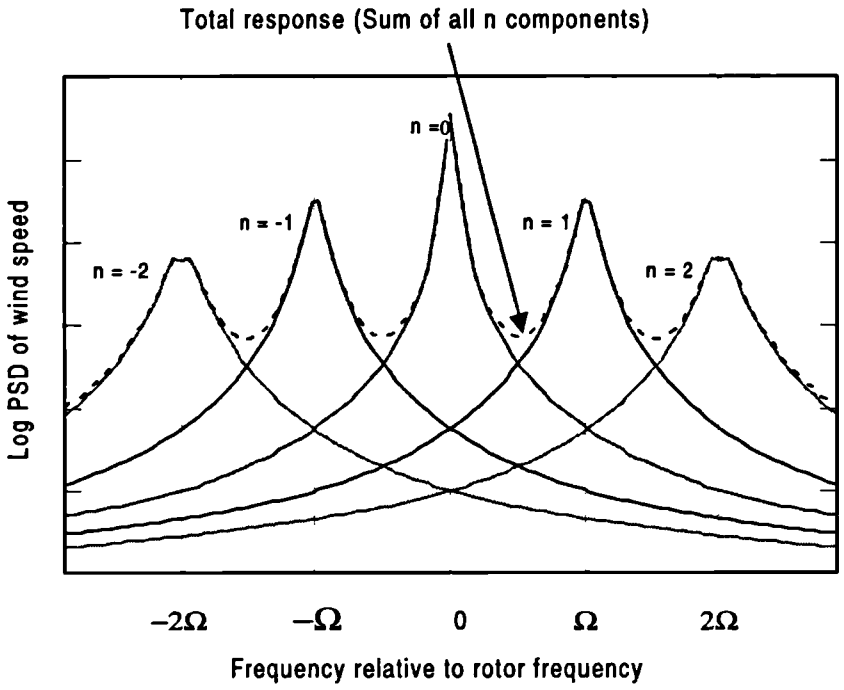

Figure 5-3 Double sided Auto-power spectrum of rotationally sampled wind

The double sided Auto-power spectrum in Figure 5-3 is seen to be real and symmetric about the origin. This can be seen in Equation 5-7 because both the Auto-power spectra of the wind $S_{uu}(\omega)$ and the Fourier coefficient $K_n(\omega)$ are symmetric. ($K_n(\omega)$ being an even function expressed as a cosine Fourier series.) Equation 5-7 can therefore be expressed as a single sided spectrum by Equation 5-8.

$$\tilde{G}_u(\omega) = \sum_{n=-\infty}^{\infty} K_n(|\omega - n\cdot\Omega|)\cdot G_{uu}(|\omega - n\cdot\Omega|) \qquad \textbf{Equation 5-8}$$

where $\tilde{G}_u(\omega)$ is the single sided rotationally sampled Auto-power spectral density function for values of $\omega \geq 0$.

Figure 5-4 shows a typical single sided PSD of rotationally sampled wind turbulence and compares this with the PSD measured at a stationary point in space. The Doppler shifts are clearly apparent in the lower frequency rotor harmonics.

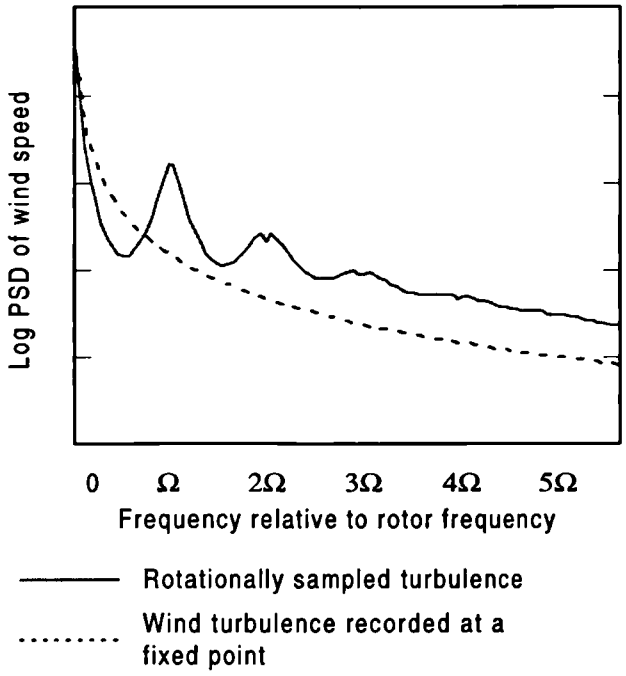

Figure 5-4 Single sided PSD of wind turbulence

5.2.1 Cross-power spectra of wind speed between two points on two rotor blades.

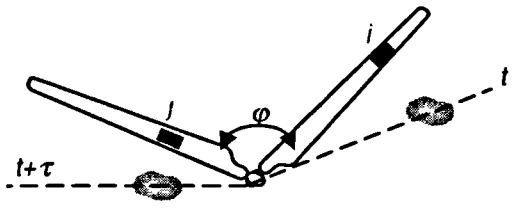

Figure 5-5 Cross-power spectra between blade elements

Consider the wind speed witnessed by two observers situated on elements *i* and *j* of two rotating turbine blades shown in Figure 5-5. The blades are rotating with constant frequency Ω *rad/sec*. At time *t*, blade element *i* passes through the random process *u*, and at time $t+\tau$ element *j* passes through process *v*. The Cross-covariance rotationally witnessed by the two blade elements is seen to be the same as the Cross-covariance between the two random processes *u* and *v*. An expression for the rotationally sampled Cross-covariance, $\tilde{C}_{ij}(\tau)$, can therefore be expressed as Equation 5-9.

$$\tilde{C}_{ij}(\tau) = E\{u(t) \cdot v(t+\tau)\} = C_{uv}(\tau)$$ **Equation 5-9**

Where $\tilde{C}_{ij}(\tau)$ is the rotationally sampled Cross-covariance function between blade elements *i* and *j*, $C_{uv}(\tau)$ is the Cross-covariance function between the two random processes *u* and *v*, and $E\{\}$ is the expectation operator.

If the processes u and v are statistically similar and have the same Auto-power spectra (i.e. the turbulence is homogeneous across the rotor plane,) the Cross-covariance function can be determined in terms of the coherence function as Equation 5-10.

$$\tilde{C}_{ij}(\tau) = C_{uv}(\tau) = \int_{-\infty}^{\infty} \gamma(\omega, d(\tau)) \cdot S_{uu}(\omega) \cdot e^{i\omega\tau} d\omega$$ **Equation 5-10**

This is a similar form to Equation 5-3, however the separation distance $d(\tau)$ is determined by the equation; $d(\tau) = \sqrt{r_i^2 + r_j^2 - 2 \cdot r_i \cdot r_j \cdot \cos(\Omega \cdot \tau + \varphi)}$ where φ is the angle between the two blades in radians and r_i and r_j are the radii along each blade to the two blade elements *i* and *j*.

Now the rotationally sampled Cross-power spectral density function $\tilde{S}_{ij}(\omega)$ can be obtained by taking the Fourier transform of the cross-covariance function $\tilde{C}_{ij}(\tau)$ as shown earlier in Equation 5-4.

$$\tilde{S}_{ij}(\omega) = \int_{-\infty}^{\infty} \tilde{C}_{ij}(\tau) \cdot e^{-i\cdot\omega\tau} d\tau$$ **Equation 5-11**

i.e.

$$\tilde{S}_{ij}(\omega) = \int_{-\infty}^{\infty} \left\{ \int_{-\infty}^{\infty} \gamma(\upsilon, d(\tau)) \cdot S_{uu}(\upsilon) \cdot e^{i\upsilon\tau} d\upsilon \right\} \cdot e^{-i\omega\tau} d\tau$$

Simplifying yields

$$\tilde{S}_{ij}(\omega) = \int_{-\infty}^{\infty} S_{uu}(\upsilon) \cdot \left\{ \int_{-\infty}^{\infty} \gamma(\upsilon, d(\tau)) \cdot e^{-i(\omega-\upsilon)\tau} d\tau \right\} d\upsilon$$

$d(\tau)$ is periodic in time τ with period $^{2\pi}/_{\Omega}$, hence the coherence function, $\gamma(\upsilon, d(\tau))$, is also periodic. The coherence function can therefore be expressed using the Fourier series, however it is not an even function as previously found in Equation 5-5 and

cannot be expressed using only the cosine series. Using the full exponential form of the Fourier series therefore, the coherence function can be defined as Equation 5-12.

$$\gamma(\upsilon,d(\tau))=\sum_{n=-\infty}^{\infty}F_n(\upsilon)\cdot e^{i\,n\,\Omega\,\tau} \qquad \textbf{Equation 5-12}$$

where $F_n(\upsilon)$ is the exponential Fourier coefficient defined as

$$F_n(\upsilon)=\frac{1}{\pi}\cdot\int_0^{\pi}\gamma(\upsilon,d(\theta))\cdot e^{-i\,n\,\theta}d\theta$$

and $d(\theta)=\sqrt{r_i^{\,2}+r_j^{\,2}-2\cdot r_i\cdot r_j\cdot\cos(\theta+\varphi)}$

An additional simplification can be carried out by observing the differences between Equation 5-12 and Equation 5-5. It can be shown that $F_n(\upsilon)=K_n(\upsilon)\cdot e^{i\,n\,\varphi}$, using this relationship Equation 5-12 may be simplified to the form given in Equation 5-13.

$$\gamma(\upsilon,d(\tau))=\sum_{n=-\infty}^{\infty}K_n(\upsilon)\cdot e^{i\cdot n\,\varphi}\cdot e^{i\,n\,\Omega\,\tau} \qquad \textbf{Equation 5-13}$$

where

$$K_n(\upsilon)=\frac{1}{\pi}\int_0^{\pi}\gamma(\upsilon,d(\theta))\cdot\cos(n\cdot\theta)d\theta$$

and $d(\theta)=\sqrt{r_i^2+r_j^2-2\cdot r_i\cdot r_j\cdot\cos(\theta)}$ and n is the Fourier variable pertaining to a frequency $n\Omega$.

Substituting Equation 5-13 into Equation 5-11 yields the following expression:

$$\tilde{S}_{ij}(\omega)=\int_{-\infty}^{\infty}S_{uu}(\upsilon)\cdot\left\{\int_{-\infty}^{\infty}\sum_{n=-\infty}^{\infty}K_n(\upsilon)\cdot e^{i\,n\,\varphi}\cdot e^{-i\,(\omega-\upsilon-n\,\Omega)\tau}d\tau\right\}d\upsilon \qquad \textbf{Equation 5-14}$$

This expression is similar to that given in Equation 5-6 and may be simplified in a similar way by using Dirac's delta function, now the expression reduces to Equation 5-15.

$$\tilde{S}_{ij}(\omega)=\int_{-\infty}^{\infty}S_{uu}(\upsilon)\cdot\left\{\sum_{n=-\infty}^{\infty}e^{i\,n\cdot\varphi}\cdot K_n(\upsilon)\cdot\delta(\omega-\upsilon-n\cdot\Omega)\right\}d\upsilon \qquad \textbf{Equation 5-15}$$

Integrating yields: $\tilde{S}_{ij}(\omega)=\sum_{n=-\infty}^{\infty}e^{i\cdot n\,\varphi}\cdot K_n(\omega-n\cdot\Omega)\cdot S_{uu}(\omega-n\cdot\Omega)$

The expression can be seen to yield the same results as Equation 5-7 when $\varphi = 0$ and $r_1 = r_2$, i.e. the rotationally sampled Auto-power spectral density function for one point on a blade. If we consider the Cross-power spectral density function between two points on one blade, the exponential term, $e^{i n \varphi} = 1$ as $\varphi = 0$. The resultant spectra will therefore be symmetric as $S_{uu}(\omega)$ and $K_n(\omega)$ are both symmetric and real. The spectra may therefore be expressed as a single sided spectra. If we now consider the Cross-power spectra between two points on different blades we now see that the resultant spectra will be complex because of the exponential term. The spectra is still symmetric however in the definition given in Chapter 2.1.5 because the negative frequency portion is the complex conjugate of the positive frequency portion. All Cross-power spectra therefore can be expressed as single sided spectra. The single sided, rotationally sampled, Cross-power spectral density function is given in Equation 5-16.

$$\tilde{G}_{ij}(\omega) = \sum_{n=-\infty}^{\infty} e^{i \cdot n \cdot \varphi} \cdot K_n(|\omega - n \cdot \Omega|) \cdot G_{uu}(|\omega - n \cdot \Omega|) \qquad \textbf{Equation 5-16}$$

If we now consider the reverse Cross-power spectra, $\tilde{G}_{ji}(\omega)$, we can note an interesting relationship with the original $\tilde{G}_{ij}(\omega)$. The Cross-power between two elements on the same blade is always real. With the reverse Cross-power we see that r_1 and r_2 are reversed and so it too will be real and equal to the original, i.e. $\tilde{G}_{ji}(\omega) = \tilde{G}_{ij}(\omega)$. If we now consider the Cross-power between two points on different blades we see that as well as r_1 and r_2 being reversed, the angle between the blades becomes negative, i.e. $-\varphi$. This changes the exponential term in Equation 5-16 and therefore yields the complex conjugate. Using this relationship then we can state the general case that the reverse Cross-power is the complex conjugate of the original Cross-power. This is expressed in Equation 5-17.

$$\tilde{G}_{ji}(\omega) = \overline{\tilde{G}_{ij}(\omega)} \qquad \textbf{Equation 5-17}$$

where $\overline{\tilde{G}_{ij}(\omega)}$ denotes the complex conjugate.

5.2.2 The Cross-power spectral matrix

The mathematical model derived so far in this chapter is based on that developed by Dragt. Use of the model for structural dynamic analysis, however, is greatly facilitated by employing a matrix formulation. The author has therefore introduced a new technique for quickly determining the cross-power spectral matrix based on the observations made in the previous section.

In Chapter 2.3.7 we introduced the matrix form of representing the various Cross-power spectral density functions. The individual Auto- and Cross-power terms calculated above may be represented in matrix form as $\left[\tilde{G}_{ij}(\omega)\right]$. The matrix is expressed as a function of frequency ω and so a different matrix will result for each frequency. Figure 5-6 illustrates the matrix for a typical 3 bladed turbine with 2 elements per blade.

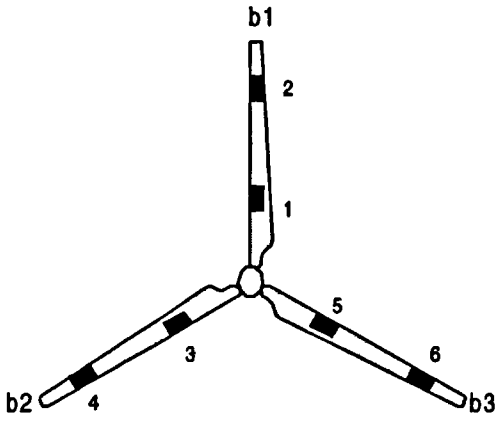

Consider a three bladed turb ne with two elements per blade. The Cross-power spectra between each element may be arranged in matrix form as given below.

The matrix can be divided into submatrices representing the Auto- and Cross- spectra between differenct blades.

$$\begin{bmatrix} G_{11} & G_{12} & G_{13} & G_{14} & G_{15} & G_{16} \\ G_{21} & G_{22} & G_{23} & G_{24} & G_{25} & G_{26} \\ G_{31} & G_{32} & G_{33} & G_{34} & G_{35} & G_{36} \\ G_{41} & G_{42} & G_{43} & G_{44} & G_{45} & G_{46} \\ G_{51} & G_{52} & G_{53} & G_{54} & G_{55} & G_{56} \\ G_{61} & G_{62} & G_{63} & G_{64} & G_{65} & G_{66} \end{bmatrix}$$

Cross-power matrix

$$\begin{bmatrix} b_{11} & b_{12} & b_{13} \\ b_{21} & b_{22} & b_{23} \\ b_{31} & b_{32} & b_{33} \end{bmatrix}$$

Cross-power between blades

Figure 5-6 Cross-power spectral density matrix of turbine elements

The matrix can be divided into sub-matrices representing the Auto- and Cross-spectra between different blades. Each sub-matrix is symmetric about its leading diagonal due to the relationship given in Equation 5-17. Furthermore if all the blades are identical then the Auto-spectra matrix for each blade will also be the same, i.e. $b_{11} = b_{22} = b_{33}$.

A relationship between the different blade Cross-spectra matrices can also be noticed. Again from Equation 5-17 we can see for instance that $[b_{21}]$ is the complex conjugate of $[b_{12}]$. Using this result we can reduce the number of calculations necessary to fill the matrix. The matrix given in Figure 5-6 may therefore be reduced to the form given in Figure 5-7. (N.B. the term $\overline{[b_{12}]}$ denotes the complex conjugate of the matrix $[b_{12}]$.)

In summary therefore we can conclude that the whole Cross-power spectral matrix given in Figure 5-6 may be populated by calculating the following terms:

$G_{11}(\omega)$, $G_{22}(\omega)$ and $G_{21}(\omega)$ from the Auto-power blade matrix

$G_{13}(\omega)$, $G_{24}(\omega)$ and $G_{23}(\omega)$ from the Cross-power blade matrix

Noting these results reduces the calculation time significantly as the number of parameters calculated reduces from 36 to 6, a square root reduction in computation time.

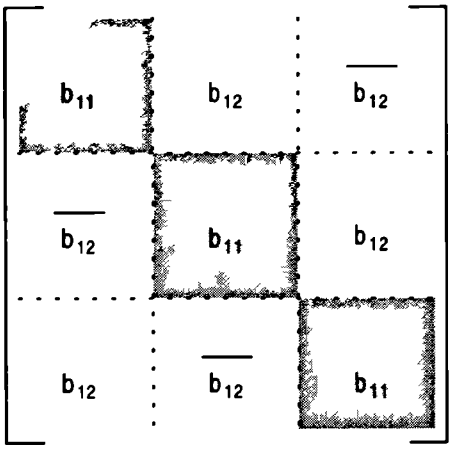

Simplified cross-power matrix between blades

A similar simplification can be made for two bladed turbines. Furthermore it can be noted that the complex conjugate $\overline{[b_{12}]}$ is equal to $[b_{12}]$ as the blade separation angle $\varphi = \pi/2$ *rad*, therefore the Cross-power spectra is real.

Figure 5-7 Blade Cross-matrices

5.3 Derivation of blade loads on a wind turbine

To this point we have considered the PSDs of wind speed witnessed by the rotating blades. We are now interested in obtaining the aerodynamic load arising because of this wind. Chapter 4 considers the aerodynamic modelling of the wind turbine and derives linear 'gain' factors that relate the wind speed to aerodynamic load for each blade element. The aerodynamic load on the i^{th} blade element is given by $Force_i(t) = g_i \cdot \tilde{v}_i(t)$, where g_i is the gain factor and $\tilde{v}_i(t)$ is the instantaneous wind speed on the i^{th} blade element.

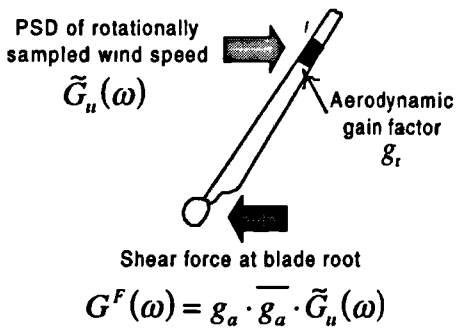

The simplest loading case is that of a blade comprising only a single element as illustrated in Figure 5-8. Now according to Equation 2-28 the PSD of shear force on the blade root is found by Equation 5-18.

Figure 5-8 Simple blade loading

$$G^F(\omega) = g \cdot \overline{g} \cdot \tilde{G}_u(\omega) \qquad \textbf{Equation 5-18}$$

To get a good resemblance of the real conditions however we need several elements per blade. In this case we must also consider the cross spectra between each element as discussed in Chapter 2.3.6. Now according to Equation 2-44, the total shear force at the blade root is given as Equation 5-19 for a blade with *N* elements.

$$G^F(\omega) = \sum_{i=1}^{N}\sum_{j-1}^{N} g_i \cdot \overline{g_j} \cdot \tilde{G}_{ij}(\omega) \qquad \textbf{Equation 5-19}$$

Where g_n is the linear aerodynamic gain factor for the n^{th} blade element.

This may also be expressed in matrix form as Equation 5-20.

$$G^F(\omega) = [g]^T \cdot \left[\tilde{G}_{ij}(\omega)\right] \cdot [\overline{g}] \qquad \textbf{Equation 5-20}$$

Where $\left[\tilde{G}_{ij}(\omega)\right]$ is the Cross-power spectral density matrix of rotationally sampled wind turbulence on one blade and [*g*] is the vector of linear aerodynamic gain factors.

The matrix representation is illustrated in Figure 5-9.

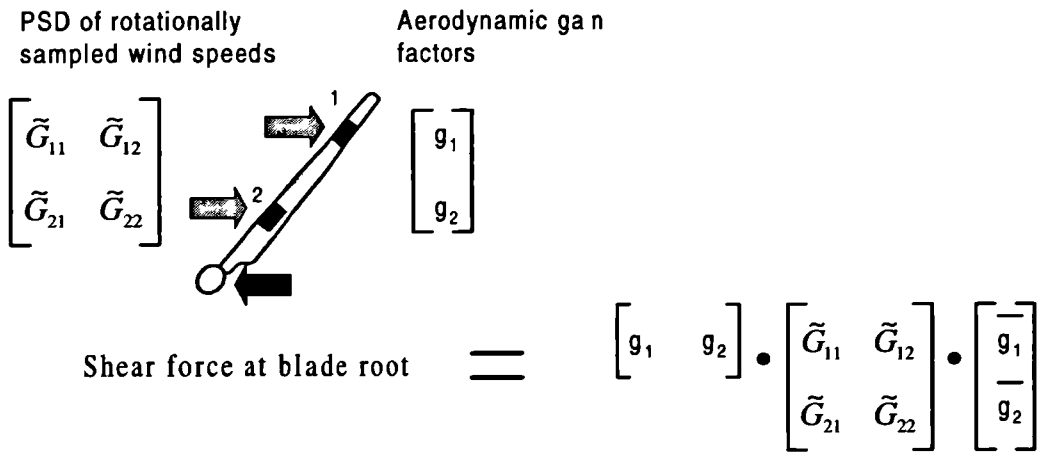

Figure 5-9 Multiple blade loads

The blade root moments are obtained in the same way as the blade root shear forces. In this case however the vector of gain factors should be replaced by a vector of the products of the gain factor and the radius to each element. The new vector of gain factors is illustrated in Equation 5-21.

$$[p]=\begin{bmatrix} r_1 \cdot g_1 \\ r_2 \cdot g_2 \\ \vdots \\ r_N \cdot g_N \end{bmatrix} \qquad \textbf{Equation 5-21}$$

Chapter 4 Derives gain factors for both in-plane and out-of-plane blade loading. These are termed g_t and g_a respectively. By substituting these for the values of g expressed in the above equations then the in- and out-of-plane shear forces and bending moments may be calculated. The formulae are summarised in Table 5-1.

Blade root shear forces	Axial direction	$G^F(\omega)=[g_a]^T\cdot[\tilde{G}_{ij}(\omega)]\cdot[\overline{g_a}]$
	Tangential direction	$G^F(\omega)=[g_t]^T\cdot[\tilde{G}_{ij}(\omega)]\cdot[\overline{g_t}]$
Blade root moments	Axial direction	$G^F(\omega)=[p_a]^T\cdot[\tilde{G}_{ij}(\omega)]\cdot[\overline{p_a}]$
	Tangential direction	$G^F(\omega)=[p_t]^T\cdot[\tilde{G}_{ij}(\omega)]\cdot[\overline{p_t}]$

Table 5-1 Summary of formulae for determining blade root forces and moments

Figure 5-10 gives the PSD of blade root shear force for a turbine operating in a 10 *m/sec* mean wind. This particular turbine is a three bladed machine and is rated at 600*kW*. Each blade is 21.5*m* in length as described by Ward[11] †.The peaks around each rotor harmonic are evident.

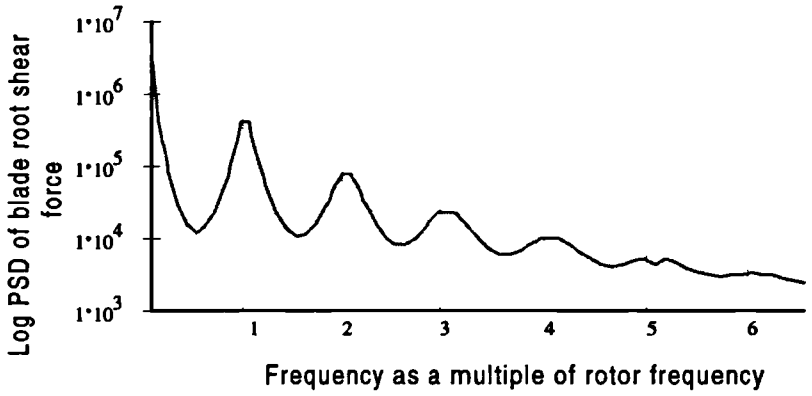

Figure 5-10 PSD of blade root shear force in the out-of-plane direction

5.4 Derivation of rotor loads on a wind turbine

In the previous section we derived formulae for calculating the shear and bending moments at the blade root. In this section we consider the loading at the tower top due to the reaction from all the rotor blades. Principally we are looking at the rotor thrust and torque. The rotor thrust is defined as the sum of the out-of-plane shear forces from all the blades; while the rotor torque is the sum of the in-plane root moments from all the blades.

The total tower top thrust and torque are determined in the same way as the blade root shear and moments were in the previous section. However, in this case the matrix $\left[\tilde{G}_{y}(\omega)\right]$ will be for all the elements on all the blades as given in Figure 5-11. The vector of gain factors must also be extended to give the corresponding values for all the elements on the blades as well. Table 5-2 summarises the formulae for determining the rotor thrust and torque, the vector [*rg*] is defined as before.

---

† The turbine manufacturer cannot be named to preserve commercial confidentiality. The analysis was carried out by W.S. Atkins using the Mathcad program developed by the author.

Rotor thrust at tower top	$G^F(\omega) = [g_a]^T \cdot [\tilde{G}_{ij}(\omega)] \cdot [\overline{g_a}]$
Rotor torque on generator	$G^F(\omega) = [p_t]^T \cdot [\tilde{G}_{ij}(\omega)] \cdot [\overline{p_t}]$

Table 5-2 Summary of formulae for calculating rotor thrust and torque

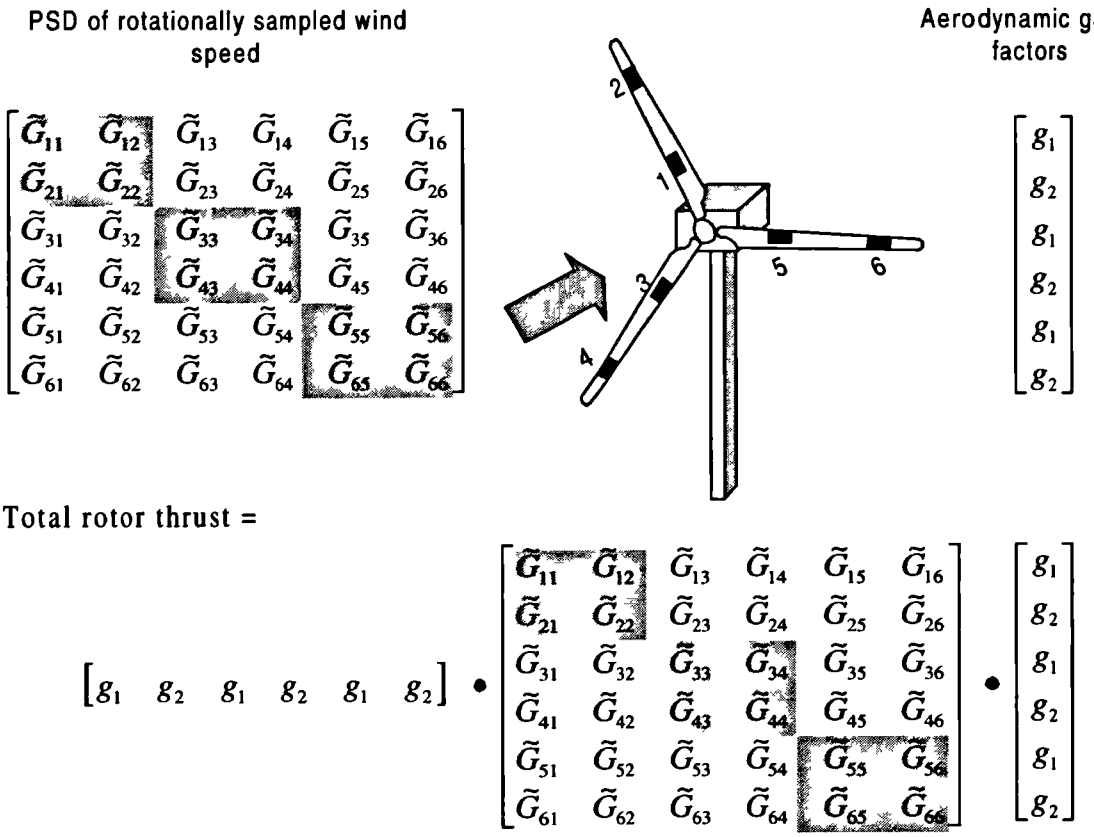

Figure 5-11 Rotor thrust

Figure 5-12 shows the PSD of thrust on the tower top for the turbine described in Figure 5-10. This is a 3 bladed turbine and the peaks are now seen at 3 times the harmonics of the rotor frequency, i.e. 3Ω, 6Ω, 9Ω, ... etc. With a two bladed we would observe peaks at 2Ω, 4Ω, 6Ω, ... etc

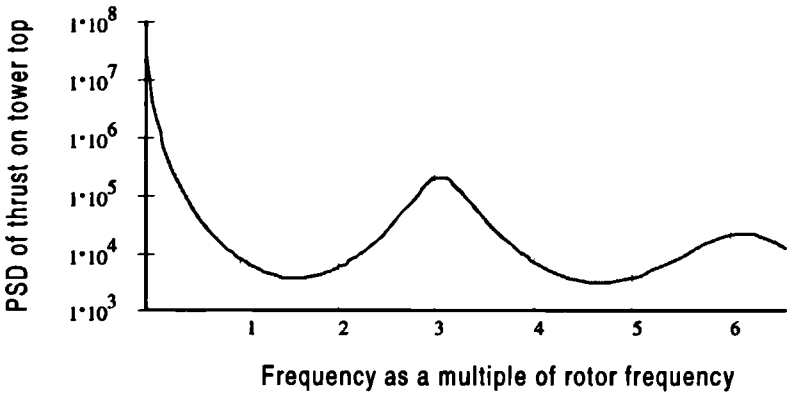

Figure 5-12 PSD of rotor thrust at tower top

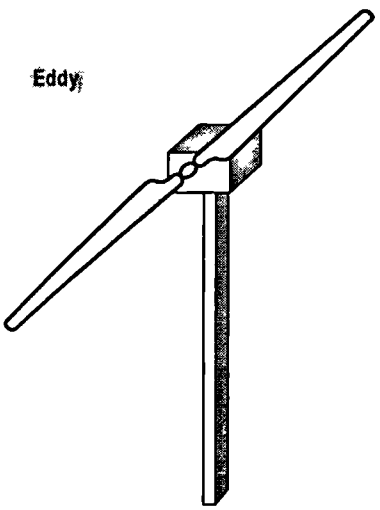

Figure 5-13 Tower top loading due to rotational sampling of a turbulent gust

This phenomenon is explained qualitatively as follows: If we first of all consider a single bladed wind turbine revolving through a single turbulent eddy, then it will witness the eddy once with each rotation. The total thrust on the tower will be from the one blade. We now consider a two bladed turbine having two equally spaced blades as illustrated in Figure 5-13. Each blade will witness the eddy once with each rotation. The thrust on the tower will now be the sum of the two blades and will be at twice the frequency. If a three bladed rotor were used then the reaction would be at three times the frequency, etc.

5.5 Derivation of a rotor 'super element' model

In the previous section we considered calculating the blade and rotor loading for the turbine. Using a form of Equation 5-20 we saw how the shear and bending moment at the blade root could be calculated, and also how the total rotor thrust and torque could be calculated at the tower top. In this section we will look at how the rotor thrust and torque may be derived using the concept of a 'super element.' This new approach proves beneficial for calculating the behaviour of the turbine for certain tower flexibilities. This is considered later in Chapter 6.

In the wind turbulence model we have assumed that the wind field is homogeneous. For most turbines we can also assume that each blade will be identical to the next. Bearing this in mind it should be possible to define an effective 'super element' which behaves exactly the same as the turbine rotor. The super element can be thought of as a special blade which exhibits the same properties as the whole rotor. This analogy is represented in Figure 5-14.

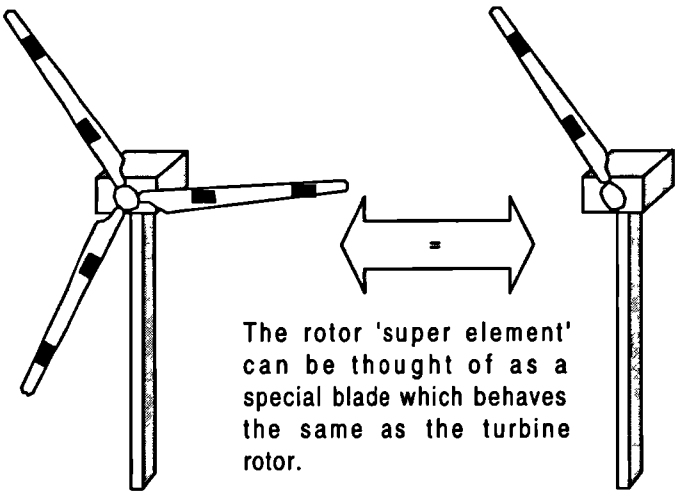

Figure 5-14 Analogy of the rotor super element

Consider the wind speed witnessed by two rotating observers situated at i and j on all the rotating blades shown in Figure 5-15. The blades are rotating with constant frequency Ω *rad/sec.* Now an equivalent rotating 'super element' will also have rotating observers situated at i and j, and would also be rotating at Ω *rad/sec.* The instantaneous wind speed witnessed by observer i or j on the super element would be equal to the sum of the instantaneous wind speeds witnessed by observers i or j on the real turbine. Therefore at time t, observer i on the super element passes through the random process u, and at time $t+\tau$ observer j passes through process v; where $u(t)=\sum_{b\ 1}^{B} u_b(t)$ and $v(t+\tau)=\sum_{c=1}^{B} v_c(t+\tau)$. (The terms b and c are ranging variables covering blades 1 to B, where B is the last blade.)

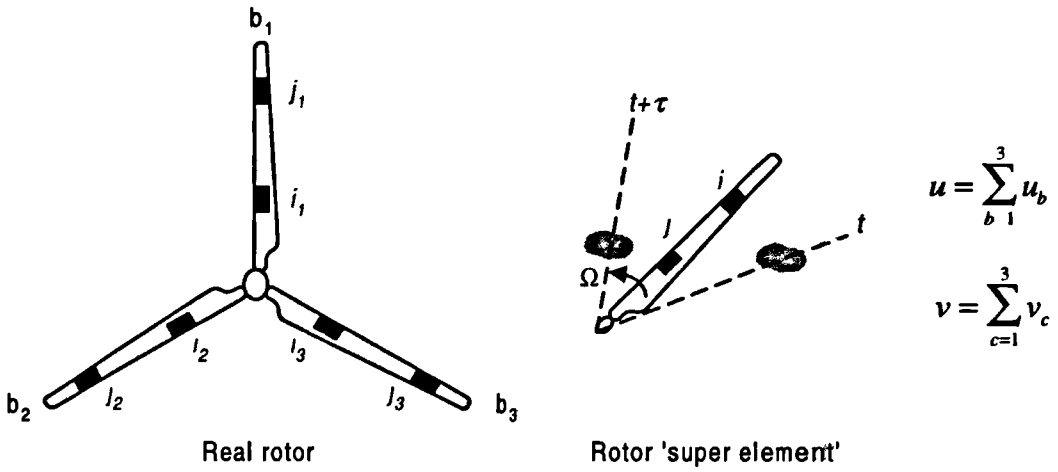

Figure 5-15 Cross-power spectra between two observers on a 'super element'

The Cross-covariance witnessed by the two observers on the super element, $\tilde{C}_{ij}(\tau)$, can be expressed as Equation 5-22.

$$\tilde{C}_{ij}(\tau) = E\left\{\sum_{b=1}^{B} u_b(t) \cdot \sum_{c=1}^{B} v_c(t+\tau)\right\} \qquad \textbf{Equation 5-22}$$

Where $\tilde{C}_{ij}(\tau)$ is the rotationally sampled Auto-covariance function between observers i and j, and $E\{\}$ is the expectation operator.

Comparing this with the expression for the Cross-power spectra derived from Equation 5-9, we can see that the rotationally sampled Cross-power spectra for the super element can be expressed as the sum of all the Cross-power spectra between the blades. This is expressed in Equation 5-23. (Conceptually it can also be given by the addition of all the blade sub-matrices illustrated in Figure 5-7.)

$$\tilde{G}_{ij}(\omega) = \sum_{b=1}^{B}\sum_{c=1}^{B}\left\{\sum_{n=-\infty}^{\infty} e^{in\frac{2\pi}{B}b} \cdot e^{in\frac{2\pi}{B}c} \cdot K_n(|\omega - n\cdot\Omega|)\cdot G_{uu}(|\omega - n\cdot\Omega|)\right\} \qquad \textbf{Equation 5-23}$$

Simplifying this yields the following expression:

$$\tilde{G}_{ij}(\omega) = \sum_{b=1}^{B}\sum_{c=1}^{B}\left\{\sum_{n=-\infty}^{\infty} e^{in\frac{2\pi}{B}(b+c)} \cdot K_n(|\omega - n\cdot\Omega|)\cdot G_{uu}(|\omega - n\cdot\Omega|)\right\} \qquad \textbf{Equation 5-24}$$

The expression may be simplified yet further by realising the following relationship:

$$\sum_{b=1}^{B}\sum_{c=1}^{B} e^{i n \frac{2\pi}{B}(b+c)} = B^2 \text{ where } n \text{ is a multiple of } B \text{ (i.e. } n = m.B)$$

$$= 0 \text{ otherwise}$$

So the Cross-power spectrum of rotationally sampled wind turbulence in the rotor super element can be expressed as Equation 5-25.

$$\tilde{G}_{ij}(\omega) = B^2 \cdot \sum_{m=-\infty}^{\infty} K_m\left(\left|\omega - m \cdot B \cdot \Omega\right|\right) \cdot G_{uu}\left(\left|\omega - m \cdot B \cdot \Omega\right|\right) \qquad \textbf{Equation 5-25}$$

The rotor thrust and torque may be calculated simply by using Equation 5-19 and substituting the Cross-power spectra of the super element. The matrix form of the solution is obtained in a similar way by Equation 5-20 where the Cross-power matrix of the super element is substituted. The frequency shifts noted in Figure 5-12 can be seen in Equation 5-25 by the terms $m \cdot B \cdot \Omega$.

5.6 Calculating the tower yaw and tilt moments

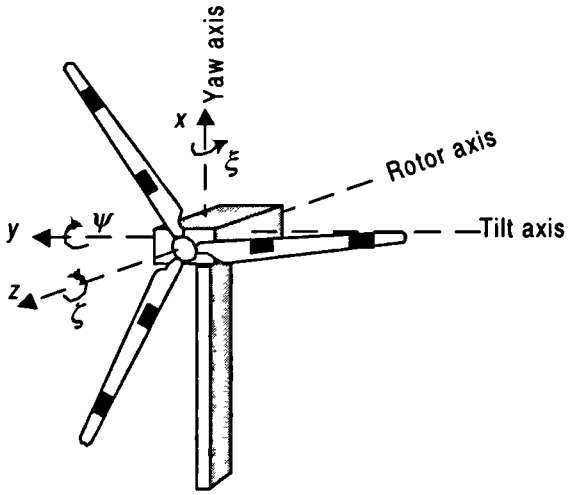

Figure 5-16 Turbine axis system

The turbulent wind pockets hitting the rotor will cause fluctuating yaw and tilt moments on the tower. This section derives formulae for determining the PSDs of these moments. If we assume that the wind turbulence is homogeneous over the rotor plane and we neglect the effect of wind shear, then we see that the yaw and tilt moments will be the same. In this section we shall therefore concentrate on deriving an expression for the yaw moment knowing that the tilt moment will result in exactly the same spectra.

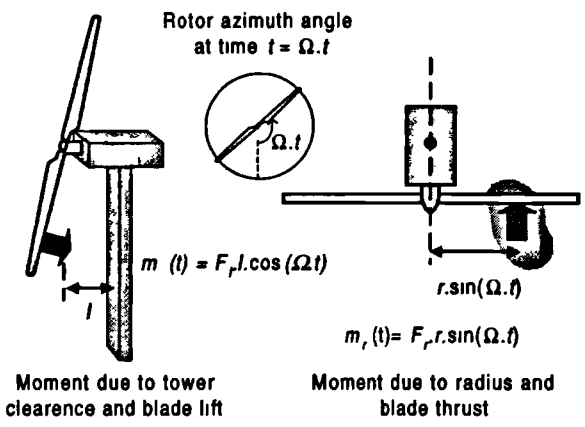

Figure 5-17 Turbine yaw

There are two effects causing the yaw and tilt moments. These are illustrated in Figure 5-17. The first is due to the blade thrust, $m_r(t) = F_r \cdot r \cdot \sin(\Omega \cdot t)$, and the second is due to the blade's lift, $m_l(t) = F_l \cdot l \cdot \cos(\Omega \cdot t)$. The total moment on the tower is therefore determined by the sum of these. In the frequency domain this is accomplished by summing the Auto- and Cross-power spectra between the two effects. (i.e. $\tilde{G}_{ll}(\omega) + \tilde{G}_{lr}(\omega) + \tilde{G}_{rl}(\omega) + \tilde{G}_{rr}(\omega)$). Oei[12] investigated this and concluded that the Cross-power terms are all imaginary and therefore do not contribute to the loading. Furthermore the moment $m_l(t)$, is considerably smaller than $m_r(t)$ and is therefore neglected in this text.

5.6.1 Cross-power spectrum of yaw moment between two blade elements

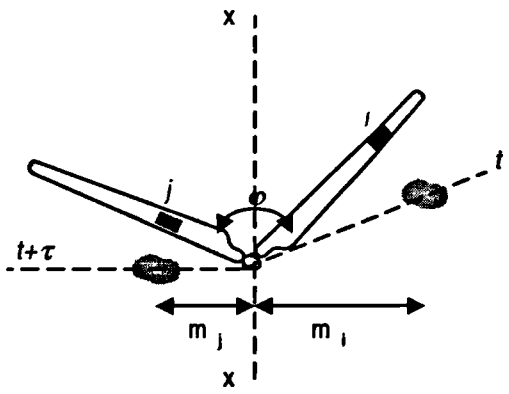

Figure 5-18 Cross-power of yaw moments

Consider the yawing moment about the x axis due to the wind speed witnessed by two rotating observers situated on elements i and j of two turbine blades. The blades are rotating with constant frequency Ω *rad/sec.* At time *t*, blade element *i* passes through random process u and at time $t+\tau$, element *j* passes through process *v*. The yawing moments of the two random processes about the *x* axis, m_i and m_j, are defined by the following expressions:

$$m_i(t) = r_i \cdot g_i \cdot u(t) \cdot \sin(\Omega \cdot t) \qquad \textbf{Equation 5-26}$$

$$m_j(t+\tau) = r_j \cdot g_j \cdot v(t+\tau) \cdot \sin(\Omega \cdot t + \Omega \cdot \tau + \varphi)$$

Where g is the aerodynamic gain factor and r is the radius to the element. To simplify the calculation let the linear function $p = r \cdot g$

Now the Cross-covariance of the rotationally sampled yaw moment from elements i and j is given by Equation 5-27.

$$\tilde{C}_{ij}(\tau) = E\left\{p_i \cdot u(t) \cdot \sin(\Omega \cdot t) \cdot p_j \cdot v(t+\tau) \cdot \sin\left(\Omega \cdot t + \Omega \cdot \tau + \varphi\right)\right\} \qquad \textbf{Equation 5-27}$$

simplifying yields $\tilde{C}_{ij}(\tau) = p_i \cdot p_j \cdot E\left\{u(t) \cdot v(t+\tau) \cdot \sin(\Omega \cdot t) \cdot \sin\left(\Omega \cdot t + \Omega \cdot \tau + \varphi\right)\right\}$

Where E{ } is the expectation operator.

Now we know that $E\{u(t) \cdot v(t+\tau)\} = C_{uv}(\tau)$ and we can also show that $E\left\{\sin(\Omega \cdot t) \cdot \sin\left(\Omega \cdot t + \Omega \cdot \tau + \varphi\right)\right\} = \frac{1}{2} \cdot \cos\left(\Omega \cdot \tau + \varphi\right)$. Therefore Equation 5-27 may be simplified to the following:

$$\tilde{C}_{ij}(\tau) = \frac{1}{2} \cdot p_i \cdot p_j \cdot C_{uv}(\tau) \cdot \cos\left(\Omega \cdot \tau + \varphi\right) \qquad \textbf{Equation 5-28}$$

If the random processes are statistically similar and have the same Auto-power spectral densities, (i.e. the turbulence is homogeneous across the rotor plane), the Cross-covariance function $C_{uv}(\tau)$ can be expressed using the coherence function as follows:

$$\tilde{C}_{ij}(\tau) = \frac{1}{2} \cdot p_i \cdot p_j \cdot \left\{\int_{-\infty}^{\infty} \gamma(\upsilon, d(\tau)) \cdot S_{uu}(\upsilon) \cdot e^{i \cdot \upsilon \cdot \tau} d\upsilon\right\} \cdot \cos\left(\Omega \cdot \tau + \varphi\right) \qquad \textbf{Equation 5-29}$$

Where $d(\tau)$ is the separation distance between the two processes u and v and is determined by the equation $d(\tau) = \sqrt{r_i^2 + r_j^2 - 2 \cdot r_i \cdot r_j \cdot \cos\left(\Omega \cdot \tau + \varphi\right)}$ where φ is the angle between the two blades in radians.

Now the rotationally sampled Cross-power spectrum $\tilde{S}_{ij}(\omega)$ can be obtained by taking the Fourier transform of the Cross-covariance function $\tilde{C}_{ij}(\omega)$.

$$\tilde{S}_{ij}(\omega) = \int_{-\infty}^{\infty} \tilde{C}_{ij}(\tau) \cdot e^{-i \cdot \omega \cdot \tau} d\tau \qquad \textbf{Equation 5-30}$$

i.e.
$$\tilde{S}_{ij}(\omega) = \int_{-\infty}^{\infty} \tfrac{1}{2} \cdot p_i \cdot p_j \cdot \left\{ \int_{-\infty}^{\infty} \gamma(\upsilon, d(\tau)) \cdot S_{uu}(\upsilon) \cdot e^{i \upsilon \tau} d\upsilon \right\} \cos(\Omega \cdot \tau + \varphi) \cdot e^{-i \cdot \omega \tau} d\tau$$

Simplifying this yields the expression given in Equation 5-31.

$$\tilde{S}_{ij}(\omega) = \tfrac{1}{2} \cdot p_i \cdot p_j \cdot \int_{-\infty}^{\infty} S_{uu}(\upsilon) \cdot \left\{ \int_{-\infty}^{\infty} \gamma(\upsilon, d(\tau)) \cdot \cos(\Omega \cdot \tau + \varphi) \cdot e^{-i(\omega - \upsilon)\tau} d\tau \right\} d\upsilon \qquad \textbf{Equation 5-31}$$

Now $d(\tau)$ is periodic in time τ with period $^{2\pi}/_{\Omega}$, hence the coherence function, $\gamma(\upsilon, d(\tau))$ is also periodic. In Equation 5-13 we expressed the coherence function in terms of the Fourier series as given in Equation 5-32.

$$\gamma(\upsilon, d(\tau)) = \sum_{n=-\infty}^{\infty} K_n(\upsilon) \cdot e^{i n \varphi} \cdot e^{i n \Omega \tau} \qquad \textbf{Equation 5-32}$$

where
$$K_n(\upsilon) = \frac{1}{\pi} \int_0^{\pi} \gamma(\upsilon, d(\theta)) \cdot \cos(n \cdot \theta) d\theta$$

and $d(\theta) = \sqrt{r_i^2 + r_j^2 - 2 \cdot r_i \cdot r_j \cdot \cos(\theta)}$ and n is the Fourier variable pertaining to a frequency $m\Omega$.

Substituting Equation 5-32 into Equation 5-31 yields the following expression:

$$\tilde{S}_{ij}(\omega) = \tfrac{1}{2} \cdot p_i \cdot p_j \cdot \int_{-\infty}^{\infty} S_{uu}(\upsilon) \cdot \left\{ \int_{-\infty}^{\infty} \sum_{n=-\infty}^{\infty} K_n(\upsilon) \cdot \cos(\Omega \cdot \tau + \varphi) \cdot e^{i \cdot n \cdot \varphi} \cdot e^{-i(\omega - \upsilon - n \cdot \Omega)\tau} d\tau \right\} d\upsilon$$

Equation 5-33

Now the cosine term may be expanded into exponential form by the relationship $\cos(\theta) = \tfrac{1}{2} \cdot \left(e^{i\theta} + e^{-i\theta} \right)$. Equation 5-33 then becomes;

$$\tilde{S}_{ij}(\omega) = \tfrac{1}{4} \cdot p_i \cdot p_j \cdot \int_{-\infty}^{\infty} S_{uu}(\upsilon) \cdot \left\{ \int_{-\infty}^{\infty} \sum_{n=-\infty}^{\infty} K_n(\upsilon) \cdot e^{i n \varphi} \cdot \left[e^{i \varphi} \cdot e^{i(\Omega - \omega + \upsilon + n\Omega)\tau} + e^{-i \cdot \varphi} \cdot e^{-i(\Omega + \omega - \upsilon - n\Omega)\tau} \right] d\tau \right\} d\upsilon$$

Equation 5-34

This expression may be simplified using Dirac's delta function and thus reduces to the following:

$$\tilde{S}_{ij}(\omega) = \tfrac{1}{4} \cdot p_i \cdot p_j \cdot \int_{-\infty}^{\infty} S_{uu}(\upsilon) \cdot \left\{ \sum_{n=-\infty}^{\infty} K_n(\upsilon) \cdot e^{i n \varphi} \cdot \begin{bmatrix} e^{i\varphi} \cdot \delta(\Omega - \omega + \upsilon + n \cdot \Omega) + \cdots \\ e^{-i\varphi} \cdot \delta(-\Omega - \omega + \upsilon + n \cdot \Omega) \end{bmatrix} \right\} d\upsilon$$

Equation 5-35

Integrating with respect to υ yields the following expression for the double sided Cross-power spectral density function of the yawing moment.

$$\tilde{S}_{ij}(\omega) = \tfrac{1}{4} \cdot p \cdot p_j \cdot \sum_{n=-\infty}^{\infty} \begin{bmatrix} e^{i(n+1)\varphi} \cdot K_n(\omega - (n+1) \cdot \Omega) \cdot S_{uu}(\omega - (n+1) \cdot \Omega) + \cdots \\ e^{i(n-1)\varphi} \cdot K_n(\omega - (n-1) \cdot \Omega) \cdot S_{uu}(\omega - (n-1) \cdot \Omega) \end{bmatrix}$$

Equation 5-36

The Auto-power spectrum is obtained from the above equation when $r_i = r_j$ and $\varphi = 0$. Figure 5-19 shows the Auto-power spectrum of the yawing moment calculated for a pair of rotating observers situated on a rotating turbine blade. The response of positive and negative values of n are plotted separated for clarity. Each n^{th} component is seen to be Doppler shifted by both $(n+1).\Omega$ and $(n-1).\Omega$ *Hz*. This results in the double peaked curves centred about the n^{th} harmonic. The total response is determined by summing all the individual n components. As with the PSDs of blade loading we see that distant harmonics have only a limited influence on each other. For instance, if we are considering the response about the $n = 1$ harmonic, then we observe that the contribution made by the $n = -1$ harmonic is so small it may be neglected. Equation 5-36 therefore may be simplified by taking the summation over a reduced number of harmonics.

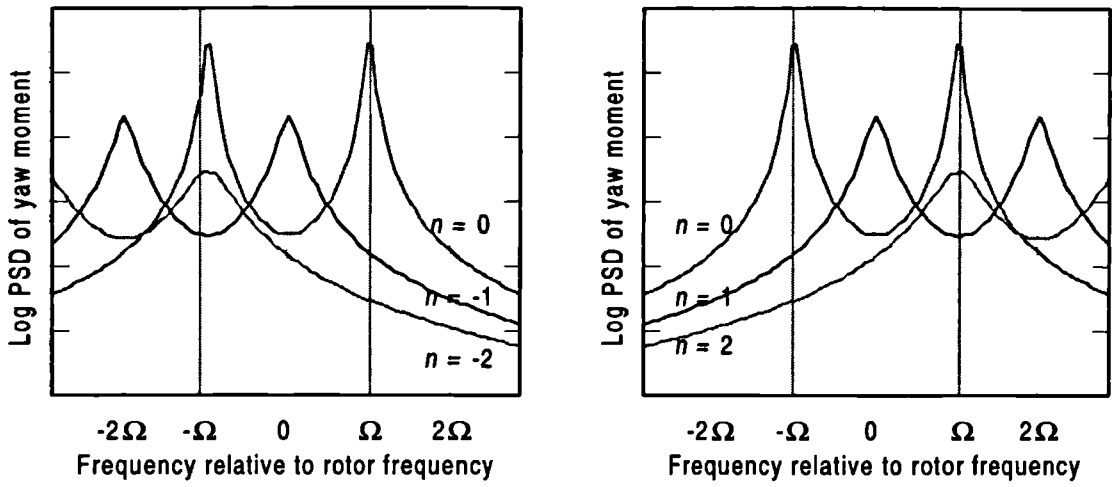

Figure 5-19 Cross-power spectra of yaw moment

The double sided Cross-power spectrum in Figure 5-19 is seen to be symmetric about the origin. This can be seen in Equation 5-36 as negative frequencies will result in the complex conjugate of the positive frequencies. Equation 5-36 can therefore be expressed as a single sided spectrum by Equation 5-37.

$$\tilde{G}_{y}(\omega) = \tfrac{1}{4} \cdot p_i \cdot p_j \cdot \sum_{n=-\infty}^{\infty} \begin{bmatrix} e^{i\cdot(|n+1|)\varphi} \cdot K_n\left(|\omega-(n+1)\cdot\Omega|\right) \cdot G_{uu}\left(|\omega-(n+1)\cdot\Omega|\right)+\cdots \\ e^{i\cdot(|n-1|)\varphi} \cdot K_n\left(|\omega-(n-1)\cdot\Omega|\right) \cdot G_{uu}\left(|\omega-(n-1)\cdot\Omega|\right) \end{bmatrix}$$

Equation 5-37

Figure 5-20 shows a typical single sided PSD of yaw moment.

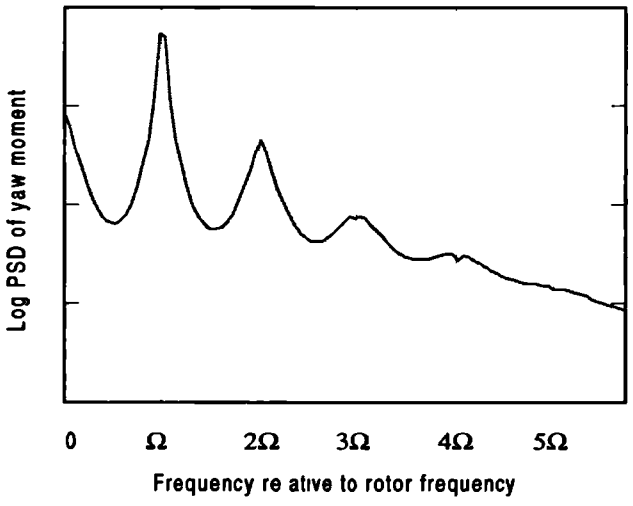

Figure 5-20 Single sided PSD of yaw moment

5.6.2 The rotor 'Super element' for modelling yaw moment

A Super element can be derived to simplify the calculation of yaw moment. This is essentially the same as that discussed in section 5.5. To simplify the formulation we should discard the linear gain factors p_i and p_j from the equation at present. This is not of great importance because we will add them back in again later when we deal with the matrix algebra. Using the results noted in Chapter 5.5, we can write the equation for the Cross-power spectrum of yaw on a super element as Equation 5-38.

$$\tilde{G}_{ij}(\omega) = \frac{B^2}{4} \cdot \sum_{n=-\infty}^{\infty} \begin{bmatrix} K_n(|\omega - B\cdot(n+1)\cdot\Omega|)\cdot G_{uu}(|\omega - B\cdot(n+1)\cdot\Omega|) + \cdots \\ K_n(|\omega - B\cdot(n-1)\cdot\Omega|)\cdot G_{uu}(|\omega - B\cdot(n-1)\cdot\Omega|) \end{bmatrix} \qquad \textbf{Equation 5-38}$$

A matrix of Cross-power spectra, $\left[\tilde{G}_{ij}(\omega)\right]$, can be expressed for the super element as described in section 5.2.2. The total yaw moment on the whole rotor can then be found using matrix algebra as given in Equation 5-39.

$$\tilde{G}_{\xi\xi}(\omega) = [p]^T \cdot \left[\tilde{G}_{ij}(\omega)\right] \cdot [\overline{p}] \qquad \textbf{Equation 5-39}$$

Where $\tilde{G}_{\xi\xi}(\omega)$ is the Auto-power spectral density of yaw moment, $\left[\tilde{G}_{ij}(\omega)\right]$ is the Cross-power spectra matrix of yaw and [p] is the vector of linear gain factors defined by $p_i = r_i \cdot g_i$.

Figure 5-21 shows the yaw moment on the turbine described in Figure 5-10. As mentioned earlier, this is also the same as the tilt moment on the turbine because it results purely from an assumed homogeneous turbulence. In reality the tilt moment would also be affected by wind shear and tower shadow, these are deterministic in nature and are not considered in this chapter.

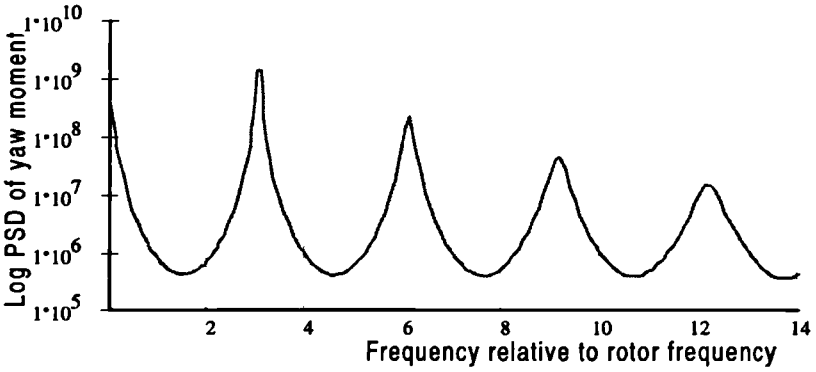

Figure 5-21 Single sided PSD of yaw moment

5.7 Yaw and tilt misalignment

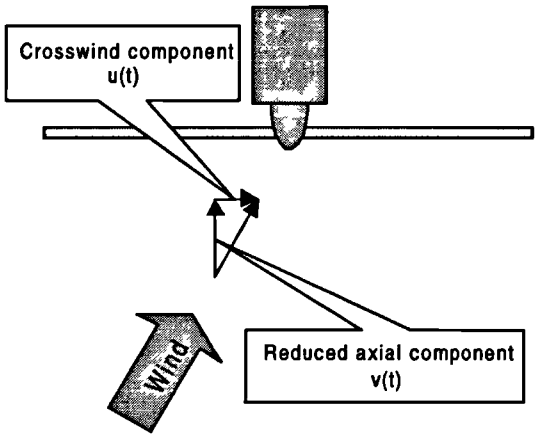

Figure 5-22 Yaw misalignment

A yaw or tilt misalignment occurs when the turbine is not perfectly aligned with the incident wind. The wind direction is constantly varying and therefore a degree of misalignment will always be present. Indeed small changes in wind direction occur so rapidly that the turbine's control system is designed to ignore them to prevent high gyroscopic loading through oscillation. In this section we shall derive the PSD of blade element loading due to a constant yaw misalignment. The effect of directional variation with time is not considered at this stage. The formulation developed in this section is equally applicable to turbines with a tilt misalignment. This is common, particularly with upwind turbines where a permanent tilt angle is applied to ensure adequate tower clearance.

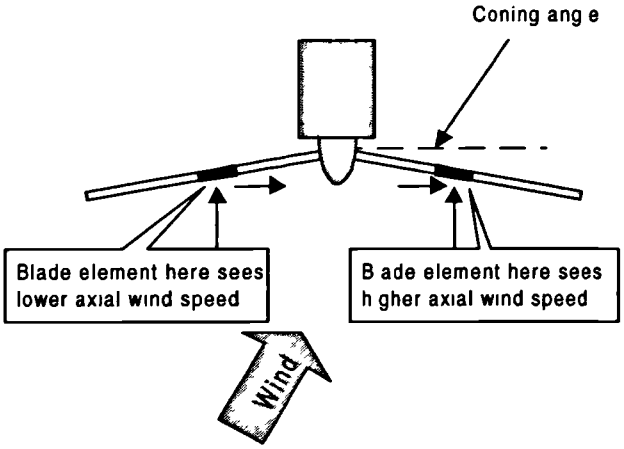

Figure 5-23 Yaw misalignment force due to rotor coning

The effect of yaw misalignment is illustrated in Figure 5-22. It results in a reduced axial wind velocity component and an additional perpendicular component known as crosswind. The crosswind component can have two effects on the blade loading. The first concerns rotors having a coning angle as shown in Figure 5-23. Here the incident wind will affect the aerodynamic loading when the blade is moving through the horizontal position, i.e. the rotor azimuth angle $\psi = 90°$ or 270°. This gives rise to a sinusoidal variation in the wind speed around from the mean. The force on an element i is expressed in Equation 5-40.

$$Force_i(t) = \left[g_i + q_i \cdot \sin(\Omega \cdot t)\right] \cdot v_i(t) \qquad \textbf{Equation 5-40}$$

Where $v_i(t)$ is the axial wind speed on the blade element, g_i is the aerodynamic gain factor and q_i is the amplitude of variation of the gain factor with respect to rotor azimuth angle.

The second effect concerns the change in inflow angle when the blades are located vertically and are heading into the crosswind or away from it. This then gives rise to the cosine variation expressed in Equation 5-41.

$$Force_i(t) = \left[c_i + d_i \cdot \cos(\Omega \cdot t)\right] \cdot v_i(t) \qquad \textbf{Equation 5-41}$$

Where $v_i(t)$ is the axial wind speed on the blade element, c_i is the aerodynamic gain factor and d_i is the amplitude of variation of the gain factor with respect to rotor azimuth angle.

From these expressions we can see that the term $g_i \cdot v_i(t)$ yields a similar result to that for the rotational sampling of turbulent wind derived earlier. The axial, turbulent wind speed $v(t)$ is reduced due to the misalignment however. For small misalignments this

reduction may be neglected and so the PSD for this term can be taken as the PSD of rotationally sampled wind turbulence calculated before. The term $c_i \cdot v_i(t)$ is evaluated in the same way except the gain factor c is used in place of g.

The terms $q_i \cdot \sin(\Omega \cdot t) \cdot v_i(t)$ and $d_i \cdot \cos(\Omega \cdot t) \cdot v_i(t)$ are similar to that determined for the yaw moment in section 5.6. The methodology given in that chapter can therefore be used to calculate the terms.

The resultant response PSD is found from the sum of the above PSDs and their corresponding Cross-spectra. However it is noted that no real Cross-power spectra exist and therefore it is sufficient to sum the PSDs given above. This operation is quite simple to perform.

5.8 Conclusion

In this chapter we have considered the aerodynamic loads acting on the turbine blades and support structure due to variations in the turbulent wind speed, In particular, blade shear and bending moments about the flatwise and edgewise axes and rotor thrust, torque, yaw and pitch. In addition we have also covered yaw and pitch misalignment. As the turbine blades rotate, they periodically sample the wind turbulence; a phenomenon referred to as 'eddy slicing'. In this chapter, closed form expressions are derived giving the rotationally sampled auto- and cross-power spectral density functions for the wind speed. These values are presented in a new matrix format to allow rapid manipulation later in the dynamic analysis. Special relationships are noted in the format of the matrices and these are exploited to reduce calculation time.

The concept of the 'Rotor Super Element' is introduced to model rotor loads on a tower and support structure. This is a hypothetical blade that exhibits the properties of the whole rotor. The super element is used throughout the thesis to cope with coordinate transformations between rotating and stationary axes and for producing rotor response matrices for sea keeping analysis. These are dealt with later.

---

[1] Rosenbrock H.H. (1955). "Vibration and stability problems in large turbines having hinged blades." ERA-report C/T 113.

[2] Connell J.R. (1982). "The spectrum of wind speed fluctuations encountered by a rotating blade of a wind energy conversion system." Solar Energy 29, 363-375.

[3] Connell J.R. (1988). "A Primer of turbulence at the wind turbine rotor." Solar Energy 41, 281-293, USA.

[4] Dragt J.B. (1984). "Wind speed fluctuation spectra on a rotating wind turbine blade, and resulting load fluctuations. Parts I and II." Internal publication, Netherlands Energy Research Foundation ECN, The Netherlands.

[5] Dragt J.B. (1984). " The spectra of wind speed fluctuations met by a rotating blade and resulting load fluctuations." European Wind Energy Conference, 1984.

[6] Dragt J.B. (1990). "Atmospheric turbulence characteristics in the rotating frame of reference of a WECS rotor." European community wind energy conference, Madrid Spain, 1990.

[7] Dragt J.B. (1985). "Load fluctuations and response of rotor systems in turbulent wind fields." WINDPOWER '85 conference, San Francisco, 1985.

[8] ESDU 86010 (1991). "Characteristics of atmospheric turbulence near the ground. Part III: variations in space and time for strong winds (neutral atmosphere)." ESDU International plc, London.

[9] ESDU 85020 (1993). "Characteristics of atmospheric turbulence near the ground. Part II: single point data for strong winds (neutral atmosphere)." ESDU International plc, London.

[10] Sørensen P. (1994). "Frequency domain modelling of wind turbine structures." Risø-R-749(EN). Risø National Laboratory, Roskilde, Denmark.

[11] Ward I.P. (1996). "Wind turbulence data measured at a turbine test site. (Location and manufacturer are confidential)." Personal correspondence.

[12] Oei T.D. (1987). "Turbulence induced yaw dynamics of horizontal axis wind turbines." Memo FYS-WIND-87-33, Internal publication, Netherlands Energy Research Foundation ECN, The Netherlands.

6. Dynamic analysis of a wind turbine subjected to turbulent wind loads

This chapter looks at the frequency domain analysis of flexible turbine structures subjected to turbulent wind loads. The previous chapter considered only the loading on a rigid turbine structure. In practice no turbine is rigid and in this chapter we shall determine how to incorporate the structural flexibilities and dynamic response in the analysis.

At the outset of this project, little work had been carried out to model the structural dynamics of a wind turbine in the frequency domain. Dragt[1] considered the effect of a hinged rotor blade in the frequency domain in 1985 and this effectively introduced a single degree of freedom flexibility to the blade model.

Through the duration of this PhD research, other organisations were developing their own models. Garrad[2], Quarton[3] and Wei[4] have in turn reported on their frequency domain program "TURBLOAD." Since 1986 this has been developing and is now able to model blade, tower and drivetrain flexibilities and can be used to model turbines with any number of blades. Very recent modifications have been made to include the effect of wave loads on floating offshore turbines. This is documented by Garrad et al[5]. The modified program is now able to deal with a single degree of freedom wave spectra at the tower base given for the fore-aft direction only. The analysis technique employed is not strictly based in the frequency domain but rather in the 'covariance domain'. The auto-power spectral density of turbulent wind speed is transformed into an autocovariance function using the inverse Fourier transform. This is then periodically sampled by the rotating blades using the coherence function to create auto- and cross-covariance functions between different stations along the blade. The auto-power spectral density functions are then determined by taking the Fourier transform of the corresponding covariance functions. The structural dynamic modelling is realised in the covariance domain.

Sørensen[6,7] reports on the work carried out at Risø in the development of their frequency domain program 'Design Basis 2.' This is capable of modelling blade, tower and drivetrain flexibilities in the frequency domain. It is, however, limited to analysing turbines with three or more blades and has no offshore capabilities.

ECN has an on-going project to add structural flexibility to its TURBU[8] program. According to Van Engelen[9] this will include blade, tower and drivetrain flexibilities. It is proposed to limit the structural model to cover only one mode in each degree of freedom.

The dynamic model described in this chapter was developed independently of the above and includes all the capabilities of these methods in addition to a new ability to analyse the turbine loads arising through random motion of the tower base. It is able to analyse blade, tower and drivetrain flexibilities for turbines with two or more blades. It is also unique in being able to analyse the turbine's response to stochastic base motions in all 6 degrees of freedom, (heave, sway, surge, yaw, tilt and roll). This makes it suitable for analysing offshore turbines mounted on floating platforms. Details of the offshore model are given in Chapter 9.

The frequency domain analysis allows the turbulent wind loads to be modelled using closed form equations as opposed to numerical sampling that is necessary in the TURBLOAD program. In practice the frequency domain approach reveals a better conceptual view of how the rotational sampling phenomenon occurs. A major advantage of the frequency domain technique becomes apparent when considering the structural dynamic analysis of the flexible turbine structure. This can now be analysed as a linear transfer function in the frequency domain that simplifies and speeds up the calculation. The TURBLOAD model, in comparison, uses a steady state convolution approach to analyse the structure in a finite element environment.

The analysis developed by the author is intuitive, fast and has been verified by operational comparison with three working turbines, Chapter 8 gives details of this comparison.

6.1 Overview of the modelling process

The dynamic analysis presented in this chapter is fairly complicated, it is therefore beneficial to introduce the concepts involved using simple structural models before continuing with the full turbine analysis.

6.1.1 Single degree of freedom blade model

Consider the simple one-degree of freedom blade model shown in Figure 6-1. The blade is subjected to a time varying wind load given by the relationship $g_a \cdot v(t)$, where $v(t)$ is the instantaneous wind speed at any time t, and g_a is the axial aerodynamic gain factor.

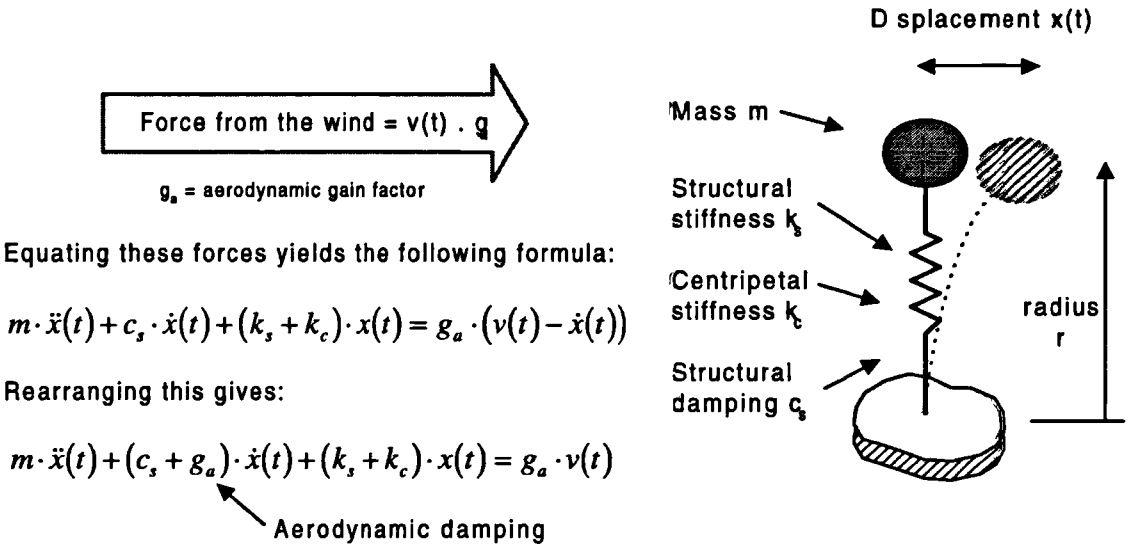

Figure 6-1 Single degree of freedom blade model

The equation of motion of the single degree of freedom blade is given as the sum of the inertial force (mass x acceleration), the viscous force (damping x velocity), the structural force (stiffness x displacement), the aerodynamic force ($g_a.v(t)$) and the centripetal force k_c. The equation of motion is given in **Equation 1**.

$$m \cdot \ddot{x}(t) + c_s \cdot \dot{x}(t) + (K_s + K_c) \cdot x(t) = g_a \cdot (v(t) - \dot{x}(t)) \qquad \textbf{Equation 1}$$

Where;

m = nodal mass

c_s = structural damping

k_s = structural stiffness

k_c = centripetal stiffness

g_a = aerodynamic gain factor

$v(t)$ = instantaneous windspeed at time t

$x(t)$ = instantaneous displacement at time t

Rearranging this expression to give the applied forces on the right hand side of the equality yields the following:

$$m \cdot \ddot{x}(t) + (c_s + g_a) \cdot \dot{x}(t) + (k_s + k_c) \cdot x(t) = g_a \cdot v(t) \qquad \textbf{Equation 2}$$

From the equilibrium equation above we see that the blade damping is taken as the sum of the structural and aerodynamic damping, and the stiffness taken as the sum of the structural and centripetal stiffness. The centripetal stiffness is obtained from Equation 3.

$$k = \frac{m \cdot r \cdot \Omega}{r} \qquad \textbf{Equation 3}$$

The solution to the differential equation in Equation 2 is described in many engineering texts such as Berg[10] and Meirovitch[11]. If the wind speed $v(t)$ is sinusoidally varying with time then the displacement $x(t)$ will also be sinusoidally varying. Expressing this sinusoidal variation in the exponential form gives the following expressions for the wind speed and displacement:

$$v(t) = V \cdot e^{i \cdot \omega \cdot t} \qquad x(t) = X \cdot e^{i \cdot \omega \cdot t} \qquad \textbf{Equation 4}$$

Where V is the amplitude of the sinusoidally varying wind speed and X is the amplitude of the induced displacement.

Differentiating displacement with respect to time yields expressions for the velocity and acceleration of the mass. These are given in Equation 5.

$$\dot{x}(t) = i \cdot \omega \cdot X \cdot e^{i \cdot \omega \cdot t} \qquad \ddot{x}(t) = -\omega^2 \cdot X \cdot e^{i \cdot \omega \cdot t} \qquad \textbf{Equation 5}$$

Substituting these into the differential equation and simplifying yields the following formula for the amplitude of displacement.

$$X = \frac{g_a}{-\omega^2 \cdot m + i \cdot \omega \cdot (c_s + g_a) + (k_s + k_c)} \cdot V \qquad \textbf{Equation 6}$$

From a structural point of view we are also interested in the amplitude of the force at the blade root. This is obtained by multiplying the displacement by the blade's structural stiffness k_s. The linear transfer function, $H(\omega)$, between wind speed and dynamic loading at the blade root is therefore given by Equation 7.

$$f = H(\omega) \cdot V \qquad \textbf{Equation 7}$$

Where f is the dynamic blade root force and $H(\omega)$ is the transfer function

defined by the formula: $H(\omega)=\dfrac{k_s \cdot g_a}{-\omega^2 \cdot m+i \cdot \omega \cdot (c_s+g_a)+(k_s+k_c)}$.

This may be expressed in the frequency domain using the relationship given in Equation 2-28, of Chapter 2.2. This is given in Equation 8.

$$G^F(\omega)=|H(\omega)|^2 \cdot \tilde{G}_u(\omega) \qquad \textbf{Equation 8}$$

Where $G^F(\omega)$ is the single sided power spectral density of blade root force, and $\tilde{G}_u(\omega)$ is the single sided auto-power spectral density function of the rotationally sampled wind speed on the blade.

Dragt[1] used the approach derived above to investigate the effect of hinged blades on dynamic loading.

6.1.2 Multiple element blade model

In this section we look at the analysis of a blade using two or more discrete elements as shown in Figure 6-2. The damping and stiffness terms given in the diagram represent the total damping and stiffness due to the structural, centripetal and aerodynamic contributions.

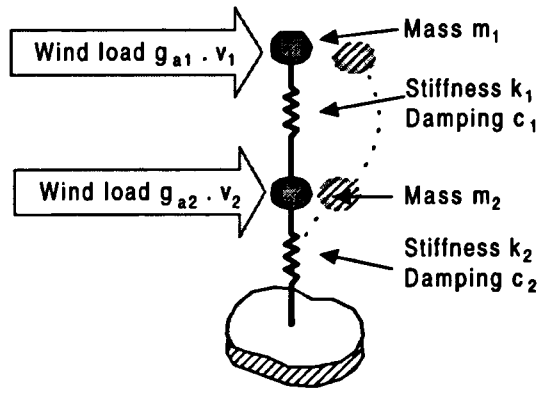

Figure 6-2 Multi-degree of freedom blade model

Wind loading will be exerted on both nodes and this will be correlated. What is required from the dynamic analysis is the transfer function between wind speed on each node and the resulting force on each of the elements. As there are two loaded nodes then there will be two transfer functions. Each transfer function will take the form of a vector where each term represents the force on a particular blade element. To explain how the transfer functions are determined, consider a unit virtual wind speed applied to each node in turn. Dynamic analysis of systems with multiple degrees of freedom is best dealt with using matrix algebra as described in Berg[10]. The equation of motion is expressed in matrix form as Equation 9.

$$\begin{bmatrix} m_1 & 0 \\ 0 & m_2 \end{bmatrix} \cdot \begin{bmatrix} \ddot{x}_1 \\ \ddot{x}_2 \end{bmatrix} + \begin{bmatrix} c_1 & 0 \\ 0 & c_2 \end{bmatrix} \cdot \begin{bmatrix} \dot{x}_1 \\ \dot{x}_2 \end{bmatrix} + \begin{bmatrix} k_1 & -k_1 \\ -k_1 & k_1 + k_2 \end{bmatrix} \cdot \begin{bmatrix} x_1 \\ x_2 \end{bmatrix} = \begin{bmatrix} g_1 \\ g_2 \end{bmatrix} \cdot \begin{bmatrix} v_1 \\ v_2 \end{bmatrix}$$

Equation 9

Using matrix algebra this is written as Equation 10.

$$M \cdot \ddot{x}(t) + C \cdot \dot{x}(t) + K \cdot x(t) = G \cdot u(t) \qquad \textbf{Equation 10}$$

Where M, C and K are the mass, damping and stiffness matrices respectively; G is the matrix of aerodynamic gain factors; and $x(t)$ and $u(t)$ are vectors of displacement and virtual wind speed respectively.

The differential equation is solved using matrix algebra in the same way as that previously discussed. A matrix of displacement amplitudes is therefore obtained from Equation 11. The n^{th} column of the matrix represents a vector of transfer functions between the force applied on the n^{th} node, and the displacement of the nodes.

$$X = [Z(\omega)]^{-1} \cdot G \cdot U \qquad \textbf{Equation 11}$$

Where U is the matrix of unit virtual loads applied to each node in turn, $[Z(\omega)]^{-1}$ is the inverse of the matrix $Z(\omega)$, and $Z(\omega) = -\omega^2 \cdot M + i \cdot \omega \cdot C + K$.

The force in each element can now be found by the process of *'back substitution.'* This process is described by Meirovitch[11] and is illustrated in Figure 6-3.

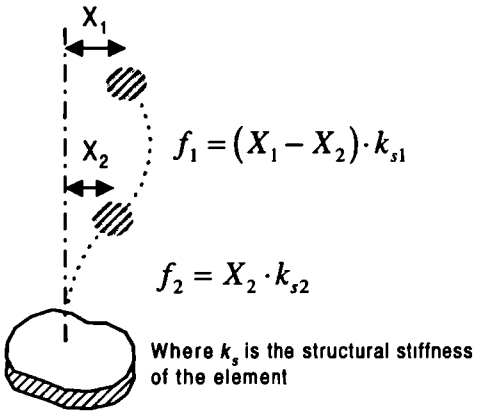

Figure 6-3 Principle of 'back substitution'

Essentially, matrix X gives the nodal displacements in terms of global coordinates. The back substitution process determines the relative displacement of the nodes. This describes how much each element has deformed between it's two nodes. It then multiples this deformation by the element's structural stiffness to obtain the force on the element. Using this process we can therefore obtain a matrix of linear transfer functions between the wind speed applied at each node and the resulting force in each element. We will use the notation $H(\omega)$ to represent

this matrix of transfer functions. The element forces can be evaluated from the transfer matrix using Equation 12.

$$f = H(\omega) \cdot U \qquad \textbf{Equation 12}$$

Where U is either a vector or matrix of wind speeds, and f is a vector or matrix of element forces.

This may also be expressed in the frequency domain using the relationship given in Equation 2-45 of Chapter 2.3.7. This is given in Equation 13.

$$G^F(\omega) = \overline{H(\omega)} \cdot \tilde{G}(\omega) \cdot H(\omega)^T \qquad \textbf{Equation 13}$$

Where $G^F(\omega)$ is the single sided, cross-power spectral density matrix of element forces and $\tilde{G}(\omega)$ is the single sided, cross-power spectral density matrix of rotationally sampled wind speed on the blade nodes.

6.1.3 Multi-degree of freedom elements

In the previous sections we have derived expressions for calculating the response of a turbine blade using simple single degree of freedom elements. In practice this is insufficient and we should employ multi-degree of freedom elements to adequately determine all the forces on the blade. In this analysis an eight degree of freedom beam element is employed. This models 2 longitudinal and 2 rotational modes at each node. The modes modelled are illustrated in Figure 6-4.

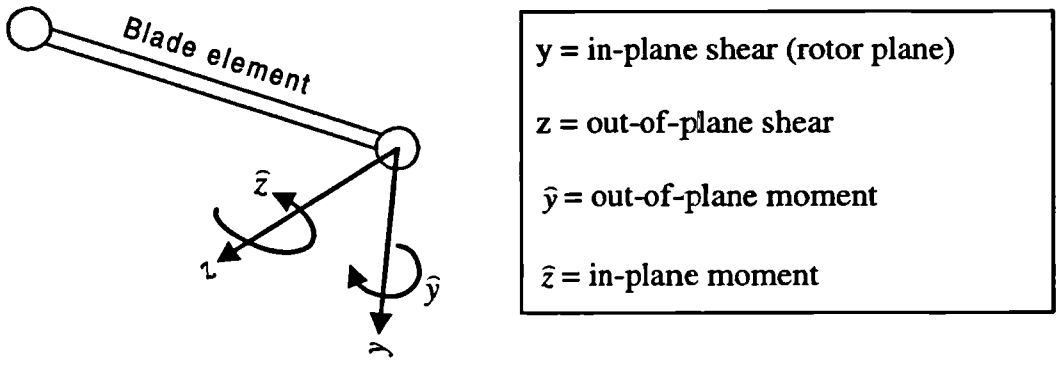

Figure 6-4 Blade element sign convention

No account is taken of the axial or torsion modes because no data is available for these. This is common for most blades and is best omitted from the analysis so as to prevent future conditioning errors in the numerical solution.

The analysis of systems comprising multi-degree of freedom elements is carried out in a similar way to that discussed earlier in Chapter 6.1.2. Differences arise however in the formation of the global system matrices. There is insufficient space available in this thesis to discuss this thoroughly and the reader is referred to other texts [References [11,12,13]] on the finite element method for details of this.

6.1.4 Natural frequency analysis and modal decomposition

The natural frequencies of the blade are obtained using an Eigen value calculation as expressed in Equation 14. (For more detailed information on Eigenvalue and vector calculations refer to Kreyszig[14]). These represent a good method for comparing the accuracy of the structural model as most blade manufactures can provide natural frequency data for the first few modes of vibration.

$$\omega_n = eigenvals\left(M^{-1} \cdot K\right) \qquad \textbf{Equation 14}$$

Where ω_n is the vector of natural frequencies, M^{-1} is the inverse mass matrix and K is the stiffness matrix. The function *eigenvals*( ) returns a vector of Eigen values, information on this is found in Berg[10] and Mathcad User's Guide[15].

The Eigen vector calculation returns a matrix of the mode shapes of each natural frequency. This is also explained in greater detail in Berg[10]. The Eigen vector formula is expressed in Equation 15.

$$\varepsilon_n = eigenvecs\left(M^{-1} \cdot K\right) \qquad \textbf{Equation 15}$$

Where ε_n is a matrix of Eigen vectors returned by the *eigenvecs*( ) function. The ε_n matrix takes the form of a series of augmented vectors as detailed in Mathcad User's Guide[15].

Using the Eigen vectors it is possible to transform the mass, stiffness and damping matrices into a general modal coordinate system, again the reader is referred to Berg[10]

for a theoretical definition. The equation of motion can be expressed in the general modal coordinate system as Equation 16.

$$M^* \cdot \ddot{q}(t) + C^* \cdot \dot{q}(t) + K^* \cdot q(t) = \varepsilon^T \cdot G \cdot u(t) \qquad \textbf{Equation 16}$$

Where

$$M^* = \varepsilon^T \cdot M \cdot \varepsilon$$
$$C^* = \varepsilon^T \cdot C \cdot \varepsilon$$
$$K^* = \varepsilon^T \cdot K \cdot \varepsilon$$
$$q(t) = \varepsilon^T \cdot x(t)$$

Working in the general modal coordinate system can be advantageous in reducing the number of degrees of freedom of the system, hence reducing the calculation time. This technique is known as modal decomposition and is employed in this analysis. Using the relationships expressed above we can decompose the mass, damping and stiffness matrices into components that are active in each mode. Higher modes occur at higher frequencies and eventually we reach a point at which insufficient load is being applied to the system at those high frequencies to contribute significantly to the overall behaviour. We can therefore choose not to consider these modes and hence reduce the number of degrees of freedom in the system matrices. This technique is used extensively to minimise computational time. For the analysis documented in Chapter 8, modal decomposition allowed a reduction from 97 degrees of freedom to only 15 with no loss of accuracy.

6.2 Derivation of blade element matrices

In this section we discuss the derivation of the mass, damping and stiffness matrices for the blade elements. The manufacturer provides structural data at a number of points along the blade. These points do not necessarily coincide with the finite element locations and so the data requires interpolation. This process is discussed for each matrix in the following sections.

6.2.1 The blade mass matrix

A number of different types of mass matrices have been compared for this research, the simplest using the 'lumped mass' approach. This type of matrix gives a fair representation of the blade but can be significantly improved by including a better

representation of the inertial terms in the rotational modes. The author's improved matrix is described in this section.

The format of the mass matrix is illustrated in Figure 6-5.

$$m = \left[\begin{array}{cccc:cccc} L_y & 0 & 0 & 0 & 0 & 0 & 0 & 0 \\ 0 & L_z & 0 & 0 & 0 & 0 & 0 & 0 \\ 0 & 0 & L_\theta & 0 & 0 & 0 & 0 & 0 \\ 0 & 0 & 0 & L_\psi & 0 & 0 & 0 & 0 \\ \hdashline 0 & 0 & 0 & 0 & R_\theta & 0 & 0 & 0 \\ 0 & 0 & 0 & 0 & 0 & R_z & 0 & 0 \\ 0 & 0 & 0 & 0 & 0 & 0 & R_{\bar{y}} & 0 \\ 0 & 0 & 0 & 0 & 0 & 0 & 0 & R_\psi \end{array}\right]$$

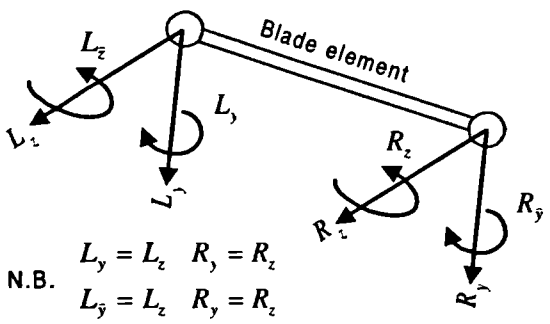

Figure 6-5 Format of the element mass matrix

The masses in the longitudinal modes (L_y, L_z, R_y and R_z) are determined assuming that each element is simply supported between its nodes. The nodal masses are then calculated by finding the reactions at the nodes due to the mass distribution. The mass distribution is determined by linear interpolation of the incremental mass data prepared by the blade manufacturer. This process is illustrated in Figure 6-6.

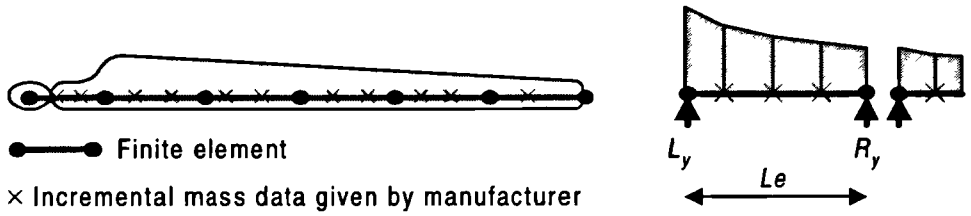

Figure 6-6 Derivation of nodal masses

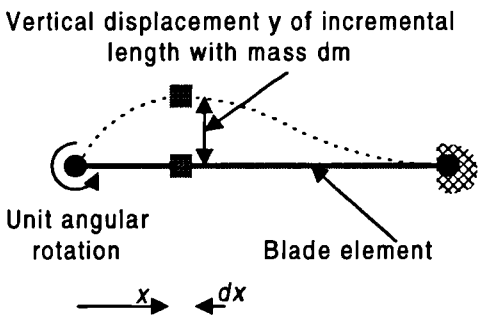

Figure 6-7 Blade shape function

The rotational inertia terms are derived using an element displacement shape function. Suppose the element shown Figure 6-7 in is rotated through an angle of 1 radian at its left-hand node.

The displacement y of an elemental length dx located at a distance x from the left hand node, can be determined by static analysis. The formula for this displacement is given in Equation 17.

$$y(x) = \frac{x}{Le^2} \cdot (x - Le)^2$$ **Equation 17**

Where Le is the length of the element.

If we differentiate twice, with respect to time, we obtain the quasi static acceleration of the element dx with respect to the rotational acceleration of the node. The inertial force on dx is obtained by taking the product of its acceleration and mass. The total moment of resistance on the node is therefore obtained as the sum of these incremental moments. This is given in Equation 18.

$$L_{\ddot{z}} = \int_0^{Le} me(x) \cdot y(x) \cdot x \cdot dx$$ **Equation 18**

Where $me(x)$ is the incremental mass in *kg/m*, at distance x from the node. This is obtained by linear interpolation of the manufactures data.

This approach is simple to compute and has shown good agreement with measured data for first and second mode natural frequency calculations. (No measured data was available to verify additional modes.) Using a blade model comprising only six elements, a maximum error of 2% was noted between the measured and calculated first mode natural frequencies. This comparison has been carried out for three different turbines, some giving better agreement than others, details are given in Chapter 8. [Reference: Halfpenny[16,17]]

6.2.2 The blade stiffness matrix

The total stiffness matrix comprises two component matrices, these are the structural stiffness and the centripetal stiffness matrices. We shall deal with the structural matrix first of all.

As with the mass properties, the structural stiffness properties are given by the manufacturer for different blade locations than those required for the finite elements. For this analysis it was found satisfactory to take the mean stiffness over the length of the finite element. The formula for this is given in Equation 19.

$$EI = \frac{1}{Le} \cdot \int_0^{Le} EI_e(x) dx$$ **Equation 19**

Where EI is the element stiffness and $EI_e(x)$ is the stiffness at a distance x

along the blade. This stiffness is obtained by linear interpolation of the manufacturers data.

The element is assumed to have a uniform stiffness profile, it is possible to derive more appropriate profiles, such as linear tapered elements, etc., but the present method yields good correlation with measured data [Reference 17] and is very simple to derive.

The element structural stiffness matrix is given in Equation 20.

$$k_e = \begin{bmatrix} \frac{12 \cdot EI_l}{Le^3} & 0 & 0 & \frac{6 \cdot EI_l}{Le^2} & -\frac{12 \cdot EI_l}{Le^3} & 0 & 0 & \frac{6 \cdot EI_l}{Le^2} \\ 0 & \frac{12 \cdot EI_f}{Le^3} & -\frac{6 \cdot EI_f}{Le^2} & 0 & 0 & -\frac{12 \cdot EI_f}{Le^3} & -\frac{6 \cdot EI_f}{Le^2} & 0 \\ 0 & -\frac{6 \cdot EI_f}{Le^2} & \frac{4 \cdot EI_f}{Le} & 0 & 0 & \frac{6 \cdot EI_f}{Le^2} & \frac{2 \cdot EI_f}{Le} & 0 \\ \frac{6 \cdot EI_l}{Le^2} & 0 & 0 & \frac{4 \cdot EI_l}{Le} & -\frac{6 \cdot EI_l}{Le^2} & 0 & 0 & \frac{2 \cdot EI_l}{Le} \\ -\frac{12 \cdot EI_l}{Le^3} & 0 & 0 & -\frac{6 \cdot EI_l}{Le^2} & \frac{12 \cdot EI_l}{Le^3} & 0 & 0 & -\frac{6 \cdot EI_l}{Le^2} \\ 0 & -\frac{12 \cdot EI_f}{Le^3} & \frac{6 \cdot EI_f}{Le^2} & 0 & 0 & \frac{12 \cdot EI_f}{Le^3} & \frac{6 \cdot EI_f}{Le^2} & 0 \\ 0 & -\frac{6 \cdot EI_f}{Le^2} & \frac{2 \cdot EI_f}{Le} & 0 & 0 & \frac{6 \cdot EI_f}{Le^2} & \frac{4 \cdot EI_f}{Le} & 0 \\ \frac{6 \cdot EI_l}{Le^2} & 0 & 0 & \frac{2 \cdot EI_l}{Le} & -\frac{6 \cdot EI_l}{Le^2} & 0 & 0 & \frac{4 \cdot EI_l}{Le} \end{bmatrix}$$

Equation 20

Where EI_l and EI_f are the edgewise and flatwise blade stiffness' respectively. These are derived from the manufactures data using Equation 19.

The manufactures data usually provides flatwise and edgewise stiffness' along the blade. The blade itself has a varying twist along its length and therefore the stiffness for each element is given along a different axis. We must therefore transform the stiffness properties into a common blade coordinate axis system and this is achieved through the coordinate transform matrix expressed in Equation 21.

$$k_s = \phi_\beta^{\,T} \cdot k_e \cdot \phi_\beta \qquad \textbf{Equation 21}$$

Where k_s is the element structural stiffness matrix expressed in the blade axis system, k_e is the element stiffness matrix derived earlier, and ϕ_β is the coordinate transformation matrix for the twist angle β of the blade element. ϕ_β is defined by the matrix:

$$\phi_\beta = \begin{bmatrix} \cos(\beta) & \sin(\beta) & 0 & 0 & 0 & 0 & 0 & 0 \\ -\sin(\beta) & \cos(\beta) & 0 & 0 & 0 & 0 & 0 & 0 \\ 0 & 0 & \cos(\beta) & \sin(\beta) & 0 & 0 & 0 & 0 \\ 0 & 0 & -\sin(\beta) & \cos(\beta) & 0 & 0 & 0 & 0 \\ 0 & 0 & 0 & 0 & \cos(\beta) & \sin(\beta) & 0 & 0 \\ 0 & 0 & 0 & 0 & -\sin(\beta) & \cos(\beta) & 0 & 0 \\ 0 & 0 & 0 & 0 & 0 & 0 & \cos(\beta) & \sin(\beta) \\ 0 & 0 & 0 & 0 & 0 & 0 & -\sin(\beta) & \cos(\beta) \end{bmatrix}$$

The centripetal stiffening effect is caused by the rotation of the blades. The centripetal stiffness matrix is given in Equation 22.

$$k_c = \begin{bmatrix} 0 & 0 & 0 & 0 & 0 & 0 & 0 & 0 \\ 0 & \frac{T_n}{Le} & 0 & 0 & 0 & -\frac{T_n}{Le} & 0 & 0 \\ 0 & 0 & 0 & 0 & 0 & 0 & 0 & 0 \\ 0 & 0 & 0 & 0 & 0 & 0 & 0 & 0 \\ 0 & 0 & 0 & 0 & 0 & 0 & 0 & 0 \\ 0 & -\frac{T_n}{Le} & 0 & 0 & 0 & \frac{T_n}{Le} & 0 & 0 \\ 0 & 0 & 0 & 0 & 0 & 0 & 0 & 0 \\ 0 & 0 & 0 & 0 & 0 & 0 & 0 & 0 \end{bmatrix}$$

Equation 22

Where T_n is the total tensile force on the n^{th} element due to centripetal acceleration.

The value of T_n is determined by Equation 23.

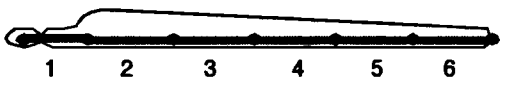

$$T_n = \sum_{i=n}^{N} m_i \cdot r_i \cdot \Omega^2$$

Equation 23

Where m_i = mass of i^{th} node
r_i = radius to i^{th} node
Ω = rotor speed in rad/sec
N = Total number of nodes

The total stiffness matrix can now be found by summing the structural and centripetal stiffness matrices.

$$k = k_s + k_c$$

Equation 24

Where k is the total stiffness matrix, k_s is the structural stiffness matrix and k_c is the centripetal stiffness matrix.

6.2.3 The blade damping matrix

The total damping matrix comprises of two component matrices, these are the aerodynamic and structural damping matrices. The aerodynamic damping matrix is a nodal matrix as opposed to an element matrix. The aerodynamic properties are calculated for each loaded node in the form of gain factors, these are discussed in Chapter 4.4. The aerodynamic damping matrix is expressed in Equation 25.

$$c_{aero} = \begin{bmatrix} c_t & -g_t & 0 & 0 \\ c_a & g_a & 0 & 0 \\ 0 & 0 & 0 & 0 \\ 0 & 0 & 0 & 0 \end{bmatrix} \qquad \textbf{Equation 25}$$

Where c_a, c_t, g_a and g_t are the aerodynamic gain factors described in Chapter 4.4.

The structural damping matrix is an element matrix. Structural damping is a difficult property to obtain and is therefore usually expressed as a percentage of critical damping for a particular mode of vibration. The relationship is given in Equation 26.

$$c_n^* = 2 \cdot \xi_n \cdot \sqrt{k^* \cdot m^*} \qquad \textbf{Equation 26}$$

Where ξ_n is the damping in the n^{th} mode expressed as a percentage of the critical damping and m^* and k^* are the mass and stiffness terms expressed in the modal coordinate system. c_n^* is the damping term associated with the n^{th} mode expressed in the modal coordinate system.

The damping matrix can be used in this form only when using modal decomposition in the analysis. In the analyses described in Chapter 8 and documented in Halfpenny[16,17], no structural damping values were available and so structural damping was not included. Later, sensitivity studies were carried out to determine the influence that structural damping has on the turbine response. It was found to be very influential in reducing the structural loads and so in future it is advisable to include some allowance for structural damping if at all possible. Due to lack of data a range of values should be considered to gain a degree of confidence in the answers obtained.

6.3 Derivation of tower and drivetrain matrices

The type of tower employed will dictate the finite element mesh required. For example, a lattice tower could use a series of simple ties and struts, whereas a concrete conical tower would require more complex beam elements. For this reason it is beneficial to analyse the tower structure as a separate sub-system and thence derive sub-system matrices. In the case of the tower, we can derive an equivalent 12 degree of freedom beam element which adequately models the first mode properties of a more complex structure, this is illustrated in Figure 6-8.

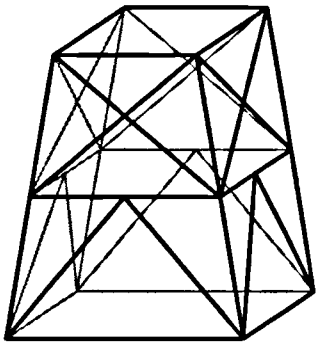

Complex lattice tower may be modelled by a single beam element sub-system

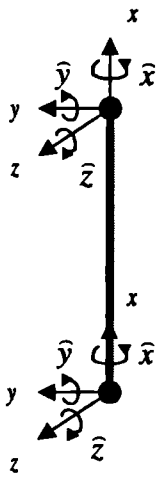

Figure 6-8 Lattice tower sub-system

The subsystem matrices are evaluated using a separate finite element analysis. In this analysis we impose unit accelerations, velocities and displacements to each degree of freedom in turn. The reaction forces from these can be calculated for each degree of freedom and the mass, damping and stiffness matrices thus determined.

Tower sub-systems allow us to develop dedicated turbine analysis programs without having the additional complexity of modelling many different tower configurations. In addition to this we often observe that the tower need only be modelled using relatively few sub-system elements and this yields a much smaller structural model. This is especially true when considering the structural design of the rotor blades. Following a detailed investigation it was found that the tower dynamics offer little contribution to the blade loading, it is therefore sufficient to model the tower using only a single element in most cases. It is worth noting that the early versions of the Garrad Hassan program, TURBLOAD, used a single degree of freedom tower element that measured

only fore-aft motion of the tower top. [Quarton[3].] Subsequent modification to TURBLOAD now allows for multiple mode response, though still only in the fore-aft direction. Wei[4] reports that this was only included to adequately model the behaviour of floating offshore turbines.

The drivetrain is modelled as a single degree of freedom element that is incorporated in the tower top element. For these investigations an induction generator has been assumed. Induction generators have negligible stiffness and behave as a damper. For this model the generator is modelled as a damper on the low speed shaft. The generator damping is calculated from the generator slip speed using Equation 27.

$$\text{Generator coefficient of damping } c_h = \frac{Torque}{Slip\ \ speed} \qquad \textbf{Equation 27}$$

$$\text{Where } Slip\ \ speed = Slip\ \ at\ \ rated\ \ power \cdot \Omega$$

$$\text{and } Torque = \frac{Rated\ \ turbine\ \ capacity\ \ [watts]}{\Omega}$$

The rotational inertia of the drive train is calculated on the low speed shaft. This is expressed in Equation 28.

$$I_h = I_L + G_R \cdot I_H \qquad \textbf{Equation 28}$$

Where I_L is the total inertia on the low speed shaft, I_H is the total inertia on the high speed shaft and G_R is the gear ratio of the gearbox.

The drivetrain element is included in the structural model by inserting an extra row and column in the tower top element matrices. The tower top is therefore modelled as a 13 degree of freedom system. This is illustrated in Figure 6-9. The drivetrain damping matrix is inserted to couple the $\hat{z}$ degrees of freedom between the rotor and tower. No other cross coupling is applied.

The additional mass of the nacelle, plant and rotor hub is added to the tower top node as lumped masses.

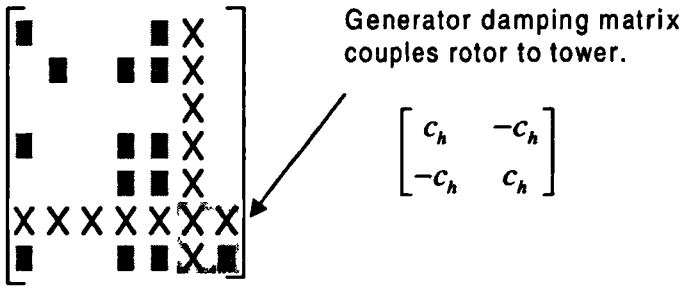

Figure 6-9 Incorporating the drivetrain element

6.4 Assembling the combined structural matrices

To this point we have considered the blade and tower element matrices in isolation. These must now be integrated into a combined global model of the turbine. Figure 6-10 illustrates a typical finite element representation of a complete turbine.

6.4.1 The global coordinate axis system

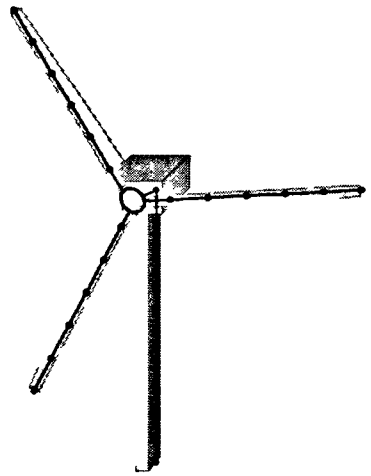

Figure 6-10 Typical element mesh of a turbine

Before assembling the global matrices it is necessary to transform all the elements into a common global coordinate axis system. A convenient axis system would be the tower axis system, therefore each blade requires a coordinate transformation.

Coordinate transformation is usually carried out using the formula expressed in Equation 21, where the transformation matrix is replaced with one covering all the degrees of freedom. (See Equation 20, chapter 9). In this particular analysis however, this method is unsuitable because the blade element has no axial nor torsional properties. This in effect violates continuity which results in 'holes' in the finite element mesh. If, on the other hand, axial and torsional degrees of freedom were incorporated in the blade, these would prolong the calculation time and risk possible matrix conditioning problems which result from having to estimate the structural properties. (Torsional properties are rarely provided by the manufactures). To circumvent these problems the author has developed a new 'transform element'. This allows each blade to be calculated in its own local

coordinate axis system while the transform element is responsible for transforming blade reactions into tower loads and visa versa. The global structural matrices, therefore, do not have to be expressed in one common axis system. In our analysis the transform element for each blade lies in the blade root as illustrated in Figure 6-11.

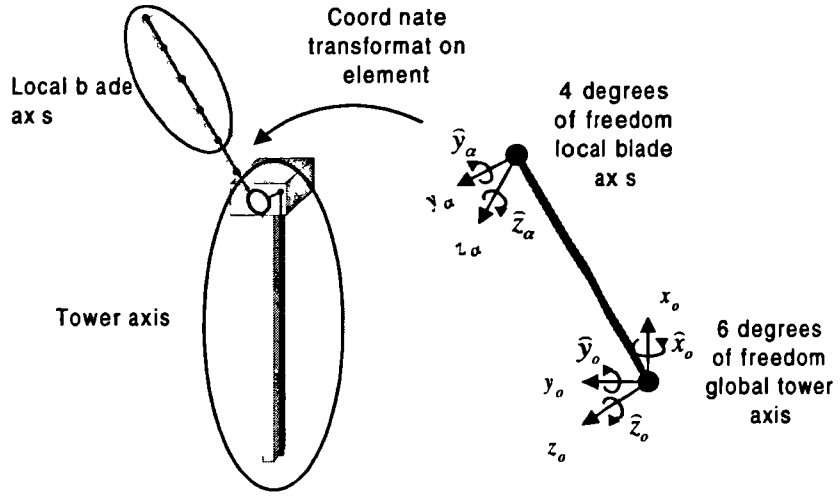

Figure 6-11 The blade coordinate transformation element

We shall now derive a method for calculating the transformation element. First of all consider the transformation matrix to transform between displacement of the tower and displacement of the blade. This is illustrated in

Figure 6-12.

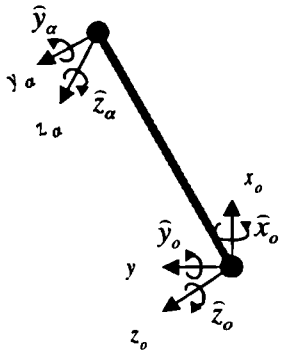

$$\begin{bmatrix} -\sin(\varphi) & \cos(\varphi) & 0 & 0 & 0 & 0 \\ 0 & 0 & 1 & 0 & 0 & 0 \\ 0 & 0 & 0 & -\sin(\varphi) & \cos(\varphi) & 0 \\ 0 & 0 & 0 & 0 & 0 & 1 \\ \cos(\varphi) & \sin(\varphi) & 0 & 0 & 0 & 0 \\ 0 & 0 & 0 & \cos(\varphi) & \sin(\varphi) & 0 \end{bmatrix} \cdot \begin{bmatrix} x_o \\ y_o \\ z_o \\ \hat{x}_o \\ \hat{y}_o \\ \hat{z}_o \end{bmatrix} = \begin{bmatrix} x_\alpha \\ y_\alpha \\ z_\alpha \\ \hat{x}_\alpha \\ \hat{y}_\alpha \\ \hat{z}_\alpha \end{bmatrix}$$

Figure 6-12 Transformation matrix between tower and blade axes.

This transformation matrix is used to transform forces and displacements between the blade and tower axes and the formulae for this is stated in Equation 29.

$$f_a = \phi \cdot f_o \qquad x_a = \phi \cdot x_o \qquad \textbf{Equation 29}$$

Where f_a and x_a represent force and displacement in the blade axis, and f_o and x_o force and displacement in the tower axis.

Rearranging these formulae yield expressions for the inverse transformations. Noting that the transformation matrix is orthogonal implies that it's inverse matrix is equal to its transverse, i.e. $\phi^{-1} = \phi^T$. The inverse transformation can therefore be expressed as Equation 30.

$$f_o = \phi^T \cdot f_a \qquad x_o = \phi^T \cdot x_a \qquad \textbf{Equation 30}$$

Using the above relationships we can state the following formulae for the forces in the blade and tower axes systems as a result of displacements in these axes. Similar formulae are found using the mass and damping matrices with the acceleration and velocities respectively.

$$f_a = k_a \cdot x_a \qquad f_a = k_a \cdot \phi \cdot x_o \qquad \textbf{Equation 31}$$

$$f_o = \phi^T \cdot k_a \cdot x_a \qquad f_o = \phi^T \cdot k_a \cdot \phi \cdot x_o$$

Where k_a is the blade element stiffness.

Consider now the original 8 degree of freedom blade element stiffness matrix at the blade root. We wish to change this into a transformation element. The element can be sub-divided into four sub-matrices as shown in

Figure 6-13.

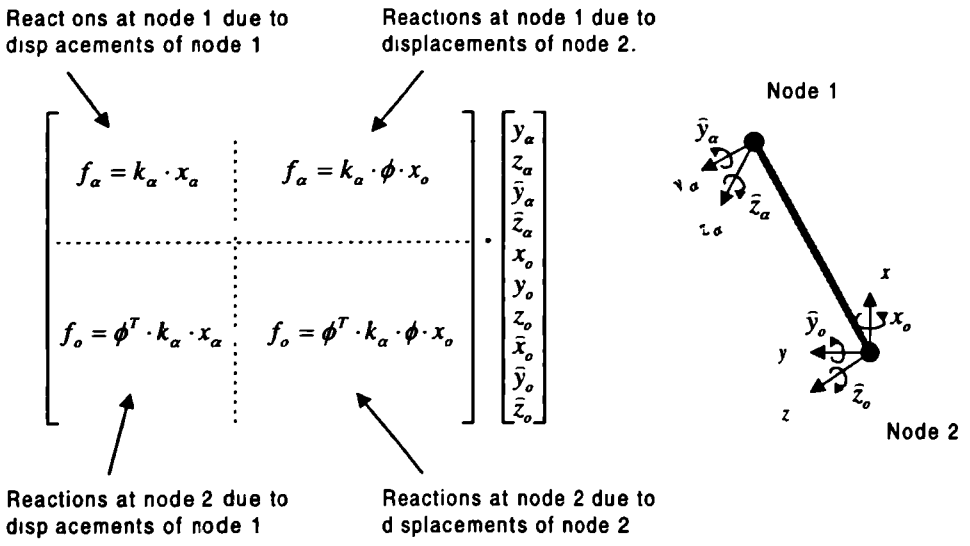

Figure 6-13 Sub-division of the stiffness matrix

The above diagram illustrates the procedure to be carried out for each quarter of the blade element matrices. However it is obvious that at present the element matrices are of incompatible size with the transform matrix. This is remedied by filling in the missing degrees of freedom in the element matrices with zeros. The transformation procedure is therefore shown in Figure 6-14.

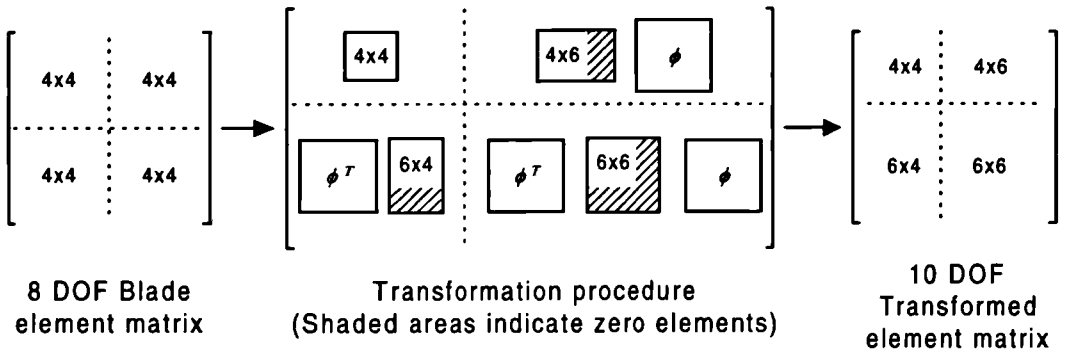

Figure 6-14 The element transformation process

6.4.2 Assembling the global structural matrices

Having dealt with the coordinate axes we can now go ahead assembling the global structural matrices in accordance with Meirovitch[11]. We shall concentrate primarily on the analysis of two and three bladed machines. Furthermore we shall restrict ourselves to the teetered hub when dealing with two bladed rotors. This is necessary to avoid azimuth dependency problems. These are discussed later.

6.4.2.1 Three bladed rotors

Three bladed rotors all have fixed hubs, this implies that all the forces and moments from each blade are transmitted to the tower. This can cause problems when considering the heave, sway, yaw and tilt modes of the tower. Essentially, the dynamic analysis described in this chapter, models the blades as stationary elements inclined at some constant azimuth angle φ. The blade rotation effect is taken into account during the rigid body aerodynamic load analysis, reported in Chapter 5, and is represented in the dynamic analysis by the cross-power spectral density matrix of wind speed, $\tilde{G}(\omega)$. Azimuth dependency problems arise when the tower loading is influenced by the particular azimuth angle φ of the rotor.

For a three bladed rotor, azimuth dependency becomes an issue when we have to consider the tower heave, sway, yaw and tilt modes. These values vary with respect to the azimuth angle of the rotor. When considering the blade dynamics this is not an important consideration as the tower dynamics have little effect on the blade loading. We can therefore say that for all analyses, with the exception of the four tower modes above, it is adequate to assign an arbitrary value to the azimuth angle. A test to confirm this assumption can be made by varying the angle. If this yields little variation in the results then the assumption is sound. In the case of the analyses documented in Chapter 8, no variation in loading was noted as we changed the arbitrary rotor azimuth angle φ.

The tower heave and sway loads are usually of little value to the turbine designer and so may be neglected. In many circumstances, however, it is still necessary to calculate the unsteady yaw and tilt moments on the turbine which are caused through turbulent wind loads. Oei[18] states the importance of this on the design of the yaw mechanism. The tower tilt and yaw moments may be calculated separately using the dynamic model described in this chapter and the concept of the 'super element' discussed in Chapter 5.

The super element is an imaginary blade which exhibits the same properties as the whole rotor. In Chapter 5 we used the super element concept to derive expressions for the yaw and tilt moments on a rigid turbine. These loads may be applied to one of the blades modelled in this dynamic analysis. In effect we are using the dynamic

properties of one blade to model the structural loading on the whole rotor. This will result in unrealistic deformation and load on the blade in question. However, the prediction of tower loads are reliable. This analysis holds because the structure is assumed to be linear elastic.

As the tower deforms in response to the applied rotor loading, it causes the rotor to be displaced also. Rotors comprising three of more blades behave as a homogeneous disk when displaced through steady air. This is proven later in Chapter 9. Rotor response is therefore independent of the azimuth angle of the rotor. Bearing this in mind, along with the assumption of linear elasticity, we can therefore conclude that the concept of the super element holds true for the dynamic analysis of three or more bladed rotors. To analyse the yaw and tilt moments on the tower we must calculate the transfer functions between super element loading and the tower moment. This is illustrated in Figure 6-15.

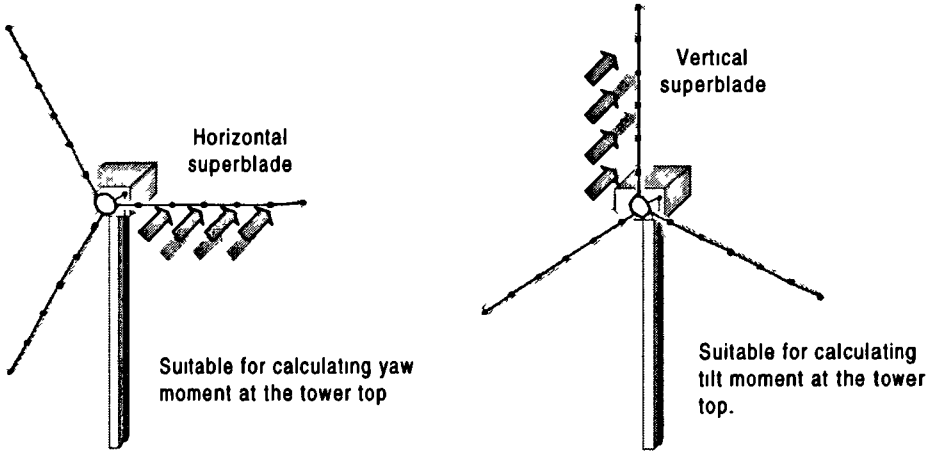

Figure 6-15 Azimuth position of super blade for modelling tilt and yaw moments on the tower

6.4.2.2 Two bladed, teetered rotors

The teetered hub eliminates the transfer of blade moments to the tower. This may be incorporated in the dynamic model by removing the coupling between the tower top and rotor in these degrees of freedom. This is accomplished by introducing additional degrees of freedom at the tower top in a similar manner to that described for incorporating the drivetrain element. Alternatively, the yaw and tilt modes may be zeroed in the tower elements. This implies that the tower base overturning moment

should be calculated separately from the product of the rotor thrust and the hub height. This method, though not so elegant, is much simpler to implement.

6.5 Calculation of element forces due to random wind turbulence

The linear transfer function between the wind speed incident on the blades and the resulting forces on the structure is evaluated as described in Chapter 6.1.2. A unit amplitude wind speed is applied along the z axis of each loaded node in turn. The transfer function G, between wind speed and wind load, is given by the following nodal matrix:

Equation 32

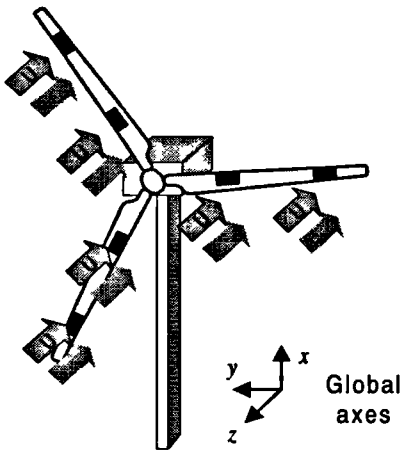

$$Virtual\ \ blade\ \ load = G \cdot U$$

$$= \begin{bmatrix} 0 & -g_t & 0 & 0 \\ 0 & g_a & 0 & 0 \\ 0 & 0 & 0 & 0 \\ 0 & 0 & 0 & 0 \end{bmatrix} \cdot \begin{bmatrix} 0 \\ 1 \\ 0 \\ 0 \end{bmatrix}$$

Where U is the unit virtual wind speed along the z axis.

The analysis results in a matrix of linear transfer functions $H(\omega)$. The cross-power spectral density matrix of element forces is obtained using Equation 33. In most cases we are only interested in the auto-power spectral densities, it is therefore acceptable to take the leading diagonal and discard the off diagonal terms. This technique is discussed in Chapter 2.3.7.

$$G^F(\omega) = \overline{H(\omega)} \cdot \tilde{G}(\omega) \cdot H(\omega) \qquad \textbf{Equation 33}$$

Where $G^F(\omega)$ is the single sided, cross-power spectral density matrix of element forces, and $\tilde{G}(\omega)$ is the single sided, cross-power spectral density matrix of rotationally sampled wind speed on the blades.

6.6 Conclusion

In this chapter the structural dynamic analysis of the turbine has been presented. Since the onset of this study, others have produced their own structural models. However,

the model presented here is unique in that the analysis is carried out wholly in the frequency domain and problems with transforming between the rotating and stationary coordinate axes have been addressed using the 'Rotor Super Element' approach.

Blade element matrices are derived in 8 degrees of freedom and a combined tower and drivetrain element in 13 degrees of freedom. The blade matrices are expressed in this way because structural property data is unavailable for both the axial and torsional modes. A new technique, termed the transfer element, is introduced to allow the tower to interface with the blade matrices despite the incompatible matrix size. This new technique is necessary to eliminate the possibility of matrix illconditioning and avoid 'holes' in the structural mesh. The finite element approach developed also allows for the inclusion of base motion spectra at the tower. These are discussed later in chapter 9.

---

[1] Dragt J.B. (1985). "Load fluctuations and response of rotor systems in turbulent wind fields." ECN-172. Internal publication.

[2] Garrad A.D. and Hassan U. (1986). "The dynamic response of wind turbines for fatigue life and extreme load prediction." Proceedings of the 1986 European Wind Energy Conference.

[3] Quarton D.C. et al. (1992). "The calculation of wind turbine loads. A frequency or time domain problem?" Proceedings of the 1992 British Wind Energy Conference.

[4] Wei J and Quarton D.C (1994). "Modelling and load prediction for offshore horizontal axis wind turbines." Proceedings, 1994 Chinese Wind Energy Conference.

[5] Garrad A.D. et al. (1995). "Study of offshore wind energy in the EC." Joule I sponsored project. Published by Verlag Natürliche Energie, Brekendorf, Germany.

[6] Sørensen P. (1994). "Frequency domain modelling of wind turbine structures." Risø-R-749(EN). Risø National Laboratory, Roskilde, Denmark.

[7] Sørensen P., Larsen G.C and Christensen C.J. (1995). "A complex frequency domain model of wind turbine structures." Journal of Solar Engineering, November 1995, Vol. 117 / 311.

[8] Van Engelen T.G. (1991). "Turbu-I Computer program for turbulence load analysis of horizontal axis wind turbines. Theory and program description." ECN, SU General Services, Petten, The Netherlands.

[9] Van Engelen T.G (1996). Personal communication with the engineer responsible for the development of TURBU. ECN, The Netherlands

[10] Berg G.V (1989) "Elements of structural dynamics." Prentice Hall. ISBN 0-13-272493-6

[11] Meirovitch L. (1986). "Elements of vibration analysis." McGraw-Hill Book Company. ISBN 0-07-100271-5

[12] Barltrop N.D.P and Adams A.J (1991). "Dynamics of fixed marine structures.) Butterworth-Heinemann Ltd. Linacre House, Jordan Hill, Oxford OX2 8DP, England.

[13] Potts J.F and Oler J.W (1989). "Finite element applications with microcomputers." Prentice-Hall International. ISBN 0-13-317439-5.

[14] Kreyszig E. "Advanced Engineering Mathematics. Seventh Edition." John Wiley & Sons, inc.

[15] MathSoft (1995). "Mathcad User's Guide (Version PLUS 6.0)." MathSoft Inc., 101 Main Street, Cambridge, MA 02142, USA.

[16] Halfpenny A (1995). "Notes on the Mathcad implementation of TURBU." Personal correspondence to W.S. Atkins Ltd.

[17] Halfpenny A (1996). "TURBUFIN. Notes of the Mathcad implementation of TURBU." Personal correspondence to W.S. Atkins Ltd.

[18] Oei T.D. (1987). "Turbulence induced yaw dynamics of horizontal axis wind turbines." Memo FYS-WIND-87-33, Internal publication, Netherlands Energy Research Foundation ECN, The Netherlands.

7. Fatigue analysis in the frequency domain

This chapter describes the analysis of fatigue life from power spectral density functions (PSDs) in the frequency domain. Material fatigue is a very large subject and it is not possible to cover the many areas of analysis and material properties in this thesis. Instead we will concentrate only on the new analysis techniques for deriving fatigue life from PSDs, because these are directly relevant to the work covered in this thesis.

For further background information on the theory and concepts of fatigue analysis the reader is referred to Bannantine[1]. A more specific account on time domain analysis techniques applicable to wind turbines is given by both Spera[2] and Stoddard[3]. An overview of the theory contained in this chapter is also given by Halfpenny[4].

7.1 Introduction to fatigue analysis

Fatigue failure arises through continually varying stresses within a component. Taken individually, each stress cycle is insufficient to cause yielding of the component but as they are repeated over a period of time they cause a gradual decay in the component until the point of eventual failure.

The path to fatigue failure is considered to occur in two stages. Firstly a crack is seen to initiate in the component at some point. This usually coincides with an imperfection in the surface structure of the component. The crack then propagates due to cyclic plasticity at the root where a local stress concentration will occur. When the crack has grown sufficiently the component becomes unable to withstand the load on it any more and failure results.

We have three methods of fatigue analysis which relate to the stages in the crack's development. The local strain approach, ε-N analysis, can be used to predict the time taken for a crack to initiate. After initiation a 'Linear Elastic Fracture Mechanics' (LEFM) model can be used to model the crack's propagation through the component. The third type of analysis is known as the 'Total Life', 'Nominal Stress' or S-N analysis, and this is used to model the whole process. Frequency domain fatigue analysis is based on a Total Life S-N approach.

7.1.1 Time domain analysis, the SN method:

To demonstrate how the frequency domain analysis proceeds it is perhaps best to set out a parallel approach in the time domain and then compare the two.

The starting point for any fatigue analysis is the response of the structure or component. In the time domain this is usually expressed as a stress or strain time history. Fatigue occurs as a result of stress or strain reversals in the time history. These are known as cycles. The significant aspects of these are the ranges of stress in the cycle and also their mean stress. Today the range and mean information is usually extracted from the time history using a procedure known as 'Rainflow Cycle Counting'. Matsuishi and Endo first introduced the concept of rainflow ranges to the scientific community over twenty years ago. An example of the way rainflow ranges are extracted from a time signal is given by Bishop[5] and Downing[6].

The output from a rainflow cycle counting exercise is usually expressed as a range mean histogram such as that shown in Figure 1[†]. The stress range of each cycle is given along the x axis, its mean stress is shown on the y axis and the z axis gives the number of cycles contained in the time history for each particular range and mean. This data was taken from the Howden HWP330 wind turbine; Bishop[7] discusses the analysis. The fatigue life quoted was obtained for an aluminium alloy 2024_HV_T4.

[†] This data was analysed and displayed using the nSoft modules; cyc and rqp. Refer to the nCode user guide for more information.

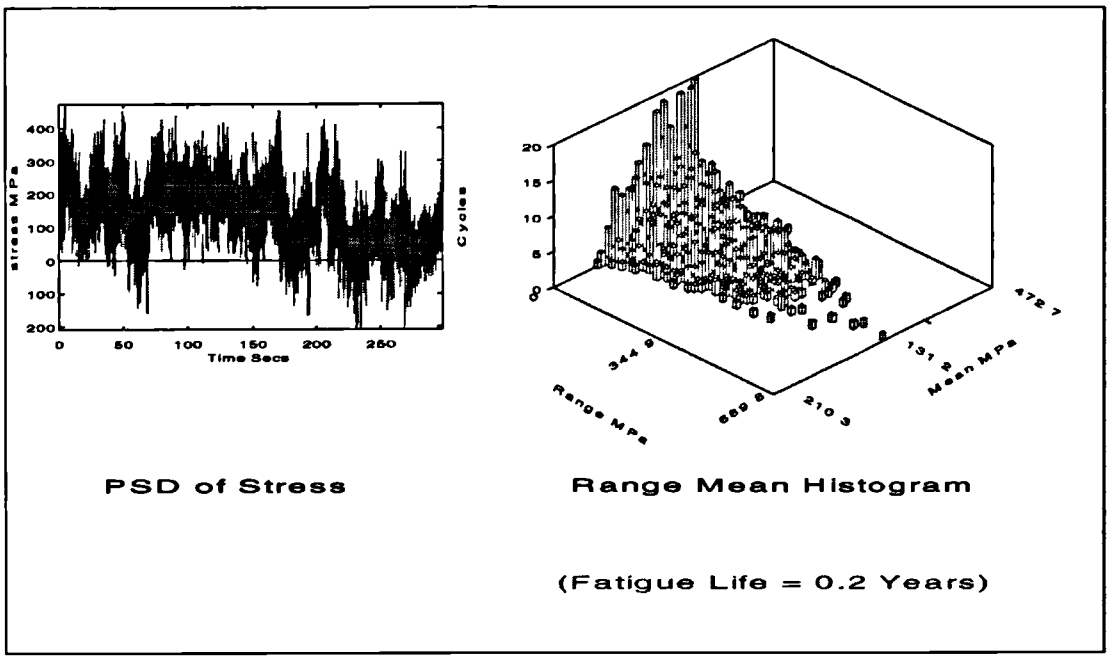

Figure 1 Range Mean Histogram Derived by Rainflow Cycle Counting

Each cycle will induce a certain amount of fatigue damage on the component. The total damage caused by the time history can therefore be obtained by summing the damage caused by each cycle shown in the stress range histogram. This approach is known as the Palmgren-Miner accumulated damage rule after the two independent people who proposed it.

The S-N approach in known to have limitations, in particular it doesn't model the sequencing effects of the cycles. This is a phenomenon where the order in which the cycles occur will influence the fatigue crack's behaviour. For example, many small stress cycles following a single large tensile cycle will cause more damage than if the small cycles followed a single large compressive cycle. This is modelled using Massing's hypothesis of stress-strain hysteresis and forms part of the local strain analysis approach. This is beyond the scope of this thesis and the reader is referred to Bannantine[1] for more details. Sequencing effects are less important for our analysis as we are dealing with stochastic events and there is an equal probability of the sequences occurring in either direction, hence one will tend to negate the other.

The damage caused by each cycle is calculated by reference to the material life curve, in this case the SN curve. The SN curve shows the number of cycles to failure, N_f, for a given stress range, S. The total damage caused by N number of cycles is therefore

obtained as the ratio of cycles to the number of cycles to failure. The Palmgren-Minor rule can therefore be expressed as Equation 1.

$$Accumulated\ Damage = \sum_i \frac{N_i}{N_f} \qquad \textbf{Equation 1}$$

Where, N_i is the number of cycles with a particular stress range and mean; i is a ranging variable covering all the possible range and mean combinations; and N_f is the number of cycles to failure for a particular stress range and mean.

The accumulated damage is expressed as a proportion of the damage required to fail the material. Therefore the fatigue life for the component can be determined from Equation 2.

$$Fatigue\ Life = \frac{Length\ of\ time\ history}{Accumulated\ Damage} \qquad \textbf{Equation 2}$$

The SN curve is used to describe a material's or component's fatigue life. The SN curve plots stress range, log(S), against the number of cycles taken to fail the material or component, log(N_f), at that particular stress range. A typical SN curve for British Standard Steel, BS4360-43C[8], is shown in Figure 2[†].

[†] This figure was produced by the nSoft module mdm using data supplied by nCode International Ltd.

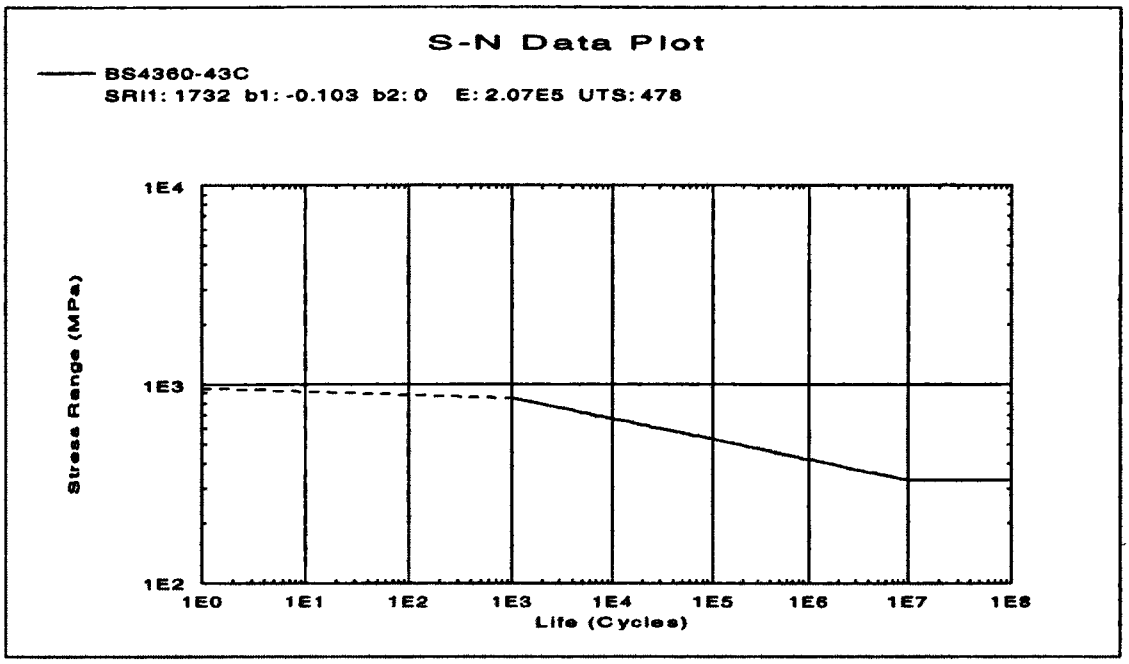

Figure 2 Typical SN curve for a British Standard Steel

The SN curve for this steel is typified by 3 stages. The first, denoted by a dotted line in the figure, represents the 'low cycle fatigue' range. The term, 'low cycle fatigue', refers to the number of cycles taken to cause fatigue damage, in this region only a few cycles are required as the stress range is high. In SN analysis this region is unreliable and the analysis technique is unsuitable for components where this is dominant. The unreliability arises because SN analysis uses a linear stress response to model what is effectively a non-linear stress strain problem. To calculate fatigue damage in this stress range region we must use a local strain approach, which is beyond the scope of this thesis.

The second stage of the SN curve relates to the high cycle fatigue portion (usually occurring after 10^3 cycles). The stress ranges here are much smaller and so the linear stress strain relationship is valid. After 10^7 cycles the third stage commences. This is known as the 'fatigue limit'. Stress ranges in this region are too small to cause any measurable fatigue damage to the component and so in theory it should last forever. This phenomenon is noticed in most carbon steels but shouldn't be relied on for other materials; aluminium, for example, has no fatigue limit.

The equation describing the important second stage of the S-N curve is expressed in Equation 3.

$$N_f \cdot S^m = k$$ **Equation 3**

Where N_f is the number of cycles to failure, S is the stress range, m is the slope of the exponential curve and k is the number of cycles to failure for a unit stress range. These are illustrated in Figure 3.

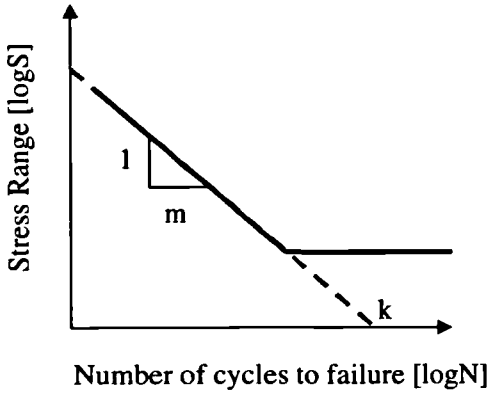

Figure 3 The S-N equation

The mean stress of a cycle also contributes to the fatigue damage caused by the cycle. Cycles with a high tensile mean stress will cause more damage than those with the same stress range but a lower mean. This phenomenon occurs because the higher tensile stresses in the component will force the crack tip to yield further and hence propagate faster. Mean stresses can be accounted for by altering the SN curve to account for the extra damage. In this way the SN curve is lowered as the mean stresses increase. In theory it is therefore necessary to determine a family of SN curves for a material with a range of mean stresses applied. In practice this is very seldom undertaken and instead empirical relationships given by Goodman (England, 1899) or Gerber (Germany, 1874) are often employed. In practice mean tensile stresses cause more damage than mean compressive stresses, in fact compressive stresses actually improve the fatigue.

7.1.2 Frequency domain analysis:

This section describes a variety of approaches for computing fatigue life, or damage, from a PSD of stress as opposed to a time history. The techniques fall into two broad categories, those that estimate fatigue life directly and those that compute range mean

histograms as an intermediate stage. These techniques are the result of a considerable amount of research around the world. As a result of this work a number of new techniques have been developed and these are summarised in this thesis. For more background information the reader is referred to Bishop[5], Sherratt[9] and Halfpenny[4]. The methods discussed here take no account of cycle mean stresses. Developments are currently underway by Bishop to address this situation and these will be documented in a proposed paper and technical manual produced in conjunction with the author[10].

In 1964 Bendat[11] proposed the first significant step towards a method of determining fatigue life from PSDs. Bendat showed that the probability density function (pdf) of peaks for a narrow band signal tended towards a Rayleigh distribution as the bandwidth reduced. Furthermore, for a narrow banded time history Bendat assumed that all positive peaks in the time history would be followed by corresponding troughs of similar magnitude regardless of whether they actually formed stress cycles. This effect was illustrated earlier in chapter 2.1.6. Using this assumption the pdf of stress range would also tend to a Rayleigh distribution. To complete his solution method, Bendat derived a series of equations to estimate the expected number of peaks using moments of area under the PSD. Bendat's narrow band solution for the range mean histogram is therefore expressed in Equation 4.

$$N(S) = E[P] \cdot T \cdot \left\{ \frac{S}{4 \cdot m_0} \cdot e^{-\frac{S^2}{8 \cdot m_0}} \right\}$$

Equation 4

Where N is the number of cycles of stress range S occurring in T seconds. m_0 is the zeroth moment of area under the PSD (i.e. the area beneath the curve), and E[P] is the expected number of peaks obtained by Equation 5.

$$E[P] = \sqrt{\frac{m_4}{m_2}}$$

Equation 5

m_4 and m_2 are the 4th and 2nd moments of area of the PSD respectively where the n^{th} moment of area is obtained as $m_n = \int f^n \cdot G(f)df$, and $G(f)$ is the value of the single sided PSD at frequency f Hz.

The term in brackets in Equation 4 is the Raleigh distribution. Figure 4 shows the range mean histogram obtained from the PSD of the time history given in Figure 1. The range mean histogram given by Bendat contains no cycle mean data.

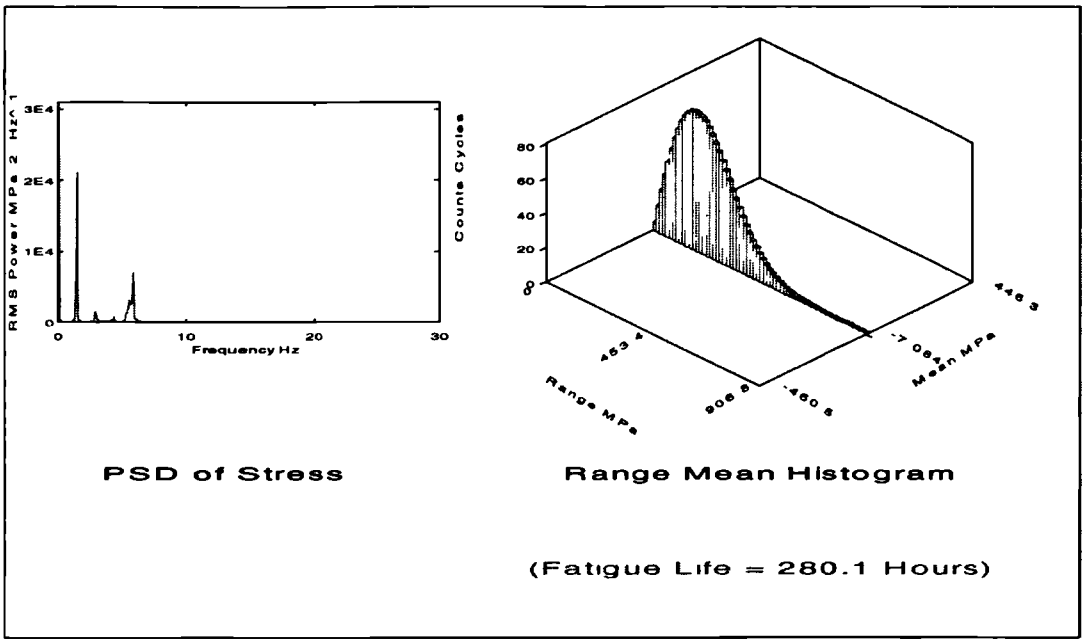

Figure 4 Range Mean Histogram Produced by Bendat's Narrow Band Solution

The problem with Bendat's narrow band solution is that it is extremely conservative when wider band time histories are used. (We now observe a fatigue life of only 280.1 hours.) The reason for this lie s in the assumption that peaks are matched with corresponding troughs of similar magnitude. This effect is illustrated in Figure 5. The wide band signal shown comprises a number of smaller cycles riding on a low frequency carrier wave. Using Bendat's assumption in this case results in the erroneous cycle extraction shown.

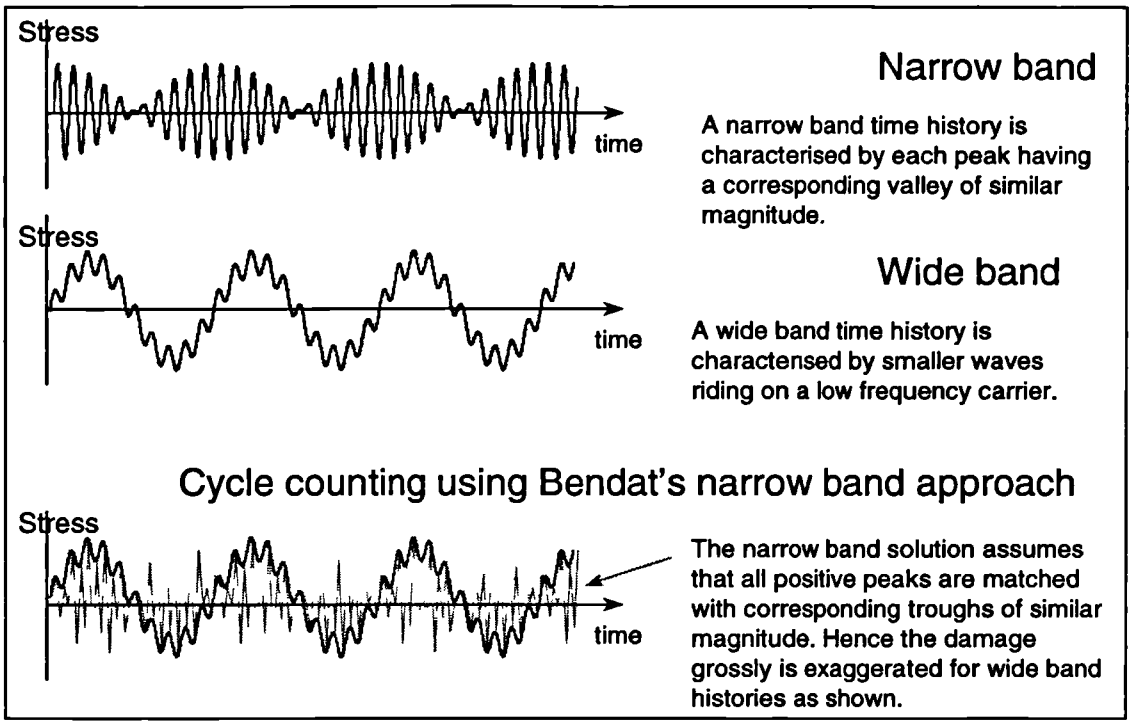

Figure 5 Why Bendat's Narrow Band Approach is Conservative

During the 1980's the need for a rapid fatigue analysis method based in the frequency domain became apparent to the offshore oil industry. Large jacket platforms were being designed and fatigue failures had to be avoided. The transient dynamic analysis proved too intensive for the time domain software because of the large structural models and high number of possible load combinations. The dynamic wave and wind load data was already provided in the frequency domain and it therefore seemed sensible to make use of the speed advantages inherent in a frequency domain analysis. The problem was how to calculate a reasonably accurate fatigue life using the resultant PSDs from the frequency domain analyses.

Sea state spectra are relatively wide banded and this effectively rules out the use of Bendat's narrow band fatigue analysis because the results prove too conservative. Several methods were developed to address this problem, the notable ones being Wirsching[12], Kam & Dover[13] and Hancock. These are semi-empirical approaches based on the narrow band solution. The latter two methods are both in the form of an equivalent stress parameter and neither tends to work particularly well when used outside the offshore platform industry. Wirsching's approach was developed for the offshore industry but has been found to be applicable to a wider class of industrial problems.

In other industries advances were also being made. Steinberg and Tunna both worked on the problem for the electronics and rail industries respectively. Again neither of these methods tend to work well outside their respective industries.

In 1985 Dirlik[14] proposed an empirical closed form solution to the problem following extensive computer simulations using the Monte Carlo technique. Although apparently more complicated than some alternative methods it is still only a function of four moments of area of the PSD, these being m_0, m_1, m_2 and m_4. This method has been found to be widely applicable and constantly outperforms all of the other available methods. The Dirlik equation is given in Equation 6.

$$N(S) = E[P] \cdot T \cdot p(S) \qquad \textbf{Equation 6}$$

Where $N(S)$ is the number of stress cycles of range S N/mm^2 expected in time T

E[P] is the expected number of peaks obtained by Equation 5.

$$p(S) = \frac{\frac{D_1}{Q} \cdot e^{\frac{-Z}{Q}} + \frac{D_2 \cdot Z}{R^2} \cdot e^{\frac{-Z^2}{2 \cdot R^2}} + D_3 \cdot Z \cdot e^{\frac{-Z^2}{2}}}{2 \cdot \sqrt{m_0}}$$

$$D_1 = \frac{2 \cdot (x_m - \gamma^2)}{1 + \gamma^2} \qquad D_2 = \frac{1 - \gamma - D_1 + D_1^2}{1 - R} \qquad D_3 = 1 - D_1 - D_2$$

$$Z = \frac{S}{2 \cdot \sqrt{m_0}} \qquad Q = \frac{1.25 \cdot (\gamma - D_3 - D_2 \cdot R)}{D_1} \qquad R = \frac{\gamma - x_m - D_1^2}{1 - \gamma - D_1 + D_1^2}$$

$$\gamma = \frac{m_2}{\sqrt{m_0 \cdot m_4}} \qquad x_m = \frac{m_1}{m_0} \cdot \sqrt{\frac{m_2}{m_4}}$$

Figure 6 shows the range mean histogram obtained using Dirlik's method for the wind turbine data used in Figure 1. Again the method ignores the cycle mean stresses but now gives an improved range mean histogram that is comparable with that obtained using a time domain approach. This is shown in Figure 7.

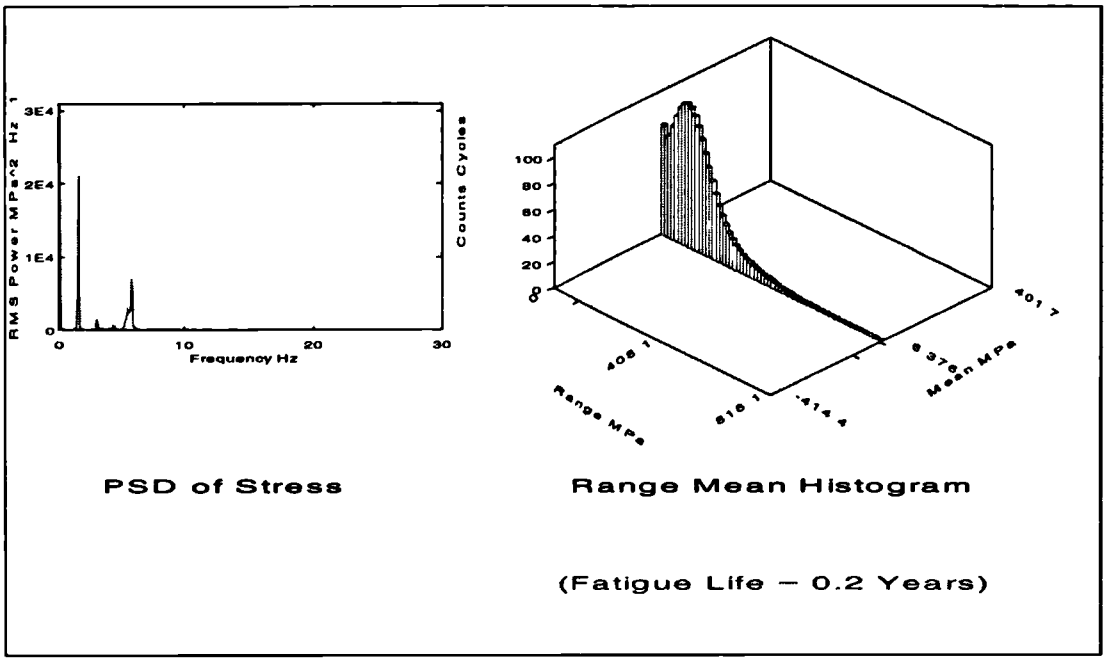

Figure 6 Range Mean Histogram Derived by Dirlik

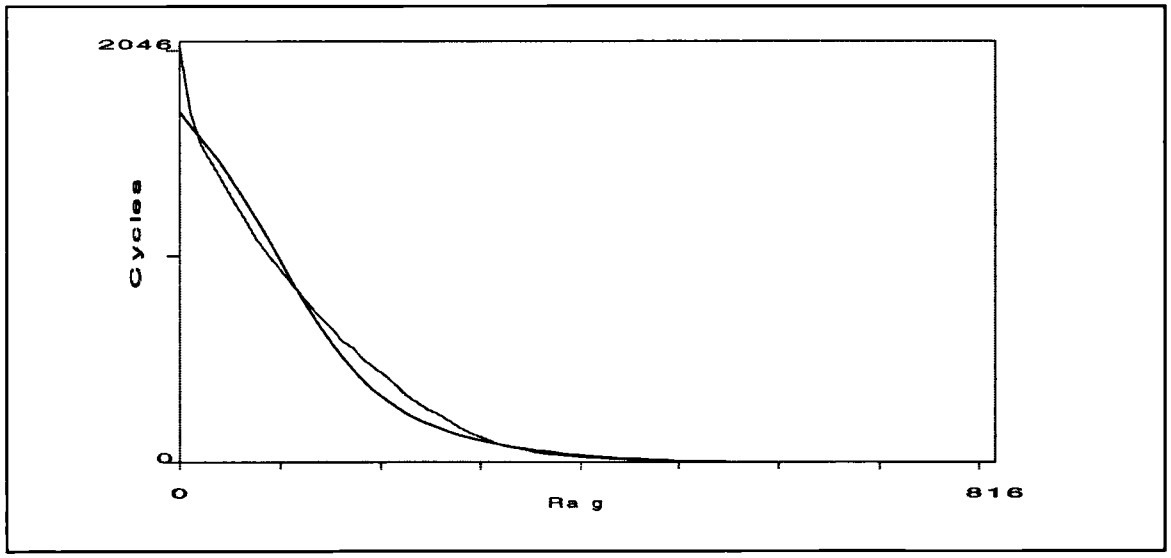

Figure 7 Exceedence Plot Comparing Time and Frequency Domain Range Mean Histograms

In terms of accuracy, Dirlik's empirical formula for rainflow ranges has been shown to be far superior to the previously available correction factors. However, the need for certification of the technique before its use meant that theoretical verification was required. This was achieved in 1988 by Bishop[15] when a theoretical solution for predicting rainflow ranges from the moments of area of the PSD was produced. Bishop[16] gives a detailed description of this method. The theoretical approach devised

by Bishop is computationally intensive and shows little improvement on accuracy over Dirlik's empirical approach. For this reason, Bishop's method gives credence to the Dirlik method but is seldom used for analysis purposes.

7.2 Comparison between fatigue analysis techniques

Many comparative studies have been carried out to ascertain the accuracy of all the various methods. Of notable significance to this thesis is the studies made by Bishop et al[7]. This study took data from the Howden HWP330 machine, computed fatigue lives in the frequency domain and then compared these with the life obtained from the time domain approach. A summary of the results is given in Table 1.

Load Case	Narrow Band	Dirlik	Wirsching	Bishop	Chaudhury	Hancock
y12a	5.14	1.03	3.91	1.52	2.13	2.75
y19a	5.15	1.00	3.92	1.54	2.14	2.77
y27a	14.34	1.59	10.91	1.74	5.12	5.83
y35a	81.87	2.34	62.23	1.95	30.08	25.08
y12b	1.91	0.77	1.46	1.13	0.98	1.25
y19b	1.98	0.81	1.50	1.22	1.04	1.31
y27b	3.67	1.07	2.79	1.29	1.47	1.92
y35b	18.34	1.48	13.95	1.84	5.68	6.10
y12c	1.98	0.76	1.51	0.86	0.95	1.25
y19c	1.87	0.73	1.43	0.86	0.92	1.20
y27c	2.03	0.74	1.54	0.72	0.87	1.14
y35c	3.22	0.76	2.45	0.66	1.15	1.42
y12d	2.09	0.84	1.59	1.15	1.03	1.33
y19d	2.03	0.83	1.54	1.17	1.02	1.31
y27d	2.92	1.01	2.22	1.15	1.23	1.62
y35d	7.50	1.12	5.70	1.23	2.75	3.29
y12e	2.80	0.99	2.13	1.27	1.50	1.95
y19e	3.06	1.01	2.33	1.44	1.64	2.12
y27e	3.50	1.03	2.67	1.53	1.65	2.16
y35e	8.81	1.11	6.71	1.99	3.31	4.15
y12f	3.86	0.98	2.93	1.43	1.66	2.18
y19f	3.97	1.00	3.02	1.61	1.78	2.33
y27f	3.96	1.01	3.01	1.57	1.76	2.31
y35f	5.59	0.98	4.25	1.65	2.17	2.80
avrg	7.98	1.04	6.08	1.36	3.08	3.32

Table 1 Comparison Between Different Frequency Domain Fatigue Analyses

The table clearly shows that the Dirlik approach is remarkably robust. It shows an average discrepancy of only 4% from the fatigue life calculated in the time domain.

7.3 Description of fatigue analysis approach adopted in this thesis

The Dirlik approach was adopted for the purpose of these studies. The decision was made in light of its superior performance over the other available techniques. Chapter 8 compares the fatigue life obtained from the theoretical results with that calculated using measured data.

The accumulated fatigue damage from all the cycles is determined by substituting Equation 3 and Equation 2 into Equation 1. This is given as Equation 7.

$$Accumulated\ Damage = \frac{E[P]\cdot T}{k}\cdot\int_0^\infty S^m\cdot p(S)\,ds \qquad \textbf{Equation 7}$$

Where $p(S)$ is the probability density function of stress ranges determined by Dirlik in Equation 6.

When comparing techniques for fatigue analysis it is often desirable to work in terms of an equivalent stress. The fatigue life curve is exponential in form implying that a small error in stress range prediction results in a large error in fatigue life. The equivalent stress is used to normalise the results and eliminate this exponential effect. The equivalent stress is calculated by Equation 8.

$$S_{eq} = \left\{\int_0^\infty S^m\cdot p(S)\,ds\right\}^{\frac{1}{m}} \qquad \textbf{Equation 8}$$

Substituting Equation 8 into Equation 7 and taking the reciprocal yields the fatigue life normalised for the exponential effect of the material S-N curve. This is given as Equation 9.

$$Normalised\ Fatigue\ Life = \frac{k}{E[P]\cdot T\cdot S_{eq}} \qquad \textbf{Equation 9}$$

7.4 Conclusions

In this chapter we have briefly introduced the theory of metal fatigue using the nominal stress (or S-N) approach. An account is given of the various methods for determining the fatigue life from PSD data of stress. The Dirlik method is recommended for general use in the wind turbine industry following the results of

previous application studies. A fatigue life model is proposed to compare results from the measured and calculated PSD analyses. This method normalises the stress data to eliminate the exponential problem in the S-N curve where small errors can be magnified substantially by the material properties.

The Dirlik method does not model cyclic mean stresses and therefore this has been ignored in these studies. Bishop has recently developed a new model that includes this effect. For more details on this approach the reader is referred to Bishop & Halfpenny[10].

[1] Bannantine JA., Comer JJ., Handrock JL (1990). "Fundamentals of Metal Fatigue Analysis." Prentice Hall, Englewood Cliffs, New Jersey 07632. ISBN 0-13-340191-X

[2] Spera D. A. (1995). "Wind Turbine Technology. Fundamental concepts of wind turbine engineering." Edited Spera D. A., ASME Press, ISBN 0-7918-1205-7

[3] Stoddard F.S. and Eggleston D.M. (1987). "Wind turbine engineering design." Von Nostrand Reinhold, ISBN 0-442-22195-9

[4] Halfpenny A. and Bishop NWM. (1997). "Vibration Fatigue." nCode International Ltd. 230 Woodbourn Road, Sheffield, S9 3LQ. England.

[5] Bishop NWM. and Sherratt F (1989). "Fatigue life prediction from power spectral density data. Part 1, traditional approaches and Part 2, recent developments." Environmental Engineering, 2.

[6] Downing SD. and Socie DF. (1982). "Simple rainflow counting algorithms." Int. J Fatigue, January 1982, 31-40.

[7] Bishop NWM, Hu Z, Wang R and Quarton D (1993). "Methods for rapid evaluation of fatigue damage on the Howden HWP330 wind turbine". British Wind Energy Conference, York.

[8] "FATIMAS user guide". nCode International Ltd, 230 Woodbourn Road, Sheffield, S9 3LQ, England.

[9] Sherratt F. (1995) "Current applications of Frequency Domain Fatigue Life Estimation." Conference volume "Product Optimisation for Integrity" pp 343-365. EMAS, West Midlands, England. ISBN 0-947817-47-6

[10] Bishop NWM and Halfpenny A. "Technical manual for MSC/FATIGUE." nCode International Ltd., 230 Woodbourn Road, Sheffield, S9 3LQ. England.

[11] Bendat JS (1964). "Probability functions for random responses." NASA report on contract NAS-5-4590.

[12] Wirsching PH and Light MC (1980). "Fatigue under wide band random loading". Journal Struct. Div. ASCE, 1593-1607.

[13] Kam JCP and Dover WD (1988). "Fast fatigue assessment procedure for offshore structures under random stress history". Procedures, Institution of civil engineers, Part 2, 85, 689-700.

[14] Dirlik T (1985). "Application of computers in fatigue analysis". PhD thesis, University of Warwick, England.

[15] Bishop NWM (1988). "The use of frequency domain parameters to predict structural fatigue." PhD thesis, University of Warwick, England.

[16] Bishop NWM and Sherratt F (1990). "A theoretical solution for the estimation of rainflow ranges from power spectral density data." Fatigue and fracture engineering of materials and structures, 13, 311-326.

8. Numerical model validation and comparison

8.1 Introduction

In this chapter we discuss the results obtained from the theoretical model and compare these, where possible, with those measured on real turbines. There have been difficulties in gaining sufficient data with which to undertake the comparative studies because of corporate confidentiality. Manufactures are reluctant to release aerodynamic data because there are no legal means by which they can prevent the turbine design being copied. For this study data has been provided by three turbine manufactures. Nedwind[1] have provided data for the Nedwind 50 turbine and this has been used to develop the analysis software. However, they have not provided measured data on which to validate the model.

Validation studies have been carried out independently by WS Atkins Ltd.[2] on two other turbines. The software developed for this PhD was made available to WS Atkins under the sponsorship agreement. They have been contracted to undertake a 'Stress audit' for a number of commercial turbines and during the course of this work have provided the author with comparative results for two of the turbines tested. No information has been given to indicate which manufactures are involved or what aerodynamic or structural properties the turbines have. We will refer to the two turbines as 'Turbine A' and 'Turbine B'. An account of the known properties of Turbines A and B are given in Table 8-1.

Turbine	A / A*	B
Method of control	Constant speed, stall regulated	Variable speed, stall regulated
Number of blades	3	3
RPM	27.7 / 25.8*	27
Coning angle	0 deg	3.5 deg
Rotor diameter	41 m / 44 m*	43 m
Number of airfoil sections per blade	2	3
Cut-in wind speed	5 m/sec*	5 m/sec
Cut-out wind speed	25 m/sec*	25 m/sec
Rated wind speed	15 m/sec*	16 m/sec
Rated power	600 kW*	600 kW
Manufacturers electrical power curves available	√*	√
Tower/Drivetrain Data		
Type	Conical steel	Cylindrical steel
Hub height	35 m	40 m
External tower diameter at the top	1.5 m	2.28 m
External tower diameter at the bottom	3.3 m	2.28 m
Plate thickness at the top	8 mm	8 mm
Plate thickness at the bottom	12 mm	32 mm
Tower top mass	31780 kg	38510 kg
Measured time history/statistical results of rotor torque	√	√
Measured time history/statistical results of tower base overturning moment	√	N/A
Blade data		
Flapwise natural frequency	1.815 Hz	N/A
Edgewise natural frequency	2.497 Hz	N/A
Measured time history/statistical results of flapwise bending moment	√	√
Measured time history/statistical results of edgewise bending moment	√	√

NOTES:

* Data has been provided for two variants of Turbine A. The blades on Turbine A* have been lengthened to enable it to deliver more power than Turbine A. Power data is provided for Turbine A* but structural loading is only given for Turbine A.

Table 8-1 Comparative data made available by WS Atkins

In this chapter we discuss the results obtained from the theoretical model and compare them with those obtained from the measured data. The theoretical model is subdivided into modules. Each module is calculated using a separate Mathcad worksheet. These are illustrated by the flow chart in Figure 8-1. We will deal, wherever possible, with each module separately.

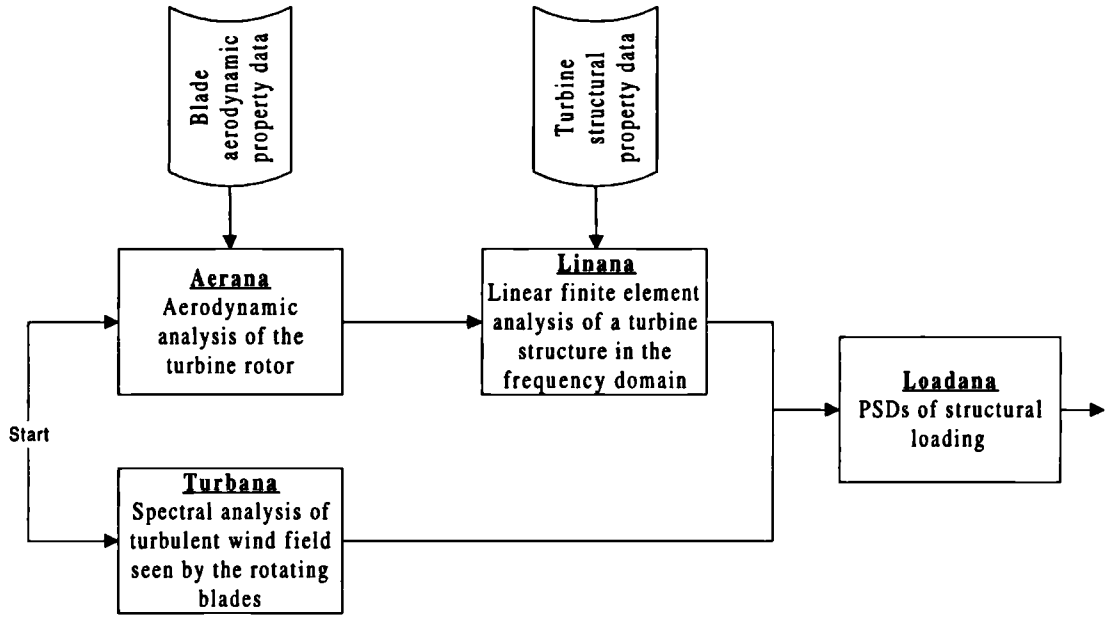

Figure 8-1 Flow chart of mathematical procedures in the analysis

8.2 Aerana: Aerodynamic pre-processor

Aerana serves as the aerodynamic pre-processor for the model and is described at length in Chapter 4. Aerana essentially performs two analyses. These are firstly; an equilibrium wake analysis for calculating the steady load and power output of the turbine; and secondly a frozen wake analysis for calculating the dynamic loading. Validation studies can be undertaken for the equilibrium analysis. However, no comparative data is available for the dynamic gain factors and these can therefore only be verified using the dynamic loads given by *Loadana.*

The equilibrium model can be validated by comparing the following results with those derived from measurements:

1. Power output with respect to the mean hourly wind speed
2. Thrust with respect to the mean hourly wind speed
3. Torque with respect to the mean hourly wind speed

4. Steady blade root moments

5. Blade parked loads

WS Atkins[2] have reported that all calculated results are in good agreement with those measured. It is unfortunate, however, that only the manufacturers published power curves have been made available to demonstrate this in the thesis. Figure 8-2 shows the comparison between the calculated rotor power and the quoted power. The curves given for Turbine A* both give rotor power and therefore can be compared directly. For the Turbine B comparison, only the electrical power is quoted by the manufacturer, this takes account of the losses in the drivetrain and generator and so cannot be compared directly with the calculated curve. According to WS Atkins, a value of approximately 10% was given for the generator loss. When this is considered then the two power curves show an excellent agreement.

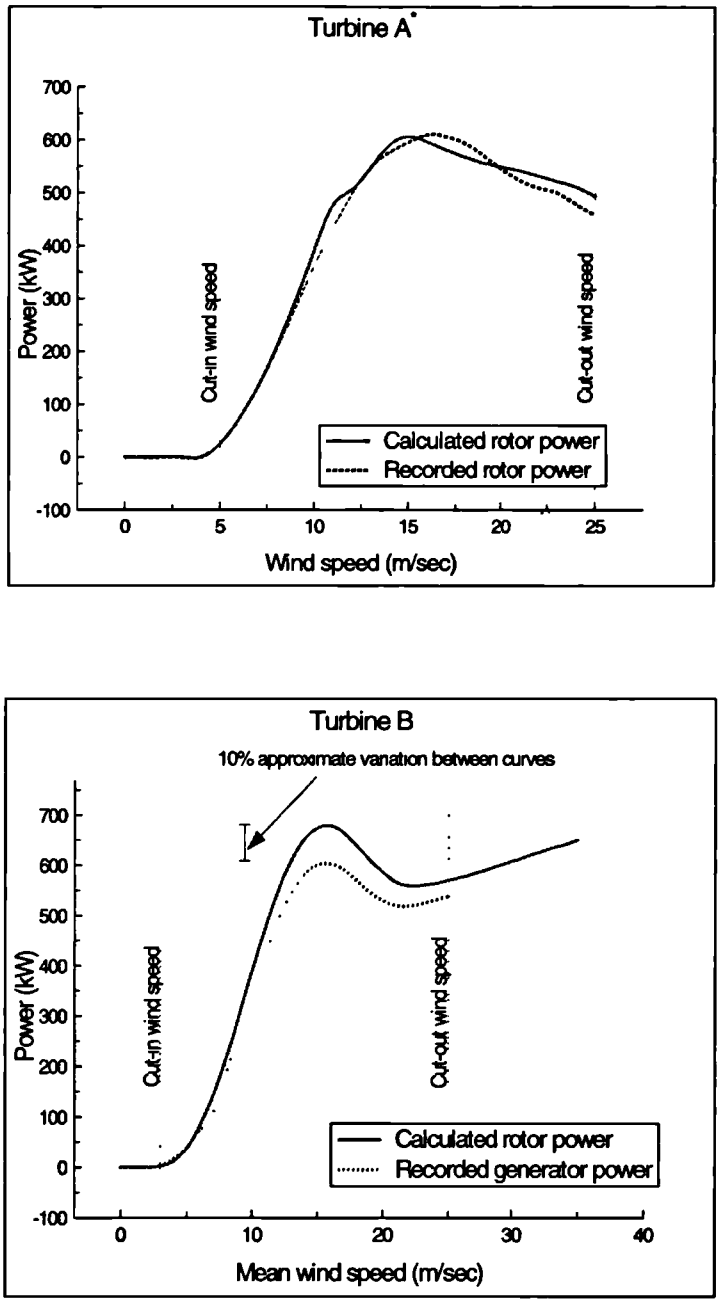

Figure 8-2 Comparison between calculated and published power curves for Turbines A* and B

8.3 Turbana: Meteorological pre-processor

Turbana effectively serves as the meteorological pre-processor for the model and can be subdivided into two parts. The first part derives the power spectral density function

of the turbulent wind speed measured at a single point in space. It then derives a coherence function to describe how the power spectral density varies with distance away from this point. These calculations are carried out using the ESDU model described in Chapter 3. The second part takes the auto-power spectrum and the coherence function and calculates the cross-power spectral density functions of wind speed seen by a number of rotating blade elements. This is described in Chapter 5. We will discuss the results from both parts separately.

8.3.1 The ESDU spectra

The ESDU model is widely used in the wind turbine community for modelling the turbulent wind field. Both TURBU[3] and TURBLOAD[4] are based on this model. However, they are based on an older version than the one discussed in this thesis. Figure 8-3 shows comparisons between the ESDU spectra and the measured spectra recorded for Turbine A (no data was provided for Turbine B). Two sets of data were provided for mean wind speeds of 10 and 20 m/sec and turbulence intensities of 8.9% and 9.3% respectively. They are each measured over a period of 10 minutes with a sample rate of 25Hz. For this comparison the power spectral density function was calculated over the whole sample length using Mathcad worksheets. The measured turbulence intensity is obtained from the time history using Equation 8-1.

$$I_u = \frac{\sigma_u}{V_z}$$ **Equation 8-1**

Where I_u is the turbulence intensity, σ_u is the standard deviation of the time history and V_z is the mean wind speed at hub height.

The ESDU spectrum is calculated using the measured turbulence intensity. Values for the ground roughness length may be substituted in the model until the required turbulence intensity is acquired.

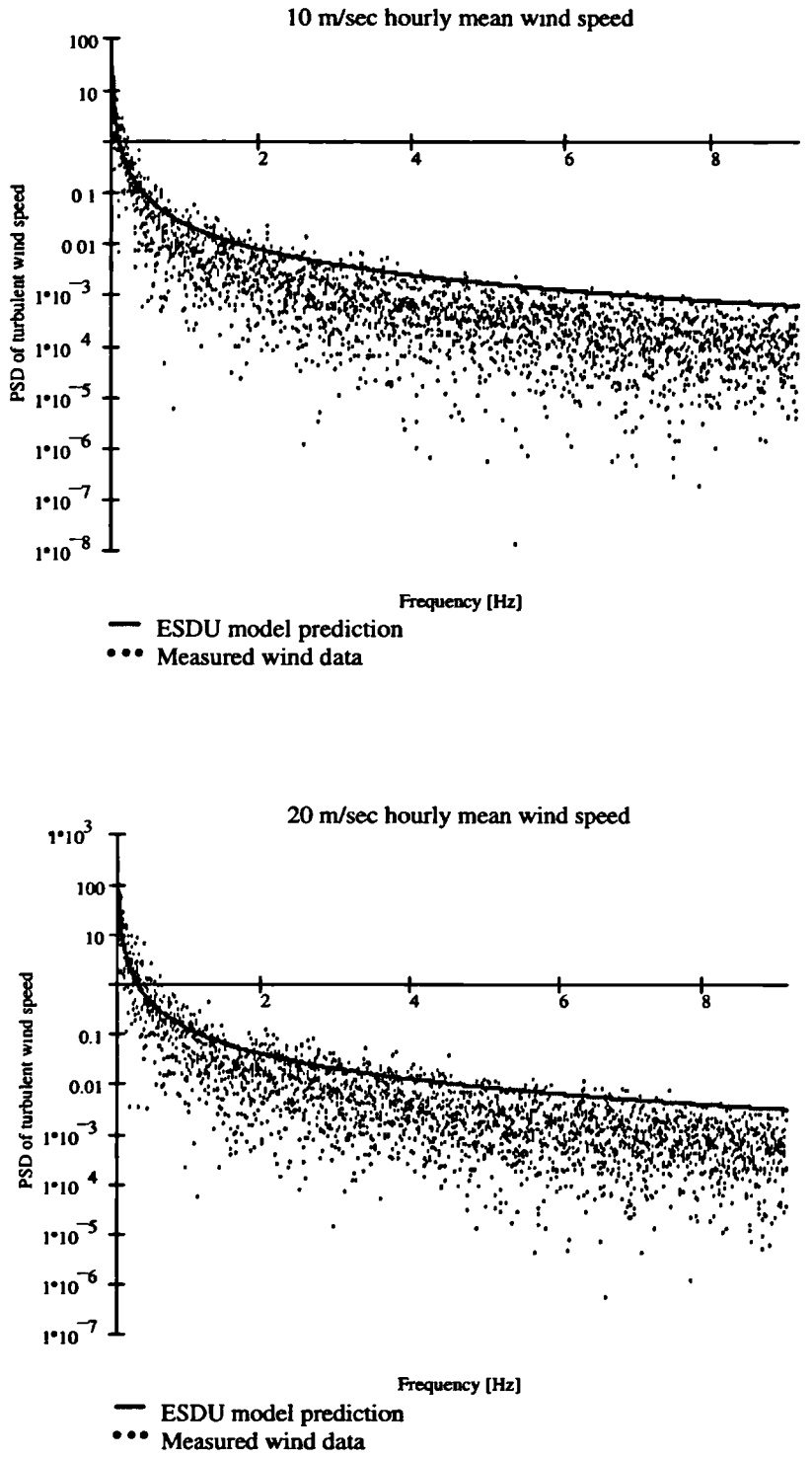

Figure 8-3 Comparison between measured and calculated PSD of wind turbulence

The ESDU model gives good agreement with the measured wind speed in the low frequency region up to approximately 2Hz. After this the model tends to over predict the turbulence intensity. For wind turbine analysis, the higher frequency range of wind

turbulence is relatively unimportant because the Doppler shifting due to blade rotation masks its energy contribution. However, for our purposes the ESDU model is still seen to be conservative in this region.

A summary of the statistical properties of the power spectra is given in Table 8-2. An equivalent normalised fatigue life is also presented to establish the effect of the errors on the fatigue predictions. This is determined using Equation 7-9.

It is important to note that the higher spectral moments are affected to a great extent by the higher frequencies. For instance, an error of 2% in the spectral ordinate at a frequency of 6Hz will incur an error in the 4^{th} moment of $2\% \times 6^4 = 2{,}592\%$. This is further complicated by the lack of accuracy in the measuring apparatus at higher frequencies. For the purpose of this thesis we shall impose a limiting frequency where 99.5% of the area of the measured PSD is taken into account. This gives a limiting frequency, in this case, of 2Hz. This approach is adopted regularly in frequency domain analysis and reference to it can be found in the nSoft user manual[5].

The table clearly shows the escalating error emerging in the spectral moments (109% error by the 4^{th} moment). However these do not severely affect the signal statistics or the equivalent normalised fatigue damage. The analysis reveals an underestimate of the fatigue damage leading to an increase in calculated fatigue life of up to 17% for the higher wind speed.

Mean wind speed = 10 m/sec. **Turbulence intensity = 8.930%**		Measured data	ESDU prediction	Discrepancy %
Ground roughness length		N/A	8.9×10^{4}m	
Spectral moments	m_0	0.809	0.78	-3.5
	m_1	0.059	0.072	22
	m_2	0.026	0.045	75
	m_4	0.035	0.073	109
Standard deviation		0.899	0.883	-1.8
Mean period		13.769	10.889	-21
Mean period between zero up-crossings		5.587	4.145	-26
Mean period between peaks		0.859	0.787	-8
Irregularity factor		0.154	0.19	24
Equivalent normalised fatigue damage		3.793	3.416	-10
Mean wind speed = 20 m/sec. **Turbulence intensity = 8.930%**				
Ground roughness length		N/A	5.02×10^{4} m	
Spectral moments	m_0	3.431	3.353	-2.3
	m_1	0.39	0.361	-7.3
	m_2	0.19	0.235	24
	m_4	0.229	0.381	66
Standard deviation		1.852	1.831	-1.1
Mean period		8.804	9.276	5.3
Mean period between zero up-crossings		4.249	3.777	-11
Mean period between peaks		0.91	0.786	-14
Irregularity factor		0.214	0.208	-2.9
Equivalent normalised fatigue damage		8.699	7 192	-17

Table 8-2 Summary of statistical data for measured and calculated PSDs

8.3.2 Rotational sampling of the turbulent wind field

No measured data exists on which to compare the algorithm for calculating the rotationally sampled wind speed. In order to validate the model, comparisons were made with the TURBU[3] program developed by ECN. TURBU is a proprietary product and has already undergone extensive validation against a time domain approach (FATAS[6]), and also with measured data taken from a number of turbines. The

validation with TURBU was carried out using the Nedwind 50[1] machine as the test bed. TURBU has no aerodynamic pre-processor and therefore the Mathcad worksheet Aerana was used for the pre-processor in both models [†]. TURBU derives Auto-power spectra for the blade root shear and moment, and the rotor thrust and torque. Turbana, on the other hand, derives the Cross-power spectra for the rotationally sampled wind speed between blade elements. From this data the necessary blade and rotor loading can be determined using Equation 8-2.

$$G^F(f) = [g]^T \cdot \left[\tilde{G}_{ij}(f)\right] \cdot \overline{[g]} \qquad \textbf{Equation 8-2}$$

Where $\left[\tilde{G}_{ij}(f)\right]$ is the Cross-power spectral density matrix given by Turbana and $[g]$ is a vector of aerodynamic gain factors given by Aerana. When considering blade moments, the vector $[g \cdot r]$ is substituted, this denotes the product of the aerodynamic gain factor of a particular blade element and the radius to the element. More details of this approach are given in Chapter 5.

The results of the validation exercise are plotted in Figure 8-4. These generally show good agreement with the TURBU-1 results but are consistently higher, especially at the higher frequency range. The reason for this anomaly is due to the ESDU model. TURBU-1 uses an older version than Turbana. Rerunning Turbana with the older ESDU model showed near identical results.

[†] Aerana has the optional capability of exporting TURBU-I data files and can therefore act as an aerodynamic pre-processor for this software.

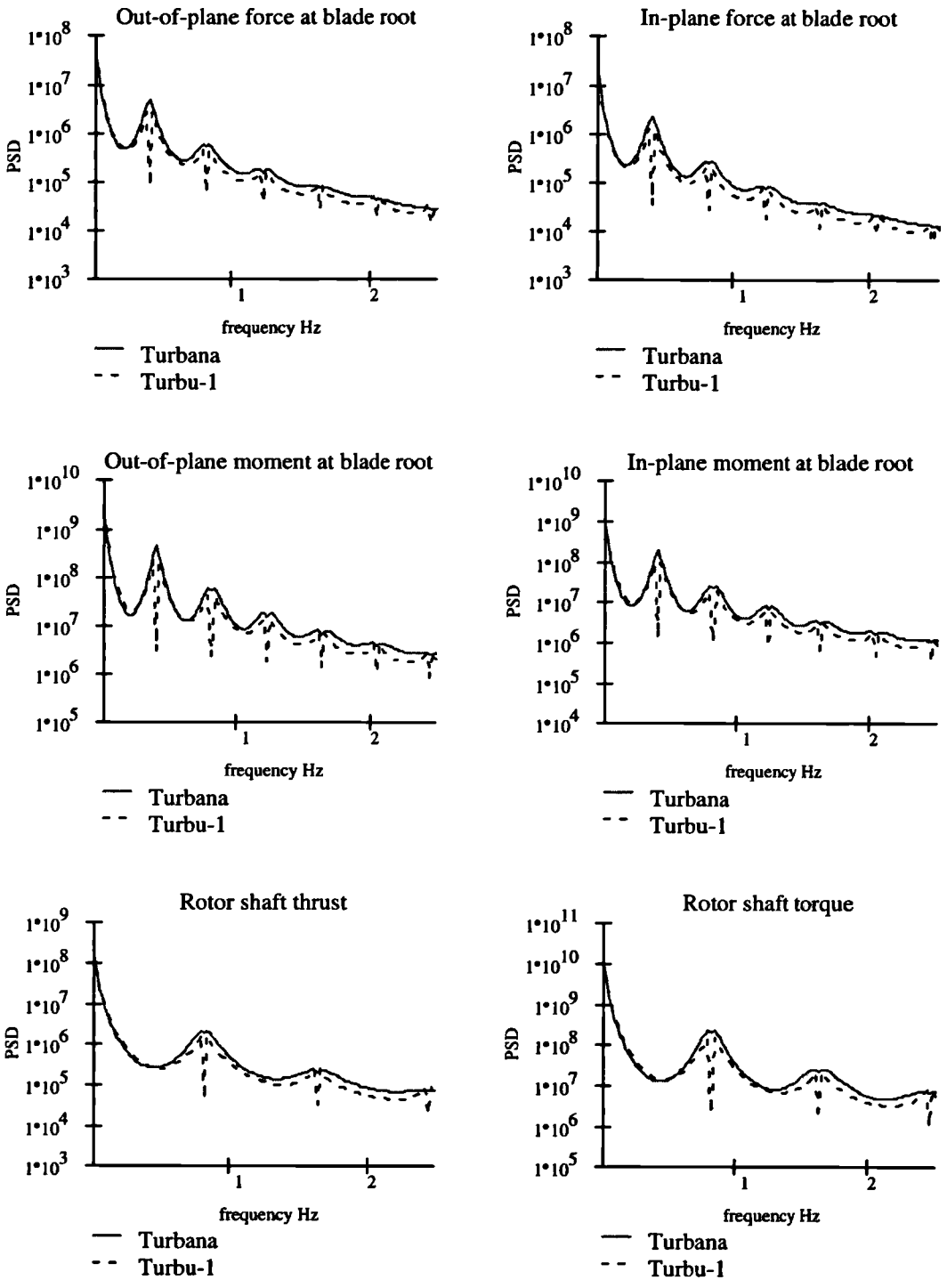

Figure 8-4 Validataion of Turbana calculation with TURBU-1

The TURBU-1 results clearly show a sharp dip at the harmonics of the rotor frequency. This is a result of the older model for calculating the coherence function. For zero relative frequencies the older model gave a unit coherence, in the revised

model this is more accurately modelled and so the dip is not apparent. It is worth noting that the dip has no significant affect on the spectral moments, and therefore is of no concern for TURBU-1 users.

The Turbana curve is seen to be higher than the TURBU-1 curve for higher frequencies and this will affect the higher spectral moments. Table 8-3 shows typical errors between the two curves. These calculations are based on a cut-off frequency of 5.2Hz in the spectral moment calculation, this represents the whole of the calculated spectra. Although these errors are quite high it is worth noting how the effect is reduced when considering the important spectral statistics and equivalent normalised fatigue damage. These errors are typical of all the calculations.

Out-of-plane blade root bending moment			
Spectral moments:	Error %	Spectral statistics:	Error %
m_0	7.1	Standard deviation	3.5
m_1	48	Mean period	-28
m_2	53	Mean period between zero up-crossings	-16
m_4	64	Mean period between peaks	-3.3
		Irregularity factor	16
		Equivalent normalised fatigue damage	-11

Table 8-3 Statistical comparison between Turbana and TURBU-1

Turbana is therefore seen to yield higher results than the corresponding TURBU-1 calculation. These are due entirely to the differences in the ESDU models and do not significantly affect the fatigue analysis results.

8.4 Linana: Structural finite element analysis of the turbine

Linana evaluates the structural response of the turbine using a finite element based approach. It can only be fully validated by comparing the predicted spectra with those measured on a real turbine, however confidence in the structural model can be gained by comparing the structural natural frequencies.

Each rotor blade is modelled using 7 blade elements. One element is used to represent the combined tower and drivetrain. The first mode natural frequency for a blade has been calculated and compared with the measured values supplied for Turbine A and also for the Nedwind 50 turbine, these are given in Table 8-4.

	Turbana prediction	Turbine A	Error %
Flat-wise 1st mode frequency	1.58Hz	1.8Hz	-12
Edge-wise 1st mode natural frequency	2.56Hz	2.5Hz	2.4
	Turbana prediction	Nedwind 50	Error %
Flat-wise 1st mode frequency	1.47Hz	1.5Hz	-2
Edge-wise 1st mode natural frequency	2.62Hz	2.6Hz	0

Table 8-4 Comparison of first mode blade frequencies

The natural frequencies show excellent agreement for the Nedwind 50 machine, however they are less good for Turbine A. There is some question about the blade properties supplied for Turbine A and an error in these cannot be ruled out. If an increase of 33% is made in the flat-wise blade stiffness, then the natural frequencies agree exactly.

Measurements were also taken for Turbine A to calculate the principal natural frequencies of the whole structure and these are summarised in Table 8-5. Linana has the facility to produce simple mode shape plots of the structure. These exaggerate the deformations to help identify the particular modes being considered. Table 8-5 illustrates the mode shapes by referring to the front and side elevations and the plan view of the turbine.

The results show reasonable agreement with the measured values but the blade modes show a rather large error which again can be eliminated by increasing the flat-wise stiffness properties by 33%. Mesh density convergence was tested and shown to have no significant influence on the results.

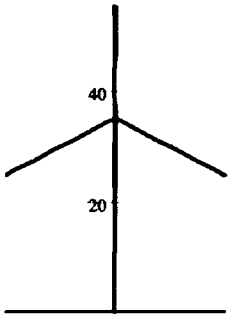

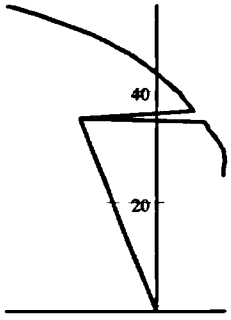

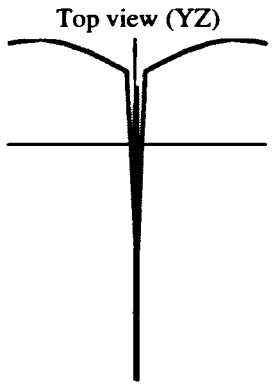

1st mode tower fore-aft bending	Turbana	Turbine A	Error
	0.79Hz	0.78Hz	1.3%

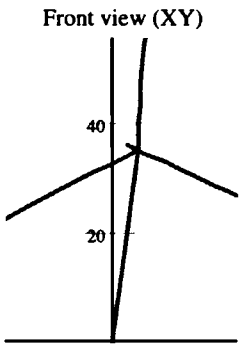

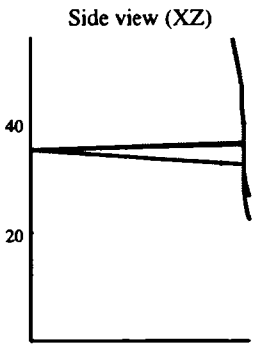

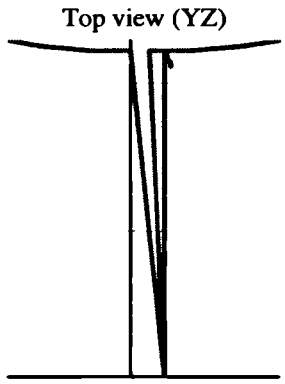

1st mode tower sway moment	Turbana	Turbine A	Error
	0.85Hz	0.85Hz	0%

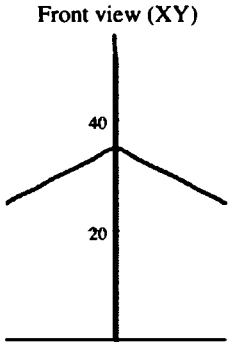

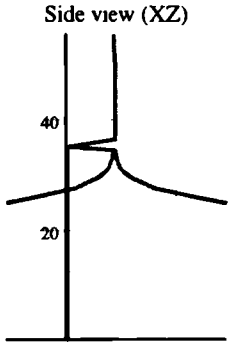

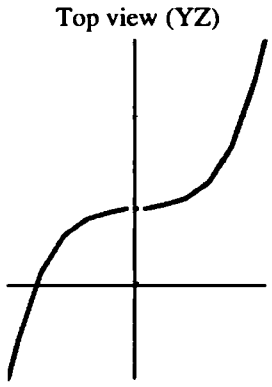

1st mode, flat wise blade bending asymmetric about the yaw axis:	Turbana	Turbine A	Error
	1.50Hz	1.76Hz	-14.7%

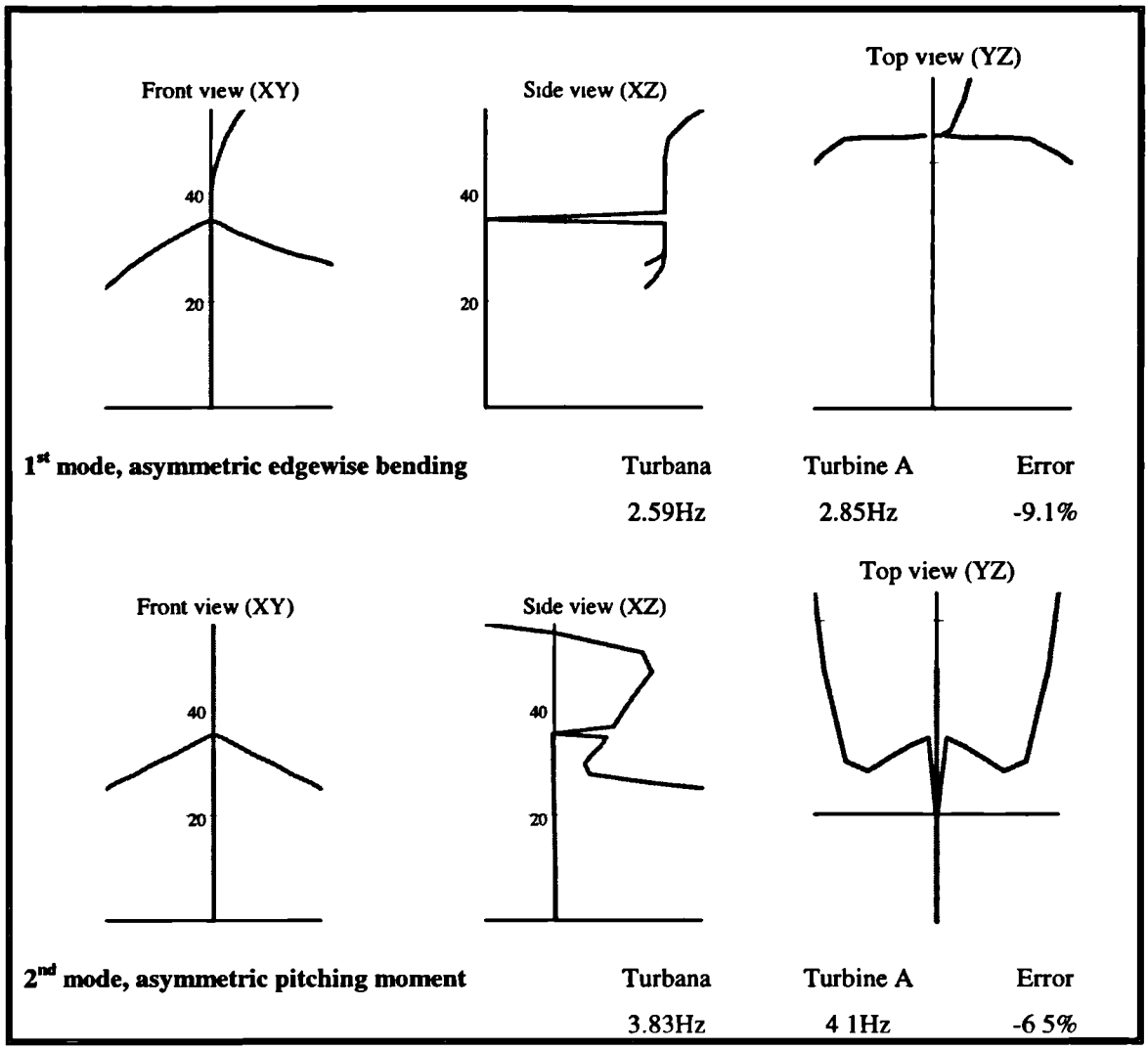

Table 8-5 Comparison of natural frequencies

8.5 Loadana: Deriving the auto-power spectra of structural forces

Loadana serves as a post-processor for the model. It takes the output from the other modules and calculates the auto-power spectra of forces on the turbine. Facilities are included to calculate the loading on a rigid turbine model as well as a flexible one. This facility enables a comparison with the TURBU-1 model and clearly highlights the effect of structural dynamics on the overall loading. The worksheet also compares the calculated spectra with measured data. PSDs are calculated from measured time histories. For this analysis measured data is taken from Turbine A. Two records have been provided with mean wind speeds of 10m/sec and 20 m/sec and turbulence intensities of 8.9% and 9.3% respectively and these are given in the following Figures:

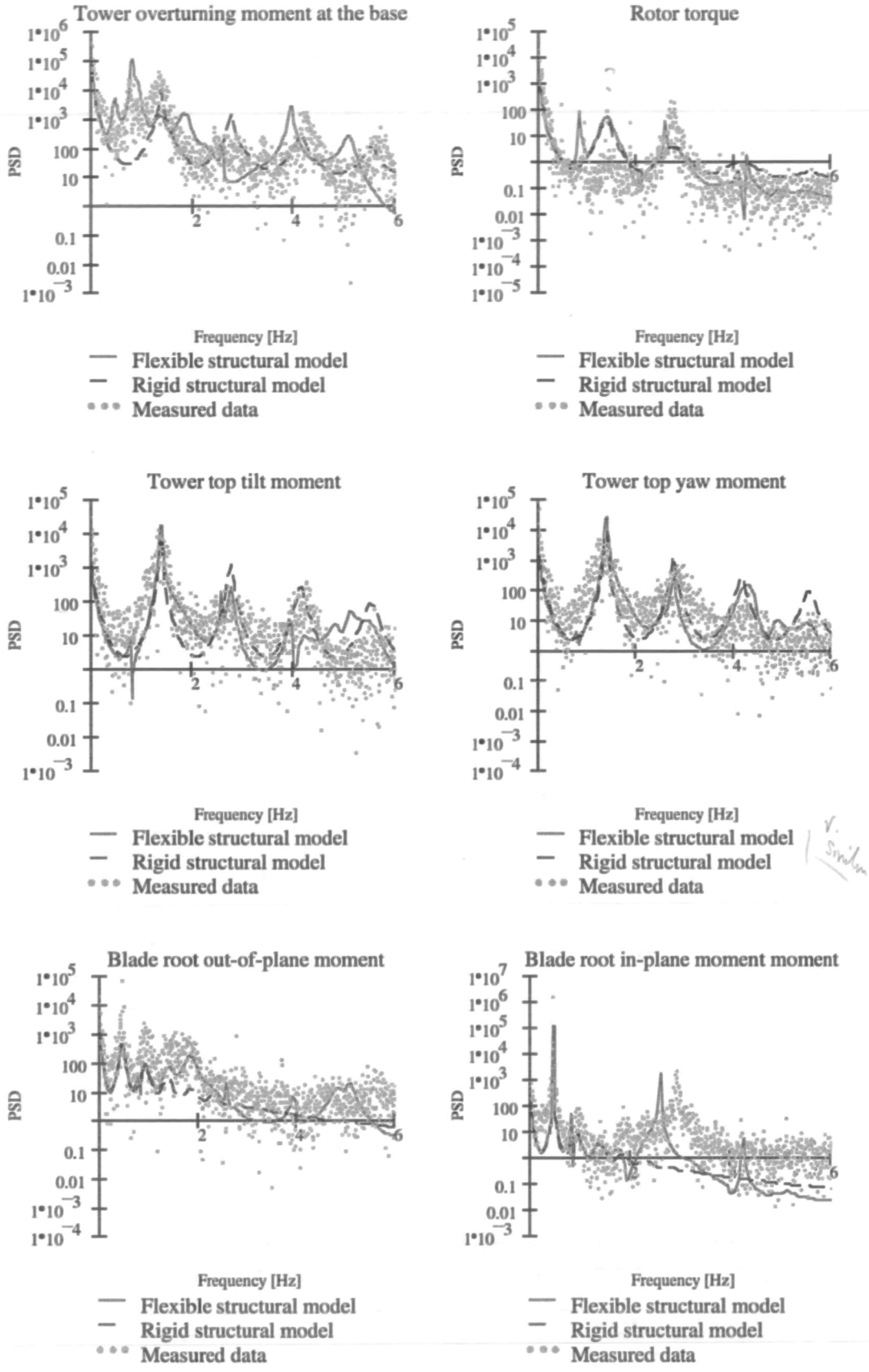

Figure 8-5 Comparison between calculated and measured PSDs for a mean wind speed of 10 m/sec, and a turbulence intensity of 8.9%.

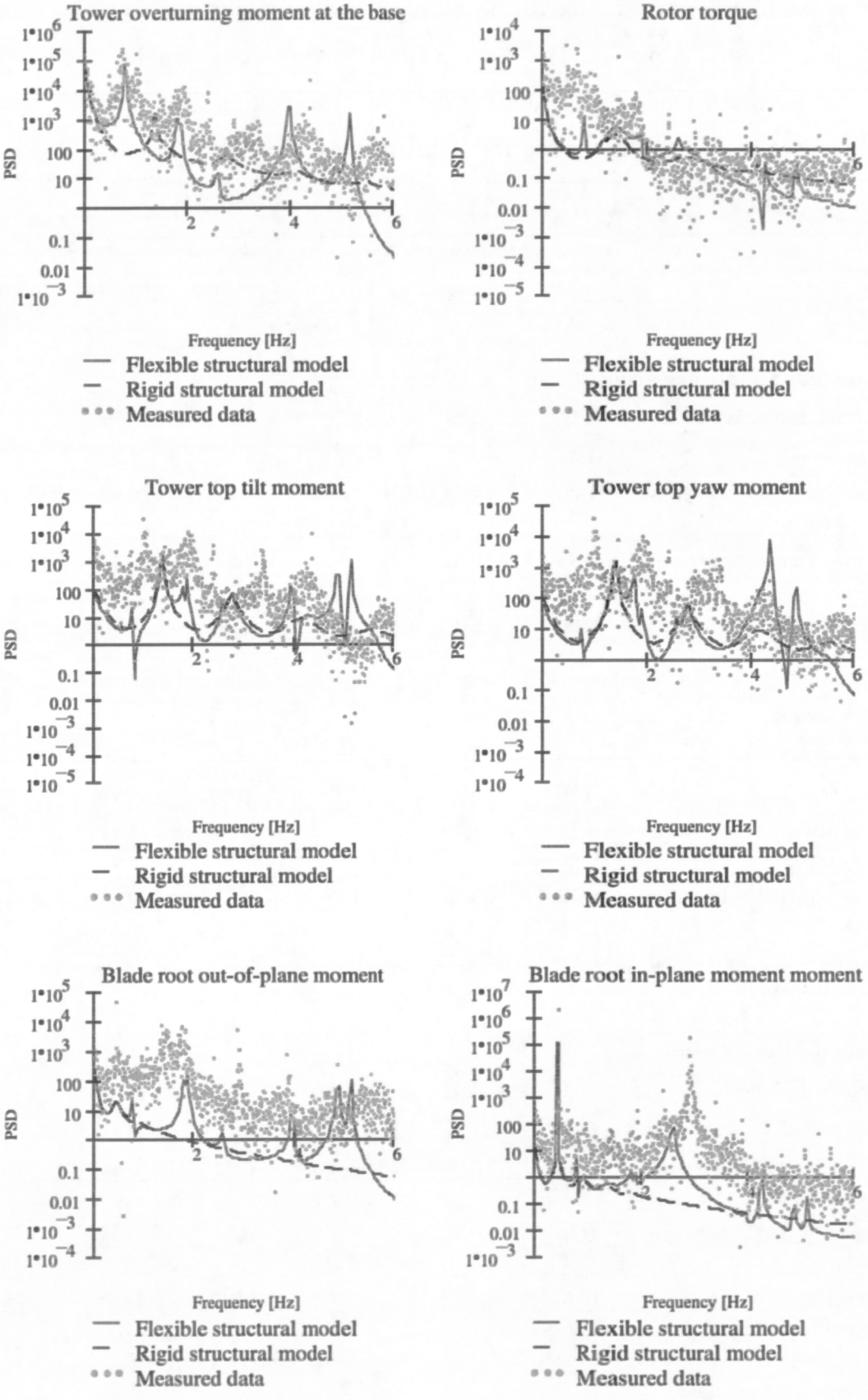

Figure 8-6 Comparison between calculated and measured PSDs for a mean wind speed of 20 m/sec, and a turbulence intensity of 9.3%.

The above figures compare the calculated spectra with those measured for two sets of data taken from Turbine A. The measured results show considerable scatter and no attempt has been made to smooth the data prior to plotting. The data can also be summarised by comparing the spectral statistics; these are given in Table 8-6.

Turbine A	Wind speed = 10 m/sec, Turbulence intensity =8.9%			Wind speed = 20 m/sec, Turbulence intensity =9.3%		
	Predicted	Measured	Error %	Predicted	Measured	Error %
Tower base overturning moment						
Standard deviation	133	129	3.1	98	156	-37
Mean period	1.41	2.23	-37	1 55	1.29	20
Mean period between zero up-crossings	1.00	1.16	14	0.93	0.99	-6
Mean period between peaks	0.33	0.32	3.1	0.28	0.37	-24
Equivalent normalised fatigue damage	2.487	2.191	13.5	1.504	3.343	-55
Rotor torque						
Standard deviation	11.8	17.0	-30	3.9	14.7	-73
Mean period	3.70	6.71	-45	1.89	1.92	-1.5
Mean period between zero up-crossings	1.58	1.80	-17	1.00	1.38	-27
Mean period between peaks	0.40	0.35	14	0.37	0.45	-18
Equivalent normalised fatigue damage	2.394	2.677	-10.5	7.708	37.52	-79
Tower top yawing moment						
Standard deviation	43.9	45.1	-2.7	27.2	49.3	-45
Mean period	0.69	1.74	-60	0.29	0.61	-52
Mean period between zero up-crossings	0.64	0.98	-35	0.27	0.54	-50
Mean period between peaks	0.40	0.39	2.5	0.24	0.36	-33
Equivalent normalised fatigue damage	10.87	9.555	13.7	4.047	10.99	-63
Tower top tilt moment						
Standard deviation	37.9	41.0	-7.5	16.3	51.0	-68
Mean period	0.69	0.97	-29	0.33	0.63	-48
Mean period between zero	0.63	0.74	-15	0 29	0.53	-45

up-crossings						
Mean period between peaks	0.35	0.36	-2.8	0.21	0.34	-38
Equivalent normalised fatigue damage	8.126	8.718	-6.7	2.121	10.6	-80
Blade root, flat-wise bending moment						
Standard deviation	14.2	33.0	-57	7.5	38.0	-80
Mean period	0.95	1.26	-25	0.53	0.68	-22
Mean period between zero up-crossings	0.64	0.88	-27	0.38	0.59	-36
Mean period between peaks	0.27	0.31	-13	0.22	0.34	-35
Equivalent normalised fatigue damage	2.19	5.816	-62	9.53	78.89	-88
Blade root, edge-wise bending moment						
Standard deviation	73.6	75.1	-2.0	78.8	88.5	-11
Mean period	1.99	1.94	2.6	2.14	1.04	106
Mean period between zero up-crossings	1.72	1.60	7.5	2.10	0.74	184
Mean period between peaks	0.60	0.45	33	1.27	0.36	253
Equivalent normalised fatigue damage	2.59	1.922	34.7	6.226	1.852	236

Table 8-6 Comparison of statistical properties of PSDs for Turbine A.

Similar tabulated data was also made available for Turbine B and is reproduced in Table 8-7.

Turbine B	Wind speed = 9.3 m/sec, Turbulence intensity =10%			Wind speed = 18.4 m/sec, Turbulence intensity =7.9%		
	Predicted	Measured	Error %	Predicted	Measured	Error %
Rotor torque						
Standard deviation	19.001	12.781	48	17.655	16.636	6.1
Mean period	11.892	15.072	-21	6.685	1.943	244
Mean period between zero up-crossings	3.533	4.475	-21	2.514	1.261	99
Mean period between peaks	0.757	0.777	-2.6	0.736	0.743	-1
Equivalent normalised fatigue damage	6.63	4.627	43	6.265	6.578	-4.7
Blade root, flat-wise bending moment						
Standard deviation	18.808	17.2-19.2	0	12.680	45.109	-72
Mean period	2.176	2.029	7.2	0.769	1.643	-53
Mean period between zero up-crossings	1.320	1.341	-1.5	0.666	1.410	-52
Mean period between peaks	0.595	0.635	-6.3	0.516	0.786	-34
Equivalent normalised fatigue damage	6.189	6.792	-8.9	3.984	21.56	-81
Blade root, edge-wise bending moment						
Standard deviation	63.828	52.16	22*	65.852	58.52	12.5
Mean period	2.236	2.23	0.3	1.832	1.85	-1.0
Mean period between zero up-crossings	2.226	2.22	0.3	1.490	1.47	1.3
Mean period between peaks	2.202	2.20	0	0.619	0.49	26
Equivalent normalised fatigue damage	9.125	7.45	22.5*	2.402	1 651	45

NOTE

* The measured result would appear to be in error for this case. The sinusoidally varying gravity load contributes much to the edge-wise bending moment, this is deterministic and very simple to compute using the formula: $\frac{1}{\sqrt{2}} \cdot M \cdot c \cdot g$; where M is the blade mass, c is the distance to the centre of gravity and g is the gravitational acceleration constant. Using this formula a value of 63.4 kN.m is given, this is larger than the measured value and for this reason the measured value is unlikely to be correct.

Table 8-7 Comparison of statistical properties of PSDs for Turbine B.

For Turbine A, the above results show a relatively good agreement between the measured and the calculated fatigue damage for the lower wind speed (nominally 10%). However, large errors are noted at the higher wind speeds where the theoretical results consistently under predict the fatigue damage by around 80%. The blade root edge-wise bending moment is a particularly erroneous figure for both cases because it is largely dependent on the periodic gravity load.

Turbine B shows reasonable agreement for the lower wind speed though it still shows some large errors for the higher winds.

No one particular reason can be proposed for the discrepancies. Instead, a number of causes may all contribute in some way. The causes are listed as follows, we shall discuss each cause separately.

1. Non-linearities and inadequacies in the aerodynamic model
2. Deterministic effects which are not modelled
3. Deficiencies in the structural model

8.5.1 Non-linearity's in the aerodynamic model

Both Turbines A and B are stall-regulated machines. Figure 8-7 shows the emphasised stall plots for both Turbines A and B. These are discussed in Chapter 4 and show where blade stall begins and how the stalled region propagates along the blade. It is apparent that for Turbine A, a stall region begins at approximately 9 m/sec and this rapidly propagates along the blade until the whole blade is operating in stall by approximately 12 m/sec. At 10 m/sec, nearly 50% of the blade is operating in stall. Turbine B shows much smoother stall propagation with stall commencing at approximately 9 m/sec and the whole blade operating in stall by approximately 17 m/sec. At 9.3 m/sec only 20% of the blade is operating in stall. This explains why the results show a much closer correlation with the measured values than those obtained for Turbine A. When turbine B is calculated for higher wind speeds, where much of the blade is operating in stall, we again observe relatively large errors between the measured and calculated values.

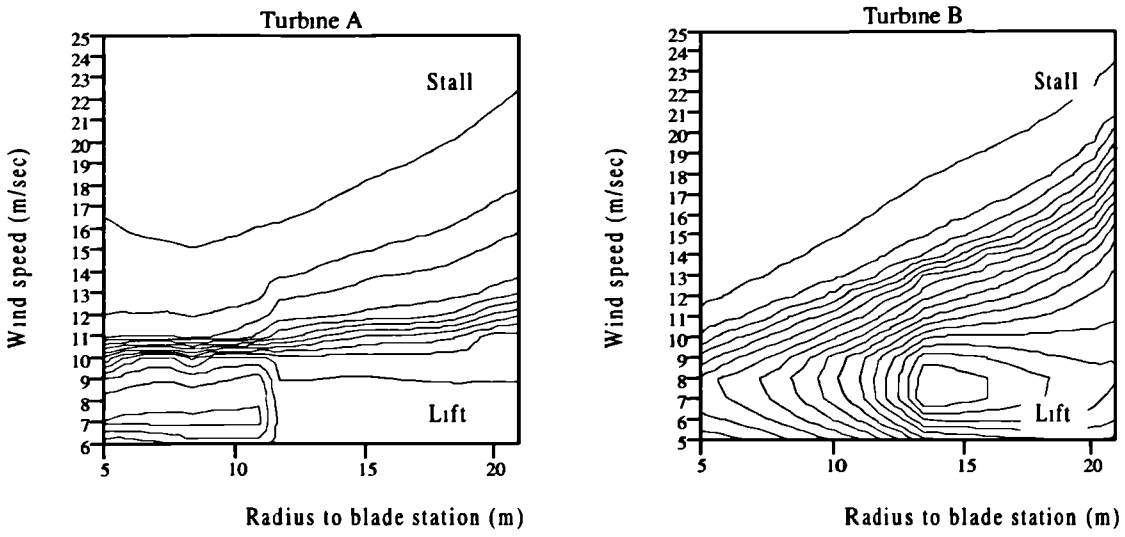

Figure 8-7 Propagation of stall along the blades of Turbines A and B

As the wind speed varies then the stalled region will also vary dynamically along the blade's length. Certain blade areas will therefore pass into, and out, of stall. In the above analysis only 4 aerodynamic elements were used to model the blade and these give inadequate resolution for modelling the propagation of stall along the blade. Although in Chapter 5, we saw that these gave sufficient resolution for calculating the equilibrium wake model, concern is now shown about their suitability for calculating the frozen wake gain factors as the blade stalls. In the future it may prove necessary to include a denser aerodynamic mesh to accurately model the post stall response of the turbine.

Stall is a highly non-linear effect that is inadequately dealt with in the Aerana worksheet. Essentially there are three non-linear factors which occur when a blade operates in stall, these are:

1. Stall transition and the hysteresis effect
2. Induced radial airflow along the blade
3. Turbulent and dynamic wake effects

8.5.1.1 Stall transition and the hysteresis effect

Stall transition and the stall hysteresis effect was discussed in Chapter 4 and is illustrated in Figure 8-8. The figure shows the variation in aerodynamic force on a particular blade element with respect to the wind speed. It was calculated for Turbine

A at a mean wind speed of 10 m/sec and a turbulence intensity of 8.9%. From Chapter 4, Table 4-1 we see that the expected range of the turbulent wind speed can be determined from the mean wind speed and the turbulence intensity by assuming that it follows a normal distribution. The expected variation and the 95.4th percentile range is therefore found by Equation 8-3 as 9.4<V<10.6 and 8.2<V<11.8 m/sec respectively.

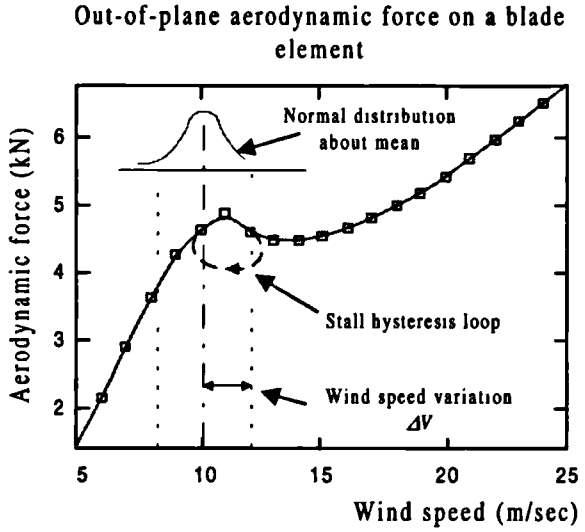

Figure 8-8 Variation in aerodynamic force on a blade element

$$\textit{Expected Variation } \Delta V = \pm 0.68 \cdot I_u \cdot V \qquad \textbf{Equation 8-3}$$

$$95.4^{th} \textit{ percentile range} = \pm 2 \cdot I_u \cdot V$$

It is quite clear that this particular blade element is likely to encounter stall during operation under these wind conditions. This will induce two non-linear effects, these being the transition into stall and the hysteresis effect as the element returns back into a lift state. We therefore see that any linearisation of the force on this element will prove difficult and further research must be undertaken to improve the model.

An attempt has been made to take account of the aerodynamic non-linearity in this study. For this the author has evaluated the weighted mean gradient of the curve between $\pm 3.\sigma_u$. This is weighted by the probability of occurrence of the gradient which is assumed to follow a normal distribution. This modification took no account of stall hysteresis and was found to have little effect on the results and so was not pursued. With a better understanding of stall hysteresis, a closer look at the problem

may yield some improvement. The gradient should then be weighted in accordance with the fatigue damage potential. This has the additional benefit of considering the damage caused from both positive and negative gradients. Under the present linearisation the negative gradients tend to negate the positive which results in a low estimate of the damage.

8.5.1.2 Induced radial airflow along the blade

Radial airflow along the blade occurs when the blade stalls. This flow condition obviously affects the airflow vector and can also affect the stall dynamics of the blade. A semi-empirical modification is included in the Aerana model to account for it and this is discussed in Chapter 4.2.2. The model appears to yield a good correlation with the measured results when considering the equilibrium wake model. However, the phenomenon is still under investigation and a clearer insight is likely to be given in the near future. A sensitivity study was carried out to investigate the contribution of this modification to the frozen wake gain factors. This revealed that the inclusion of the modification may have a significant contribution to blade gain factors during stall and would therefore warrant closer investigation.

8.5.1.3 Turbulent and dynamic wake effects

The Aerana model assumes that the wake vector is frozen at the equilibrium established for the mean wind speed. Rapid variations in the wind speed therefore have no effect on the wake. In practice this does not happen because the wake will be dynamically changing in response to the wind speed variations. This dynamic wake is still an area of active research and requires further investigation so that it may be incorporated in the aerodynamic model. Particular attention is needed for the linear application of the stalled wake model. It is apparent that the frozen wake model proves quite satisfactory for the pre-stalled case but requires more investigation in the post-stall case.

8.5.2 Deterministic effects which are not modelled

The analysis described in this chapter takes account only of the stochastic loads arising from the turbulent wind field and the deterministic, gravity effect of the edgewise blade bending moment. There are a number of other deterministic effects that are not modelled. These include:

1. Vertical wind shear
2. Tower shadow
3. Yaw misalignment and shaft tilt
4. Gravity effect caused by the coning angle of the blades

Wind shear and tower shadow both result in an increase in blade loading which occurs at multiples of the rotor frequency. Failure to model these effects could contribute to the relatively large under prediction of the blade loading. Yaw misalignment and shaft tilt result in an increase in load at the rotor frequency. This contribution to the load was not modelled as no data was provided. In future it may be beneficial to impose a notional misalignment of say 10° in the analysis to account for possible misalignment.

8.5.3 Deficiencies in the structural model

It was noted earlier that the stiffness properties of the blades were thought to be incorrect. Despite increasing the structural mesh density, little improvement of the first and second mode natural frequencies could be achieved. However, an increase in the blade flat-wise stiffness of around 33% resulted in near perfect correlation of the first mode frequency. From Figure 8-5 we see a definite lag in the position of the blade harmonics when compared with the measured results. Again, it was noted that this difference disappeared for the first mode response when the blade stiffness correction was made. This would seem to suggest an error in some of the blade stiffness properties given. It was noted, however, that this had only a small impact on the statistical properties of the spectra.

Structural damping of the turbine was not modelled in the analysis because no data was available on which to base this. However, the author carried out a separate sensitivity study to investigate the contribution made by structural damping. Damping was modelled by assuming a percentage of critical damping for the first 6 modes of the structure. Values were applied ranging from 0.05% to 10%. It was noted that this has a very significant effect on the calculated spectra, especially on the statistical mean period results. No structural damping was included in the comparison listed in this chapter however as this would have been pure guesswork as the construction of the blades was unknown.

8.6 Conclusion

This chapter has presented a case study to validate the mathematical models with measured values obtained from two production turbines. In conclusion we see that there are many factors which influence the accuracy of the analysis. These include the following:

1. Quality of the turbulent wind model (ESDU spectra).
2. Quality of the material property and structural data.
3. Non-linearities in the aerodynamic analysis caused by; stall hysteresis, induced radial airflow along the blades, and the turbulent dynamic wake. These effects influence the analysis of stalled blades.
4. Deterministic effects that are not modelled such as; vertical wind shear, tower shadow, yaw misalignment and shaft tilt, and gravity effects caused by the coning angle of the blades. These will influence all results, stalled and unstalled.

The ESDU model has been shown to agree well with the measured wind speeds giving an overall underestimate of approximately 10% to 20% in equivalent normalised fatigue damage. The calculated turbulent wind loads on the rotor have been verified against the existing TURBU program by ECN and been found to agree very well with an overestimate of only 10% in normalised fatigue damage. If the old ESDU model were implemented in Turbana, then the agreement is perfect.

There are some concerns over the material properties provided for this study. In particular the blade mass and stiffness properties for Turbine A show a consecutive error in natural frequency and PSD results. Applying a correction of 33% to the flat-wise bending stiffness largely improves this situation. Another major concern is the omission of structural damping data by the manufacturer. With today's composite materials, high structural damping is likely and this should be included because it appears to have quite a large influence on the results (approximately 10% to 20% in equivalent normalised fatigue damage). The largest contribution is noticed in the edgewise blade loads as these have negligible aerodynamic damping.

The results of this exercise have clearly identified the non-linear aerodynamic analysis as the main source of errors. The results show generally good correlation for the pre-stalled case. These give approximately 10% errors in equivalent normalised fatigue life between the predicted and measured loads. Under blade stall the results show an increasing error in the region of 80%. For a frequency domain analysis to succeed we must concentrate on developing a good linearisation for the aerodynamic model to replace the Aerana model described in Chapter 4. The new analysis must consider stall hysteresis in particular. A number of research studies are currently being undertaken to address this in the time domain and many time domain programs now include the ability to model some of the effects mentioned. However, more research is necessary on the effective linearisation of these models so they can be incorporated into a frequency domain package. The author sees this as essential to the future of frequency domain analysis of stalled rotors.

An investigation was also carried out to look at the effect on accuracy of limiting the dynamic analysis to cover only the first blade mode response, an approach proposed by Van Engelen[7]. This showed large errors in the analysis and it was found necessary to include at least the second blade mode and preferably the first 6. The errors occur because of the rapid attenuation of the higher frequency responses following the first mode natural frequency. A similar study also considered reducing the number of modes taken to represent the tower. This showed that an effective tower model need only include a single mode in the fore-aft direction. For an offshore analysis modes are also necessary for pitch and yaw.

---

[1] Nedwind (1995). "Design data for the Nedwind 50 turbine." Nedwind.

[2] WS Atkins Ltd. (1996). "Summary of results for validation of wind turbine model." Personal correspondence with Ian Ward, WS Atkins Ltd. Woodcote Grove, Ashley Road. Epsom, Surrey. England.

[3] Van Engelen T.G. (1991). "Turbu-I computer program for turbulence load analysis of horizontal axis wind turbines. Theory and program description." ECN, SU General Services, Petten, The Netherlands.

[4] Wei J and Quarton D.C (1994). "Modelling and load prediction for offshore horizontal axis wind turbines." Proceedings, 1994 Chinese Wind Energy Conference.

[5] nCode International Ltd. (1996). "FATIMAS spectral user manual." nCode International Ltd. 230 Woodbourn Road, Sheffield. England

[6] Lindenburg C. "Technical manual for the FATAS computer program." ECN, SU General Services, Petten, The Netherlands.

[7] Van Engelen T.G. (1996). Personal communication with the engineer responsible for the development of TURBU. ECN, The Netherlands.

9. Wind turbine loading due to stochastic base motions

An offshore wind turbine is subjected to both turbulent wind and wave loading. In response to this. The turbine will be forced to move in the water. For floating turbines the motions induced take the form of structural vibrations, where the structure will bend and twist; and rigid body motions, where the whole platform will move as one. For fixed base turbines only the structural vibrations are relevant.

Rigid body motions are typically characterised by their large amplitude and low frequencies, whereas structural motions have a lower amplitude but occur at higher frequencies. In this chapter we shall consider the effect on rotor loading due to fairly large amplitude motions, such as those found with floating turbines.

A floating turbine will contribute in three ways to the rigid body motions of the platform. Firstly, it exerts a steady thrust force due to the mean wind speed: this results in a constant trim error on the platform. Secondly, it imposes turbulent loads due to the gusting wind; and thirdly, it offers resistance to the platform motions.

In this, and the following chapter we wish to answer two questions:

1. How much does the wind turbine move in the water? (Chapter 9)
2. What dynamic loads are exerted on the wind turbine blades due to this motion? (Chapter 10)

In order to compute the amplitude of the rigid body motions in various sea and wind conditions it is necessary to derive terms for the dynamic equilibrium formula. The classical equilibrium formula is expressed in Equation 9-1.

$$M \cdot \ddot{s}(t) + C \cdot \dot{s}(t) + K \cdot s(t) = F(t) \qquad \textbf{Equation 9-1}$$

Where M = Mass matrix

C = Damping matrix

K = Stiffness matrix

$F(t)$ = Force vector

s = Displacement vector

The rigid body mass, damping and stiffness matrices for the wind turbines are derived in this chapter. These can be exported to commercial hydrodynamic analysis

packages, such as the AQWA package by WS Atkins Ltd., for inclusion in seakeeping and stability analyses. The force vector comprises hydrodynamic and aerodynamic components. The hydrodynamic analysis is beyond the scope of this thesis and the reader is referred to Patel[1] and Patel & Witz[2] for further details. The aerodynamic loads are obtained from the analysis documented previously in this thesis. Although this assumes that the turbine is stationary, this will only incur small errors in the analysis and is quite suitable for frequency domain work. A simplified illustration of the rigid body model is shown in Figure 9-1.

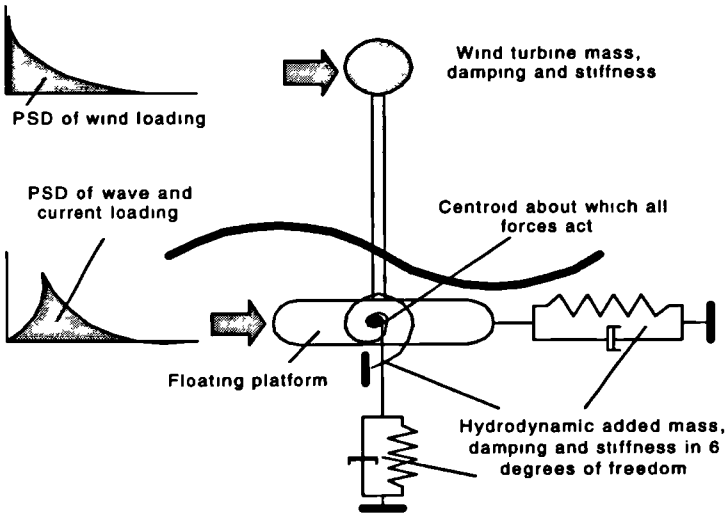

Figure 9-1 Idealisation of a floating wind turbine

There are two methods of evaluating the amplitude response to the turbulent loads:

1. Time history analysis (time domain)
2. Power spectral density analysis (PSD frequency domain)

In this chapter we shall derive the matrices describing the rotor forces induced by the motion of the turbine in six degrees of freedom. These are first derived in the time domain for rotors with any number of blades. For rotors with three or more blades it is shown that the response simplifies substantially. For this special case we shall also derive formulae for a frequency domain calculation.

The derivations are carried out in the local blade and the global tower axis systems. Figure 9-2 illustrates the notation employed for longitudinal and rotational motion about each axis. It should be noted that the term 'Tilt' is used in place of the more conventional 'Pitch.' This is to avoid confusion with the blade's 'Pitch' angle.

Each blade is split up into a number of aerodynamic elements. Linear gain factors are used for calculating the aerodynamic loading on each of these elements due to changes in the various wind directions, these are derived in Chapter 4. Figure 9-3 illustrates the notation used to represent each gain factor for changes of wind speed and blade angle of attack.

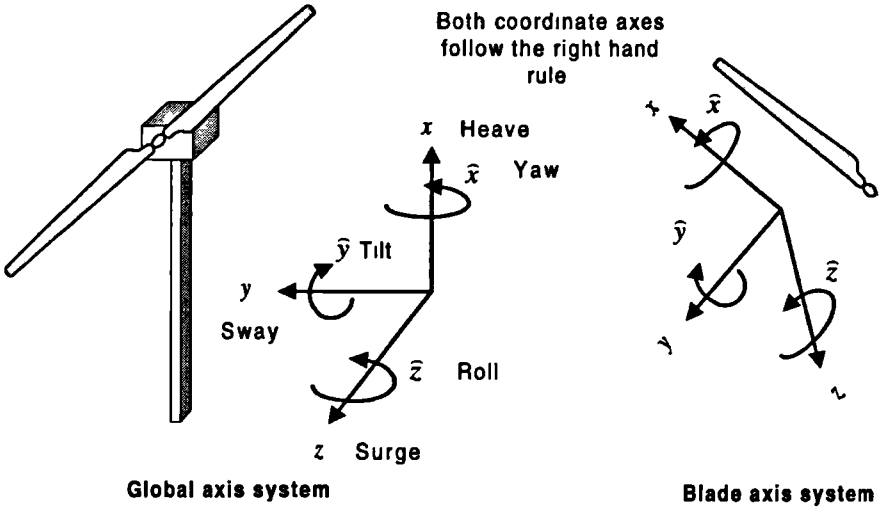

Figure 9-2 Global and blade axes systems

Heave	Translation along the x axis
Sway	Translation along the y axis
Surge	Translation along the z axis
Yaw	Rotation about the x axis
Tilt	Rotation about the y axis
Roll	Rotation about the z axis

Table 9-1 Rigid body degrees of freedom

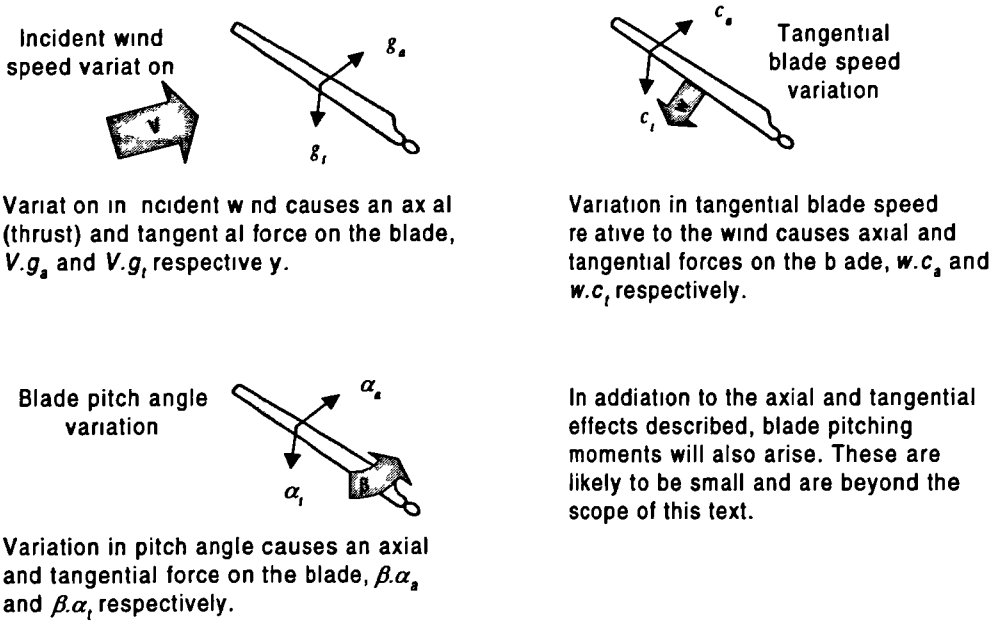

Figure 9-3 Notation for linear gain factors

This chapter is split into several sections to facilitate a clear explanation of the derivations. It is prudent to say a little about the content of each section at this point as this will help the reader understand the derivation procedure.

9.2 The loading on a blade element as the turbine is moved through space: This section describes the loading on a single blade element as it rotates and is subjected to additional nacelle motions. The section starts by tracing the locus of the element in space, from this the velocity and acceleration of the element is found and hence the damping and inertial forces determined.

9.3 Derivation of transfer matrices relating blade loads to motions of the nacelle: This section considers the blade loading, represented in the blade's local coordinate axis, to nacelle motions occurring in the global coordinate axis. Nacelle motion in one direction results in blade loads along a number of local blade axes. This section derives matrices which relate the blade loads to nacelle motions.

9.4 Derivation of rotor transformation matrices relating rotor load in the global axis system to motions of the nacelle: This section considers the blade loading, represented in the global coordinate axis system, to nacelle

motions also occurring in the global coordinate axis. Essentially the blade loads derived in item 2 are transformed into the global coordinate axis. These are then summed over the number of blades in the rotor, therefore giving the total force exerted on the rotor due to motions of the nacelle. Forces are presented as mass, damping and stiffness matrices and can be used to determine the equilibrium motion of the floating turbine. Results are presented for rotors consisting of one, two or three or more blades.

9.5 Derivation of rotor loading on a three bladed turbine in the frequency domain: In item 3 we discover that rotors which have 3 or more blades behave as homogeneous disks and this enables us to analyse them very easily in the frequency domain. This section derives the formulation in the frequency domain for determining rotor loading for rotors with three or more blades.

9.6 Comments on the solution technique for analysing 1 or 2 bladed rotors in the frequency domain: A three bladed rotor is relatively easy to analyse in the frequency domain. However, we see that single and two bladed rotors are extremely complicated. In this section we look at the processes involved when considering the calculation of single and two bladed rotors.

9.1 Previous relevant studies

Many studies have been made in the time domain for fixed base turbines. Notable among these is the study by Oscar and Paez[3]. They derived a computer model in 1988 to predict the dynamic response of an offshore turbine. The analysis is carried out through a time domain simulation and the results transformed into the frequency domain. Delft University of Technology have, more recently, undertaken quite an extensive research programme and have published a number of reports discussing the analysis of fixed based machines. These range from cost analyses to detailed load and structural analysis (Kortlever[4] and Kühn[5]). At present only Garrad Hassan have carried out a full frequency domain analysis of a fixed base, offshore turbine. Garrad Hassan and Germanischer Lloyd[6] document this. For this analysis they have used a modified version of their TURBLOAD program, which has been modified to include

wave loading input in the form of a sea state spectra. Wei and Quarton[7] describe this analysis. All of the above studies highlight the importance of an integrated model for the wind turbine rotor and the support structure.

Floating offshore concepts have received less attention. Floating platforms are likely to undergo much larger motions than fixed base platforms and the effect on the turbine loading needs to be considered. Garrad Hassan, in collaboration with Tecnomare UK Ltd., has recently undertaken a large project to investigate the behaviour of floating platforms (Tong and Cannell[8]). This project, named 'FLOAT,' concentrated on a single turbine mounted on a spa buoy platform. The platform is secured to the seabed using an eight point catenary mooring and a piled anchor system. Analysis is carried out in the frequency domain again using the modified version of their TURBLOAD program. The program, however, only models the turbine response in surge and does not appear to include the additional degrees of freedom for heave, sway, yaw and tilt. However, it does include structural flexibilities for the blades, tower and drivetrain.

Previous work carried out on Wind Assisted Ship Propulsion (WASP) is also useful. Sinclair and Clayton[9] have undertaken considerable work in this field. Relevant to this study is the research carried out on ship roll stabilisation using wind turbines. They later extended their studies to consider the analysis of offshore wind turbines (Sinclair and Clayton[10,11]). These were based on a theoretical aerodynamic model of the rotor where various aerodynamic coefficients were determined using wind tunnel tests on a scaled 3 bladed wind turbine. Properties were calculated for the rotor as a whole. Individual blade properties were not derived and the rotor was assumed infinitely stiff. Analyses were carried out to investigate the effect of aerodynamic damping on a flexible tower structure. An experimental verification of the work was later present by Sinclair[12]. This work however has concentrated only on the aerodynamic roll damping of the rotor and has not considered all the effects such as gyroscopic coupling, rotor inertia, etc. Furthermore it does not model the dynamics of the individual blades and therefore the consequence on the fatigue life of the turbine.

In this chapter we derive new theoretical techniques for analysing the motion response of a floating turbine. These include all the inertial, damping and stiffness terms for all rigid body degrees of freedom. The technique represents a completely new integrated

analysis capability. A special model is derived in the frequency domain to investigate the rigid body motion dynamics of a three bladed turbine rotor. This is seen to behave as a homogeneous disk when displaced through the air. The chapter assumes a fully rigid structure and considers only the rigid body modes. Chapter 10 discusses the effect of system flexibilities on the loading. Together these two chapters combine all the structural flexibilities of the turbine and the rigid body dynamics in an integrated approach not seen before.

9.2 The loading on a blade element as the turbine is moved through space

In this section we observe the locus of a single blade element as the nacelle is moved through space with six degrees of freedom. Having established this locus we can differentiate with respect to time to determine the velocity and acceleration of the element. Using these values the forces on the blade element can be determined. This proves a very intuitive method for determining the rather complicated loading on rotating bodies. We will first of all consider the response to yawing and tilting.

9.2.1 Yawing and tilting motions

Consider the displacement of a blade element rotating about an inclined axis as shown in Figure 9-4. The rotor tilt is varying sinusoidally with respect to time.

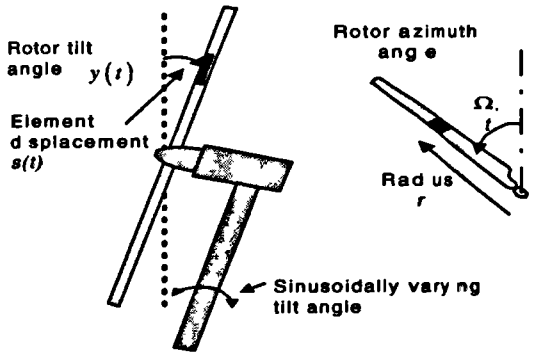

Figure 9-4 Rotor tilt

Now the displacement *s(t)* is found by the following expression:

$$s(t) = -r \cdot \sin(\tilde{y}(t)) \cdot \cos(\Omega \cdot t)$$

Assuming that the pitching motion is small yields a more friendly expression that can be employed in the frequency domain.

$$s(t) = -r \cdot \tilde{y}(t) \cdot \cos(\Omega \cdot t) \qquad \textbf{Equation 9-2}$$

Gravitational acceleration acting on the blade element will result in an overturning moment on the blade due to this displacement. The overturning moment is given in Equation 9-3.

$$Fs(t) = -\gamma \cdot r \cdot \tilde{y}(t) \cdot \cos(\Omega \cdot t) \qquad \textbf{Equation 9-3}$$

Where $Fs(t)$ is the rotor moment and γ is the gravitational force found by the product of the elemental mass m and the acceleration due to gravity.

A similar force can also arise with a self aligning rotor. It is known that all downwind rotors and some upwind rotors will self align with the wind, occasionally it may also act in a negative sense and this is the reason why upwind rotors are usually fitted with active yawing systems. The self-aligning moment can be expressed in the form of Equation 9-3 by substituting γ with an appropriate gain factor. In this text we shall not consider this effect because it is found to be quite small for upwind rotors.

Now, if we picture the locus of this blade element as it progresses through space, we can see that the changing displacement gives rise to velocity and acceleration of the element. These in turn will cause aerodynamic and inertial loads.

The velocity of the blade element is determined by differentiating Equation 9-2 with respect to time t. This is expressed in Equation 9-4.

$$\dot{s}(t) = -r \cdot \dot{\tilde{y}}(t) \cdot \cos(\Omega \cdot t) + r \cdot \tilde{y}(t) \cdot \Omega \cdot \sin(\Omega \cdot t) \qquad \textbf{Equation 9-4}$$

The first part of this equation arises due to the angular velocity at which the rotor is moved through the air. The aerodynamic forces due to this term are obtained using the aerodynamic gain factors g_a and g_t for the element. The second part is 90° out of phase with the first and deals with the variation in in-flow angle of the incident wind. The forces caused by this are obtained after multiplying by the pitch gain factors β_a and β_t. The force is therefore given by Equation 9-5.

$$F\dot{s}(t) = -r \cdot g \cdot \dot{\tilde{y}}(t) \cdot \cos(\Omega \cdot t) + \beta \cdot \tilde{y}(t) \cdot \sin(\Omega \cdot t) \qquad \textbf{Equation 9-5}$$

Where $F\dot{s}(t)$ is the damping force, and g and β are the aerodynamic gain factors. (g_a and β_a represent axial force, while g_t and β_t represent tangential). It should be noted that sign convention may change when dealing with the

tangential component. This is covered more fully in later sections.

The acceleration of the blade element is found by differentiating the velocity with respect to time as given in Equation 9-6.

$$\ddot{s}(t) = \underbrace{-r\cdot\ddot{y}(t)\cdot\cos(\Omega\cdot t)}_{\text{Inertial}} + \underbrace{2r\cdot\dot{y}(t)\cdot\Omega\cdot\sin(\Omega\cdot t)}_{\text{Gyroscopic}} + \underbrace{r\cdot\bar{y}(t)\cdot\Omega^2\cdot\cos(\Omega\cdot t)}_{\text{Centripetal}} \qquad \textbf{Equation 9-6}$$

The three parts of this equation are clearly recognised as the inertial, gyroscopic and centripetal components of force. The force due to these components is obtained by multiplying by the mass *m* of the element. The gyroscopic force is 90° out of phase with the inertial and centripetal as expected. The inertial force on the element is therefore expressed as Equation 9-7.

$$F\ddot{s}(t) = -m\cdot r\cdot\ddot{\bar{y}}(t)\cdot\cos(\Omega\cdot t) + 2m\cdot r\cdot\dot{\bar{y}}(t)\cdot\Omega\cdot\sin(\Omega\cdot t) + m\cdot r\cdot\bar{y}(t)\cdot\Omega^2\cdot\cos(\Omega\cdot t)$$

Equation 9-7

Expressing the sum of all these forces yields the following:

$$\begin{aligned}&\left\{-m\cdot r\cdot\cos(\Omega\cdot t)\right\}\cdot\ddot{\bar{y}}(t) + \left\{2m\cdot r\cdot\Omega\cdot\sin(\Omega\cdot t) - g\cdot r\cdot\cos(\Omega\cdot t)\right\}\cdot\dot{\bar{y}}(t) + \cdots\\ &\left\{m\cdot r\cdot\Omega^2\cdot\cos(\Omega\cdot t) + \beta\cdot\sin(\Omega\cdot t) - \gamma\cdot r\cdot\cos(\Omega\cdot t)\right\}\cdot\bar{y}(t) = f(t)\end{aligned}$$

Where *f(t)* is the total force on the blade element. **Equation 9-8**

Simplifying this expression yields Equation 9-9:

$$m\cdot\ddot{\bar{y}}(t) + c\cdot\dot{\bar{y}}(t) + k\cdot\bar{y}(t) = f(t) \qquad \textbf{Equation 9-9}$$

Where

$$\begin{aligned}m &= -m\cdot r\cdot\cos(\Omega\cdot t)\\ c &= 2m\cdot r\cdot\Omega\cdot\sin(\Omega\cdot t) - g\cdot r\cdot\cos(\Omega\cdot t)\\ k &= m\cdot r\cdot\Omega^2\cdot\cos(\Omega\cdot t) + \beta\cdot\sin(\Omega\cdot t) - \gamma\cdot r\cdot\cos(\Omega\cdot t)\end{aligned}$$

The above formula clearly shows the dynamic equilibrium equation for the blade element when the rotor is subjected to a tilting motion. A similar expression is obtained when the rotor is subjected to a yawing motion. In this case, however, the gravity term will be excluded and the phase relationships will all be shifted through 90°.

9.2.2 Rolling motions

If the nacelle is subjected to a rolling motion then the rotor will be forced to rotate through the air at varying speed. The axial and tangential blade forces resulting from this variation are obtained from Equation 9-10.

$$f(t) = -m \cdot r \cdot \ddot{z}(t) + c \cdot r \cdot \dot{z}(t) \qquad \textbf{Equation 9-10}$$

Where $c = c_a$ or c_t depending on whether the axial or tangential blade force is required.

9.2.3 Heave and sway motions

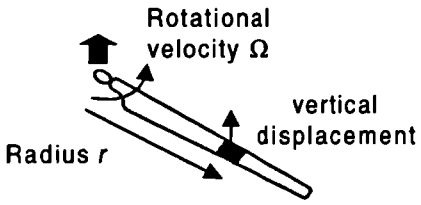

Figure 9-5 locus due to heaving motion

Consider the locus of a rotating blade element when the nacelle is subjected to a sinusoidal heaving motion *x(t)* with respect to time. This is illustrated in Figure 9-5.

Now the displacement *s(t)* resolved in the *x* direction is found by the following expression:

$$s(t) = r \cdot \cos(\Omega \cdot t) + x(t) \qquad \textbf{Equation 9-11}$$

There is no force associated with this displacement. The velocity of the vertical displacement is obtained by differentiating the above with respect to time *t*. This is expressed in Equation 9-12.

$$\dot{s}(t) = -r \cdot \Omega \cdot \sin(\Omega \cdot t) + \dot{x}(t) \qquad \textbf{Equation 9-12}$$

The force associated with this is due to the aerodynamics of the blade. To obtain this force we need to resolve the heave velocity so it is in a direction perpendicular to the blade. The resulting aerodynamic force on the blade element is given in Equation 9-13.

$$F\dot{s}(t) = c \cdot r \cdot \Omega + c \cdot \dot{x}(t) \cdot \sin(\Omega \cdot t) \qquad \textbf{Equation 9-13}$$

Where c may be the axial or tangential aerodynamic gain factor, c_a or c_t, depending on the direction of loading required.

The acceleration of the blade element is found by differentiating Equation 9-12 with respect to time t as follows:

$$\ddot{s}(t) = -r \cdot \Omega^2 \cdot \cos(\Omega \cdot t) + \ddot{x}(t) \qquad \textbf{Equation 9-14}$$

The force associated with this acceleration is found after multiplying by the elemental mass m. This is expressed in Equation 9-15.

$$F\ddot{s}(t) = \underbrace{-m \cdot r \cdot \Omega^2 \cdot \cos(\Omega \cdot t)}_{\text{Centripetal}} + \underbrace{m \cdot \ddot{x}(t)}_{\text{Inertial}} \qquad \textbf{Equation 9-15}$$

The first term of this is the centripetal component of axial force along the blade. This is not taken into account in the structural analysis described in this text. However, it is included here as an additional loading. Expressing the sum of all these forces yields the following:

$$M \cdot \ddot{x}(t) + C \cdot \dot{x}(t) + K \cdot x(t) + H = f(t) \qquad \textbf{Equation 9-16}$$

Where
$$M = m$$
$$C = c \cdot \sin(\Omega \cdot t)$$
$$K = 0$$
$$H = c \cdot r \cdot \Omega - m \cdot r \cdot \Omega^2 \cdot \cos(\Omega \cdot t)$$

9.2.4 Surge motion

If the nacelle is subjected to a surge motion then the rotor will see a corresponding change in the incident wind speed. The axial and tangential blade forces resulting from this variation is obtained from Equation 9-17.

$$f(t) = m \cdot \ddot{z}(t) + g \cdot \dot{z}(t) \qquad \textbf{Equation 9-17}$$

Where $g = g_a$ or g_t depending on whether the axial or tangential blade force is required.

9.3 Derivation of transfer matrices relating blade loads to motions of the nacelle

In the previous section we derived expressions for the forces acting on a single blade element as a wind turbine is subjected to motions in six degrees of freedom. The

expressions are given in terms of mass, damping and stiffness in the blade coordinate axis system. In this section we shall look at the matrix representation of all these loads. This allows us to see how a turbine motion in a particular degree of freedom will affect the blade's loading in the all of its degrees of freedom.

We could derive all the expressions for the entire blade forces and moments as we did in the previous section. A more elegant approach makes use of the coordinate transformation matrix and this is utilised in this section.

We determined that five different loading conditions arise from the turbine's motions. These are listed in Table 9-2 along with the type of matrix, (Mass, Damping or Stiffness) that these give. We shall derive each matrix in turn. The resulting mass, damping and stiffness matrices are then found by summing the relevant matrices.

Aerodynamic loads	(Damping matrix)
Inertial loads	(Mass matrix)
Gyroscopic loads	(Damping matrix)
Gravity load	(Stiffness matrix)
In-flow angle	(Stiffness matrix)

Table 9-2 Loading conditions due to turbine motion

9.3.1 Aerodynamic loading

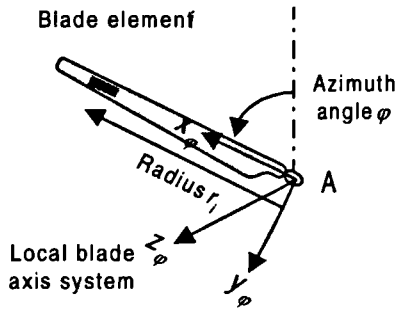

Consider the reaction forces and moments at point A due to the motion of element *i* through the air along its local axis system. The reactions are expressed in the local blade axis system as shown in the diagram. The forces and moments may be found using matrix algebra as given in Equation 9-18.

$$f_\varphi = G_\varphi \cdot s_\varphi \qquad \textbf{Equation 9-18}$$

Where f_φ represents a vector of force and s_φ a vector of displacement in the blade axis system, and G_φ is the matrix of aerodynamic gain factors in the local axis system. This is defined by Equation 9-19:

$$G_\varphi = \begin{bmatrix} 0 & 0 & 0 & 0 & 0 & 0 \\ 0 & c_t & -g_t & 0 & g_t \cdot r & c_t \cdot r \\ 0 & c_a & g_a & 0 & -g_a \cdot r & c_a \cdot r \\ 0 & 0 & 0 & 0 & 0 & 0 \\ 0 & -c_a \cdot r & -g_a \cdot r & 0 & g_a \cdot r^2 & -c_a \cdot r^2 \\ 0 & c_t \cdot r & -g_t \cdot r & 0 & g_t \cdot r^2 & c_t \cdot r^2 \end{bmatrix}$$ **Equation 9-19**

We now need to know what the blade forces are when the turbine is moved through the air along the various tower coordinate axes. To find the blade loading matrix we will use the coordinate transformation matrix $\phi(\varphi)$ as defined in Equation 9-20.

$$\phi(\varphi) = \begin{bmatrix} \cos(\varphi) & \sin(\varphi) & 0 & 0 & 0 & 0 \\ -\sin(\varphi) & \cos(\varphi) & 0 & 0 & 0 & 0 \\ 0 & 0 & 1 & 0 & 0 & 0 \\ 0 & 0 & 0 & \cos(\varphi) & \sin(\varphi) & 0 \\ 0 & 0 & 0 & -\sin(\varphi) & \cos(\varphi) & 0 \\ 0 & 0 & 0 & 0 & 0 & 1 \end{bmatrix}$$ **Equation 9-20**

Where φ is the azimuth angle of the blade at some time.

We use the subscripts φ and o to represent the local blade and global tower coordinate axes respectively. We use the transformation matrix to transform displacements and forces from one axis system into the other. To transform from the tower axis system to the blade axis system we use the following formulae:

$$f_\varphi = \phi(\varphi) \cdot f_o \qquad s_\varphi = \phi(\varphi) \cdot s_o$$ **Equation 9-21**

Where f represents a vector of force and s a vector of displacement.

The reverse transformation can be found by rearranging the above formulae using matrix algebra. Now transformation matrices have the property that their inverse ϕ^{-1} is equal to their transpose ϕ^{T}. The reverse transformations may therefore be expressed as follows:

$$f_o = \phi(\varphi)^T \cdot f_\varphi \qquad s_o = \phi(\varphi)^T \cdot s_\varphi$$ **Equation 9-22**

Now we want the blade's loading to be represented in the local coordinate axis, while the motion is expressed in the tower coordinate axis. To accomplish this we arrange the above formulae as follows:

$$f_\varphi = \underbrace{G_\varphi \cdot \phi \cdot s_o}_{G_{\varphi o}}$$

Equation 9-23

Where $G_{\varphi o}$ is the matrix of gain factors relating global tower motions with local blade forces and moments.

Evaluating Equation 9-23 yields the following expression for the aerodynamic gain matrix $G_{\varphi o}$.

$$G_{\varphi o} = \begin{bmatrix} 0 & 0 & 0 & 0 & 0 & 0 \\ -c_t \cdot \sin(\varphi) & c_t \cdot \cos(\varphi) & -g_t & -g_t \cdot r \cdot \sin(\varphi) & g_t \cdot r \cdot \cos(\varphi) & c_t \cdot r \\ -c_a \cdot \sin(\varphi) & c_a \cdot \cos(\varphi) & g_a & g_a \cdot r \cdot \sin(\varphi) & -g_a \cdot r \cdot \cos(\varphi) & c_a \cdot r \\ 0 & 0 & 0 & 0 & 0 & 0 \\ c_a \cdot r \cdot \sin(\varphi) & -c_a \cdot r \cdot \cos(\varphi) & -g_a \cdot r & -g_a \cdot r^2 \cdot \sin(\varphi) & g_a \cdot r^2 \cdot \cos(\varphi) & -c_a \cdot r^2 \\ -c_t \cdot r \cdot \sin(\varphi) & c_t \cdot r \cdot \cos(\varphi) & -g_t \cdot r & -g_t \cdot r^2 \cdot \sin(\varphi) & g_t \cdot r^2 \cdot \cos(\varphi) & c_t \cdot r^2 \end{bmatrix}$$

Equation 9-24

9.3.2 Inertial loading

The inertial loading analysis is carried out in the same way as the aerodynamic case above. Here the matrix of inertial gain factors expressed in the local blade axis system is given by Equation 9-25.

$$G_\varphi = \begin{bmatrix} m & 0 & 0 & 0 & 0 & 0 \\ 0 & m & 0 & 0 & 0 & m \cdot r \\ 0 & 0 & m & 0 & -m \cdot r & 0 \\ 0 & 0 & 0 & 0 & 0 & 0 \\ 0 & 0 & -m \cdot r & 0 & m \cdot r^2 & 0 \\ 0 & m \cdot r & 0 & 0 & 0 & m \cdot r^2 \end{bmatrix}$$

Equation 9-25

The matrix of gain factors giving blade forces in the local blade axis due to tower motions in the global tower axis is therefore expressed as follows:

$$G_{\varphi o} = \begin{bmatrix} m\cdot\cos(\varphi) & m\cdot\sin(\varphi) & 0 & 0 & 0 & 0 \\ -m\cdot\sin(\varphi) & m\cdot\cos(\varphi) & 0 & 0 & 0 & m\cdot r \\ 0 & 0 & m & m\cdot r\cdot\sin(\varphi) & -m\cdot r\cdot\cos(\varphi) & 0 \\ 0 & 0 & 0 & 0 & 0 & 0 \\ 0 & 0 & -m\cdot r & -m\cdot r^2\cdot\sin(\varphi) & m\cdot r^2\cdot\cos(\varphi) & 0 \\ -m\cdot r\cdot\sin(\varphi) & m\cdot r\cdot\cos(\varphi) & 0 & 0 & 0 & m\cdot r^2 \end{bmatrix}$$

Equation 9-26

9.3.3 Gyroscopic loading

The loading on the turbine blade due to gyroscopic action cannot be derived using the local blade gain matrix as described above. In the above cases we first of all derived this matrix by observing the way in which the blade behaved when moved along its local axes. Gyroscopic loading however results from the blade motion about the global axis. It so happens, however that we can easily derive the gain matrix $G_{\varphi o}$ by observation. Thus the previous steps described above are therefore unnecessary. The gain matrix relating blade force, in the blade's local axis, to motion in the global axis is therefore given as Equation 9-27.

$$G_{\varphi o} = \begin{bmatrix} 0 & 0 & 0 & 0 & 0 & 0 \\ 0 & 0 & 0 & 0 & 0 & 0 \\ 0 & 0 & 0 & 2m\cdot r\cdot\Omega\cdot\cos(\varphi) & 2m\cdot r\cdot\Omega\cdot\sin(\varphi) & 0 \\ 0 & 0 & 0 & 0 & 0 & 0 \\ 0 & 0 & 0 & -2m\cdot r^2\cdot\Omega\cdot\cos(\varphi) & -2m\cdot r^2\cdot\Omega\cdot\sin(\varphi) & 0 \\ 0 & 0 & 0 & 0 & 0 & 0 \end{bmatrix}$$

Equation 9-27

9.3.4 Gravity loading

The gravity loading discussed here relates to that brought about by the stochastic tilting of the turbine. The deterministic loading due to the blades rotation is not considered. The gain matrix relating blade force, in the blade's local axis, to motion in the global axis is given by observation as Equation 9-28.

$$G_{\varphi o} = \begin{bmatrix} 0 & 0 & 0 & 0 & 0 & 0 \\ 0 & 0 & 0 & 0 & 0 & 0 \\ 0 & 0 & 0 & 0 & \gamma \cdot r & 0 \\ 0 & 0 & 0 & 0 & 0 & 0 \\ 0 & 0 & 0 & 0 & -\gamma \cdot r^2 & 0 \\ 0 & 0 & 0 & 0 & 0 & 0 \end{bmatrix}$$ **Equation 9-28**

9.3.5 Loading brought about by a cyclic variation in in-flow angle

By observation, the gain matrix relating blade force, in the blade's local axis, to motion in the global axis is given as Equation 9-29.

$$G_{\varphi o} = \begin{bmatrix} 0 & 0 & 0 & 0 & 0 & 0 \\ 0 & 0 & 0 & -\beta_t \cdot \cos(\varphi) & -\beta_t \cdot \sin(\varphi) & 0 \\ 0 & 0 & 0 & \beta_a \cdot \cos(\varphi) & \beta_a \cdot \sin(\varphi) & 0 \\ 0 & 0 & 0 & 0 & 0 & 0 \\ 0 & 0 & 0 & -\beta_a \cdot r \cdot \cos(\varphi) & -\beta_a \cdot r \cdot \sin(\varphi) & 0 \\ 0 & 0 & 0 & -\beta_t \cdot r \cdot \cos(\varphi) & -\beta_t \cdot r \cdot \sin(\varphi) & 0 \end{bmatrix}$$ **Equation 9-29**

9.3.6 The mass, damping and stiffness matrices of blade loading caused by motion of the turbine

Using the matrices derived above we can now arrange these to form mass, damping and stiffness matrices for the blade loading. These are expressed in Equation 9-30.

$$M_{\varphi o} \cdot \ddot{s}_o + C_{\varphi o} \cdot \dot{s}_o + K_{\varphi o} \cdot s_o = f_\varphi$$ **Equation 9-30**

Where

$$M_{\varphi o} = \begin{bmatrix} m \cdot \cos(\varphi) & m \cdot \sin(\varphi) & 0 & 0 & 0 & 0 \\ -m \cdot \sin(\varphi) & m \cdot \cos(\varphi) & 0 & 0 & 0 & m \cdot r \\ 0 & 0 & m & m \cdot r \cdot \sin(\varphi) & -m \cdot r \cdot \cos(\varphi) & 0 \\ 0 & 0 & 0 & 0 & 0 & 0 \\ 0 & 0 & -m \cdot r & -m \cdot r^2 \cdot \sin(\varphi) & m \cdot r^2 \cdot \cos(\varphi) & 0 \\ -m \cdot r \cdot \sin(\varphi) & m \cdot r \cdot \cos(\varphi) & 0 & 0 & 0 & m \cdot r^2 \end{bmatrix}$$

$$K_{\varphi o} = \begin{bmatrix} 0 & 0 & 0 & 0 & 0 & 0 \\ 0 & 0 & 0 & -\beta_t \cdot \cos(\varphi) & -\beta_t \cdot \sin(\varphi) & 0 \\ 0 & 0 & 0 & \beta_a \cdot \cos(\varphi) & \beta_a \cdot \sin(\varphi) + \gamma \cdot r & 0 \\ 0 & 0 & 0 & 0 & 0 & 0 \\ 0 & 0 & 0 & -\beta_a \cdot r \cdot \cos(\varphi) & -\beta_a \cdot r \cdot \sin(\varphi) - \gamma \cdot r^2 & 0 \\ 0 & 0 & 0 & -\beta_t \cdot r \cdot \cos(\varphi) & -\beta_t \cdot r \cdot \sin(\varphi) & 0 \end{bmatrix}$$

$$C_{\varphi o} = \begin{bmatrix} 0 & 0 & 0 & 0 & 0 & 0 \\ -c_t \cdot \sin(\varphi) & c_t \cdot \cos(\varphi) & -g_t & -g_t \cdot r \cdot \sin(\varphi) & g_t \cdot r \cdot \cos(\varphi) & c_t \cdot r \\ -c_a \cdot \sin(\varphi) & c_a \cdot \cos(\varphi) & g_a & g_a \cdot r \cdot \sin(\varphi) + 2m \cdot r \cdot \Omega \cdot \cos(\varphi) & -g_a \cdot r \cdot \cos(\varphi) + 2m \cdot r \cdot \Omega \cdot \sin(\varphi) & c_a \cdot r \\ 0 & 0 & 0 & 0 & 0 & 0 \\ c_a \cdot r \cdot \sin(\varphi) & -c_a \cdot r \cdot \cos(\varphi) & -g_a \cdot r & -g_a \cdot r^2 \cdot \sin(\varphi) - 2m \cdot r^2 \cdot \Omega \cdot \cos(\varphi) & g_a \cdot r^2 \cdot \cos(\varphi) - 2m \cdot r^2 \cdot \Omega \cdot \sin(\varphi) & -c_a \cdot r^2 \\ -c_t \cdot r \cdot \sin(\varphi) & c_t \cdot r \cdot \cos(\varphi) & -g_t \cdot r & -g_t \cdot r^2 \cdot \sin(\varphi) & g_t \cdot r^2 \cdot \cos(\varphi) & c_t \cdot r^2 \end{bmatrix}$$

9.4 Derivation of rotor transformation matrices relating rotor load in the global axis system to motions of the nacelle

This section considers the blade loading, represented in the global coordinate axis, to nacelle motions also occurring in the global coordinate axis. Essentially the local blade loads derived above are transformed into the global coordinate axis, these are then summed over the number of blade elements and the number of blades in the rotor giving the total force exerted on the rotor due to motions of the nacelle. These forces are presented as 6 degree of freedom, mass, damping and stiffness matrices and can therefore be incorporated into hydrodynamic analysis programs such as AQWA, by WS Atkins Ltd., or into structural dynamic analysis programs. The use of these matrices proves very beneficial as they can be used with existing offshore analysis software and so can be brought into production very swiftly. Typical applications include stability and seakeeping analyses. Matrices are defined for rotors consisting one, two or three or more blades.

To accomplish the coordinate transformation we use the transform matrix $\phi(\varphi)$ as described earlier. This time we are only interested in the sum of the loading on the blades and not the individual load on each blade element. The formula is therefore given in Equation 9-31.

$$G_o = \phi^T \cdot \sum_{i=1}^{N} G_{\varphi o_i} \qquad \textbf{Equation 9-31}$$

Where $G_{\varphi o_i}$ is the 6x6 matrix of gain factors for the i^{th} blade element, N is the number of aerodynamic elements along the blade and G_o is the 6x6 matrix of gain factors relating to the blade reaction loading. This is given in the tower's global coordinate axis and pertains to turbine motions, also expressed in the global axis.

Now the matrix G_o is given as a function of the azimuth angle, φ. We need to find out the total reaction forces from all the blades and therefore have to take the sum of the matrix $G_o(\varphi)$ over all the blades. This is expressed in Equation 9-32.

$$G_o^R = \sum_{b=0}^{B-1} G_{o_i}\left(\varphi + b \cdot \frac{2\pi}{B}\right) \qquad \textbf{Equation 9-32}$$

Where G_o^R is the matrix of total rotor loading resulting from all the blades and B is the number of blades, evenly spaced around the rotor.

We notice a very complicated loading response in the case of a single bladed turbine. However once we consider the two and three bladed cases we see that many of the terms begin to cancel. In the following section we use the trigonometric identities given in Equation 9-33 to simplify the matrix expressions.

$$\sum_{b=0}^{B-1}\cos\left(\varphi+b\cdot\frac{2\pi}{B}\right) \qquad \sum_{b=0}^{B-1}\sin\left(\varphi+b\cdot\frac{2\pi}{B}\right) \qquad = 0 \text{ for values of } B \geq 2$$

$$\sum_{b=0}^{B-1}\cos\left(\varphi+b\cdot\frac{2\pi}{B}\right)\cdot\sin\left(\varphi+b\cdot\frac{2\pi}{B}\right) \qquad = 0 \text{ for values of } B \geq 3$$

$$\sum_{b=0}^{B-1}\cos^2\left(\varphi+b\cdot\frac{2\pi}{B}\right) \qquad \sum_{b=0}^{B-1}\sin^2\left(\varphi+b\cdot\frac{2\pi}{B}\right) \qquad = \frac{B}{2} \text{ for values of } B\geq 3$$

Equation 9-33

The equations presented in the next few pages represent the simplified expressions for G_o. These are given for single, two and multi-bladed machines and take account of the relationships expressed in Equation 9-33 to allow for the simplification.

The formulae clearly show the benefit of using three bladed turbines over two bladed or single bladed machines. The lack of the sine and cosine terms means that the rotor acts as a balanced homogeneous disk as the turbine is tossed around in the sea. With the two bladed turbine we start to see blade azimuth dependencies appearing in the form of sine and cosine expressions. These result in Doppler shifting in the loading spectra. Physically this implies that if the turbine is moved in the water with a certain frequency, then the resultant loads would occur at different frequencies. To illustrate this problem consider the axial force on the tower in response to a sinusoidal heaving motion of a two bladed turbine. To simplify this we shall only consider the aerodynamic components of the force.

Now the force on the tower due to a sinusoidal heaving velocity is obtained from the gain matrix in Equation 9-35 as the following:

$$f(t) = \dot{y}(t) \cdot \sin^2(\Omega \cdot t) \cdot c_t \qquad \text{Where } \dot{y}(t) = \sin(\omega \cdot t)$$

Expanding this expression yields:

$$f(t) = \tfrac{1}{4} c_t \cdot \left\{ \sin\left((2\Omega - \omega) \cdot t\right) - \sin\left((2\Omega + \omega) \cdot t\right) + 2 \cdot \sin(\omega \cdot t) \right\}$$

We therefore see that for an input at a single frequency, the output will occur at three separate frequencies. This dramatically increases the complexity of the calculation and also results in possible dynamic problems. These occur when frequencies interfere with certain natural frequencies.

If we carry out a similar study on a three bladed turbine we see from Equation 9-36 that the force due to sinusoidal heaving is now linear and therefore much easier to deal with in the frequency domain. The force response is given as follows:

$$f(t) = \dot{y}(t) \cdot \tfrac{1}{2} \cdot c_t \qquad \text{Where } \dot{y}(t) = \sin(\omega \cdot t)$$

$$M(\varphi) \begin{bmatrix} m & 0 & 0 & 0 & 0 & -m\cdot r\cdot\sin(\varphi) \\ 0 & m & 0 & 0 & 0 & m\cdot r\cdot\cos(\varphi) \\ 0 & 0 & m & m\cdot r\cdot\sin(\varphi) & m\cdot r\cdot\cos(\varphi) & 0 \\ 0 & 0 & m\cdot r\cdot\sin(\varphi) & \sin(\varphi)^2\cdot m\cdot r^2 & \sin(\varphi)\ m\cdot r^2\cdot\cos(\varphi) & 0 \\ 0 & 0 & m\cdot r\cdot\cos(\varphi) & \sin(\varphi)\cdot m\cdot r^2\cdot\cos(\varphi) & \cos(\varphi)^2\cdot m\cdot r^2 & 0 \\ m\cdot r\cdot\sin(\varphi) & m\cdot r\cdot\cos(\varphi) & 0 & 0 & 0 & m\cdot r^2 \end{bmatrix} \quad K(\varphi) : \begin{bmatrix} 0 & 0 & 0 & \sin(\varphi)\cdot\beta_t\cdot\cos(\varphi) & \sin(\varphi)^2\cdot\beta_t & 0 \\ 0 & 0 & 0 & \cos(\varphi)^2\cdot\beta_t & \sin(\varphi)\cdot\beta_t\cdot\cos(\varphi) & 0 \\ 0 & 0 & 0 & \beta_a\cdot\cos(\varphi) & \beta_a\cdot\sin(\varphi) & 0 \\ 0 & 0 & 0 & \sin(\varphi)\cdot\beta_a\cdot r\cdot\cos(\varphi) & \sin(\varphi)^2\cdot\beta_a\cdot r & 0 \\ 0 & 0 & 0 & \cos(\varphi)^2\cdot\beta_a\cdot r & \sin(\varphi)\cdot\beta_a\cdot r\cdot\cos(\varphi) & 0 \\ 0 & 0 & 0 & \beta_t\cdot r\cdot\cos(\varphi) & \beta_t\cdot r\cdot\sin(\varphi) & 0 \end{bmatrix}$$

$$C(\varphi) \begin{bmatrix} \sin(\varphi)^2\cdot c_t & \sin(\varphi)\cdot c_t\cdot\cos(\varphi) & \sin(\varphi)\cdot g_t & \sin(\varphi)^2\cdot g_t\cdot r & \sin(\varphi)\cdot g_t\cdot r\cdot\cos(\varphi) & c_t\cdot r\cdot\sin(\varphi) \\ \sin(\varphi)\cdot c_t\cdot\cos(\varphi) & \cos(\varphi)^2\cdot c_t & \cos(\varphi)\cdot g_t & \sin(\varphi)\cdot g_t\cdot r\cdot\cos(\varphi) & \cos(\varphi)^2\cdot g_t\cdot r & c_t\cdot r\cdot\cos(\varphi) \\ c_a\cdot\sin(\varphi) & c_a\cdot\cos(\varphi) & g_a & g_a\cdot r\cdot\sin(\varphi)+2\cdot m\cdot r\cdot\Omega\cdot\cos(\varphi) & -g_a\cdot r\cdot\cos(\varphi)+2\cdot m\cdot r\cdot\Omega\cdot\sin(\varphi) & c_a\cdot r \\ \sin(\varphi)^2\cdot c_a\cdot r & c_a\cdot\sin(\varphi)\cdot r\cdot\cos(\varphi) & g_a\cdot r\cdot\sin(\varphi) & \sin(\varphi)^2\cdot g_a\cdot r^2+2\cdot\sin(\varphi)\cdot m\cdot r^2\cdot\Omega\cdot\cos(\varphi) & \sin(\varphi)\cdot g_a\cdot r^2\cdot\cos(\varphi)+2\cdot\sin(\varphi)^2\cdot m\cdot r^2\cdot\Omega & c_a\cdot\sin(\varphi)\cdot r^2 \\ c_a\cdot\sin(\varphi)\ r\cdot\cos(\varphi) & \cos(\varphi)^2\cdot c_a\cdot r & g_a\cdot r\cdot\cos(\varphi) & \sin(\varphi)\cdot g_a\cdot r^2\cdot\cos(\varphi)-2\cdot\cos(\varphi)^2\cdot m\cdot r^2\cdot\Omega & \cos(\varphi)^2\cdot g_a\cdot r^2\quad 2\cdot\sin(\varphi)\cdot m\cdot r^2\cdot\Omega\cdot\cos(\varphi) & c_a\cdot\cos(\varphi)\cdot r^2 \\ c_t\cdot r\cdot\sin(\varphi) & c_t\cdot r\cdot\cos(\varphi) & g_t\cdot r & g_t\cdot r^2\cdot\sin(\varphi) & g_t\cdot r^2\cdot\cos(\varphi) & c_t\cdot r^2 \end{bmatrix}$$

Equation 9-34 Single bladed turbine

$$M(\varphi) \begin{bmatrix} m & 0 & 0 & 0 & 0 & 0 \\ 0 & m & 0 & 0 & 0 & 0 \\ 0 & 0 & m & 0 & 0 & 0 \\ 0 & 0 & 0 & \sin(\varphi)^2 \cdot m \cdot r^2 & \sin(\varphi) \cdot m \cdot r^2 \cdot \cos(\varphi) & 0 \\ 0 & 0 & 0 & \sin(\varphi) \cdot m \cdot r^2 \cdot \cos(\varphi) & \cos(\varphi)^2 \cdot m \cdot r^2 & 0 \\ 0 & 0 & 0 & 0 & 0 & m \cdot r^2 \end{bmatrix}$$

$$K(\varphi) \begin{bmatrix} 0 & 0 & 0 & \sin(\varphi) \cdot \beta_t \cdot \cos(\varphi) & \sin(\varphi)^2 \cdot \beta_t & 0 \\ 0 & 0 & 0 & \cos(\varphi)^2 \cdot \beta_t & \sin(\varphi) \cdot \beta_t \cdot \cos(\varphi) & 0 \\ 0 & 0 & 0 & 0 & 0 & 0 \\ 0 & 0 & 0 & \sin(\varphi) \cdot \beta_a \cdot r \cdot \cos(\varphi) & \sin(\varphi)^2 \cdot \beta_a \cdot r & 0 \\ 0 & 0 & 0 & \cos(\varphi)^2 \cdot \beta_a \cdot r & \sin(\varphi) \cdot \beta_a \cdot r \cdot \cos(\varphi) & 0 \\ 0 & 0 & 0 & 0 & 0 & 0 \end{bmatrix}$$

$$C(\varphi) \begin{bmatrix} \sin(\varphi)^2 \cdot c_t & \sin(\varphi) \cdot c_t \cdot \cos(\varphi) & 0 & \sin(\varphi)^2 \cdot g_t \cdot r & \sin(\varphi) \cdot g_t \cdot r \cdot \cos(\varphi) & 0 \\ \sin(\varphi) \cdot c_t \cdot \cos(\varphi) & \cos(\varphi)^2 \cdot c_t & 0 & \sin(\varphi) \cdot g_t \cdot r \cdot \cos(\varphi) & \cos(\varphi)^2 \cdot g_t \cdot r & 0 \\ 0 & 0 & g_a & 0 & 0 & c_a \cdot r \\ \sin(\varphi)^2 \cdot c_a \cdot r & c_a \cdot \sin(\varphi) \cdot r \cdot \cos(\varphi) & 0 & \sin(\varphi)^2 \cdot g_a \cdot r^2 + 2 \cdot \sin(\varphi) \cdot m \cdot r^2 \cdot \Omega \cdot \cos(\varphi) & \sin(\varphi) \cdot g_a \cdot r^2 \cdot \cos(\varphi) + 2 \cdot \sin(\varphi)^2 \cdot m \cdot r^2 \cdot \Omega & 0 \\ c_a \cdot \sin(\varphi) \cdot r \cdot \cos(\varphi) & \cos(\varphi)^2 \cdot c_a \cdot r & 0 & \sin(\varphi) \cdot g_a \cdot r^2 \cdot \cos(\varphi) \quad 2 \cdot \cos(\varphi)^2 \cdot m \cdot r^2 \cdot \Omega & \cos(\varphi)^2 \cdot g_a \cdot r^2 \quad 2 \cdot \sin(\varphi) \cdot m \cdot r^2 \cdot \Omega \cdot \cos(\varphi) & 0 \\ 0 & 0 & g_t \cdot r & 0 & 0 & c_t \cdot r^2 \end{bmatrix}$$

Equation 9-35 Two bladed turbine

$$M \begin{bmatrix} m & 0 & 0 & 0 & 0 & 0 \\ 0 & m & 0 & 0 & 0 & 0 \\ 0 & 0 & m & 0 & 0 & 0 \\ 0 & 0 & 0 & \frac{1}{2}\cdot m\cdot r^2 & 0 & 0 \\ 0 & 0 & 0 & 0 & \frac{1}{2}\cdot m\cdot r^2 & 0 \\ 0 & 0 & 0 & 0 & 0 & m\cdot r^2 \end{bmatrix}$$

$$K - \begin{bmatrix} 0 & 0 & 0 & 0 & \frac{1}{2}\cdot\beta_t & 0 \\ 0 & 0 & 0 & -\frac{1}{2}\cdot\beta_t & 0 & 0 \\ 0 & 0 & 0 & 0 & 0 & 0 \\ 0 & 0 & 0 & 0 & \frac{1}{2}\cdot\beta_a\cdot r & 0 \\ 0 & 0 & 0 & -\frac{1}{2}\cdot\beta_a\cdot r & 0 & 0 \\ 0 & 0 & 0 & 0 & 0 & 0 \end{bmatrix}$$

$$C \begin{bmatrix} \frac{1}{2}\cdot c_t & 0 & 0 & \frac{1}{2}\cdot g_t\cdot r & 0 & 0 \\ 0 & \frac{1}{2}\cdot c_t & 0 & 0 & \frac{1}{2}\cdot g_t\cdot r & 0 \\ 0 & 0 & g_a & 0 & 0 & c_a\cdot r \\ \frac{1}{2}\cdot c_a\cdot r & 0 & 0 & \frac{1}{2}\cdot g_a\cdot r^2 & m\cdot r^2\cdot\Omega & 0 \\ 0 & \frac{1}{2}\cdot c_a\cdot r & 0 & m\cdot r^2\cdot\Omega & \frac{1}{2}\cdot g_a\cdot r^2 & 0 \\ 0 & 0 & g_t\cdot r & 0 & 0 & c_t\cdot r^2 \end{bmatrix}$$

Equation 9-36 Three or more bladed turbine

9.5 Derivation of rotor loading on a three bladed turbine in the frequency domain

In the previous section we discovered that rotors consisting 3 or more blades behave as homogeneous disks when moved in space and this enables us to analyse them very easily in the frequency domain. This section derives the formulation in the frequency domain for determining rotor loading for rotors with three or more blades.

As the mass, damping and stiffness matrices are all linear it is very simple to determine the cross-spectral response matrix between all the degrees of freedom, this is given in Equation 9-37

$$S_{ij}^{R}(\omega) = H^{R}(\omega) \cdot S_{o}(\omega) \cdot \overline{H^{R}(\omega)}^{T} \qquad \textbf{Equation 9-37}$$

Where $H^{R}(\omega) = B \cdot \sum_{i=1}^{N} \left\{ -\omega^{2} \cdot M_{i}^{R} + i \cdot \omega \cdot C_{i}^{R} + K_{i}^{R} \right\}$, N is the number of blade elements along each blade, B is the number of blades (B must be at least three) and $S_{o}(\omega)$ is the cross-power spectral matrix of displacements in all 6 degrees of freedom.

For most cases we are only interested in the auto-power of these forces and so can extract a vector of terms from the leading diagonal and discard the off-diagonal terms, this is expressed in Equation 9-38.

$$S^{R}(\omega) = ldiag\left(S_{ij}^{R}(\omega)\right) \qquad \textbf{Equation 9-38}$$

Where *ldiag*(Π) is a function which extracts a vector from the leading diagonal of the matrix Π.

9.6 Comments on the solution technique for analysing 1 or 2 bladed rotors in the frequency domain

We have only derived an expression in the frequency domain to analyse the rotor response for 3 or more bladed rotors. This is essentially because the analysis is very simple and linear. We could not analyse the response of 1 or 2 bladed rotors in this way because of there sinusoidal components. It is still possible to express these terms

in the frequency domain, but it becomes almost impossible to manage the cross-correlation between them.

A far simpler method of calculation may involve the response analysis to a series of unit amplitude sine waves at various frequencies in the time domain. These can then be transformed numerically into the frequency domain using the Fourier transform. In this way we can build up a frequency domain transfer matrix and not have to worry about the cross-correlation problems.

Not withstanding the above, we can still gain some information about the behaviour of the turbines. Table 9-3 summarises the auto-power spectral densities that are obtained from the general trigonometric terms for the mass, damping and stiffness matrices. In these tables, κ is a constant gain factor that can represent mass or aerodynamic properties, etc.

Table 9-3 Auto-power spectral density functions for general sinusoidal motion

General Form	$\kappa \cdot \sin^2(\Omega \cdot t)$ $\kappa \cdot \cos^2(\Omega \cdot t)$
1 blade	$\tilde{G}_{ij}^{\ B}(\omega) = \frac{B^2}{16} \cdot \kappa_i \cdot \kappa_t \cdot \left\{4 \cdot G_\Psi(\omega) + G_\Psi(\lvert\omega - 2\Omega\rvert) + G_\Psi(\lvert\omega + 2\Omega\rvert)\right\}$
2 Blades	As 1 blade
3 or more blades	$\tilde{G}_{ij}^{\ B}(\omega) = \frac{B^2}{4} \cdot \kappa_i \cdot \kappa_t \cdot G_\Psi(\omega)$

General Form	$\kappa \cdot \sin(\Omega \cdot t) \cdot \cos(\Omega \cdot t)$
1 blade	$\tilde{G}_{ij}^{\ B}(\omega) = \frac{B^2}{16} \cdot \kappa_t \cdot \kappa_t \cdot \left\{G_\Psi(\lvert\omega - 2\Omega\rvert) + G_\Psi(\lvert\omega + 2\Omega\rvert)\right\}$
2 Blades	As 1 blade
3 or more blades	$\tilde{G}_{ij}^{\ B}(\omega) = 0$

General Form	$\kappa \cdot \sin(\Omega \cdot t)$ $\kappa \cdot \cos(\Omega \cdot t)$
1 blade	$\tilde{G}_{ij}^{B}(\omega) = \frac{1}{4} \cdot \kappa_i \cdot \kappa_i \cdot \{G_\Psi(\lvert\omega - \Omega\rvert) + G_\Psi(\lvert\omega + \Omega\rvert)\}$
2 Blades	$\tilde{G}_{ij}^{B}(\omega) = 0$
3 or more blades	$\tilde{G}_{ij}^{B}(\omega) = 0$

The above tables clearly show the frequency shifts that result from each trigonometric term in the matrices. When we consider the simple sine and cosine case for a single bladed turbine, we notice that the energy is shifted to frequencies around the rotor frequency. When considering 2 or 3 bladed turbines however, we note that this then equates to zero indicating no net load.

The sine and cosine square term's result in frequency shifts around the second harmonic of the rotor frequency. This effect is noticeable with single and two bladed rotors but does not occur with three or more blades.

Frequency shifting can cause problems when trying to avoid interaction with the structure's natural frequencies. With all turbine design we try to avoid natural frequencies occurring at multiples of the rotor frequency. However, the frequency shifts still result in greater fatigue damage due to higher amplitudes of load occurring at higher cycle counts. With one or two bladed turbines sited on floating platforms, the additional loading in this high frequency band may cause fatigue problems.

9.7 Conclusions

In this chapter we have considered the loads on a rotor hub in response to rigid body tower motions in six degrees of freedom. Mass, damping and stiffness matrices have been derived to represent the effect of a wind turbine mounted on an offshore floating platform. These matrices can be incorporated into existing hydrodynamic analysis software packages to facilitate the sea keeping and stability analyses of offshore wind turbines. This technique proves very powerful because it can be incorporated into most defraction analysis software packages without change. It forms part of the original work contained in this thesis.

Turbines with 3 or more blades are found to behave as homogeneous disks when subjected to nacelle motions, this makes frequency domain analysis very simple. Single or twin bladed turbines, however, prove very complex to analyse because harmonics are added to the response. The presence of additional harmonics is likely to prove damaging to the structure because they will result in greater fatigue loads. Although methods of analysing these in the frequency domain are discussed, analysis in the time domain would prove most sensible.

A case study is presented in chapter 11 which considers the loads on a 3 bladed turbine subjected to typical offshore motion. A comparison is made between motion induced loads and those resulting due to wind turbulence.

---

[1] Patel M.H. (1989). "Dynamics of offshore structures." Butterworth-Heinemann.

[2] Patel M.H. and Witz J.A. (1991). "Compliant offshore structures." Butterworth-Heinemann.

[3] Oscar D.S. Paez T.L. (1988). "Analysis of wind turbines on offshore support structures excited by random wind and random waves." Sandia National Laboratories, Albuquerque, New Mexico 87 185. Report reference SAND87-1689 UC-60.

[4] Kortlever W. (1992). "The use of the discrete element method to model an offshore wind turbine." Master's thesis, Faculty of Civil Engineering, Delft University of Technology.

[5] Kühn M. (1994). "Simulation of offshore wind turbines under stochastic loading." Procedures, European Wind Energy Conference 1994.

[6] Garrad Hassan and Germanischer Lloyd. (1995). "Study of offshore wind in energy in the EC." EC JOULE I research program, published by Verlag Natürliche Energie,24811 Brekendorf, Germany.

[7] Wei J. and Quarton D.C. (1994). "Modelling and load prediction for offshore horizontal axis wind turbines." Proceedings, 1994 Chinese Wind Energy Conference.

[8] Tong K and Cannell C. (1993). "Technical and economical aspects of a floating offshore windfarm." Proceedings of a BWEA/DTI seminar, Cockroft Hall, Harwell, June 1993.

[9] Sinclair F.M. Clayton B.R. (1988). "The use of wind energy devices as ship stabilisers." Procedures, British Wind Energy Association, Annual conference, 1988.

[10] Sinclair F.M. Clayton B.R. (1989). "Excitation and damping forces on offshore wind turbines." Wind Engineering. Vol. 13 No. 6.

[11] Sinclair F.M. Clayton B.R. (1989). "The effects of wave loading on offshore wind turbines." Procedures, European Wind Energy Conference 1989.

[12] Sinclair F.M. (1994). "Aerodynamic damping on offshore installations-a comparison of experimental measurements with theory." Journal of Wind Engineering and Industrial Aerodynamics. SSDI 0167-6105(93)E0064-6.

10. Wind turbine blade loads due to stochastic base motions

In the previous chapter, a method for determining the rigid body motions of a floating turbine was derived. Having computed the amplitude of the rigid body motions, we are in a position to calculate the resulting forces on the rotor blades.

Each turbine blade will witness sinusoidally varying loads as it rotates in the rotor plane. When considering multiple bladed rotors some of these forces begin to negate each other. For rotors with three or more symmetric blades, all the sinusoidal forces negate and the rotor behaves as a homogeneous disk as derived in chapter 9. This enabled us to derive a closed form solution for determining the rigid body motions of the floating wind turbines that have three or more blades. When considering the individual blade forces however, it is necessary to include the sinusoidal loads and this is the reason why a separate calculation is made after the equilibrium rigid body motions have been established.

In chapter 9 we derived mass, damping and stiffness matrices which give the blade forces, in the blade's local coordinate axis, in response to turbine motions along the global axis. In this section we shall derive expressions to perform the structural dynamic analysis of the turbine in the frequency domain. The contents of this chapter contribute to the original research documented in this thesis.

The turbine blade is sub-divided into a number of elements. The force imposed on each element node, as the turbine is tossed around in the sea, is obtained in matrix form using the relationships expressed in Equation 9-30. To analyse these in the frequency domain, the auto-power and cross-power spectra between each blade element must be derived in the same way as described in chapter 6.

10.1 Calculate the cross-power force matrices between a pair of blade elements

The dynamic equilibrium formula is expressed in Equation 9-30. Now assuming that the force and displacement is sinusoidal with respect to time, we can express them in exponential form as Equation 10-1.

$$s_o(t) = A_o \cdot e^{i\omega t} \qquad f_\varphi(t) = F_\varphi \cdot e^{i\omega t} \qquad \textbf{Equation 10-1}$$

Where A_o and F_φ are the amplitude of global displacement and blade force respectively.

Now the velocity and acceleration may be determined by differentiating the displacement $s_o(t)$ with respect to time as follows:

$$\dot{s}_o(t) = i \cdot \omega \cdot A_o \cdot e^{i\omega t} \qquad \ddot{s}_o(t) = -\omega^2 \cdot A_o \cdot e^{i\omega t} \qquad \textbf{Equation 10-2}$$

Equation 9-30 can therefore be simplified to Equation 10-3.

$$H(\omega) \cdot A_o = F_\varphi \qquad \textbf{Equation 10-3}$$

Where $H(\omega)$ is the transfer function defined by the following expression:

$$H(\omega) = -\omega^2 \cdot M_{\varphi o} + i \cdot \omega \cdot C_{\varphi o} + K_{\varphi o}$$

Now the matrices given in Equation 9-30 are non-linear and contain many sine and cosine terms. These terms are given with respect to the rotor azimuth angle φ at any time t. We can rewrite φ with respect to t as $\varphi(t) = \Omega \cdot t$.

Now a very neat simplification is found for calculating the force in the frequency domain. To realise this we must first of all separate the matrices into sinusoidally varying and constant matrices as Equation 10-7. (Constant matrices will be denoted by the superscript '*C*' and sinusoidally varying matrices by the superscript '*S*'. e.g. M^C and M^S.) We shall then derive two cross-power matrices, one for the sinusoidally varying part and the other for the constant part. Following this we must establish whether there is a cross-correlation between the sinusoidal and constant matrices and add these too if necessary. We will prove, however, that the e is no such cross-correlation. This simplifies our procedure slightly so the total load is found from the sum of the constant and sinusoidal response spectra.

10.1.1 Constant cross-power force matrices

Now the constant mass, damping and stiffness matrices may be substituted directly into Equation 10-3 and the constant transfer function $H_i^C(\omega)$ for the ith blade element

evaluated. This is a linear transfer function and so the response in the frequency domain is easily found using the matrix formula given in Equation 2-43.

$$S_{ij}^{CF}(\omega) = H_i^C(\omega) \cdot S_{ij}(\omega) \cdot \overline{H_j^C(\omega)}^T \qquad \textbf{Equation 10-4}$$

Where $S_{ij}^{CF}(\omega)$ represents the cross-power spectral matrix of force between the various degrees of freedom and on elements i and j. $S_{ij}(\omega)$ represents the cross-power spectra of displacement between each degree of freedom and on elements i and j.

10.1.2 Sinusoidally varying cross-power force matrices

It is more difficult to deal with the sinusoidally varying matrices. When we calculate the transfer function, by substituting them into Equation 10-3, we notice that the result is a very long and complex addition of sine and cosine terms. The addition of these trigonometric terms is simplified by resorting to complex number theory in a similar manner to that described in Chapter 2.1.2. Here, the following complex identity shall be used:

$$\alpha \cdot \cos(\Omega \cdot t) + \beta \cdot \sin(\Omega \cdot t) = \tfrac{1}{2} \cdot \left(\Lambda \cdot e^{i \cdot \Omega \cdot t} + \overline{\Lambda} \cdot e^{-i \cdot \Omega \cdot t}\right) \qquad \textbf{Equation 10-5}$$

Where $\Lambda = \alpha - i\beta$ and $\overline{\Lambda}$ is the complex conjugate defined as $\overline{\Lambda} = \alpha + i\beta$.

So, the sinusoidally varying matrices can be simplified using the following substitutions for all the sine and cosine terms:

$$\alpha \cdot \cos(\Omega \cdot t) = \alpha \quad \text{and} \quad \beta \cdot \sin(\Omega \cdot t) = -i\beta \qquad \textbf{Equation 10-6}$$

The complex sinusoidally varying matrices and the constant matrices are given in Equation 10-7 for the mass, damping and stiffness terms.

<u>Mass,</u> constant: **Equation 10-7**

$$M_{\varphi o}^{C} = \begin{bmatrix} 0 & 0 & 0 & 0 & 0 & 0 \\ 0 & 0 & 0 & 0 & 0 & m \cdot r \\ 0 & 0 & m & 0 & 0 & 0 \\ 0 & 0 & 0 & 0 & 0 & 0 \\ 0 & 0 & -m \cdot r & 0 & 0 & 0 \\ 0 & 0 & 0 & 0 & 0 & m \cdot r^2 \end{bmatrix}$$

sinusoidal:

$$M^{S}_{\varphi o} = \begin{bmatrix} m & -i\cdot m & 0 & 0 & 0 & 0 \\ i\cdot m & m & 0 & 0 & 0 & 0 \\ 0 & 0 & 0 & -i\cdot m\cdot r & -m\cdot r & 0 \\ 0 & 0 & 0 & 0 & 0 & 0 \\ 0 & 0 & 0 & i\cdot m\cdot r^2 & m\cdot r^2 & 0 \\ i\cdot m\cdot r & m\cdot r & 0 & 0 & 0 & 0 \end{bmatrix}$$

Damping,

constant:

$$C^{C}_{\varphi o} = \begin{bmatrix} 0 & 0 & 0 & 0 & 0 & 0 \\ 0 & 0 & -g_t & 0 & 0 & c_t\cdot r \\ 0 & 0 & g_a & 0 & 0 & c_a\cdot r \\ 0 & 0 & 0 & 0 & 0 & 0 \\ 0 & 0 & -g_a\cdot r & 0 & 0 & -c_a\cdot r^2 \\ 0 & 0 & -g_t\cdot r & 0 & 0 & c_t\cdot r^2 \end{bmatrix}$$

sinusoidal:

$$C^{S}_{\varphi o} = \begin{bmatrix} 0 & 0 & 0 & 0 & 0 & 0 \\ i\cdot c_t & c_t & 0 & i\cdot g_t\cdot r & g_t\cdot r & 0 \\ i\cdot c_a & c_a & 0 & 2m\cdot r\cdot\Omega - i\cdot g_a\cdot r & -g_a\cdot r - i\cdot 2m\cdot r\cdot\Omega & 0 \\ 0 & 0 & 0 & 0 & 0 & 0 \\ -i\cdot c_a\cdot r & -c_a\cdot r & 0 & -2m\cdot r^2\cdot\Omega + i\cdot g_a\cdot r^2 & g_a\cdot r^2 + i\cdot 2m\cdot r^2\cdot\Omega & 0 \\ i\cdot c_t\cdot r & c_t\cdot r & 0 & i\cdot g_t\cdot r^2 & g_t\cdot r^2 & 0 \end{bmatrix}$$

Stiffness,

constant:

$$K^{C}_{\varphi o} = \begin{bmatrix} 0 & 0 & 0 & 0 & 0 & 0 \\ 0 & 0 & 0 & 0 & 0 & 0 \\ 0 & 0 & 0 & 0 & \gamma\cdot r & 0 \\ 0 & 0 & 0 & 0 & 0 & 0 \\ 0 & 0 & 0 & 0 & -\gamma\cdot r^2 & 0 \\ 0 & 0 & 0 & 0 & 0 & 0 \end{bmatrix}$$

sinusoidal:

$$K^{S}_{\varphi o} = \begin{bmatrix} 0 & 0 & 0 & 0 & 0 & 0 \\ 0 & 0 & 0 & -\beta_t & i\cdot\beta_t & 0 \\ 0 & 0 & 0 & \beta_a & -i\cdot\beta_a & 0 \\ 0 & 0 & 0 & 0 & 0 & 0 \\ 0 & 0 & 0 & -\beta_a\cdot r & i\cdot\beta_a\cdot r & 0 \\ 0 & 0 & 0 & -\beta_t\cdot r & i\cdot\beta_t\cdot r & 0 \end{bmatrix}$$

Using these sinusoidally varying matrices we can now express Equation 10-3 as Equation 10-8.

$$\frac{1}{2}\left\{H_i^S(\omega)\cdot e^{i\Omega t}+\overline{H_i^S(\omega)}\cdot e^{-i\Omega t}\right\}\cdot A_o = F_\varphi \qquad \textbf{Equation 10-8}$$

Where $H_i^S(\omega)$ is the sinusoidally varying transfer function for the ith element. This is defined as $H_i^S(\omega)=-\omega^2\cdot M_{\varphi o}^S+i\cdot\omega\cdot C_{\varphi o}^S+K_{\varphi o}^S$.

We now need to transfer this expression into the frequency domain to determine its power spectral density.

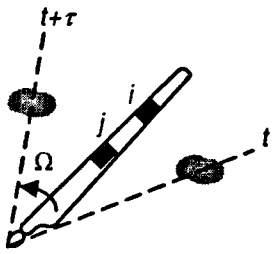

Figure 10-1 Cross-power spectra of loading

Consider the loading witnessed by two observers situated on elements *i* and *j* of a rotating turbine blade as shown in Figure 10-1. The blade is rotating with constant frequency Ω *rad/sec*. At time *t*, blade element *i* passes through the random process *u*, and at time $t+\tau$ element *j* passes through process *v*. The random loading associated with the two processes is found using Equation 10-9.

$$u(t)=\frac{1}{2}\left(h_i^S(\omega)\cdot e^{i\cdot\Omega\cdot t}+\overline{h_i^S(\omega)}\cdot e^{-i\cdot\Omega\cdot t}\right)\cdot s(t) \qquad \textbf{Equation 10-9}$$

$$v(t+\tau)=\frac{1}{2}\left(h^S(\omega)_j\cdot e^{i(\Omega\cdot t+\Omega\cdot\tau)}+\overline{h^S(\omega)_j}\cdot e^{-i\cdot(\Omega\cdot t+\Omega\cdot\tau)}\right)\cdot s(t+\tau)$$

Where $s(t)$ is the random displacement in a particular degree of freedom at time *t*. $h_i^S(\omega)$ is the sinusoidal transfer function, taken from the transfer matrix for the ith blade element, for the particular degree of freedom.

The Cross-covariance rotationally witnessed by the two rotating blade elements is seen to be the same as the Cross-covariance between the two random processes *u* and *v*. An expression for the rotationally sampled Cross-covariance, $\tilde{C}_{ij}(\tau)$, can therefore be expressed as Equation 10-10.

$$\tilde{C}_{ij}(\tau)=E\{u(t)\cdot v(t+\tau)\}=C_{uv}(\tau) \qquad \textbf{Equation 10-10}$$

Where $\tilde{C}_{ij}(\tau)$ is the rotationally sampled Cross-covariance function between blade elements *i* and *j*, $C_{uv}(\tau)$ is the Cross-covariance function between the

two random processes u and v, and $E\{\}$ is the expectation operator defined by the expression $E\{y(t)\} = \lim_{T\to\infty}\left\{\frac{1}{T}\cdot\int_{-T/2}^{T/2} y(t)dt\right\}$

Substituting Equation 10-9 into Equation 10-10 and evaluating the expectation function yields the following expression for the Cross-covariance function:

$$\tilde{C}_{ij}(\tau) = C_s(\tau)\cdot h_i^S(\omega)\cdot\overline{h_j^S(\omega)}\cdot\tfrac{1}{2}\cdot\cos(\Omega\cdot t) \qquad \textbf{Equation 10-11}$$

Where $C_s(\tau)$ is the Auto-covariance of displacement of the turbine in one of the degrees of freedom. This is obtained from the double sided Auto-power spectral density function, $S_s(\upsilon)$, by taking the inverse Fourier transform, i.e. $C_s(\tau) = \int_{-\infty}^{\infty} S_s(\nu)\cdot e^{i\cdot\nu\cdot t}d\nu$.

The Cross-power spectral density function is determined by taking the Fourier transform of Equation 10-11 as follows:

$$\tilde{S}_{ij}(\omega) = \int_{-\infty}^{\infty}\left\{\tfrac{1}{2}\cdot h_i^S(\omega)\cdot\overline{h_j^S(\omega)}\cdot\cos(\Omega\cdot t)\cdot\int_{-\infty}^{\infty} S_s(\nu)\cdot e^{i\cdot\nu\cdot\tau}d\nu\right\}\cdot e^{-i\cdot\omega\cdot\tau}d\tau \qquad \textbf{Equation 10-12}$$

Simplifying yields $\tilde{S}_{ij}(\omega) = \tfrac{1}{2}\cdot h_i^S(\omega)\cdot\overline{h_j^S(\omega)}\cdot\int_{-\infty}^{\infty} S_s(\nu)\cdot\left\{\int_{-\infty}^{\infty}\cos(\Omega\cdot t)\cdot e^{-i(\omega-\nu)\tau}d\tau\right\}d\nu$

Now we express the cosine term in the exponential form. Substituting this notation and simplifying yields the following expression:

$$\tilde{S}_{ij}(\omega) = \tfrac{1}{4}\cdot h_i^S(\omega)\cdot\overline{h_j^S(\omega)}\cdot\int_{-\infty}^{\infty} S_s(\nu)\cdot\left\{\int_{-\infty}^{\infty} e^{i(\Omega\ \omega+\nu)\tau} + e^{-i(\Omega+\omega-\nu)\tau}d\tau\right\}d\nu \qquad \textbf{Equation 10-13}$$

This can be simplified further using Dirac's delta function. Noting that $\int_{-\infty}^{\infty} e^{i\sigma\tau}d\tau = \delta(\sigma)$, where $\delta(\sigma)$ is Dirac's delta function defined by the relationships $\delta(\sigma)=1$ when $\sigma=0$ and $\delta(\sigma)=0$ for all non zero values of σ, the expression reduces to Equation 10-14.

$$\tilde{S}_{ij}(\omega) = \tfrac{1}{4} \cdot h_i^S(\omega) \cdot \overline{h_j^S(\omega)} \cdot \int_{-\infty}^{\infty} S_s(\nu) \cdot \{\delta(\Omega - \omega + \nu) + \delta(-\Omega - \omega + \nu)\} d\nu \qquad \textbf{Equation 10-14}$$

Integrating with respect to υ yields: $\tilde{S}_{ij}(\omega) = \tfrac{1}{4} \cdot h_i^S(\omega) \cdot \overline{h_j^S(\omega)} \cdot \{S_s(\omega - \Omega) + S_s(\omega + \Omega)\}$

We can see from the above formula that if $h_i^S(\omega) = h_j^S(\omega)$ then $\tilde{S}_{ij}(\omega)$ will be real and symmetric and can therefore be expressed as a single sided spectrum. However if $h_i^S(\omega) \neq h_j^S(\omega)$ then $\tilde{S}_{ij}(\omega)$ will be complex. In this case the negative frequencies terms will be the same as the positive (they will not be complex conjugates) and therefore a double sided spectrum is necessary to describe the events. In a typical design situation we deal with the cross-power spectra where $h_i^S(\omega) \neq h_j^S(\omega)$ and so will have to resort to using the double sided PSD in this analysis.

We can now express Equation 10-14 in matrix notation in the same way as Equation 10-4.

$$S_{ij}^{SF}(\omega) = H_i^S(\omega) \cdot S_{ij}^S(\omega) \cdot \overline{H_j^S(\omega)}^T \qquad \textbf{Equation 10-15}$$

Where $S_{ij}^{SF}(\omega)$ represents the double sided cross-power spectral matrix of force between the various degrees of freedom and on elements *i* and *j*. $H_i^S(\omega)$ is the sinusoidal transfer function matrix for the ith blade element, defined in Equation 10-7. $S_{ij}^S(\omega)$ is a special rotationally sampled cross-power spectra of displacement between each degree of freedom, defined by Equation 10-16.

$$S_{ij}^S(\omega) = \tfrac{1}{4} \cdot \{S_{ij}(\omega - \Omega) + S_{ij}(\omega + \Omega)\} \qquad \textbf{Equation 10-16}$$

10.1.3 Cross-power between the constant and sinusoidally varying cases.

In the previous section we derived the cross-power spectral densities between blade elements for the sinusoidally varying matrices. Prior to this we also derived them for the constant matrices. From Chapter 2.3.6 we know that there may be some cross-

correlation between the constant and sinusoidal terms which must also be considered. In this section we prove that no such cross-correlation exists and therefore we need only take the sum of the sinusoidal and constant results.

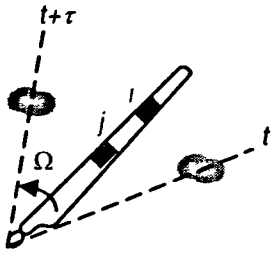

Consider the loading witnessed by two observers situated on elements *i* and *j* of a rotating turbine blade as shown in the diagram. The blade is rotating with constant frequency Ω *rad/sec*. At time *t*, blade element *i* passes through the random process *u*, and at time $t+\tau$ element *j* passes through process *v*. For this cross-correlated case, process *u* is given as the sinusoidally varying case and *v* as the constant case. The random loading associated with the two processes is found by Equation 10-17.

$$u(t) = \tfrac{1}{2}\left(h_i^S(\omega)\cdot e^{i\cdot\Omega\cdot t} + \overline{h_i^S(\omega)}\cdot e^{-i\cdot\Omega\cdot t}\right)\cdot s(t) \qquad \textbf{Equation 10-17}$$

$$v(t+\tau) = \kappa_j \cdot s(t+\tau)$$

Where $s(t)$ is the random displacement in a particular degree of freedom at time *t*. $h_i^S(\omega)$ is the sinusoidal transfer function for the ith blade element, and κ_j is the constant transfer function for the jth blade element.

The Cross-covariance rotationally witnessed by the two rotating blade elements is seen to be the same as the Cross-covariance between the two random processes *u* and *v*. An expression for the rotationally sampled Cross-covariance, $\tilde{C}_{ij}(\tau)$, can therefore be expressed as Equation 10-18.

$$\tilde{C}_{ij}(\tau) = E\{u(t)\cdot v(t+\tau)\} = C_{uv}(\tau) \qquad \textbf{Equation 10-18}$$

Where $\tilde{C}_{ij}(\tau)$ is the rotationally sampled Cross-covariance function between blade elements *i* and *j*, $C_{uv}(\tau)$ is the Cross-covariance function between the two random processes *u* and *v*, and $E\{\}$ is the expectation operator.

Substituting Equation 10-17 into Equation 10-18 and evaluating the expectation function yields a value of zero for the Cross-covariance function. We therefore see there is no cross-correlation between the sinusoidal and constant cases.

10.1.4 Summary of cross-power force matrix between elements i and j

The total response is obtained by taking the sum of the constant and sinusoidal power spectral densities as given in Equation 10-19.

$$S_{ij}^{F}(\omega) = S_{ij}^{CF}(\omega) + S_{ij}^{SF}(\omega) \qquad \textbf{Equation 10-19}$$

Where $S_{ij}^{CF}(\omega) = H_i^{C}(\omega) \cdot S_{ij}(\omega) \cdot \overline{H_j^{C}(\omega)}^{T}$ | $H_i^{C}(\omega) = -\omega^2 \cdot M_{\varphi o}^{C} + i \cdot \omega \cdot C_{\varphi o}^{C} + K_{\varphi o}^{C}$ (for the i^{th} blade element.)

$S_{ij}^{SF}(\omega) = H_i^{S}(\omega) \cdot S_{ij}^{S}(\omega) \cdot \overline{H_{ij}^{S}(\omega)}^{T}$ | $H_i^{S}(\omega) = -\omega^2 \cdot M_{\varphi o}^{S} + i \cdot \omega \cdot C_{\varphi o}^{S} + K_{\varphi o}^{S}$ (for the i^{th} blade element.)

and $S_{ij}^{S}(\omega) = \frac{1}{4} \cdot \left\{ S_{ij}(\omega - \Omega) + S_{ij}(\omega + \Omega) \right\}$

10.2 Dynamic analysis of the blade loading

The previous sections have dealt with the derivation of blade loads on a rigid blade being moved through the air. In practice the blade will have a finite stiffness and will deflect under the influence of the loads. The blade deflection has a further influence on the incident loading and to complete a full dynamic analysis it proves necessary to perform an iterative calculation to find the equilibrium blade forces and deflections. The iterative procedure is illustrated by the flow chart given in Figure 2.

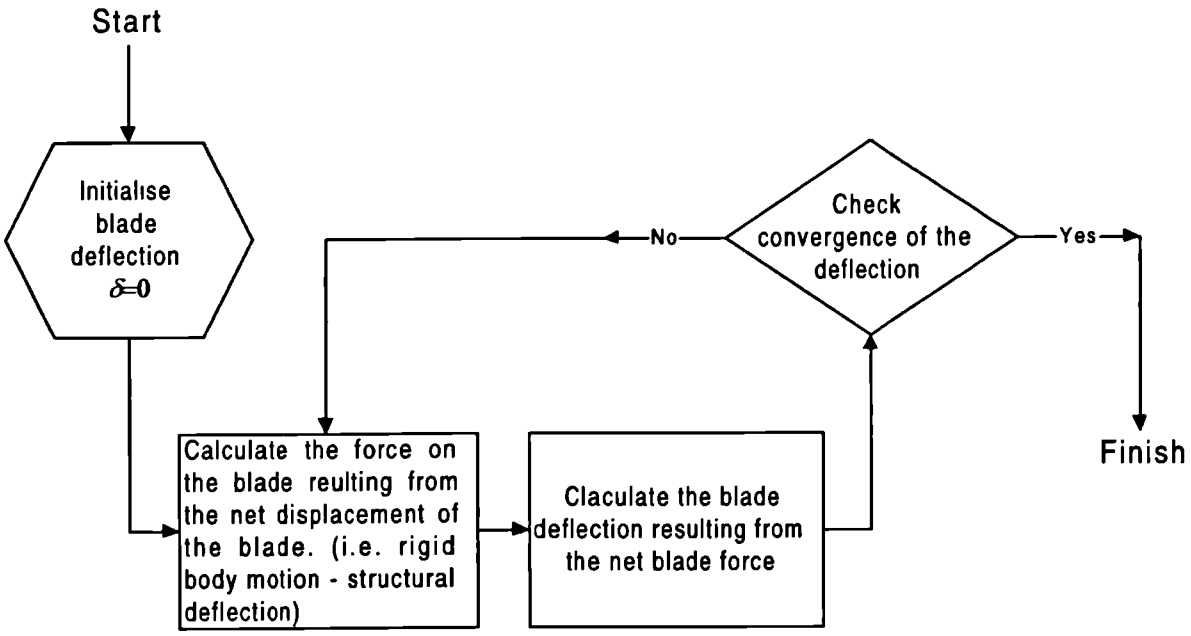

Figure 2 Flow chart showing iterative calculation of equilibrium blade forces

The above procedure is simplified if the assumption is made that structural deflections are small when compared with the rigid body motions. In this case the iterative cycle can be removed and the structural deflection calculated using the dynamic equilibrium formula given in Equation 20. This technique is termed a 'first order' solution.

$$\left(M\cdot\ddot{\delta}+C\cdot\dot{\delta}+K\cdot\delta\right)\cdot e^{i\omega t}=\left\{H^{C}(\omega)+\tfrac{1}{2}\cdot\left(H^{S}(\omega)\cdot e^{i\cdot\Omega t}+\overline{H^{S}(\omega)\cdot e^{-i\,\Omega\cdot t}}\right)\right\}\cdot e^{i\cdot\omega\cdot t}\cdot A_{0}$$

Equation 20

Where M, C and K are the blades structural mass, damping and stiffness properties respectively; δ is the blade's structural deflection; and A_0 is the amplitude of the rigid body displacement of the blades through the air.

Equation 20 may be expressed in the frequency domain using the following matrix formulation:

$$S_{ij}^{R}(\omega)=H(\omega)\cdot S_{t}^{F}(\omega)\cdot\overline{H(\omega)}^{T}$$

Equation 21

Where $S_{ij}^{F}(\omega)$ is the cross-power spectral density function of blade loads for each blade element and between each degree of freedom. $H(\omega)$ is the structural transfer function calculated using a Finite Element based analysis similar to the

one discussed in Chapter 6, and $S_{ij}^{R}(\omega)$ is the cross-power spectral density function of blade deflection.

In most cases we are only interested in the Auto-power spectral density functions of the blade deflections and forces, in this case only the leading diagonal of the matrix $S_{ij}^{R}(\omega)$ need be considered.

10.3 Conclusion

In this chapter expressions have been derived for the blade loads resulting from motions of the turbine in 6 degrees of freedom. Motion induced loading arises with floating turbine structures and is complicated by additional harmonics which are introduced by the rotation of the blades. A unique method for evaluating this complex phenomenon is presented in this chapter.

11. Case study: The analysis of a floating offshore wind turbine mounted on a tensioned buoyant platform

11.1 Introduction

In this chapter we consider the application of the mathematical models derived in the previous two chapters, to a typical floating offshore turbine. At this point in time, no floating wind turbines are in existence and therefore an appropriate concept is proposed on which to base the case study.

There are few published reports available that discuss likely floating turbine concepts. Two notable concepts are, however, discussed by Tong and Cannell[1], Barltrop[2] and Halfpenny et al[3].

Tong and Cannell[1] propose a spar buoy type platform similar to the one shown in Figure 1. The platform is moored using an eight-point catenary mooring system and anchored to the sea bed using a piled anchor system. The cost of this particular system was found to be relatively high and this was mainly due to the expense of the mooring system.

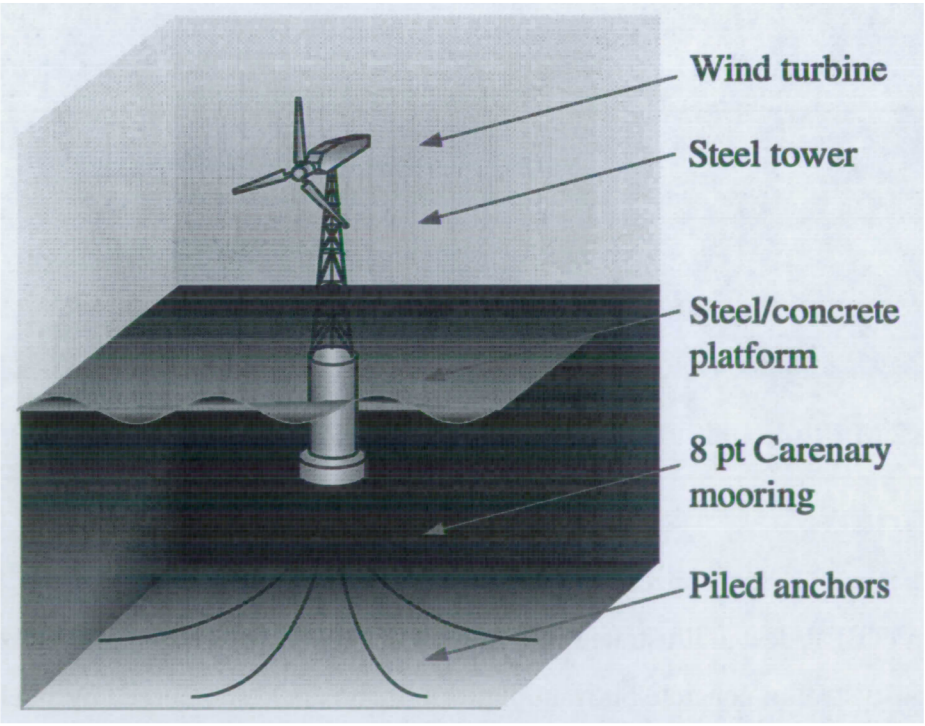

Figure 1 Catenary moored spar buoy platform (after Tong & Cannell)

Barltrop[2] and Halfpenny et al[3] suggest using a large 'Multiple Unit Floating Offshore Windfarm (MUFOW)'. The platform would have a single, eight point catenary mooring system connected to a turret on the platform that enables the whole platform to weather vane and effectively track the wind. This feature permits the turbines to be mounted closer together without them suffering excessive damage by having to operate in each other's wake for prolonged periods. It also removes the need for having individual yawing mechanisms on each turbine and therefore reduces the maintenance overhead. The cables would be anchored to the seabed using either a piled, a gravity or a bucket anchor system. By having as many as eight turbines sharing the same mooring system, the MUFOW concept is expected to dramatically reduce mooring costs. A detailed cost analysis is documented by Halfpenny et al[3]. An artist's illustration of the proposed concept is given in Figure 2.

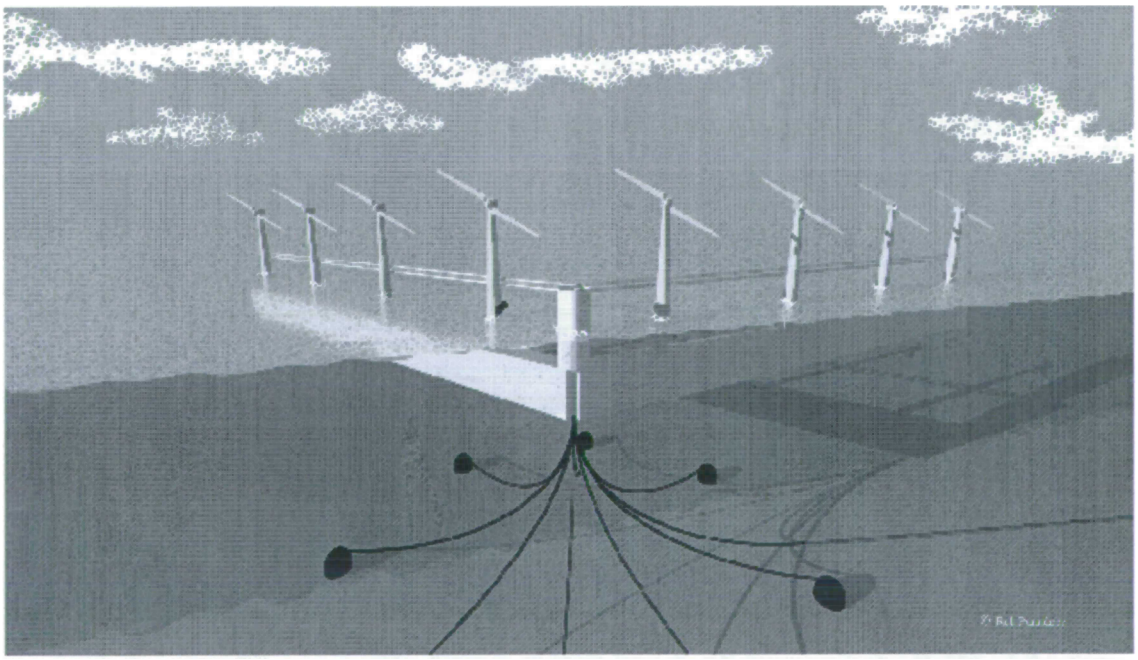

Figure 2 Multiple Unit Floating Offshore Windfarm (MUFOW) (after Barltrop and Halfpenny et al.)

For this thesis a new concept has been proposed based on a 'Tensioned Buoyant Platform (TBP)' design illustrated in Figure 3. The concept is based around relatively inexpensive steel or concrete buoyant platform than is held submerged by steel tension cables. The cables are secured to the seabed by inverted bucket anchors. Only the relatively slender tower protrudes through the sea surface hence reducing the wave loads on the structure.

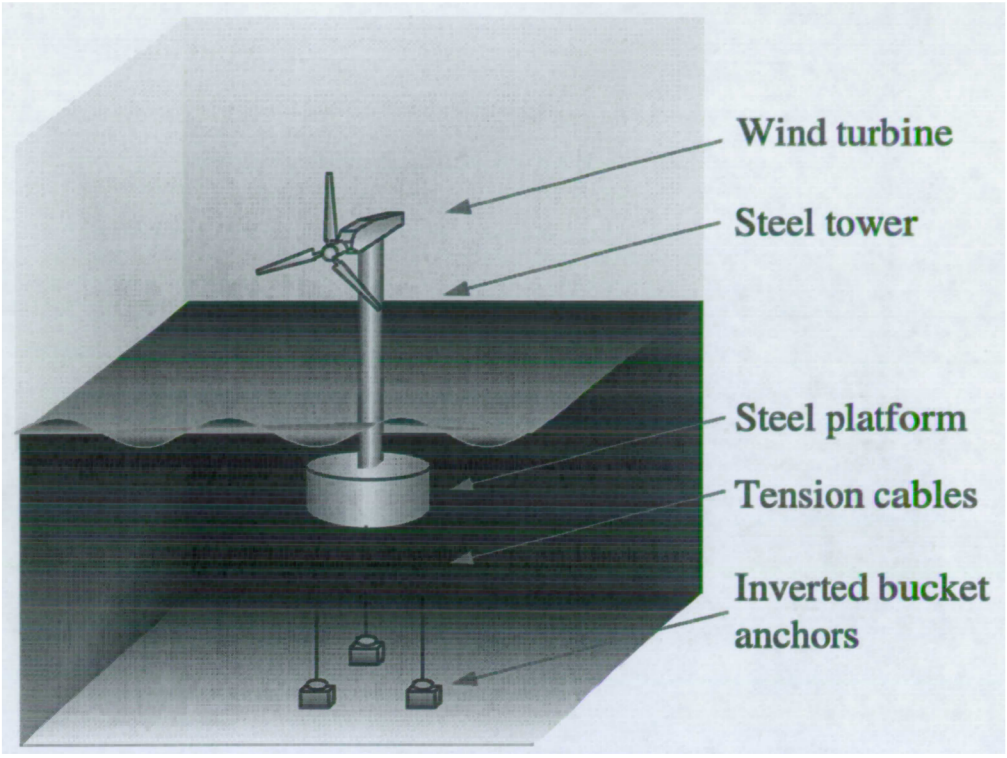

Figure 3 Tensioned buoyant platform (TBP) concept

The response of the TBP system follows the simple principle of an inverted pendulum with the excess buoyancy force on the platform acting to oppose the platform's motion. This concept is particularly appealing because of its superior dynamic response. Only the surge and sway modes are significant while the roll, tilt and heave modes are negligible. A degree of yaw may occur due to the relatively low stiffness in this mode but it should cause few problems. By removing the rotational modes many of the more complicated processes, such as gyroscopic coupling between modes, are also removed thus making the response easier to predict and reducing the blade loads.

No hydrodynamic analysis has been carried out on the TBP concept as this was beyond the scope of this thesis. Instead, typical motion spectra are used which have been derived for two similar TBP structures as documented by Patel and Witz[4]. The platforms discussed are similar to the one illustrated in Figure 4. Details of the two TBPs are given in Table 1.

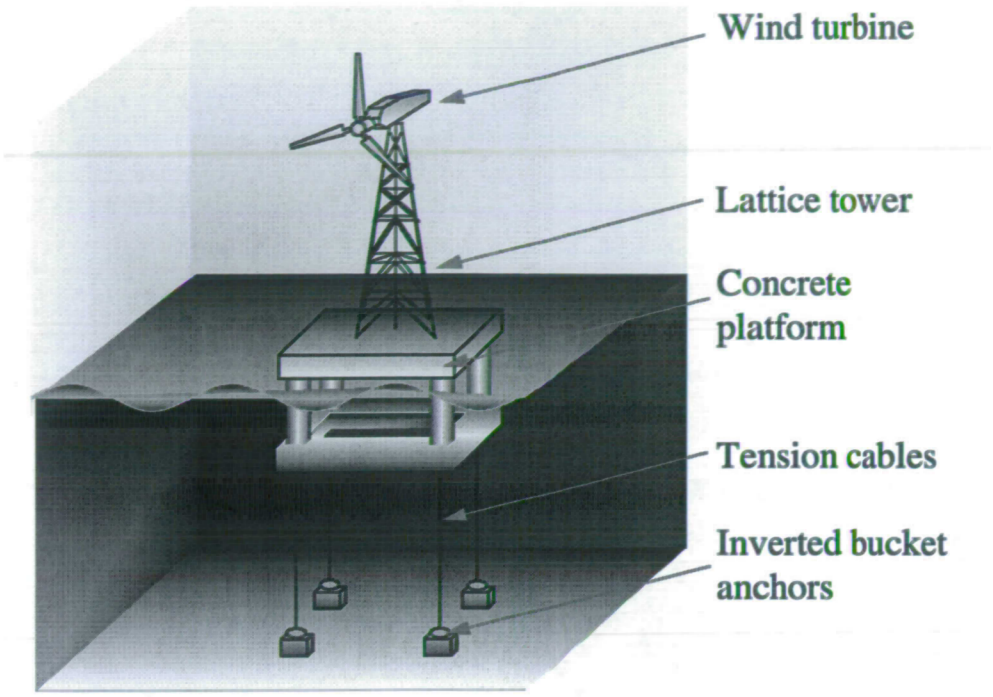

Figure 4 Typical TBP concept

	4 Column TBP	6 Column TBP
Displacement (tonnes)	47700	74360
Vertical centre of gravity above keep	38.32 m	28 m
Draught	42.5 m	32 m
Outer column spacing	99.4 m	78 m length
		74 m width
Outer column radius	7.07 m	9.06 m
Inner column radius		7.25 m
Cable axial stiffness (kN/m)	56528.8	258307.7
Cable pretension (tonnes)	3750	4000
Natural periods (seconds)		
Surge	93.7	60.8
Sway	103.8	60.1
Heave	2.9	1.8
Roll	3.2	1.8
Tilt (Pitch)	3.0	1.8
Yaw	91.8	49.9

Table 1 Summary of TBP data after Patel and Witz[4]

11.2 Motion analysis of the Tensioned Buoyant Platforms

The motion response spectra of the TBPs is obtained in any sea state from the 'Response Amplitude Operator (RAO)' given by Patel and Witz[4]. RAOs are given for surge and sway modes only because heave, tilt, roll and yaw responses are negligible. The PSD of motion response is then determined for a particular sea state using Equation 11-1.

$$G_{yy}(\omega) = [RAO(\omega)]^2 \cdot G_w(\omega) \qquad \textbf{Equation 11-1}$$

Where $G_{yy}(\omega)$ is the PSD of surge motion, $RAO(\omega)$ is the Response Amplitude Operator and $G_w(\omega)$ are the wave elevation spectra.

A number of wave elevation spectra are commonly used including the Pierson-Moskowitz[5] spectrum and the JONSWAP (Joint North Sea Wave Project) spectrum. (Hasselmann et al[6].) In this analysis the Pierson Moskowitz spectrum is used because a better range of sea state data was available for the analysis. The theory of wave loading is beyond the scope of this thesis and the reader is referred to Barltrop[7] and Patel and Witz[8] for more information on these spectra.

The Pierson Moskowitz spectrum is given by Equation 11-2.

$$G_w(\omega) = \frac{H_s^2 \cdot T_z}{16\pi^3} \cdot \left(\frac{\omega}{2\pi} \cdot T_z\right)^{-5} \cdot \exp\left\{-\frac{1}{\pi} \cdot \left(\frac{\omega}{2\pi} \cdot T_z\right)^{-4}\right\} \qquad \textbf{Equation 11-2}$$

Where $G_w(\omega)$ is the Pierson Moskowitz spectrum of wave elevation expressed in $m^2/rad/sec$

H_s is the significant wave height in m

T_z is the zero crossing wave period in *sec* and is found by $T_z = \frac{T_D}{1.408}$; where T_D is the period corresponding to the dominant frequency.

For this case study, representative values for H_s and T_D were obtained for the North Sea from Bishop[9], these values are listed in Table 2. The probability density function of significant wave height is shown in Figure 5.

Sea State	Significant wave height H	Dominant wave period T_D	Percentage duration of the sea state
1	16.01	17.3	0.00368 %
2	14.48	16.5	0.00932 %
3	12.96	15.8	0.037 %
4	11.43	14.7	0.22 %
5	9.9	13.6	0.73 %
6	8.38	12.7	1.35 %
7	6.86	11.6	2.65 %
8	5.53	10.3	6 %
9	3.81	9.1	21 %
10	2.28	7.7	49 %
11	0.76	4.4	19 %

Table 2 Sea state parameters for the Pierson Moskowitz spectra

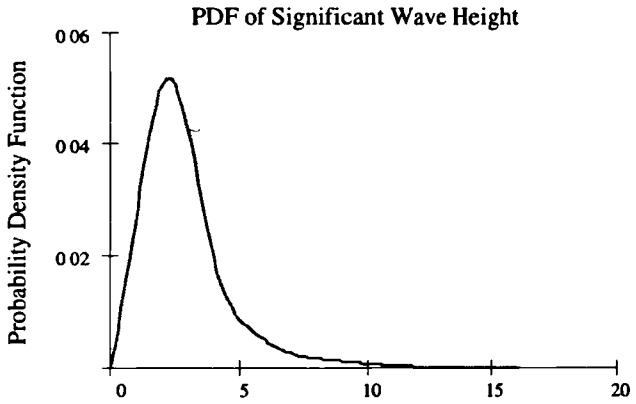

Figure 5 The PDF of significant wave height

Patel and Witz[4] give the RAOs for the two TBPs. These are shown with respect to frequency in the form of Figure 6.

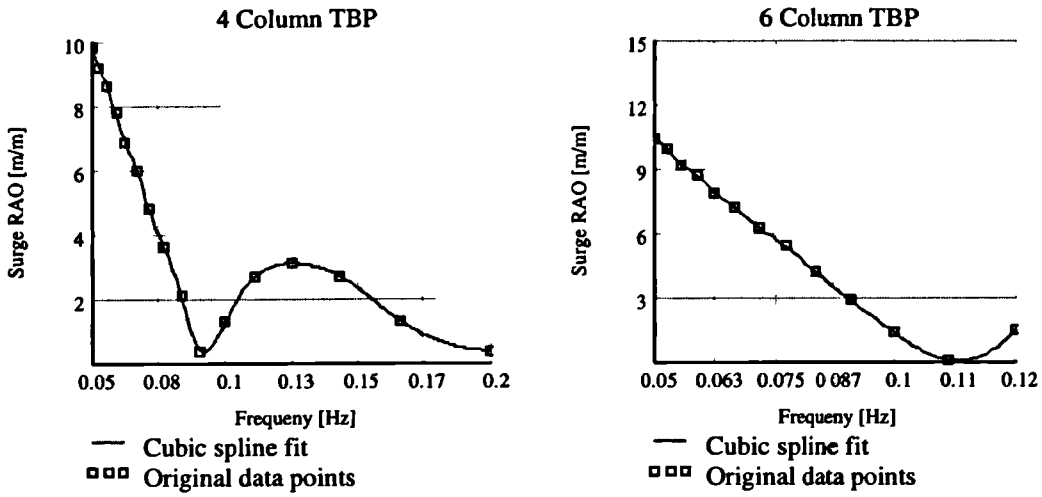

Figure 6 Response Amplitude Operators for both 4 and 6 column TBPs

Substituting Equation 11-2 into Equation 11-1 and using the above RAOs yields PSDs of surge motion similar to the one shown in Figure 7.

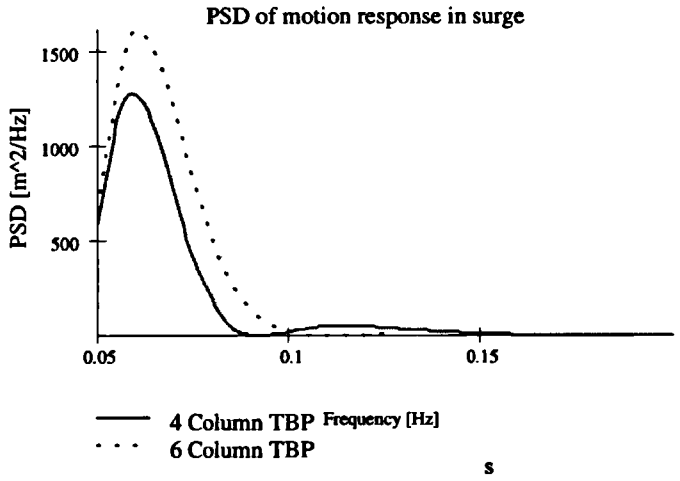

Figure 7 PSD of surge response for TBPs in the sea state 4

Sea states 8 to 11 cannot be adequately analysed using the RAOs given above. These only cover the frequency ranges 0 to 0.2 Hz and 0 to 0.12 Hz respectively for the 4 and 6 column platforms. Sea states 8 to 11 have dominant frequencies outside this range and so the analysis will under predict the actual damage. Patel and Witz[4] chose these frequency ranges because they relate to the more severe sea states. In platform design it is usually the severe sea states that cause most of the damage to the platform. Later in the thesis we see that this assumption is invalid for offshore wind turbine

design where wave induced fatigue damage is still significant in the less severe sea states.

11.3 Rotor loads resulting from platform surge

Platform surge gives rise to aerodynamic forces on the rotor, these act to oppose the platform's motion and also cause oscillating torsion moments on the shaft. In this section we compare the PSDs of rotor force caused by the surge motion with those caused by the turbulent wind speed variation. This will allow us to predict the ratio of structural damage caused by the platform motions with that caused by the turbulent wind.

The presence of the turbines will also contribute to the damping of the platform. Using the platform data given in Table 1 the degree of rotor damping may be expressed as a percentage of the critical damping. This provides information on the influence of the rotor to the overall dynamic behaviour of the platform.

In this analysis, Turbine A has been employed as a representation of the actual turbine. In practice it may be more cost effective to employ larger machines than this. However, no turbine data has been made available to include such a turbine in this analysis.

Figure 8 shows the PSD of rotor thrust caused by the surging motion of the platform in comparison with that caused by the turbulent wind. The turbulent wind is calculated for an upper mean wind speed of 20 m/sec and a lower of 10 m/sec. Turbulent wind loading is a wide band process where as the wave induced motions occur in a much narrower frequency band. The frequency of the wave loading is very low with respect to the first natural frequency of the rotor blades or the tower, this implies that the turbine will behave in a quasi-static manner and no dynamic amplification will occur. This simplifies the analysis considerably because the structural dynamic behaviour of the turbine need not be modelled. The amplitude of the wave-induced loads is found to be larger than that caused by the turbulent wind indicating a significant amount of fatigue damage. The affect on the statistics and the equivalent normalised fatigue damage of the two spectra are shown in Table 4. The comparable fatigue damage caused by the turbulent wind is summarised in Table 3.

Mean Hourly Wind Speed m/sec	Equivalent Normalised Fatigue Damage (Rotor Thrust)	Equivalent Normalised Fatigue Damage (Rotor Torque)
10	$6.23 \cdot 10^{-5}$	$2.4 \cdot 10^{-5}$
20	$4.0 \cdot 10^{-4}$	$7.7 \cdot 10^{-5}$

Table 3 Comparable Fatigue Damage for Wind Turbulence

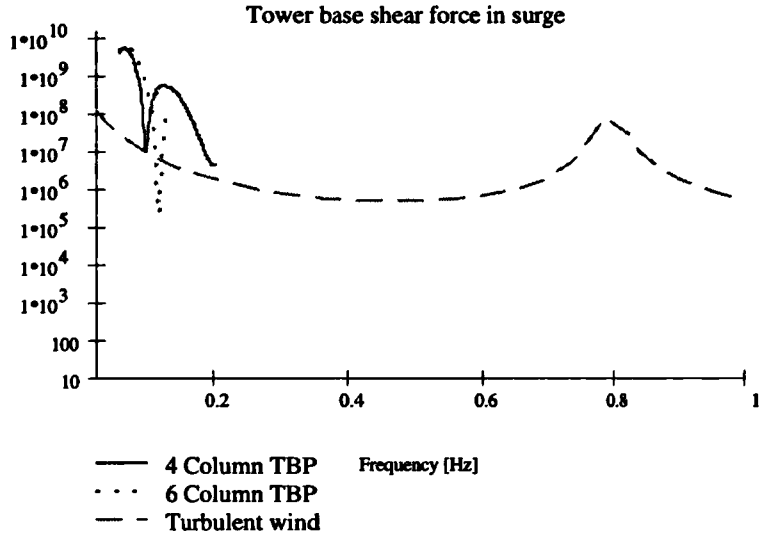

Sea state 1 with 20 m/sec windspeed

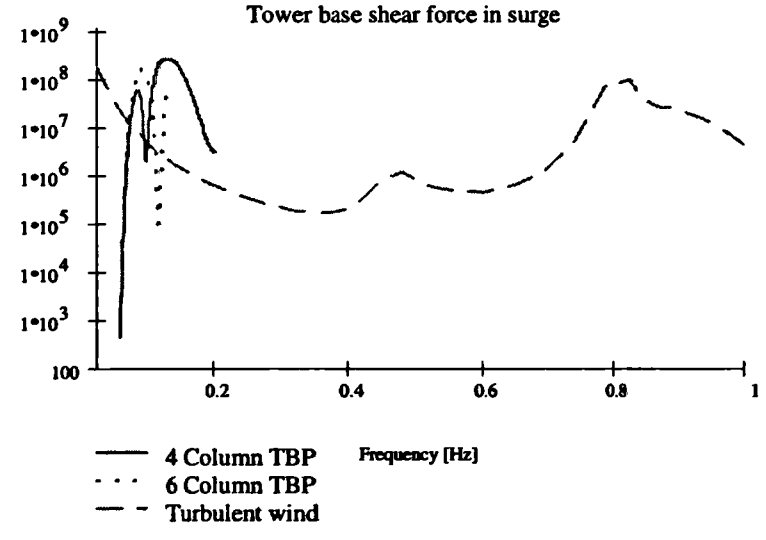

Sea state 8 with 10 m/sec windspeed

Figure 8 PSD of rotor thrust caused by wave induced motions and the turbulent wind

Rotor Thrust on 4 Column TBP

Sea State	Standard Deviation σ	Mean Period T_m	Period btn. zero up-crossings T_o	Peak period T_p	Equivalent Fatigue Damage
1	9483	13.469	12.61	9.505	5.7
2	8607	12.955	12.111	9.212	5.0
3	7671	12.42	11.607	8.941	4.3
4	6646	11.424	10.705	8.508	3.58
5	5626	10.305	9.739	8.101	2.89
6	4712	9.407	8.995	7.815	2.35
7	3914	8.497	8.255	7.541	1.89
8	3370	7.821	7.706	7.317	1.59
9	2.522	7.499	7.427	7.156	1.17
10	1564	7.202	7.146	6.925	0.70
11	114	5.771	5.751	5.671	0.04

Rotor Thrust on 6 column TBP

Sea State	Standard Deviation σ	Mean Period T_m	Period btn. zero up-crossings T_o	Peak period T_p	Equivalent Fatigue Damage
1	10550	15.195	14.978	14.085	9.6
2	9527	14.935	14.723	13.86	8.53
3	8428	14.669	14.464	13.635	7.42
4	7130	14.177	13.989	13.232	6.10
5	5731	13.607	13.442	12.772	4.73
6	4430	13.103	12.957	12.359	3.54
7	3097	12.458	12.333	11.807	2.37
8	1879	11.64	11.528	11.047	1.34
9	861	10.732	10.619	10.141	0.57
10	256	9.233	9.144	8.825	0.15
11	0.319	8.049	8.049	8.047	0

Table 4 Statistical properties and fatigue damage in rotor thrust PSDs

The table clearly shows that the overall fatigue damage due to the wave-induced motion is significantly higher than that caused by the turbulent wind. Wave loading is therefore an important part of fatigue analysis for floating offshore platforms. For this

analysis we should also carry out better analyses in the less severe sea states as these also contribute more fatigue damage than the turbulent wind.

Figure 9 shows the equivalent fatigue damage plotted with respect to the sea state.

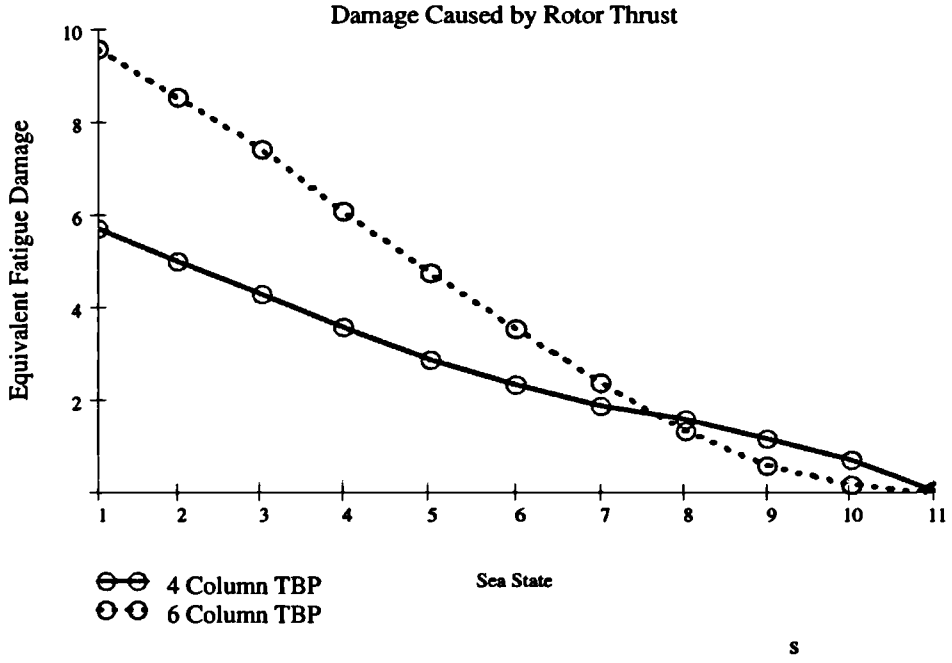

Figure 9 Fatigue Damage V's Sea State

Figure 9 show's how the damage decreases as the wave height reduces. The plot shows a near linear relationship between fatigue damage and sea state. The sea states between 8 and 11 are seen to digress from this linear relationship and this is perhaps due to the lack of RAO data to adequately analyse the response.

The same information can be presented for the variation in rotor torsion. This is shown in Figure 10 with the statistical properties and equivalent normalised fatigue damage given in Table 5.

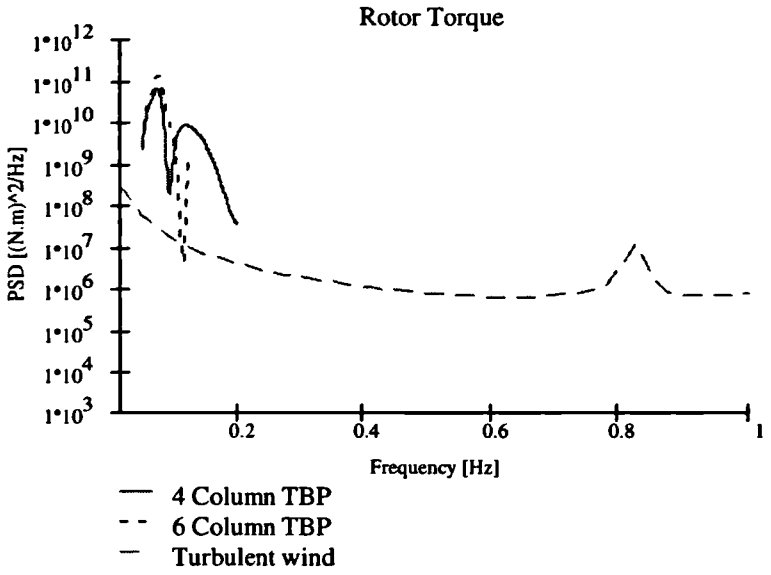

Sea State 1 with 20 m/sec windspeed

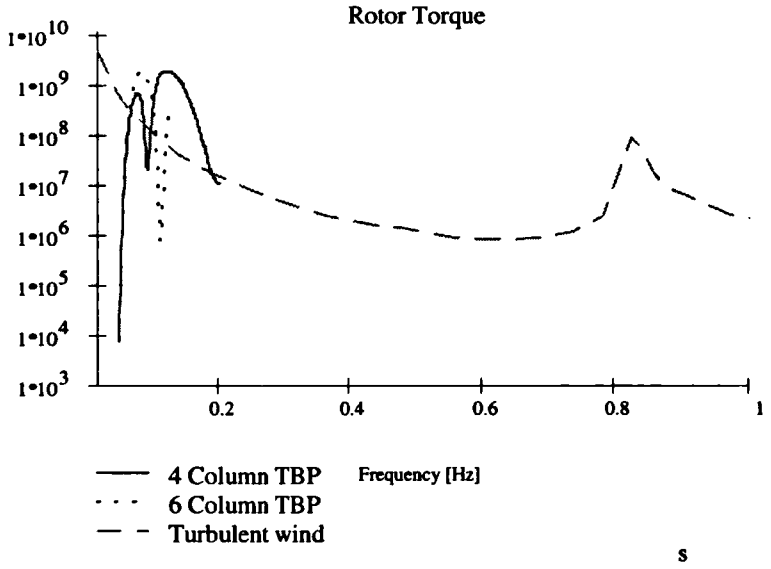

Sea state 8 with 10 m/sec windspeed

Figure 10 PSD of rotor torque caused by wave induced motions and the turbulent wind

Rotor Torque on 4 column TBP

Sea State	Standard Deviation σ	Mean Period T_m	Period btn. zero up-crossings T_o	Peak period T_p	Equivalent Fatigue Damage
1	34150	14.833	14.16	11.087	24.0
2	30550	14.387	13.687	10.671	20.7
3	26790	13.903	13.186	10.271	17.4
4	22390	12.931	12.215	9.594	13.6
5	18010	11.699	11.051	8.916	10.2
6	14300	10.571	10.042	8.418	7.66
7	11050	9.265	8.93	7.936	5.61
8	8880	8.192	8.043	7.565	4.33
9	6408	7.709	7.632	7.347	3.05
10	3852	7.365	7.309	7.088	1.77
11	236	5 84	5.819	5.735	0.09

Rotor Torque on 6 column TBP

Sea State	Standard Deviation σ	Mean Period T_m	Period btn. zero up-crossings T_o	Peak period T_p	Equivalent Fatigue Damage
1	39170	15.519	15.314	14.466	36.6
2	35150	15.258	15.056	14.232	32.3
3	30880	14.988	14.792	13.997	27.9
4	25780	14.483	14.301	13.571	22.6
5	20370	13.889	13.729	13.085	17.2
6	15490	13.36	13.22	12.652	12.7
7	10580	12.688	12.57	12.082	8.28
8	6211	11.856	11.754	11.32	4.56
9	2731	10.967	10.865	10.425	1.84
10	745	9.464	9.368	9.013	0.43
11	0.841	8 05	8.049	8.048	0

Table 5 Statistical properties and fatigue damage in rotor torsion PSDs

Again we see that the fatigue damage caused by the wave-induced motion is greater than that caused by the turbulent wind. The values given for sea states 8 to 11 cannot be relied upon because insufficient RAO data was available in this frequency range.

Figure 11 shows a plot of the equivalent fatigue damage with respect to the sea state.

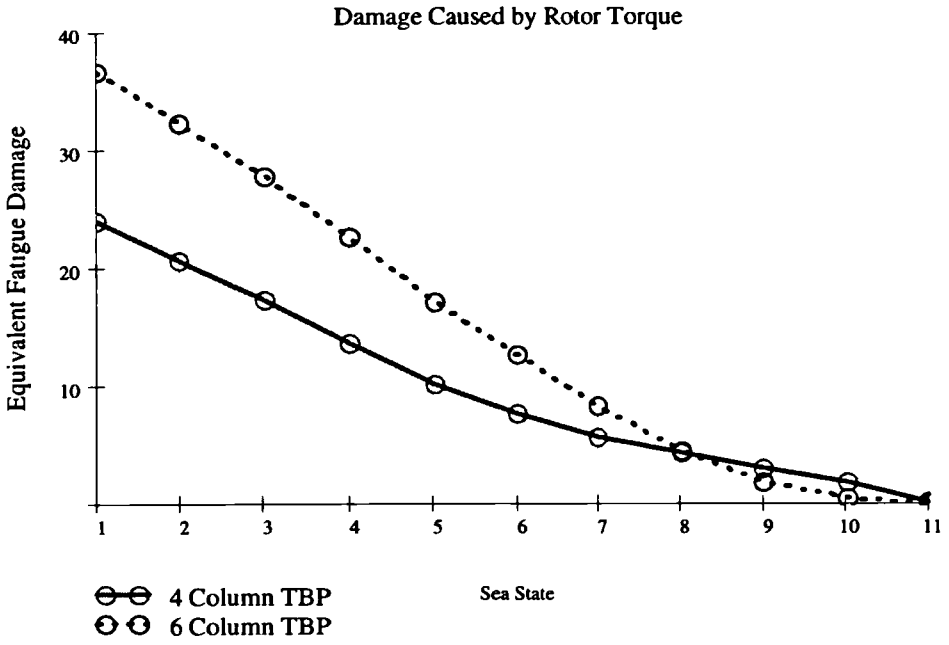

Figure 11 Fatigue Damage V's Sea State

Although the PSD of wind turbulence is much broader than that of the motion induced loads, the damage caused by the latter is found to be significantly greater. This indicates that fatigue damage will result from the platform's motion even though the frequency of the motion is low. This implies that motion analysis should be carried out and the results included in the fatigue analysis of the turbine.

11.4 The effect of rotor damping on rigid body motion response

The presence of the turbines acts to damp the dynamic response of the platform motion. The degree of damping offered by the turbines can be determined as a percentage of the estimated critical damping. The critical damping coefficient is obtained from Equation 11-3.

$$C_{crit} = 2\sqrt{K \cdot M} \qquad \textbf{Equation 11-3}$$

Where K is the stiffness of the platform in surge and M is the sum of the physical mass and the hydrodynamic added mass of the platform. For this approximation the added mass is assumed equal to the physical mass. This is acceptable where circular cylinders are employed (Ref. Barltrop et al[7] Chapter 6.8.3).

The stiffness of the platform in surge can be estimated, assuming that it responds as a linear inverted pendulum, from the natural period. The natural period is found using Equation 11-4.

$$T = 2\pi \cdot \sqrt{\frac{M}{K}} \qquad \textbf{Equation 11-4}$$

Where T is the natural period in seconds, K is the stiffness of the platform and M is the sum of the physical and the hydrodynamic added mass.

Rearranging Equation 11-4 to find an equivalent stiffness and substituting into Equation 11-3 yields values for the critical damping coefficients. The rotor damping offered by Turbine A is determined from the mathematical model derived in Chapter 9 and is expressed as a percentage of critical in Table 6.

	4 Column TBP N/m/sec	6 Column TBP N/m/sec
Critical damping	$1.28\ 10^7$	$2.00\ 10^7$
Rotor damping	2085	2085
Rotor damping expressed as a percentage of the critical damping	0.016%	0.01%

Table 6 Effect of rotor damping in surge

These results indicate a relatively low damping coefficient and show that the rotor damping is unlikely to play a significant part in suppressing the rigid body surge motions. This is as expected because the rigid body surge displacement is typically characterised by a large amplitude and low frequency motion; therefore the velocities will be relatively low. The same phenomenon also occurs with the inertial properties. The mass of the turbine in relation to the overall platform mass is given in Table 7. The turbine's mass is extremely low in comparison with the platform's and so has little significance in the overall rigid body dynamic behaviour.

	4 Column TBP N/m/sec	6 Column TBP N/m/sec
Platform mass	47700	74360
Turbine mass (inc. tower)	60	60
Turbine mass expressed as a percentage of the platform mass	0.13%	0.08%

Table 7 Turbine mass in relation to platform mass

In conclusion we see that the presence of the turbine has little influence on the surge dynamics of the platform. The constant rotor thrust will, however, influence the motion of the platform by applying a steady displacement.

Platform surge will arise due to the wave loading effects on the platform. These will result in additional loads on the rotor blades. The loading occurs at a relatively low frequency and therefore the blades will respond in a quasi-static manner. This simplifies the analysis because a rigid turbine model may be used. The motion-induced loads are relatively high in comparison with the turbulent wind loads and will therefore influence the fatigue design of the turbine. It therefore proves necessary to analyse the motion response of the platform and include this in the fatigue damage assessment.

11.5 The influence of rotor damping on structural vibrations

The previous section demonstrated the insignificance of rotor damping and inertia on the rigid body surge motion of the platform. Damping is very slight because of the relatively slow movement of the platform through the water. The rotor is able to offer significantly better damping for structural vibrations however, because these are typically characterised by small amplitude high frequency motions that result in larger velocities and accelerations.

Sinclair[10,11] investigated the effect of rotor damping on structural vibrations. In particular she considered the effect of roll damping and found that the damping provided by the wind turbine was always at least as good as structural damping. Using the techniques derived in this thesis we are now able to carry out a more detailed analysis which includes all the vibration modes and all the interrelating effects between each mode.

It is assumed that Turbine A is mounted on the platform as shown in Figure 12. The platform is assumed to be rigid in this example, although in practice it can be modelled in the same finite element program as the tower.

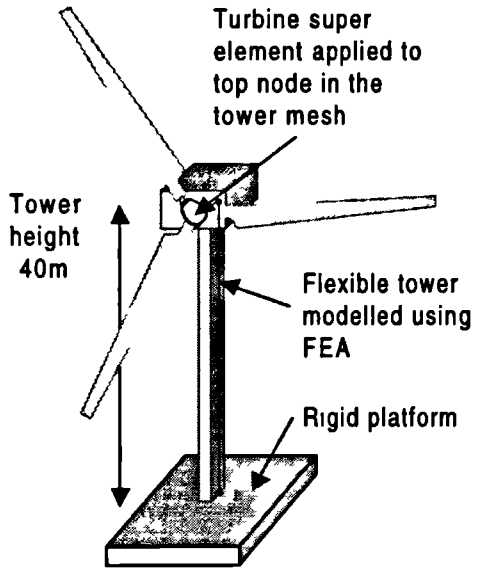

Figure 12 FEA model of turbine mounted on TBP

The tower is modelled using a number of beam elements, the turbine properties are added to the tower top node using the super element model derived in Chapter 10. From this analysis the damping coefficient may be expressed as a percentage of critical in each mode. The surge and tilt modes are found to benefit most from the additional damping of the turbine rotor. First mode surge damping results in 0.3% of critical while the first tilt mode gives 1.29%. These figures are of the same order as the structural damping properties and so should be taken into account when considering the structural dynamic design.

The results given by Sinclair[11] reveal damping values of at least 2% for the first tilt mode. This is similar to that derived above using the new method. The difference between the values is most likely due to differences between the two turbines modelled. An attempt was made to apply Sinclair's empirical technique to Turbine A so that both methods could be compared. Sinclair uses an empirical relationship to derive the coefficients of thrust and lift on the rotor. These are expressed as a function of the tip speed ratio (λ) of the rotor. It proved impossible to compare the two techniques in this way because the empirical expressions did not correctly model this particular turbine. Using Sinclair's empirical equation, the coefficient of thrust was found to be C_D = 1.924. This implies that the turbine is operating in propeller brake state and clearly this can not true. Using the aerodynamic analysis derived in this thesis an actual value of C_D = 0.409 is obtained. This compares well with the measured data referred to in Chapter 8.

11.6 Conclusion

In this chapter a case study is described which demonstrates the application of the 'Rotor Super Element' for calculating rotor loads on floating platforms. A 'Tensioned Buoyant Platform (TBP)' is proposed and analysed for motion in the surge and sway

directions. The platform motion is characterised by a low frequency oscillation. This frequency is below the first mode natural frequency of the rotor and therefore the rotor blades can be modelled as rigid elements.

Studies reveal that the motion-induced loads on the blades cause significant levels of fatigue damage. The damage is more severe than that caused by the turbulent wind even in slight seas. For this reason hydrodynamic analysis is always necessary in fatigue life calculations.

The influence of the turbine on motion damping of the platform was found to be negligible in the case of the TBP. The TBP was chosen for its excellent motion characteristics and this is born out by the low surge and sway responses. This suggests that the sea keeping analyses may be performed separately without concern for the influence of the wind turbine (the steady thrust from the turbine should still be considered however). This may not be true for other floating concepts such as the spar buoy platforms where tilting motions will induce yaw moments and can lead to other coupled effects.

The turbine rotor has been found to have a large influence on damping the structural vibrations in the turbine. This is particularly true in the tilt direction where damping of 1.3% of critical was noted. This is the same order as structural damping and should therefore be considered in any structural dynamic analysis.

---

[1] Tong K and Cannell C (1993). "Technical and economic aspects of a floating offshore windfarm." Proceedings of a BWEA/DTI seminar, Cockroft Hall, Harwell, June 1993.

[2] Barltrop N. (1993). "Multiple unit floating offshore wind farm (MUFOW)." Proceedings of a BWEA/DTI seminar, Cockroft Hall, Harwell, June 1993.

[3] Halfpenny A., Kerr S., Quinlan M, Bishop NWM (1995). "A technical feasibility study and economic assessment of an offshore floating wind farm." Proceedings of the seventeenth BWEA Wind Energy Conference 1995.

[4] Patel M.H. and Witz J.A. (1985). "On improvements to the design of tensioned buoyant platforms." Proceedings of the fourth international conference on behaviour of offshore structures (BOSS '85) pp 563-575. Elsevier Science Publishers B.V., Amsterdam, The Netherlands.

[5] Pierson W.J. and Moskowitz L. (1964). "A proposed spectral form of fully developed wind seas based on the similarity theory of S.A. Kitaigorodskii." Journal of Geophysics. Res., Vol. 69.

[6] Hasselmann K. et al (1973). "Measurements of wind wave growth and swell decay during the JONSWAP project." Deut Hydrog Z, Supplement A, 8 No. 12 p 95.

[7] Barltrop N.D.P. and Adams A.J. (1991). "Dynamics of fixed marine structures." Butterworth-Heinemann Ltd. Linacre House, Jordan Hill, Oxford OX2 8DP, England.

[8] Patel M.H. and Witz J.A. (1991). "Compliant offshore structures." Butterworth-Heinemann.

[9] Bishop (1994). "Spectral methods for estimating the integrity of structural components subjected to random loading." Handbook of Fatigue Crack Propagation in Metallic Structures, volume 2. Elsevier.

[10] Sinclair F.M. Clayton B.R. (1989). "The effects of wave loading on offshore wind turbines." Procedures, European Wind Energy Conference 1989.

[11] Sinclair F.M. (1994). "Aerodynamic damping on offshore installations-a comparison of experimental measurements with theory." Journal of Wind Engineering and Industrial Aerodynamics. SSDI 0167-6105(93)E0064-6.

12. Conclusion

12.1 Contributions of the work

This thesis describes mathematical techniques in the frequency domain that can analyse the stress and motion response characteristics of floating offshore wind turbines. Some of these models have also been employed on a commercial basis to analyse the fatigue damage caused to onshore turbines. The work concludes with new mathematical techniques that perform the following analyses:

1. Stress analysis of a flexible wind turbine structure subjected to random wind loads. This model differs from other analysis methods available at the time as it also models the blade, drivetrain and tower flexibilities and works entirely in the frequency domain.
2. A 'Rotor Super Element' model to derive response matrices for a turbine rotor subjected to platform motions. The response matrices may be used in conjunction with commercial hydrodynamic analysis software to model the effect of a wind turbine on the sea keeping of a floating platform. This analysis has never been undertaken before. The model can be used in the time or frequency domains.
3. A new procedure for calculating the dynamic loads on rotating turbine blades subject to random platform motions. This again represents a new analysis capability in the time and frequency domains.

Case studies are presented to validate the models with data measured from working turbines and also to demonstrate how a turbine will affect the dynamics of a floating offshore platform.

12.2 Conclusions from each chapter

12.2.1 Chapter 2: Frequency domain representation of random processes

The turbulent wind and wave loads acting on an offshore turbine can be modelled as partially correlated random processes. In this chapter a full description of the theory used for analysing random processes is presented. Emphasis is given to presenting a

conceptual understanding of the theories involved as these are used extensively through the rest of the thesis. The chapter concludes by deriving an efficient matrix approach to represent the various auto- and cross-power spectra. This approach is convenient when considering structural dynamic analysis that uses matrix methods.

The use of matrix techniques for frequency domain turbine analysis has not been employed before. They allow a very neat and fast algorithm that easily integrates with finite element analysis. Previous algorithms prove limited for structural analysis because they require separate consideration of each vibration mode. The matrix methodology described in this chapter is not constrained by this requirement.

12.2.2 Chapter 3: Modelling the turbulent wind

In this chapter a literature review is documented discussing the mathematical model used for describing wind turbulence. The ESDU model is proposed for modelling both the on and offshore winds. The model assumes atmospheric equilibrium, this proves a satisfactory solution for isolated turbines given an unrestricted fetch of approximately 30km. These conditions are considered appropriate for the offshore applications covered in this thesis. Further research is necessary, however, to improve the model's description of the real wind field over complex terrain with multiple wind turbine interaction. These conditions are typically associated with onshore windfarms.

The model also assumes a neutrally stable atmosphere that is commonly found in the case of strong winds. This assumption is justified because most of the fatigue damage is likely to be caused under these conditions.

The mathematical model presented in this chapter is considered state-of-the-art and is currently being implemented in a number of commercial software packages for both on and offshore analysis.

12.2.3 Chapter 4: Aerodynamic modelling of a wind turbine

In this chapter a detailed description of the aerodynamic behaviour of wind turbines is presented. The mathematical model chosen for the analysis is based on Glauert's annulus momentum vortex theory (strip theory) which was chosen because of its relative simplicity and rapid calculation. Various modification factors are introduced to improve the model's representation, in particular a new correction factor to take

account of the 3 dimensional flow regime in the post stall state. The model has been verified and found to give excellent agreement with measured power curves.

The post stall behaviour of wind turbines is a complicated non-linear problem and hence difficult to model in the frequency domain. A very simple linearisation method is proposed in this chapter and various aerodynamic gain factors derived which are used throughout the thesis to obtain the aerodynamic loads on the structure. Further research is still required however, to improve the linearisation of the post stall regions as these have been found erroneous. (See Chapter 8 for more details.)

12.2.4 Chapter 5: Modelling the wind turbine loads

This chapter considers the loads acting on the turbine blades and support structure due to variations in the turbulent wind speed. As the turbine blades rotate, they periodically sample the wind turbulence; a phenomenon referred to as 'eddy slicing'. Closed form expressions are derived giving the rotationally sampled auto- and cross-power spectral density functions for the wind speed. These values are presented in a new matrix format to allow rapid manipulation later in the dynamic analysis. Special relationships are noted in the format of the matrices and these are exploited to reduce calculation time.

The concept of the 'Rotor Super Element' is introduced. This is a hypothetical blade that exhibits the properties of the whole rotor. This novel technique is used throughout the thesis to cope with coordinate transformations between rotating and stationary axes and for producing rotor response matrices for sea keeping analysis.

12.2.5 Chapter 6: Dynamic analysis of a wind turbine subjected to turbulent wind loads

In this chapter the structural dynamic analysis of the turbine is presented. Since the onset of this study, others have produced their own structural models. However, the model presented here is unique in that the analysis is carried out wholly in the frequency domain and problems with transforming between the rotating and stationary coordinate axes have been addressed using the 'Rotor Super Element' approach.

Blade element matrices are derived in 8 degrees of freedom and a combined tower and drivetrain element in 13 degrees of freedom. The blade matrices are expressed in this

way because structural property data is unavailable for both the axial and torsional modes. A new technique is introduced to allow the tower to interface with the blade matrices despite the incompatible matrix size. This new technique is necessary to eliminate the possibility of matrix illconditioning and avoid 'holes' in the structural mesh.

12.2.6 Chapter 7: Frequency domain fatigue analysis

In this chapter a brief introduction to the theory of metal fatigue is presented. Particular attention is paid to using the nominal stress (or S-N) approach. An account is given of the various methods for determining the fatigue life from PSD data of stress. The Dirlik method is recommended for general use in the wind turbine industry following the results of previous application studies.

The Dirlik method does not model cyclic mean stresses and therefore this has been ignored in these studies. Bishop has recently developed a new model that includes this effect. Further studies should be undertaken to establish the effect of this new technology on frequency domain turbine analyses.

12.2.7 Chapter 8: Numerical model validation and comparison

This chapter presents a case study to validate the mathematical models with measured values obtained from two production turbines and other software packages. The ESDU model of wind turbulence was compared with measured data and found to agree well for the purpose of turbine analysis. The turbulent loading on the rotor blades was compared with other existing software and also found to agree well. The results of the dynamic and fatigue analysis were compared with measured data and some significant errors were observed. Many factors are highlighted which contribute to these errors. Of primary importance is the calculation of the linear aerodynamic gain factors derived in Chapter 4. The results of this exercise have clearly identified the non-linear aerodynamic analysis as the main source of errors. The results show generally good correlation for the linear pre-stalled case. These give approximately 10% errors in equivalent normalised fatigue life between the predicted and measured loads. Under blade stall the results show an increasing error in the region of 80%. For a frequency domain analysis to succeed we must concentrate on developing a good

linearisation for the aerodynamic model to replace the model described in Chapter 4. The new analysis must consider stall hysteresis in particular.

Another major concern is the omission of structural damping data by the manufacturer. With today's composite materials, high structural damping is likely and this should be included because it appears to have quite a large influence on the results (approximately 10% to 20% in equivalent normalised fatigue damage). The largest contribution is noticed in the edgewise blade loads as these have negligible aerodynamic damping.

12.2.8 Chapter 9: Wind turbine loading due to stochastic base motions

This chapter considers the loads on the rotor hub in response to platform motions. The motions are expressed in six degrees of freedom. Mass, damping and stiffness matrices are derived to represent the effect of a wind turbine mounted on an offshore floating platform. The matrices can be incorporated into existing hydrodynamic analysis software packages to facilitate the sea keeping and stability analyses of offshore wind turbines.

Turbines with 3 or more blades are found to behave as homogeneous disks when subjected to nacelle motions, this makes frequency domain analysis very simple. Single or twin bladed turbines, however, prove very complex to analyse as harmonics are added to the response. The presence of additional harmonics is likely to prove damaging to the structure because they will entail greater fatigue loads. This is discussed in the chapter. Although methods of analysing these in the frequency domain are discussed, analysis in the time domain would prove most sensible. In conclusion it is recommended that offshore turbines have 3 blades.

The new analysis techniques derived in this chapter prove valuable in the analysis of offshore floating turbines. They enable a floating turbine installation to be modelled using any existing hydrodynamic analysis software that accepts additional mass, damping and stiffness matrices. All rigid body forces are modelled including gyroscopically coupled modes.

12.2.9 Chapter 10: Wind turbine blade loads due to stochastic base motions

In this chapter expressions are derived to calculate the blade loads resulting from motions of the turbine in 6 degrees of freedom. Motion induced loading arises with floating turbine structures and is complicated by additional harmonics that are introduced by the rotation of the blades. A unique method for evaluating this complex phenomenon in the frequency domain is presented.

12.2.10 Chapter 11: The analysis of a floating offshore wind turbine mounted on a tensioned buoyant platform

A case study is described which demonstrates the application of the 'Rotor Super Element' for calculating rotor loads on floating platforms. A 'Tensioned Buoyant Platform (TBP)' is proposed and analysed for motion in the surge and sway directions. The platform motion is characterised by a low frequency oscillation, this frequency is below the first mode natural frequency of the rotor and therefore the rotor blades are modelled as rigid elements.

The results show that the platform motions contribute significantly to the overall fatigue damage of the turbine. Their effect is always more severe than the turbulent wind even in the slightest sea conditions. It is therefore necessary to include detailed hydrodynamic analyses when performing a fatigue analysis.

The influence of the turbine on motion damping of the platform is investigated and found to be negligible in the case of the TBP. The TBP is chosen for its excellent motion characteristics and this is born out by the low surge and sway responses. This suggests that the sea keeping analyses may be performed for the platform separately without concern for the influence of the wind turbine (the steady thrust from the turbine should still be considered however). This may not be true for other floating concepts such as the spar buoy platforms where tilting motions will induce yaw moments and can lead to other coupled effects.

The turbine rotor is found to have a large influence on damping the structural vibrations in the turbine. This is particularly true in the tilt direction where damping of 1.3% of critical was noted. This is of the same order as structural damping and should therefore be considered in any structural dynamic analysis.

12.3 Suggestions for further study

12.3.1 Further developments necessary in the mathematical model

The new work discussed in this thesis has been aimed at developing the structural and offshore dynamic models. No significant research effort was applied to the aerodynamic analysis techniques. These have since proved to be the limiting factor in undertaking a successful analysis. The aerodynamic model presented in this thesis is based on a simple linearisation of the Glauert's annulus momentum theory (strip theory). This analysis was considered state of the art at the commencement of the research and proves very capable when considering the steady equilibrium analysis. However, with dynamic analysis in the post stall region it proves inadequate. The reasons for this are discussed in Chapter 8 and include, stall hysteresis, stall non-linearity, dynamic wake effects and 3 dimensional airflow.

Today many turbine manufactures agree that passive or active stall control is the most promising method for regulating turbine power and loading. If frequency domain techniques are to be successfully employed in the future then more attention should be paid to improving the linearised aerodynamic model. Such linearisation should be weighted on a fatigue damage criterion and should include the effects mentioned above. This research is beyond the scope of this study and is recommended for further study.

The finite element analysis documented in this thesis was carried out using beam elements. In many design applications these will prove inadequate and various triangular or square plate elements would have to be used instead. Further research is required to successfully integrate the frequency domain fatigue analysis with other finite element models. The new techniques should allow multiple partially correlated loads to be applied to a structural finite element mesh. The resulting stress PSDs are required along the principal stress vectors at each element node. Fatigue life can then be computed based on the maximum principal stress or using some stress invariant such as von-Mises or the Tresca effective stress.

In addition to the above analysis it is also necessary to determine whether the stress state at a node is uni or multiaxial. This can be achieved by determining whether the

principal stress tensor is stationary or mobile. A stationary tensor indicates a uniaxial or proportional multiaxial stress state while a mobile tensor indicates a non-proportional multiaxial stress state.

12.3.2 Further case studies

The work documented in this thesis is largely concerned with the development of frequency domain tools for analysing the dynamic behaviour of both on and offshore wind turbines. The development of these new techniques has taken a considerable length of time and has therefore left little opportunity for detailed application studies. If offshore floating turbine concepts are to be reality then many more case studies are required to determine how they behave.

- **Case studies to determine the sea keeping ability of floating concepts**

  The case study documented in Chapter 11 has considered the response of a 'Tensioned Buoyant Platform (TBP)'. This was chosen because of its superior motion characteristics as significant displacements are only found in the surge and sway directions. From this study it is shown that the turbine contributes little to the rigid body dynamics and therefore may be ignored in all sea keeping analyses. Further studies are required to determine whether this is true for all concepts. One particular concern is for the Spar Buoy type concept. In this case considerable tilt motion is also expected and this will result in a coupling between the modes due to gyroscopic effects. This will induce, among other things, a high yaw moment on the turbine which will contribute to rigid body yaw as a result of the low stiffness and damping present in this mode. With these concerns in mind, it is advisable to carry out a study to determine the significance of the turbine on the sea keeping of a number of different floating platforms.

- **Case study to determine the turbine's contribution to motion damping**

  Chapter 11 has shown that rigid body motions are likely to contribute to the fatigue damage of the turbine. In this example, only the surge response was found to be significant as insufficient motion is induced in the other modes. This beneficial result is unlikely to be observed with other floating concepts, especially those like the Spar Buoy where tilt and yaw motions will induce

higher harmonics in the blade loading which will also contribute to the fatigue damage. For this reason it is advised that further study be performed to determine which modes cause significant fatigue damage on different turbine concepts.

- **Case study to determine the turbine's contribution to vibration damping**

  The turbine has been shown to contribute to the structural vibration damping of a platform. In this case the contribution is of the same order as the structural contribution. The analysis method adopted in this study assumes that the rotor blades are rigid and so the model becomes inaccurate at higher frequencies approaching blade resonance. It is possible to develop the super element and include blade flexibility, however it may prove more desirable to simply develop the finite element representation given in Chapter 6 to include a full description of the platform structure as well as the tower. This approach is adequate for turbines with three or more blades. However, for those with fewer blades, account must be paid to the additional harmonics resulting from rotor azimuth dependencies. Further case studies are therefore recommended to determine the damping contribution made by the turbine for the higher modes.

- **Cost benefit analysis for proposing 1, 2 or 3 bladed turbines for use offshore**

  The frequency domain Rotor Super Element assumes that the rotor has three blades. Many onshore turbines have only two blades and a few have only one. These turbines may prove cheaper to manufacture but also induce harmonic shifts in the platform load spectra. The harmonics result in energy being moved from lower to higher frequencies hence increasing the fatigue damage to the structure. A cost benefit analysis should be considered to determine whether it is reasonable to use single or twin bladed turbines or whether the additional fatigue loads would result in the three bladed rotor being the most economical proposal.

- **Analysis of transient and highly non-linear loads on the turbine structure**

  The research documented in this thesis is concerned with the linear analysis of steady state loading on the turbine structure. Many structural failures, however, are attributed to large transient or non-linear loads that occur throughout the life of the turbine. These can accumulate significant levels of fatigue damage and include control scenarios such as start-up and shutdown procedures and turbine yawing. We must also consider the rare extreme loads such as emergency shutdown on loss of grid connection, etc. These may only occur a few times during the turbine's life but can cause catastrophic damage. In order to design for these loads requires a quasi-static or transient dynamic analysis in the time domain. Before offshore turbines are employed it is therefore necessary to develop computational models in the time domain to analyse these loads.

- **Detailed component analysis**

  The analysis documented has concentrated on the overall loading on the turbine. Before we can build a real turbine it is necessary to investigate the stresses and fatigue damage accumulated in many individual components, these include gearbox and generator mountings, yaw drive systems, etc. This could be done in the frequency domain when steady-state linear loads are observed, or in the time domain when transient or non-linear loads are apparent. To accurately predict the stress distribution for components on this level, a more detailed finite element model is required. Overall analysis models, such as the one documented in this thesis, are then used to provide loading input into these component specific models. Further studies are therefore required to ensure that suitable output loads are available for subsequent detailed component analyses.

Appendix A

Aerana Listing

QUASI-STATIC WIND TURBINE ANALYSIS

Set origin for all matrix addressing ORIGIN 1

Set tolerance limit for numerical routines TOL 0 01

Define units of force N newton kN 1000·N Define unit of power MW kW 10^3

Introduction

This worksheet performs the following functions:

- visualisation of blade airfoil aerodynamic characteristics
- visualisation of turbine rotor stall characteristics
- analysis of blade loads and power output using equilibrium and frozen wake assumptions
- aerodynamic pre-processing required for entry into the dynamic analysis worksheets.

The aerodynamic analysis method employed is based on the revised momentum equations and includes terms for tip losses from the blades. An equilibrium wake is calculated at a given average wind speed and this is then assumed frozen for the calculation of the aerodynamic blade forces under the fluctuating turbulent wind speed. The turbulent wake state is modeled using Willson's linear approximation, the method is based on the one given in the book *'Wind Turbine Engineering Design* by *'Eggleston and Stoddard'*

Input data files· aprofile prn, apitch prn, ffaw3cl prn, nacacl prn, boncd.prn, acm prn
Output data files · gaindamp prn

Number of blade elements:

Set the number of blade elements to be considered N_B 20 i 1 . N_B

Define the rotor parameters:

Number of blades B 3

Rotational speed rpm 25 8 f_o $\frac{rpm}{min}$ $f_o = 0.43 \cdot Hz$

Ω $f_o 2\pi$ $\Omega = 2.702 \cdot rad\ sec^{-1}$

Hub height hub_{height} 35 m

Coning angle ψ 0 deg

Read in blade profile data

bladprof READPRN(aprofilv $_{prn}$)

This file contains 4 columns of data.

- radius along blade (m) measured from the hub centre (this data should start at the root radius and finish at the tip radius)
- chord at this blade location (m)
- twist at this blade location (degrees)
- thickness of the blade (m)

bladprof =

	1	2	3	4
1	3	1 075	9	1 075
2	3 33	1 075	9	1 075
3	3 8	1 075	9	1 075
4	4 5	1 252	12 5	1 017
5	5	1 383	15	0 964
6	5 5	1 516	17 5	0 919
7	6	1 65	20	0 881
8	6 5	1 624	18 1	0 82
9	7	1 597	16 3	0 759
10	7.5	1 569	14 8	0 696
11	8	1 54	13	0 638
12	8 5	1 511	11 5	0 581
13	9	1 481	10 05	0 528
14	9 5	1 451	8 3	0 48
15	10	1 42	7 46	0 433

Overall radius R_{tip} $bladprof_{(length\ bladprof^{<1>},1}$ m $R_{tip} = 22 \cdot m$

Root radius R_{root} $bladprof_{(1\ 1)}$ m $R_{root} = 3 \cdot m$

Blade profile start and change position

Radius to start of aerodynamic profile R_{prof} 6 m

Radius to change of aerodynamic profile R_{chang} 12 5 m

linearly interpolate to find the chord and the twist as a function of radius.

c(rad) linterp$\left(bladprof^{<1>} \cdot m, bladprof^{<2>}, rad\ m\right)$

alpha(rad) linterp bladprof$^{<1>}$ m, bladprof$^{<3>}$, rad) deg

Bonus chord distribution used for load case 2.1

$$c(rad) := 1\ 65\ m + (rad - 4\ 5\ m)\ \frac{1\ 65\ m - 0\ 4\ m}{4\ 5\ m - 22\ m}$$

$c(10\ m) = 1\ 42 \cdot length$

Set up the blade elements

Δr $\frac{R_{tip} - R_{prof}}{N_B}$ Length of element $\Delta r = 0\ 8 \cdot m$

Radius to i^{th} element r_i $\left[\left(R_{prof} + \frac{\Delta r}{2} + \Delta r (i - 1)\right.\right.$

i.e.... $r^T =$

1	2	3	4	5	6	7	8	9	10	11
6 4	7 2	8	8 8	9 6	10 4	11 2	12	12 8	13 6	14 4

$\cdot m$

Read in variation of pitch angle with wind speed

This file contains two columns:
- velocity (m/s)
- pitch angle (degrees)

pitch READPRN(apitch)

pitch angle as a function of velocity $\beta(\text{velocity})$ linterp pitch$^{\langle 1\rangle}$ m sec^{-1}, pitch$^{\langle 2\rangle}$ deg, velocity

vel 1 25

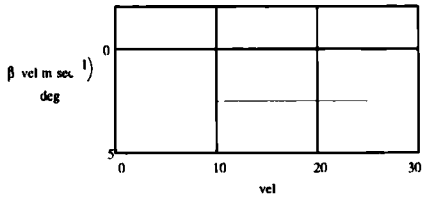

pitch angle as a function of tip speed ratio $\beta(\text{lambda})$ $\beta\left(\frac{f_o \cdot 2\pi R_{tip}}{\text{lambda}}\right)$

Therefore the pitch angle as a function of r and λ is:- $\beta(r,\lambda)$ alpha(r) + $\beta(\lambda)$

Aerodynamic Coefficients (lift, drag, pitching moment)

Read in aerodynamic coefficients for the blade

ACL1 READPRN(ffaw3cl)
ACL2 READPRN(nacacl)
ACD READPRN(boncd)
ACM READPRN(acm)

These files contain two columns:
- angle of incidence (degrees)
- aerodynamic coefficient

Define functions for C_l, C_d and C_m

This function returns an angle between 0 and 360 degrees $OTP(\alpha)$ $2\cdot\pi\cdot\frac{\alpha}{2\pi} - \text{floor}\left(\frac{\alpha}{2\cdot\pi}\right)$

$C_{l\,2d}(\alpha,\text{rad})$ if(rad<R_{prof}, 0, linterp ACL1$^{\langle 1\rangle}$ deg, ACL1$^{\langle 2\rangle}$, OTP(α))

$C_{l\,2d}(\alpha,\text{rad})$ if rad<R_{chang}, $C_{l.2d}(\alpha,\text{rad})$, linterp ACL2$^{\langle 1\rangle}$·deg, ACL2$^{\langle 2\rangle}$, OTP(α))

$C_d(\alpha,\text{rad})$ if rad<R_{prof}, 1 linterp ACD$^{\langle 1\rangle}$ deg, ACD$^{\langle 2\rangle}$, OTP(α))

$C_m(\alpha)$ linterp ACM$^{\langle 1\rangle}$ deg, ACM$^{\langle 2\rangle}$, OTP(α)

Plot out the aerodynamic coefficients

ang 0 deg, 1 deg .. 390 deg

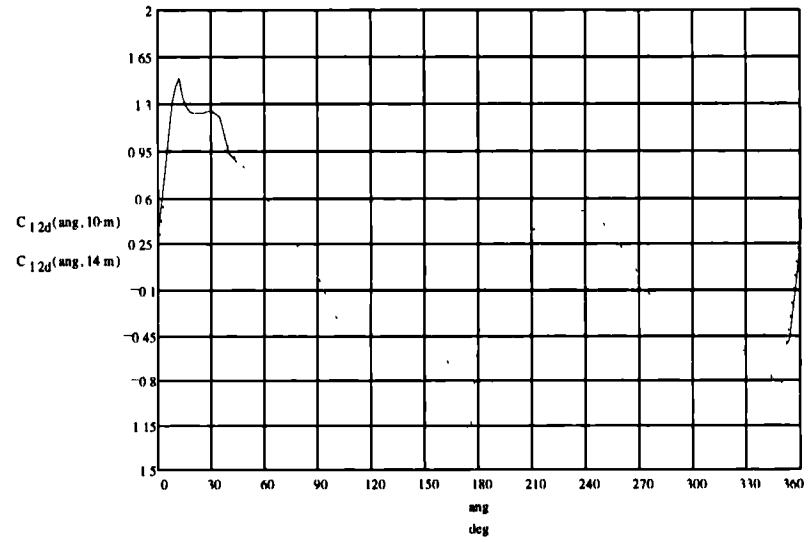

Functions to plot the coefficients out on a polar diagram.

CP(α, rad) if($C_{l\,2d}(\alpha,\text{rad})>0, C_{l\,2d}(\alpha,\text{rad}), 0$) CN(α, rad) if $C_{l\,2d}(\alpha,\text{rad})<0, C_{l\,2d}(\alpha,\text{rad}), 0$)

$C_{mp}(\alpha)$ if($C_m(\alpha)>0, C_m(\alpha), 0$) $C_{mn}(\alpha)$ if($C_m(\alpha)<0, C_m(\alpha), 0$)

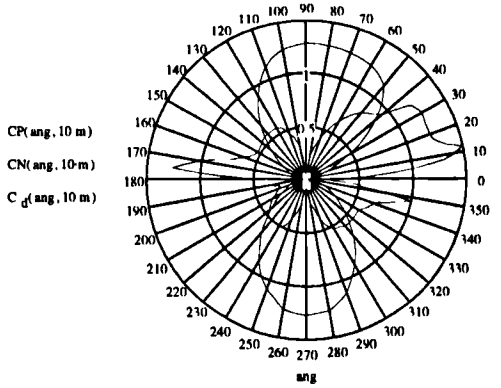

The 2D coefficients for lift and drag Cl_{2d} and Cd are obtained from library files for the 4 blade profile types used The values for each coefficient are derived by linear interpolation from the files and automatically adjust to find the required blade profile given the radius along the blade under question A 3D modification is made to the lift coefficient,Cl_{3d}, after Snel.

Cl at $\alpha = 0$ $\quad Cl_0(r) \quad C_{l\,2d}(0\ r)$

Define the linear Cl curve from potential flow theory $\quad Cl_{lin}(\alpha,r) \quad Cl_0(r) + 2\cdot\pi\,\alpha$

Define the term ΔCl for the difference between the linear potential flow theory assumption and the actual $\quad \Delta Cl(\alpha,r) \quad Cl_{lin}(\alpha\ r) \quad C_{l\,2d}(\alpha,r)$

Define the 3D lift coefficient: $\quad C_{l\,3d}(\alpha,r) \quad C_{l\,2d}(\alpha\ r) + \Delta Cl(\alpha,r)\ \tanh\left[3\cdot\left(\frac{c(r)}{r}\right)^2\right]$

Define the lift and drag coefficients: $\quad Cl(\phi,r,\lambda) \quad C_{l\,3d}(\phi\ \ \beta(r,\lambda),r)$

$Cd(\phi\ r,\lambda) \quad C_d(\phi\ \ \beta(r,\lambda),r)$

Define the calculation parameters: $\quad$ Density of air $\quad \rho \quad 1\,225\cdot kg\ m^{-3}$

$N_v \quad 20$ $\quad$ Number of wind speeds to be calculated $\quad j \quad 1\ N_v$

$V_{min} \quad 6\ m\ sec^{-1} \quad V_{max} \quad 25\ m\ sec^{-1}$ $\quad$ Minimum & maximum wind speed in range

Therefore the wind speeds calculated are given by: $\quad V_j \quad V_{min} + \left(\frac{V_{max} \quad V_{min}}{N_v \quad 1}\right)(j \quad 1)$

V^T

1	2	3	4	5	6	7	8	9	10	11	12
6	7	8	9	10	11	12	13	14	15	16	17

$\cdot m\ sec^{-1}$

The respective tip speed ratios for these wind speeds are: $\quad \lambda_j \quad \frac{\Omega\ R_{tip}}{V_j}$

λ^T

1	2	3	4	5	6	7	8	9
9 906	8 491	7 43	6 604	5 944	5 404	4 953	4 572	4 246

Define the main momentum equations, loss factors, etc.:

$\sigma(r) \quad \frac{B\ c(r)}{\pi\ r}$ $\quad$ Local solidity ratio for each blade element. ie. area of a small length δr along the blade with respect to the swept area of the same length taken over the whole rotor disk.

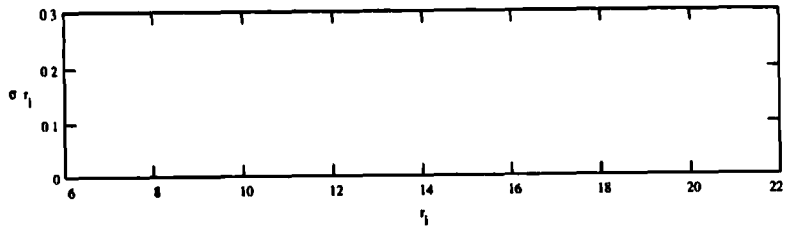

Determine the tip loss coefficient:

The tip loss coefficient F can be obtained from the expression: $\quad F \quad \frac{2}{\pi}\ acos(exp(\ f))$

where *f* is given as:- $\quad f_{tip} \quad \frac{B}{2}\cdot\frac{R_{tip} \quad r}{r\cdot\sin(\phi)}$

Therefore the tip loss function *F* with respect to *r* and ϕ can be defined as:-

$$F(\phi,r) \quad \frac{2}{\pi}\cdot acos\left[\exp\left[\frac{1}{2}B\left(\frac{R_{tip} \quad r}{(r\sin(\phi))}\right)\right]\right]$$

Define the iterative procedure to evaluate axial and radial interference factors a & a`.

In order to obtain solutions for the factors required it is necessary to use an iterative process. First it is necessary to make initial guesses for the values and then by process of iteration refine these to reach the required solutions. For this purpose the *MathCad Solve block*^ has been employed.

Initial guesses:

$a \quad \frac{1}{3} \qquad \phi \quad a \qquad a' \quad 0 \qquad C_H \quad a$

given

$$\phi = atan\left[\frac{R_{tip} \quad (1 \quad a)\cdot\cos(\psi)}{r \qquad (1+a)\,\lambda}\right]$$ $\quad$ Direction of resultant wind wrt rotor plane

$$C_H = \frac{\sigma(r)}{2}\cdot(1 \quad a)^2\cdot\frac{\cos(\psi)^2}{\sin(\phi)^2}\cdot(Cl(\phi,r,\lambda)\cos(\phi) + Cd(\phi,r\ \lambda)\sin(\phi))$$ $\quad$ Local *Head Loss Coefficient* for the rotor element Δr

$$a = if\left[C_H < 0\,9424, \left[\frac{1}{2\,F(\phi\ r)}\cdot\left(1 \quad \sqrt{1 \quad C_H}\right), \left[\frac{1}{F(\phi,r)} \quad \frac{C_H \quad 0\,5776}{0\,96}\right]\right]\right]$$ $\quad$ Axial interference factor. If a>0.38 then use momentum equation else use linear turbulent wake model.

$$a' = \sigma(r)\ \frac{Cl(\phi,r,\lambda)\sin(\phi) \quad Cd(\phi\ r,\lambda)\cos(\phi)}{8\,F(\phi,r)\cdot\cos(\phi)\sin(\phi) \quad \sigma(r)\,(Cl(\phi,r,\lambda)\sin(\phi) \quad Cd(\phi\ r\ \lambda)\cos(\phi))}$$ $\quad$ Radial interference factor

$Solution(r,\lambda) \quad minerr\ a,a',\phi\ C_H$ $\quad$ Nb. '*Solution*' is defined as a function of *r* and λ and returns a vector of matrices giving values for *a*, *a'*, ϕ and C_H.

Start main iterative calculations to determine interference factors for each TSR:

$a_{i,j}$
$a'_{i,j}$ Solution r_i, λ_j
$\phi_{i,j}$
$C_{H_{i,j}}$

i.e.. calculate a vector of vectors for the axial induction factors, the radial induction factors, the inflow angle and the local head loss coefficient. These are calculated at each radius i.

Plot induction factors along the length of the blade:

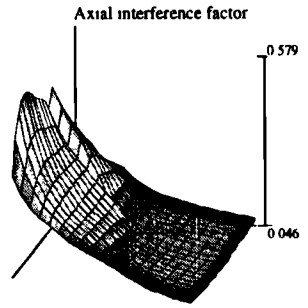

a

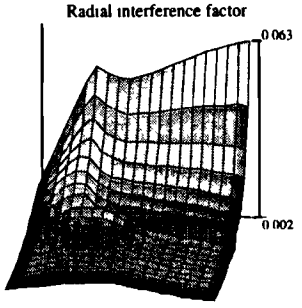

a'

N.B.. TSR increases from left to right; Radius increases out of the page.

To gain a better indication of which regions go into stall a plot of Cl/Cd may be made for all radii and tip speed ratios. The plot is shown below as a contour and surface plot.

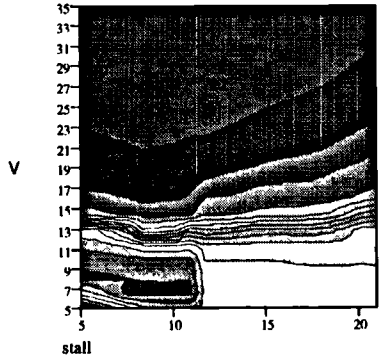

stall

radius

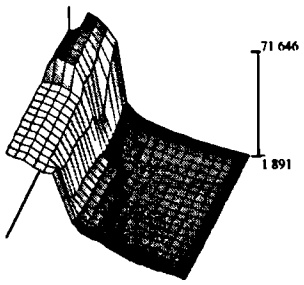

stall

Cl/Cd vertical, Radius increases out of the page & wind speed increases to the right

Find torque, thrust and power coefficients for the rotor at each TSR λ:

Find the relative wind velocity w:

$$W_{i,j} \left[(1 - a_{i,j}) \cdot \begin{pmatrix} \cos(\psi) \\ \sin \phi_{i,j} \end{pmatrix} \right] V_j$$

Torque coefficient C_Q:

$$C_{q_j} \frac{\frac{1}{2} \cdot \left[\sum_1 r_i \; W_{i,j}{}^2 \cdot \left(Cl\, \phi_{i,j}, r_i, \lambda_j \right) \sin \phi_{i,j} \quad Cd\left(\phi_{i,j}\, r_i, \lambda_j \right) \cos \phi_{i,j} \quad B\, c\, r_i \; \Delta r \right]}{\pi R_{tip}{}^2 \; \Omega R_{tip}{}^2 R_{tip}}$$

$C_q{}^T =$

	1	2	3	4	5
1	$1.829 \cdot 10^{-4}$	$3.358 \cdot 10^{-4}$	$5.304 \cdot 10^{-4}$	$7.54 \cdot 10^{-4}$	0.001

Power P:

$$P_j \; \frac{1}{2} \rho \left[\sum_1 r_i \, \Omega \cdot \left(W_{i,j} \right)^2 \left(Cl\, \phi_{i,j}, r_i, \lambda_j \right) \sin \phi_{i,j} \quad Cd\, \phi_{i,j}\, r_i\, \lambda_j \cos \phi_{i,j} \quad B\, c\, r_i \; \Delta r \right.$$

Coefficient of power C_P:

$$C_P \; \frac{\overrightarrow{P}}{\frac{1}{2} \cdot \rho \, V^3 \cdot \left(\pi R_{tip}{}^2 \right)}$$

$C_P{}^T =$

	1	2	3	4	5	6	7	8	9
1	0.356	0.411	0.435	0.434	0.42	0.385	0.315	0.268	0.231

Thrust coefficient C_T:

$$C_{T_j} \; \frac{\sum_1 \left(W_{i,j} \right)^2 \left(Cl\, \phi_{i,j}, r_i, \lambda_j \right) \cos\left(\phi_{i,j} \right) + Cd\left(\phi_{i,j}, r_i, \lambda_j \right) \sin \phi_{i,j} \quad B\, c\, r_i \; \Delta r}{\left(V_j{}^2 \pi R_{tip}{}^2 \right.}$$

$C_T{}^T =$

	1	2	3	4	5	6	7	8	9
1	0.904	0.83	0.767	0.707	0.644	0.572	0.498	0.441	0.388

Plot power coefficient vs wind speed

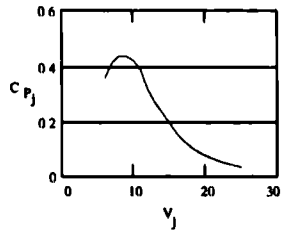

Plot thrust coefficient vs wind speed:

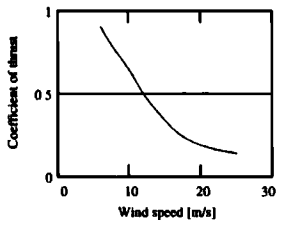

Plot torque coefficient vs TSR:

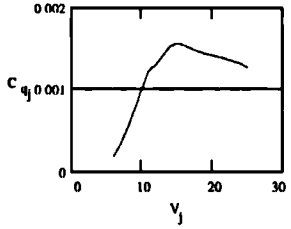

Power vs wind speed:

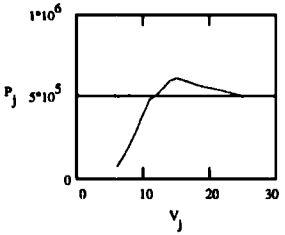

Find local lift and drag forces:

From the above Axial and Radial Interference factors the velocity of swirl and axially induced wake velocities may be determined. These velocities are then assumed '*frozen*' for the calculations of the blade angles of attack ϕ and α used for the upper and lower bounds of the wind class.

Choose the wind speed to be used from the previous calculations:

J 3 Wind speed calculation to be used -> relates to wind speed of: $V_j = 8 \cdot m\ sec^{-1}$

Number of wind speeds to be calculated around this mean (should be odd): $N_u \quad 21 \qquad n \quad 1..N_u$

Lowest wind speed calculated: $U_{min} \quad 5\ m\ sec^{-1}$

Highest wind speed calculated: $U_{max} \quad 25\ m\ sec^{-1}$

Therefore the windspeeds are: $U_n \quad U_{min} + \left(\frac{U_{max} - U_{min}}{N_u - 1}\right)(n - 1)$

I.e. the wind speeds are:

U^T

n	1	2	3	4	5	6	7	8	9	10	11	12
U_n	5	6	7	8	9	10	11	12	13	14	15	16

$\cdot m\ sec^{-1}$

Axially induced wake velocity $\quad v_i \quad V_j\, a_{i,j}$

Velocity of swirl in wake $\quad w_i \quad r_i\, \Omega\, a'_{i,j}$

Find the direction of resultant wind wrt rotor plane ϕ and the blade angle of attack for each blade section α at the upper and lower bounds of the wind class:

$$\phi_{frozen_{i,n}} \quad -\operatorname{atan}\left(\frac{U_n - v_i}{\Omega \cdot r_i + w_i} \cdot \cos(\psi)\right) \qquad \alpha_{i,n} \quad \phi_{frozen_{i,n}} - \beta\, r_i, \lambda_j$$

Find the relative wind velocity w: $\quad \psi = 0 \cdot deg$

$$W_{i,n} \quad (U_n - v_i) \cdot \begin{pmatrix} \cos(\psi) \\ \sin\left(\phi_{frozen_{i,n}}\right) \end{pmatrix}$$

Find lift force on blade [N]: $\quad l_{i,n} \quad \frac{1}{2} \rho \left(W_{i,n}\right)^2 (c\ r)\, \Delta r)\, Cl\left(\phi_{frozen_{i,n}}, r_i, \lambda_j\right)$

Drag force on blade [N]: $\quad d_{i,n} \quad \frac{1}{2} \rho \left(W_{i,n}\right)^2 (c\ r_i)\, \Delta r\ \ Cd\ \phi_{frozen_{i,n}}, r_i, \lambda_j$

calculate the forces at each blade element in the in-plane and out-of-plane directions

$$Force_{inplane_{i,n}} = l_{i,n} \sin\left(\phi_{frozen_{i,n}}\right) \quad d_{i,n} \cdot \cos\left(\phi_{frozen_{i,n}}\right)$$

$$Force_{outplane_{i,n}} \quad l_{i,n} \cos\left(\phi_{frozen_{i,n}}\right) + d_{i,n} \sin\left(\phi_{frozen_{i,n}}\right)$$

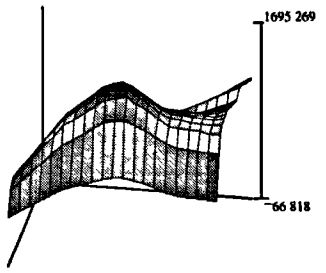

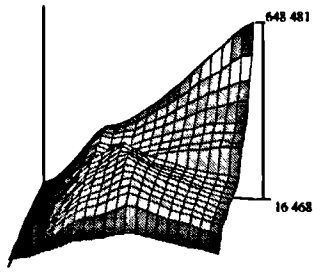

$Force_{outplane}$ $\qquad$ $Force_{inplane}$

Radius increases out of the page & wind speed increases to the right

Calculate steady state Torque, Thrust and Power for the rotor for upper & lower class wind:

Torque Q:

$$Q_n \quad B \cdot \sum_1 r_i \cdot \left(l_{i,n} \cdot \sin\left(\phi \text{frozen}_{i\ n}\right) \quad d_{i,n} \cdot \cos\left(\phi \text{frozen}_{i,n}\right) \right]$$

Thrust T:

$$T_n \quad B \cdot \sum_1 \left(l_{i,n} \cdot \cos\left(\phi \text{frozen}_{i,n} + d_{i,n} \cdot \sin \phi \text{frozen}_{i,n}\right)\right)\Bigg]$$

Power P:

$$P_n \quad Q_n \Omega$$

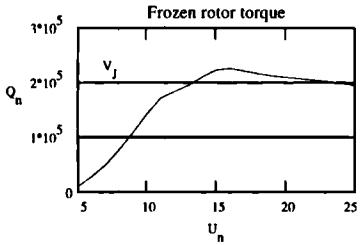

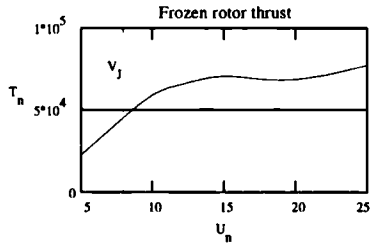

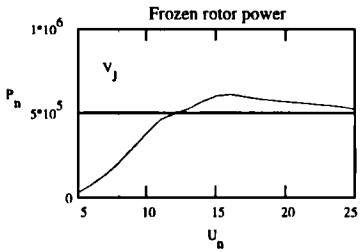

Calculate the Lead-lag damping coefficients:

Velocity of swirl in the equilibrium wake: $\text{swirl}_i \quad a'_{i,J} \Omega r_i$

$\text{swirl}^T =$

1	2	3	4	5	6	7	8	9
0 479	0 471	0 474	0 474	0 481	0 461	0 441	0 415	0 358

$\cdot m\ sec^{-1}$

variation in swirl speed calculated: $\Delta sw \quad 0\,2 \cdot m\ sec^{-1}$

Therefore the swirl speeds are. $sw_{i,n} \quad \text{swirl}_i \quad \Delta sw\ \text{floor}\left(\frac{N_u}{2}\right) + \Delta sw\ n$

Calculate the inflow angle for the frozen wake for all rotor frequencies and all blade elements:

$$\phi \text{edge}_{i,n} \quad \text{atan}\left(\frac{V_J \quad v_i}{\Omega r_i + sw_{i,n}} \cdot \cos(\psi)\right) \qquad \alpha_{i\ n} \quad \phi \text{edge}_{i\ n} \quad \beta\left(r_i, \lambda_J\right)$$

Find the relative wind velocity at each blade element in each wind speed:

$$W_{i,n} \quad \left(V_J \quad v_i\right) \cdot \frac{\cos(\psi)}{\sin\left(\phi \text{edge}_{i,n}\right)}$$

Find the lift force on each element $l_{i,n} \quad \frac{1}{2} \rho \left(W_{i\ n}\right)^2 \left(c\left(r_i\right) \Delta r\right) Cl\left(\phi \text{edge}_{i,n}, r_i, \lambda_J\right)$

Find the drag force on each element $d_{i\ n} \quad \frac{1}{2} \rho \left(W_{i,n}\right)^2 \left(c\left(r_i \quad \Delta r \quad Cd\left(\phi \text{edge}_{i,n}, r_i, \lambda_J\right)\right.\right.$

Axial force on the blade element (flap-wise) $F_{a_{i\ n}} \quad l_{i,n} \cos\left(\phi \text{edge}_{i,n}\right) + d_{i\ n} \sin\left(\phi \text{edge}_{i\ n}\right)$

Tangential force on the blade element (lead-lag) $F_{t_{i\ n}} \quad l_{i,n} \sin\left(\phi \text{edge}_{i\ n}\right) \quad d_{i\ n} \cos\left(\phi \text{edge}_{i\ n}\right)$

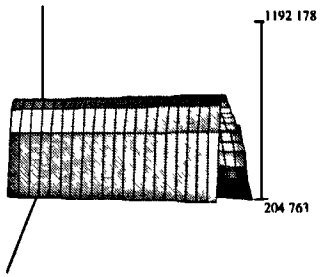

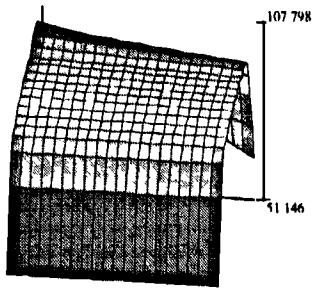

F_a F_t

Radius increases out of the page & blade speed increases to the right

Reset the variables: $I := 0$ $d := 0$ $F_a := 0$ $F_t := 0$ $\alpha := 0$ $W := 0$

$swirl := 0$ $\phi_{frozen} := 0$ $\phi_{edge} := 0$ $v := 0$ $w := 0$ $sw := 0$

$Force_{inplane} := 0$ $Force_{outplane} := 0$

The gain factors are used in subsequent Mathcad sheets for calculating the blade forces.

$N_B := 4$ Enter number of blade elements to be calculated $i := 1 .. N_B$

Set up the new blade elements:

$\Delta r := \frac{R_{tip} - R_{prof}}{N_B}$ Length of elements $\Delta r = 4 \cdot m$

Radius to the i^{th} element: $r := 0$ $r_i := \left(R_{prof} + \frac{\Delta r}{2}\right) + \Delta r \cdot (i - 1)$

i.e.... $r^T = (8 \quad 12 \quad 16 \quad 20)\cdot m$

<u>Evaluate the blade interference factors, etc. for the equilibrium wake at these blade locations:</u>

Define the initial guesses for the SOLVE block given earlier:

$a := \frac{1}{3}$ $\phi := a$ $a' := 0$ $C_H := a$

Calculate the interference factors:

$\begin{bmatrix} a_i \\ a'_i \\ \phi_i \\ C_{H_i} \end{bmatrix}$ Solution (r_i, λ_j)

i.e.. calculate a vector of vectors for the axial induction factors, the radial induction factors, the inflow angle and the local head loss coefficient. These are calculated at each radius i.

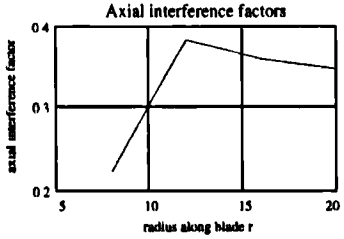

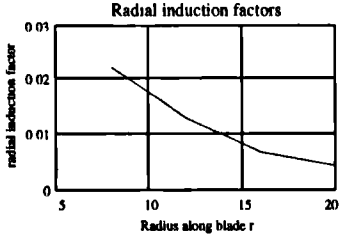

This section can be used as an indication of the accuracy lost using a more limited number of blade elements.

Find the relative wind velocity w: $W := 0$

$$W_i := \left[(1 - a_i) \cdot \left(\frac{\cos(\psi)}{\sin(\phi_i)}\right)\right] \cdot V_j$$

Torque coefficient C_Q:

$$CC_q := \frac{\frac{1}{2} \cdot \left[\sum_i r_i \left(W_i^{\,2} \left(Cl(\phi_i, r_i, \lambda_j) \sin(\phi_i) - Cd(\phi_i, r_i, \lambda_j) \cos(\phi_i)\right) B\, c\, r_i\right) \Delta r\right]}{\left(\pi R_{tip}^{\,2}\right) \left(\Omega R_{tip}\right)^2 R_{tip}}$$

$CC_q = 5.467 \cdot 10^{-4}$ Compares with the value obtained from the full analysis $C_{q_j} = 5.304 \cdot 10^{-4}$ Error.... $\frac{CC_q - C_{q_j}}{C_{q_j}} = 3.072 \cdot \%$

Power P:

$$PP := \frac{1}{2} \cdot \rho \cdot \left[\sum_i r_i \Omega \left(W_i\right)^2 \cdot \left(Cl(\phi_i, r_i, \lambda_j) \cdot \sin(\phi_i) - Cd(\phi_i, r_i, \lambda_j) \cos(\phi_i)\right) B\, c\, r_i\, \Delta r\right]$$

$PP = 213.828 \cdot kW$

Coefficient of power C_P:

$$CC_P := \frac{PP}{\frac{1}{2} \cdot \rho \cdot \left(V_j\right)^3 \cdot \left(\pi R_{tip}^{\,2}\right)}$$

$CC_P = 0.448$ Compares with the value obtained from the full analysis $C_{P_j} = 0.435$ Error. .. $\frac{CC_P - C_{P_j}}{C_{P_j}} = 3.072 \cdot \%$

Thrust coefficient C_T:

$$CC_T := \frac{\sum_i \left(W_i\right)^2 \cdot \left(Cl(\phi_i, r_i, \lambda_j) \cdot \cos(\phi_i) + Cd(\phi_i, r_i, \lambda_j \sin(\phi_i))\right) B\, c\, r_i\, \Delta r}{\left(V_j^{\,2} \cdot \pi R_{tip}^{\,2}\right)}$$

$CC_T = 0.798$ Compares with the value obtained from the full analysis $C_{T_j} = 0.767$ Error.... $\frac{CC_T - C_{T_j}}{C_{T_j}} = 4.101 \cdot \%$

Calculate the variation in inplane and out of plane forces with respect to wind speed assuming a frozen wake:

Mean wind speed being calculated: $V_J = 8 \cdot m\ sec^{-1}$

$\Delta V \quad 2\ m\ sec^{-1}$ Wind class interval. i.e. difference between upper and lower bound wind speeds

The upper and lower bound wind speeds u_s may therefore be obtained by: $s \quad 1..2$

$u_1 \quad V_J - \frac{\Delta V}{2}$ i.e.... Lower bound of wind class $u_1 = 7 \cdot m\ sec^{-1}$

$u_2 \quad V_J - \frac{\Delta V}{2}$ i.e.... Upper bound of wind class $u_2 = 9 \cdot m\ sec^{-1}$

The frozen wake velocities are given by:

Axially induced wake velocity $v_i \quad V_J\, a_i$

Velocity of swirl in wake $w_i \quad r_i \cdot \Omega \cdot a'_i$

Find the direction of resultant wind wrt rotor plane ϕ and the blade angle of attack for each blade section α at the upper and lower bounds of the wind class:

$$\phi frozen_{i,n} \quad atan\left(\frac{U_n - v_i}{\Omega r_i + w_i}\cos(\psi)\right) \qquad \alpha_{i,n} \quad \phi frozen_{i,n} - \beta(r_i, \lambda_J)$$

Find the relative wind velocity w: $\psi = 0 \cdot deg$

$$W_{i,n} \quad U_n - v_i\left(\begin{matrix}\cos(\psi)\\ \sin\phi frozen_{i,n}\end{matrix}\right)$$

Find lift force on blade [N] $l_{i,n} \quad \frac{1}{2}\cdot\rho\cdot W_{i,n}^2\cdot\left(c(r_i)\cdot\Delta r\cdot Cl\left(\phi frozen_{i,n}, r_i, \lambda_J\right)\right)$

Drag force on blade [N]: $d_{i,n} \quad \frac{1}{2}\rho\, W_{i,n}^2\,(c\, r_i\, \Delta r)\, Cd\left(\phi frozen_{i,n}, r_i, \lambda_J\right)$

calculate the forces at each blade element in the in-plane and out-of-plane directions

$$Force_{inplane_{i,n}} \quad l_{i,n}\sin\left(\phi frozen_{i,n}\right) - d_{i,n}\cdot\cos\left(\phi frozen_{i,n}\right)$$

$$Force_{outplane_{i,n}} \quad l_{i,n}\cos\left(\phi frozen_{i,n}\right) + d_{i,n}\sin\left(\phi frozen_{i,n}\right)$$

View the change in force for the blade elements between the upper and lower bound wind speeds:

These plots allow you to see the effect of the linearisation assumptions for each blade element. For stall regulated machines especially there are points of non linearity and these are likely to produce gain factors substantially different from the actual blade unless care is taken in selecting the mean wind speeds and the wind class interval for the calculations.

$I \quad 1$ View the I^{th} blade element Mean wind speed $V_J = 8 \cdot m\ sec^{-1}$

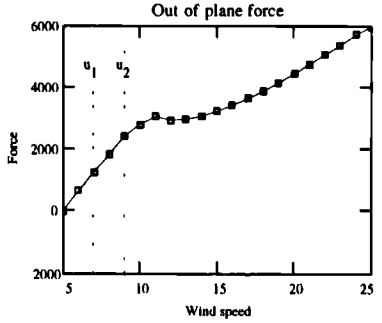

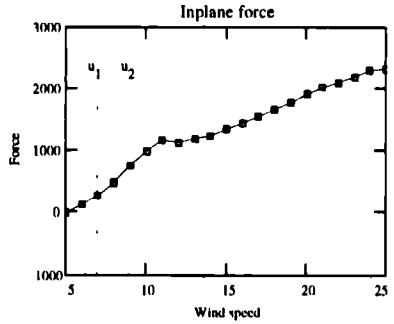

Calculate the variation in blade forces due to variations in the inplane wind speed:

$\Delta w \quad 0.2 \cdot m \cdot sec^{-1}$ Swirl velocity class interval. i.e difference between the upper and lower bound swirl velocities

The upper and lower swirl velocities vs_s may therefore be found by:

$vs_{i,1} \quad w_i - \frac{\Delta w}{2}$ i.e.... Lower bound swirl velocity

$vs_{i,2} \quad w_i + \frac{\Delta w}{2}$ i.e ... Upper bound swirl velocity

Velocity of swirl in the equilibrium wake: $swirl_i \quad a'_i\, \Omega\, r_i$

$swirl^T = (\ 0.474 \quad 0.415 \quad 0.289 \quad 0.234\ ) \cdot m\ sec^{-1}$

Therefore the swirl speeds are: $sw_{i,n} \quad swirl_i \quad \Delta w\ floor\left(\frac{N_u}{2}\right) + \Delta w\, n$

Calculate the inflow angle for the frozen wake for all rotor frequencies and all blade elements:

$$\phi edge_{i,n} \quad atan\left(\frac{V_J - v_i}{\Omega r_i + sw_{i,n}}\cos(\psi)\right) \qquad \alpha_{i,n} \quad \phi edge_{i,n} - \beta(r_i, \lambda_J)$$

$$W_{i,n} \quad (V_j \quad v_i)\cdot \frac{\cos(\psi)}{\sin\left(\phi_{edge_{i,n}}\right)}$$

Find the lift force on each element $l_{i,n} \quad \frac{1}{2}\rho\cdot(W_{i,n})^2\left(c(r_i)\,\Delta r\right) Cl\left(\phi_{edge_{i,n}}, r_i, \lambda_j\right)$

Find the drag force on each element $d_{i,n} \quad \frac{1}{2}\rho\,(W_{i,n})^2\cdot\left(c(r_i)\cdot\Delta r\cdot Cd\left(\phi_{edge_{i,n}}, r_i, \lambda_j\right)\right.$

Axial force on the blade element (flap-wise) $F_{a_{i,n}} \quad l_{i,n}\cos\left(\phi_{edge_{i,n}}\right) + d_{i,n}\cdot\sin\left(\phi_{edge_{i,n}}\right)$

Tangential force on the blade element (lead-lag) $F_{t_{i,n}} \quad l_{i,n}\sin\left(\phi_{edge_{i,n}}\right) \quad d_{i,n}\cos\left(\phi_{edge_{i,n}}\right)$

View the change in force between the upper and lower swirl velocities:

I 4 View the I^{th} blade element Mean wind speed $V_j = 8\cdot m\,sec^{-1}$

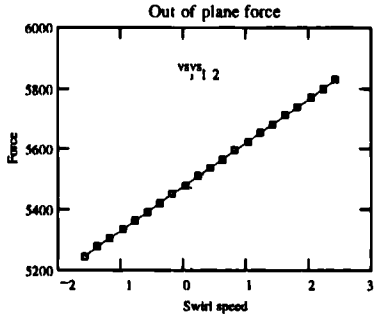

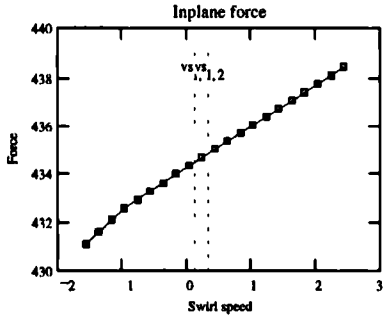

Calculate the variation in blade forces due to variation in the blade pitch angle:

We shall calculate the axial and tangential force variation due to changes n angle of attack of the blade. We shall calculate this for a number of different angle variations to check linearity.

$\Delta\theta$ 1 deg Blade pitch variation interval.

Now because we are considering negative and positive variations we need to find the position in the vector for zero variation.

$$pos_{zero} \quad ceil\left(\frac{N_u}{2}\right) \qquad pos_{zero} = 11$$

Therefore the pitch angle variation vector is given by: $\theta_n \quad \Delta\theta \quad n \quad pos_{zero}\right)$

$$\theta^T = (\ 10\ -9\ \ 8\ \ 7\ -6\ \ 5\ -4\ \ 3\ \ 2\ \ 1\ \ 0\ \ 1\ \ 2\ \ 3\ \ 4\ \ 5\ \ 6\ \ 7\ \ 8\ \ 9\ \ 10\ )\cdot deg$$

choose best range.)

$\Delta\phi$ 1·deg Therefore the corresponding angles are: $v\theta_1 \quad \frac{\Delta\phi}{2} \qquad v\theta_2 \quad \frac{\Delta\phi}{2}$

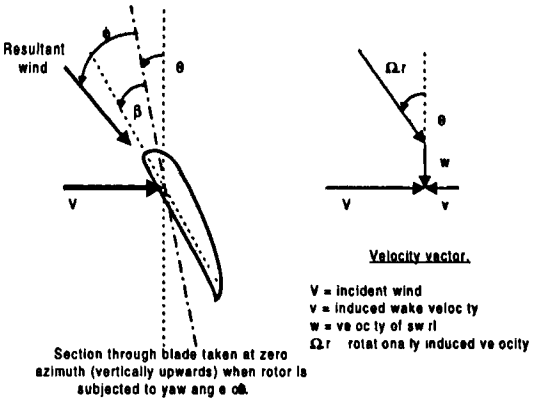

Calculate the relative wind velocity and direction of inflow at each blade element with the blade pitch variations given above.

$$\phi_{pitch_{i,n}} \quad atan\left[\frac{(V_j \quad v_i) + \Omega\, r_i \sin\left(\theta_n\right)}{w_i + \Omega\, r_i \cos\left(\theta_n\right)}\cdot\cos(\psi)\right] \quad \theta_n$$

$$W_{i,n} \quad \sqrt{\left[(V_j \quad v_i) + \Omega\, r_i\cdot\sin\ \theta_n\ \right]\cos(\psi)\Big]^2 + \left(w_i + \Omega\, r_i\cdot\cos\ \theta_n\ \right)^2}$$

Find lift force on blade [N]: $l_{i,n} \quad \frac{1}{2}\rho\,(W_{i,n})^2\left(c(r_i)\,\Delta r \quad Cl\,\phi_{pitch_{i,n}}, r_i, \lambda_j\right)$

Drag force on blade [N]: $d_{i,n} \quad \frac{1}{2}\rho\,(W_{i,n})^2\left(c\ r_i\right)\Delta r\right) Cd\left(\phi_{pitch_{i,n}}, r_i\ \lambda_j\right)$

Calculate the forces at each blade element in the in-plane and out-of-plane directions

$$F_{a_{i,n}} \quad l_{i,n}\cdot\cos\left(\phi_{pitch_{i,n}}\right) + d_{i,n}\cdot\sin\left(\phi_{pitch_{i,n}}\right)$$

$$F_{t_{i,n}} \quad l_{i,n}\sin\left(\phi_{pitch_{i,n}}\right) - d_{i,n}\cdot\cos\left(\phi_{pitch_{i,n}}\right)$$

View the change in force between the upper and lower pitch angle variations:

I 4 View the I^{th} blade element Mean wind speed $V_J = 8 \cdot m\ sec^{-1}$

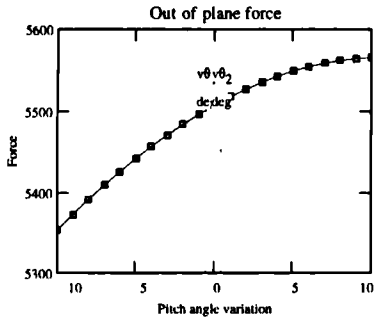

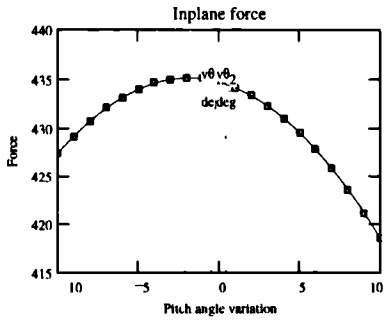

Calculate the gain factors for the blade elements:

Having accepted the linearisation given above, this section calculates the linear gain factors:

Calculate the axial and tangential gain factors for the blade elements:

Find the direction of resultant wind wrt rotor plane ϕ and the blade angle of attack for each blade section α at the upper and lower bounds of the wind class:

Reset variables: $\phi_{frozen} \quad 0 \qquad \alpha \quad 0 \qquad I \quad 0 \qquad d \quad 0 \qquad Force_{inplane} \quad 0$

$Force_{outplane} \quad 0 \qquad F_a \quad 0 \qquad F_t \quad 0$

$$\phi frozen_{i,s} \quad atan\left(\frac{u_s \quad v_i}{\Omega\, r_i + w_i} \cdot \cos(\psi)\right) \qquad \alpha_{i,s} \quad \phi frozen_{i,s} \quad \beta\left(r_i, \lambda_j\right)$$

Find the relative wind velocity w: $\psi = 0 \cdot deg$

$$W_{i,s} \quad u_s \quad v_i \left(\begin{matrix}\cos(\psi) \\ \sin\left(\phi frozen_{i,s}\right)\end{matrix}\right)$$

Find lift force on blade [N] $$l_{i,s} \quad \frac{1}{2}\rho \cdot \left(W_{i,s}\right)^2 \cdot \left(c\left(r_i\right) \Delta r \quad Cl\left(\phi frozen_{i,s}, r_i\ \lambda_j\right)\right.$$

Drag force on blade [N]: $$d_{i,s} \quad \frac{1}{2}\rho \left(W_{i,s}{}^2 \quad c\ r_i \quad \Delta r\right) Cd\ \phi frozen_{i,s}, r_i, \lambda_j\right)$$

calculate the forces at each blade element in the in-plane and out-of-plane directions

$$Force_{inplane_{i,s}} \quad l_{i,s} \sin \phi frozen_{i,s} \quad d_{i,s} \cos\left(\phi frozen_{i,s}\right)$$

$$Force_{outplane_{i,s}} \quad l_{i,s} \cos\left(\phi frozen_{i,s}\right) + d_{i,s} \sin\left(\phi frozen_{i,s}\right)$$

Evaluate the gain factors:

$$g_{a_i} \quad \frac{Force_{outplane_{i,2}} \quad Force_{outplane_{i,1}}}{\Delta V} \qquad g_{t_i} \quad \frac{Force_{inplane_{i,2}} \quad Force_{inplane_{i,1}}}{\Delta V}$$

$$g_a{}^T = (\ 591.557 \quad 754.295 \quad 695.136 \quad 589.168\ ) \cdot \frac{N}{m\ sec^{-1}}$$

$$g_t{}^T = (\ 240.474 \quad 214.15 \quad 178.137 \quad 144.451\ ) \cdot \frac{N}{m\ sec^{-1}}$$

Augment these ready for exporting to file:

$$gain \quad augment\left(g_a \cdot \frac{m\ sec^{-1}}{N}, g_t \cdot \frac{m\ sec^{-1}}{N}\right)$$

Calculate the Axial and tangential damping factors for inplane motion:

Reset the variables: $\phi_{edge} \quad 0$

Calculate the inflow angle for the frozen wake for all rotor frequencies and all blade elements:

$$\phi edge_{i,s} \quad atan\left(\frac{V_j \quad v_i}{\Omega\, r_i + vs_{i,s}} \cos(\psi)\right) \qquad \alpha_{i,s} \quad \phi edge_{i,s} \quad \beta\left(r_i\ \lambda_j\right)$$

Find the relative wind velocity at each blade element in each wind speed:

$$W_{i,s} \quad \left(V_j \quad v_i\right) \cdot \frac{\cos(\psi)}{\sin\left(\phi edge_{i,s}\right)}$$

Find the lift force on each element $$l_{i,s} \quad \frac{1}{2}\rho \quad W_{i,s}\right)^2 \left(c\ r_i\right) \Delta r\right) Cl\left(\phi edge_{i,s}, r_i, \lambda_j\right)$$

Find the drag force on each element $$d_{i,s} \quad \frac{1}{2}\rho \left(W_{i,s}\right)^2 \quad c\left(r_i\right) \Delta r\right) Cd\left(\phi edge_{i,s}, r_i, \lambda_j\right)$$

Axial force on the blade element (flap-wise) $$F_{a_{i,s}} \quad l_{i,s} \cos\left(\phi edge_{i,s}\right) + d_{i,s} \sin\left(\phi edge_{i,s}\right)$$

Tangential force on the blade element (lead-lag) $$F_{t_{i,s}} \quad l_{i,s} \sin\left(\phi edge_{i,s}\right) \quad d_{i,s} \cos\left(\phi edge_{i,s}\right)$$

Evaluate the damping factors:

Axial and tangential damping coefficients $$c_{a_i} \quad \frac{F_{a_{i,2}} \quad F_{a_{i,1}}}{\Delta w} \qquad c_{t_i} \quad \frac{F_{t_{i,2}} \quad F_{t_{i,1}}}{\Delta w}$$

$c_a = (\ 2.096 \quad 113.063 \quad 158.736 \quad 145.016\ )\ \frac{}{m\ sec^{-1}}$

$c_t^{T} = (\ 23.21 \quad 1.433 \quad 0.983 \quad 1.728\ )\ \frac{N}{m\ sec^{-1}}$

Augment these ready for exporting to file:

$damp \quad augment\left(c_a \frac{sec}{kg}, c_t \frac{sec}{kg}\right)$

Calculate the blade pitch damping coefficients:

Reset the variables $\phi_{pitch} \quad 0$

Calculate the relative wind velocity and direction of inflow at each blade element with the blade pitch variations given above.

$$\phi_{pitch_{i,s}} \quad atan\left[\frac{\left(V_j \quad v_i\right) + \Omega\, r_i \sin\left(\theta_s\right) \cos(\psi)}{w_i \quad \Omega\, r_i \cos\left(\theta_s\right)}\right] \quad \theta_s$$

$$W_{i,s} \quad \sqrt{\left[\left(V_j \quad v_i\right) + \Omega\, r_i \sin\left(\theta_s\right) \cos(\psi)\right]^2 + \left[w_i + \Omega\, r_i \cos\left(\theta_s\right)\right]^2}$$

Find lift force on blade [N] $l_{i,s} \quad \frac{1}{2} \rho\, W_{i,s}^{\ 2}\, c\, r_i\, \Delta r\, Cl\left(\phi_{pitch_{i,s}}, r_i, \lambda_j\right)$

Drag force on blade [N]: $d_{i,s} \quad \frac{1}{2} \rho\, W_{i,s}^{\ 2}\, c\, r_i\, \Delta r\, Cd\left(\phi_{pitch_{i,s}}, r_i, \lambda_j\right)$

Calculate the forces at each blade element in the in-plane and out-of-plane directions

$F_{a_{i,s}} \quad l_{i,s} \cos\left(\phi_{pitch_{i,s}}\right) \quad d_{i,s} \sin\left(\phi_{pitch_{i,s}}\right)$

$F_{t_{i,s}} \quad l_{i,s} \sin\left(\phi_{pitch_{i,s}}\right) \quad d_{i,s} \cos\left(\phi_{pitch_{i,s}}\right)$

Evaluate the damping factors:

Axial and tangential damping coefficients $\beta_{a_i} \quad \frac{F_{a_{i,2}} \quad F_{a_{i,1}}}{\Delta\phi} \qquad \beta_{t_i} \quad \frac{F_{t_{i,2}} \quad F_{t_{i,1}}}{\Delta\phi}$

$\beta_t^{T} = (-0.172 \quad 1.396 \quad 1.849 \quad 1.781\ )\ \frac{N}{deg}$

Augment these ready for exporting to file: $Pdamp \quad augment\left(\beta_a \frac{1}{N}, \beta_t \frac{1}{N}\right)$

Create augmented matrix of values and write results to a file for subsequent use in the dynamic calculations. (N.B. This MUST be dimensionless):

$WRITEPRN(gaindamp) \quad augment\left(\frac{r}{m}, augment\left(\frac{\overrightarrow{c(r)}}{m} \quad augment \quad \frac{\overrightarrow{alpha(r)}}{deg}\right)\right) \quad augment(gain \quad augment(damp, Pdamp))$

Compare with formula given by Fiona Sinclair.

Define coefficient of lift wrt yaw angle ξ degrees $C_L(\xi) \quad 0.016 \lambda_J \xi \cdot (23 \quad \lambda_J$

Define coefficient of drag: $C_D \quad 0.035 \cdot \lambda_J \cdot (17 \quad \lambda_J)$

λ is the tip speed ratio given, for this wind speed $V_J = 8 \cdot m\ sec^{-1}$ as $\lambda_J = 7.43$

The forces are found from these coefficients by multiplying by $\frac{1}{2} \rho (V_J)^2 A$

Where A is the rotor swept area: $A \quad \pi R_{tip}^2$ $A = 1.521 \cdot 10^3 \cdot m^2$

Therefore a force multiplier can be defined as: $F_m \quad \frac{1}{2} \rho \cdot (V_J)^2 \cdot A$ $F_m = 59.605 \cdot kN$

Find the coefficient of drag and the total thrust on the turbine:

$C_D = 2.489$ Therefore force is $F_m C_D = 148.337 \cdot kN$

Compare this with that calculated for the rotor: $C_{T_J} = 0.767$ $F_m C_{T_J} = 45.719 \cdot kN$

Find the lift with ξ degrees of yaw misalignment: $\xi \quad 1 \cdot deg$

$C_L(\xi) = 0.032$ Therefore the force is $F_m C_L(\xi) = 1.926 \cdot kN$

This compares with a force calculated in Rotormat as follows:

$Sway(\xi) \quad \frac{B}{2} \xi \cdot \sum_{n=1}^{4} \beta_{t_n}$ $Sway(\xi) = 0.007 \cdot kN$

Transfer this into the stationary tower system $Sway(\xi) + F_m C_{T_J} \cdot \xi = 0.805 \cdot kN$

Rotormat also gives a tilt moment on the rotor as follows:

$Tilt(\xi) \quad \frac{B}{2} \cdot \xi \cdot \sum_{n=1}^{4} \beta_{a_n} r_n$ $Tilt(\xi) = 1.385 \cdot kN\ m$

Appendix B

Turbana Listing

Turbana

Frequency Domain Modelling of Rotationally Sampled Wind

Andrew Halfpenny

This worksheet performs the stochastic loading calculations to determine the forces applied to a wind turb ne blade and tower The stochastic wind field is modelled using the ESDU spectra given in ESDU 85020 Amended 1993) and ESDU 86010 The spectra is rotationally sampled by a revolving rotor blade This is modelled using the method documented in the TURBU-1 manual. An additional simpl fication is in uded to mprove the speed of calcu ation. This is based on the results documented in the R SØ report but in th s study a more precise value is used.

TOL-1 ^{8} N newton kN 1000 newton ORIGIN=1

Define parameters for the ESDU spectra:

U_{ave} 10 Average steady state wind speed

z 35 Hub height [m]

z_o 0 00087 Terrain roughness length [m]

h 0 General obstruction height of surrounding obstacles [m]

RPM 27 7 Rotor frequency [rpm] $\Omega \quad \frac{RPM}{60} 2\pi$ $\Omega = 2\,901$ [rad/sec]

ESDU 85020 (Amended 1993)

Angu ar velocity of the earth $\Omega_{earth} \quad 72\,9\,10^{-6}$

Angle of latitude of the site $\phi_{lat} \quad 60\,deg$

Coriolis parameter $f_c \quad 2\,\Omega_{earth} \sin(\phi_{lat})$

Friction velocity $u_* \quad \frac{U_{ave}}{2\,5 \ln\left(\frac{z}{z_o}\right)}$ $u_* = 0\,377$

Boundary layer height $h_{bl} \quad \frac{u_*}{6\,f_c}$ $h_{bl} = 497\,987$

Parameters from (Eqn 4.2) $\eta \quad 1 \frac{z}{h_{bl}}$ $\eta = 0\,93$

$\rho \quad \eta^{16}$ $\rho = 0\,312$

Standard deviation of wind turbulence (Eqn 4.2) $\sigma_u \quad u_* \left(7\,5\,\eta \quad 0\,538 + 0\,09 \ln\left(\frac{z}{z_o}\right)^{\rho}\right)^{-1} \left(1 \quad 0\,156 \ln\left(\frac{u_*}{f_c z_o}\right)\right)$ $\sigma_u = 0\,89$

Turbulence Intensity $\frac{\sigma_u}{U_{ave}} = 8\,9021\,\%$ (choose the value of roughness length above to give the correct turbulence intensity)

Height above which $K_z = K_\infty$ (Eqn. A2.17) $z_c \quad 0.39\,h_{bl}\left(\frac{u_*}{f_c z_o}\right)^{\frac{1}{8}}$ $z_c = 29\,601$

$K_\infty \quad 0.188$

Kolmogorov parameter Eqn. A2 16) $K_z \quad \text{if}\left[z>z_c, K_\infty, K_\infty\left[1 \quad 1 \left(\frac{z}{z_c}\right)^{\frac{1}{2}}\right]^{\frac{1}{2}}\right]$ $K_z = 0\,188$

(Eqn. A2 15) $A \quad 0\,115 \quad 1 + 0\,3151\,\eta^{\frac{2}{3}}$ $A = 0\,13$

Long tudinal length scale Eqn. A2.14 $x_{Lu} \quad \frac{A^{\frac{3}{2}} \sigma_u^{3} z}{u_* \left(2\,5\,K_z^{2}\,\eta^{2}\right)^{3} \left(1 \quad 5\,75 \frac{z}{h_{bl}}\right)}$ $x_{Lu} = 87\,252$

Employ ESDU modification to incorporate low frequencies:

Calculate factors in modified von Karman equations.

Eqn. B.5.10 $a \quad 0\,535 + 2\,76\,(0\,138 \quad A)^{0\,68}$

Eqn. B.5 8 $\beta_1 \quad 2\,357\,a \quad 0\,761$

Eqn. B 5 7 $\beta_2 \quad 1 \quad \beta_1$

Calculate the function n_u: $n_u(n) \quad \frac{n \cdot x_{Lu}}{U_{ave}}$

Calculate the factor F1 (Eqn B 4 3) $F_1(n) \quad \text{if}\left[n = 0.1,\ 1 + 0.455\, e^{0.76 \left(\frac{n_u(n)}{a}\right)^{0.8}}\right]$

Calculate the modified autopower spectra:

$$G_u(n) = \frac{\sigma_u^2}{n}\left[\beta_1 \frac{2.987 \left(\frac{n_u(n)}{a}\right)^5}{\left(1 + \left(\frac{2\pi n_u(n)}{a}\right)^2\right)^6} + \beta_2 \frac{1.294 \left(\frac{n_u(n)}{a}\right)^5}{\left(1 + \left(\frac{\pi n_u(n)}{a}\right)^2\right)^6}\right] F_1(n)$$

OR in circular coordinates.

Define parameter $b \quad \frac{x_{Lu}}{U_{ave}}$

$$G_u(\omega) \quad \frac{\sigma_u^2}{2\pi}\left[\beta_1 \frac{2.987 \left(\frac{b}{a}\right)^5}{\left(1 + \left(\frac{2\pi n_u \frac{\omega}{2\pi}}{a}\right)^2\right)^6} + \beta_2 \frac{1.294 \left(\frac{b}{a}\right)^5}{\left(1 + \left(\frac{\pi n_u \frac{\omega}{2\pi}}{a}\right)^2\right)^6}\right] F_1\left(\frac{\omega}{2\pi}\right)$$

$cc \quad 1 \ldots 100 \quad freq_{cc} \quad \frac{cc}{100}$

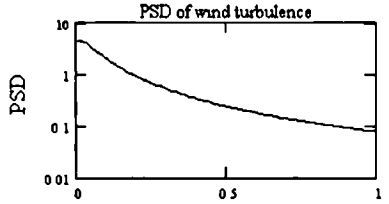

Determine the coherence function:

ESDU 86010

Longitudinal length scale $x_{Lu} \quad 87.252$

Calculate the lateral length scales (Eqns 6.3 & 6.4)

$$z_{Lu} \quad x_{Lu}\left[0.5 + 0.34\, e^{-3.5 \left(\frac{z}{h_{bl}}\right)^{1.7}}\right] \qquad z_{Lu} = 23.409$$

$$y_{Lu} \quad x_{Lu}\left[0.16 + 0.68 \frac{z_{Lu}}{x_{Lu}}\right] \qquad y_{Lu} = 29.878$$

Calculate the radial length scale $r_{Lu} \quad \sqrt{z_{Lu} \cdot y_{Lu}} \qquad r_{Lu} = 26.446$

Determine the coherence function (ESDU procedure 7.1.2):

$$r_g(d) \quad \frac{d}{2 r_{Lu}}$$

$$b(d) \quad 0.35\, r_g(d)^{0.2}$$

$$\eta(n,d) \quad \left[0.747\, r_g(d)^2 + \left(2\pi n \frac{d}{U_{ave}}\right)^2\right]^{\frac{1}{2}}$$

$$c_1(n,d) \quad \frac{16\, r_g(d)^{0.13}}{\eta(n,d)^{b(d)}} \qquad c(n,d) \quad \text{if}\left(c_1(n,d) > 1.0,\ c_1(n,d),\ 1.0\right)$$

$$\eta_1(n,d) \quad \left[0.747\, r_g(d)^2 + c(n,d)\left(2\pi n \frac{d}{U_{ave}}\right)^2\right]^{\frac{1}{2}}$$

Coherence function. $\gamma(n,d) \quad e^{-11.5 \eta_1(n,d)^{1.5}}$

OR in circular coordinates $\chi(\omega,d) \quad e^{-11.5 \eta_1 \left(\frac{\omega}{2\pi}, d\right)^{1.5}} \qquad dist_{cc} \quad cc$

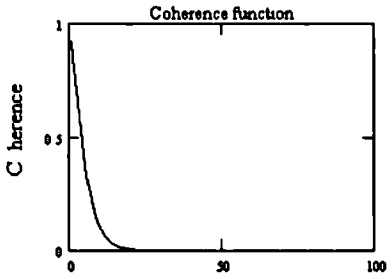

Define the admittance function:

distance in rotor plane $d(r_1, r_2, \theta) := \sqrt{r_1^2 + r_2^2 - 2 r_1 r_2 \cos(\theta)}$

$$K_n(r_1, r_2, n, \omega) := \frac{1}{\pi} \int_0^{\pi} \chi(\omega, d(r_1, r_2, \theta)) \cos(n\theta)\, d\theta$$

Define the cross power spectra for the turbine blade:

The cross power spectra may be written as follows This equation allows harmonic contribution cut offs at nΩ frequencies (simplification from RISØ) .-

Define the highest and lowest harmonic contribution to each frequency calculation.

$lo(\omega) := \text{floor}\left(\frac{\omega}{\Omega}\right) - 2$ $\qquad$ $hi(\omega) := \text{floor}\left(\frac{\omega}{\Omega}\right) + 3$

Therefore the revised cross spectra is determined by -

$$G_{uu}(r_1, r_2, \varphi, \omega) := \sum_{n=lo(\omega)}^{hi(\omega)} e^{i \cdot n \cdot \varphi} K_n(r_1, r_2, n, n\Omega - \omega)\, G_u(n\Omega - \omega)$$

Input the blade radii from PREBU-2b.

Hawtload mcd created an output file ca led *Gaindamp prn*. This contains the ga n and drag coefficients for the blade loading. The first column of this data shows the radii to the blade sections which have been calculated and are required for the *Turbana* calculation The axial & tangential gains will also be required later

gains READPRN("gaindamp prn r gains$^{\langle 1 \rangle}$

$r^T = (6.5\ 10.5\ 14.5\ 18.5)$

Calculate the number of elements $N_e := last(r)$

Define the ranging variable for the Spectral calculation $i := 1 .. N_e$

Calculate the cross power spectra for rotationally sampled wind speeds for various frequencies ω:

The following section determines the frequencies over which the calculation will take place Low frequency wind is likely to play a large role and so a separate interva is included to improve the resolution in this area. As rotational sampling is observed then the same interval is also used for all areas around the required P frequencies

Number of b ades	$B := 3$	
Enter starting frequency [rad/sec]	$\omega_{start} := 0.1$	
Enter frequency interval around the P frequencies	$\delta\omega_p := 0.1$	
Enter number of points to be calcu ated at this interval	$n_1 := 6$	
Enter number of P's to be included at this interval	$n_p := 3$	$\Omega := 2.901$
Enter frequency interval for the rest of the spectra	$\delta\omega_r := 0.3$	
Enter last frequency to be calculated	$\omega_{last} := 40$	

```
ω | for k ∈ 1 .. n1
      ω1_k ← ω_start + δω_p·(k − 1)
      ω2_k ← Ω − ω_start − δω_p·(n1 − k)
    end1 ← ω1_(n1)
    end2 ← ω2_1
    n3 ← ceil((end2 − end1)/δω_r)
    δ ← (end2 − end1)/n3
    for k ∈ 1 .. n3 − 1
      ω3_k ← end1 + δ·k
    ω4 ← stack(stack(ω1, ω3), ω2)
    for i ∈ 1 .. np − 1                    if np > 2
      ω4 ← stack(ω4, ω4 − Ω_i)
    ω5 ← ω4
    end ← ω5_(last(ω5))
    n4 ← ceil((ω_last − end)/δω_r)
    δ ← (ω_last − end)/n4
    for k ∈ 1 .. n4
      ω6_k ← end + δ·k
    stack(ω5, ω6)
```

ω =

0.1
0.2
0.3
0.4
0.5
0.6
0.883
1.167
1.45
1.734
2.017
2.301
2.401
2.501
2.601

Number of calculations $no_{calcs} := last(\omega)$ $no_{calcs} = 163$

Define frequency calculation number $k := 1 .. no_{calcs}$

Save the frequency information WRITEPRN("freq.prn") := ω

Now the cross power spectra is required between each blade element on each blade. For both 2 and 3 bladed turbines it is noted that the matrices follow similar patterns. As this calculation is potentially very time consuming then use is made of these known patterns to reduce the number of calculations involved. To explain the pattern in the matrices formed consider the following 3 bladed turbine.

The cross spectral matrix is comprised of a number of smaller cross matrices. These are for the cross power between blade elements on the same blade and cross power between elements on different blades. The rotor cross power matrix can thus be illustrated as follows for the 3 bladed turbine:

Cross Power Spectra between blade elements

$$\begin{bmatrix} b1,b1 & b1,b2 & b1,b3 \\ b2,b1 & b2,b2 & b2,b3 \\ b3,b1 & b3,b2 & b3,b3 \end{bmatrix}$$

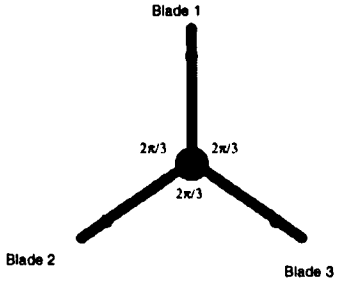

3 bladed turbine rotor

The cross power terms between elements on different rotors such as b1,b2 are affected by the angle between the two blades given by the equation: $\varphi_{b1,b2} = \frac{2\pi}{B}(b2 - b1)$. It can be seen that for the three bladed case then this angle can be either 2π/3 or 4π/3 rads. Now 4π/3 is the same as 2π/3 and so it should only be necessary to calculate one of these angles.

The following routines calculate only the necessary angles and then manipulate the matrices to fill in the other missing sections. For a three bladed turbine these angles are 0 and 2π/3 rads., while for two bladed rotors they are 0 and π rads. The corresponding angle for -2π/3 is derived by taking the complex conjugate of the submatrix obtained for the +2π/3 case. For the two bladed turbine the angle of -π is simply the same as for +π.

The sub matrices for the primary angles can be seen to be symmetric about the leading diagonal. To further reduce the calculation time only the lower half of the matrix shall be evaluated and then this then mirrored about the leading diagonal to form the completed submatrix. This is accomplished using the following Mathcad sub program.

```
SG_ij(G, φ, ω) | M ← 0
               | for i ∈ 1 .. N_e
               |   for j ∈ 1 .. i
               |     M_i,j ← G_ri,rj(φ, ω)
               | for j ∈ 2 .. N_e                 < Calculate the bottom half of the matrix
               |   for i ∈ 1 .. j − 1
               |     M_i,j ← M_j,i                < Mirror the matrix about the leading diagonal
               | M
```

Now we can calculate the sub matrices for the primary angles for a range of frequencies ω. These take the form of a vector of nested matrices. Expressions are presented for both two and three bladed turbines. The 0th angle is common to both. The global cross power matrix is then formed directly and the form is given below for either turbine. Disable the equations you do not wish to use.

Common to 2 & 3 bladed rotors: $G_{0_k} \quad SG_{ij}(G_{uu}, 0, \omega_k)$

2 bladed rotors

$G_{\pi_k} \quad SG_{ij}(G_{uu}, \pi, \omega_k)$

$TG_k \quad \begin{bmatrix} G_{0_k} & G_{\pi_k} \\ G_{\pi_k} & G_{0_k} \end{bmatrix}$

3 bladed rotors:

$G_{\varphi_k} \quad SG_{ij}(G_{uu}, \frac{2\pi}{3}, \omega_k)$

$TG_k \quad \begin{bmatrix} G_{0_k} & G_{\varphi_k} & G_{\varphi_k} \\ G_{\varphi_k} & G_{0_k} & G_{\varphi_k} \\ G_{\varphi_k} & G_{\varphi_k} & G_{0_k} \end{bmatrix}$

Toggle as appropriate

The above calculations have derived the cross spectra in terms of a 5 dimensional matrix (i.e. for each value of k, TG gives a matrix of nested matrices. These are combined into one matrix using the following Mathcad sub program

```
combine(G)   M ← G[1,1]
             for k ∈ 2..B
               M ← stack(M, G[k,1])
             for l ∈ 2..B
               tmp ← G[1,l]
               for k ∈ 2..B
                 tmp ← stack(tmp, G[k,l])
               M ← augment(M, tmp)
             M
```

Calculate the cross spectral matrices for each frequency ω. The matrices are nested in a vector G_{blade} where each vector element represents a frequency ω_k.

$G_{blade_k} \quad combine(TG_k)$

Save the matrix

WRITEPRN('blade.prn") G_{blade}

OR - >

Read in a previously saved matrix:

G_{blade} READPRN("blade.prn")

View the graphs for some of the above cross spectra:

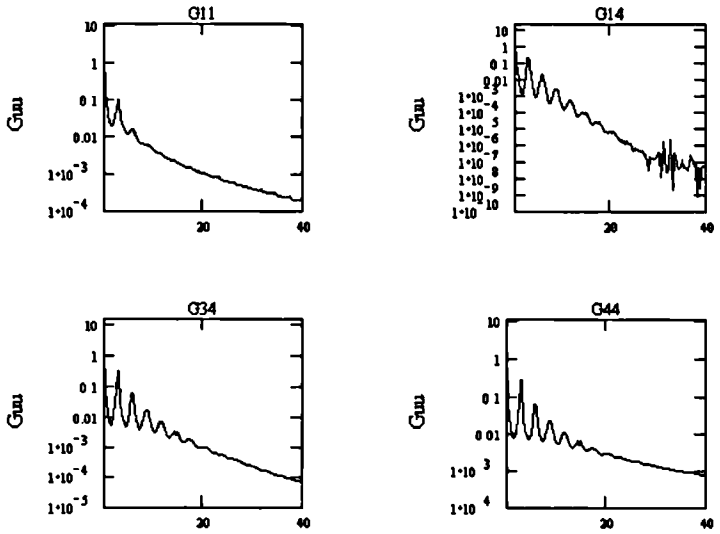

Determine the cross power spectra for the tower loading:

Assuming that the all the blades are identical in a turbine then the behaviour of the complete rotor may be modelled to find such things as tower loading etc. (N.B. This is assuming that the blades are rigid. The following calculation derives cross spectra between each node on an equivalent blade this effectively is a single virtual blade which exhibits all the properties of the entire rotor.

Using the pre-combined 5 dimensional matrix sum each nested matrix of TG_k to give a single cross power matrix at each frequency ω_k for the virtual blade.

$$G_{rotor_k} \quad \sum_{i=1}^{B} \sum_{j=1}^{B} (TG_k)_{i,j}$$

Save this matrix to file.

WRITEPRN("rotor.prn") G_{rotor}

OR -->

Read in a previously saved matrix

G_{rotor} READPRN("rotor.prn")

View some of the rotor cross spectra:

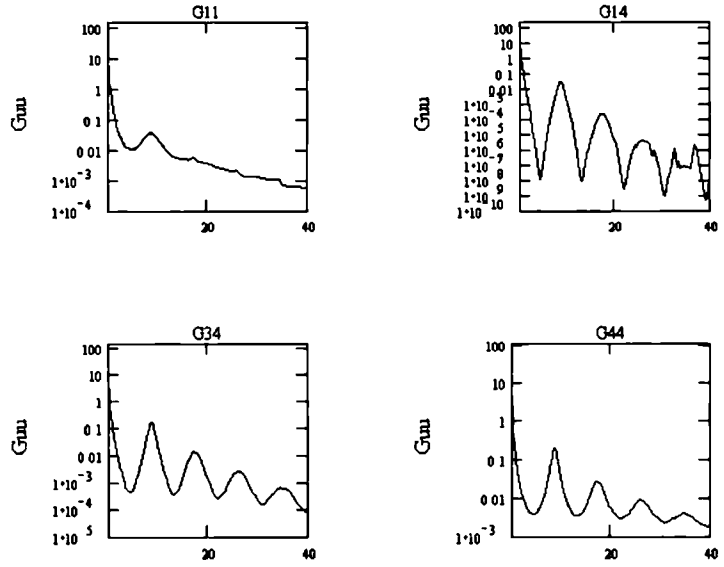

Determine the cross-power spectra for yaw and pitching moments at the tower top:

Define the hi and lo cut off points for variable n

$$lo(\omega) \quad floor\left(\frac{\omega}{B\,\Omega}\right) \quad 2 \qquad\qquad hi(\omega) \quad floor\left(\frac{\omega}{B\,\Omega}\right) + 3$$

Define the cross-power terms between portions on the super element.

$$G_y(r_1, r_2, \varphi, \omega) \quad \frac{B^2}{4}\left[\sum_{n=lo(\omega)}^{hi(\omega)} K_n(r_1, r_2, n, (|\omega - B(n+1)\Omega|)\, G_u(\omega - B(n+1)\Omega) + K_n(r_1, r_2, n, (\omega - B(n-1)\Omega))\, G_u(\omega - B(n-1)\Omega)\right]$$

N B. φ is a dummy variable only included to maintain compatibility with the SG_{ij}( ) function

Calculate the cross-power matrix of yaw pitch loading

$$G_{yaw_k} \quad SG_{IJ}(G_y, 0, \omega_k)$$

Save the matrix: WRITEPRN("yaw prn") G_{yaw} OR > G_{yaw} READPRN("yaw prn

View some of the rotor cross spectra:

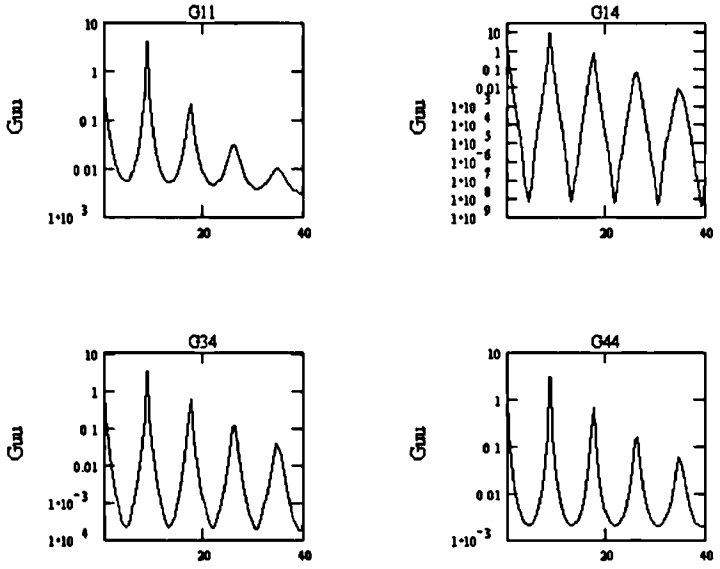

Appendix C

Linana Listing

Linana

Structural Dynamic Analysis of a Wind Turbine Rotor Blade

for the Turbana Development Model

Andrew Halfpenny ORIGIN 1

This worksheet calculates the dynamic response of a three bladed turbine to a turbulent wind field. It is split into several sections as follows.-

1) Dynamic analysis of a single rotor b ade This evaluates the undamped natural frequency of the b ade and can be used to check the FEA mesh and the input parameters.

2) Dynamic analysis of the tower This evaluates the undamped natural frequency of the tower structural with a lumped mass at the top This allows the tower model to be checked and also high ights any likely dynamic problems.

3) Dynamic analysis of the complete rotor and tower system including the generator and drive train This allows the force and moment to be calculated at any node in the structure due to virtual, oscillating forces being applied to the blades These results form a transfer function between blade loading and structural response at some location. These are passed to another worksheet to evaluate the PSD response to turbulent wind loading

The equation of motion:

The dynamic motions can be obtained from the expression:-

$$M\ddot{x} + c\dot{x} + kx = F(t)$$

Where x(t) d splacement as a function of time
k G obal stiffness matrix
c Global damping matrix
M Global Mass/Inertia matrix

The Global stiffness matrix is derived in this worksheet from the element stiffnesses A co ordinate transform is carried out to take account of the twist and pitch of the blade so that the effective motions are determined in the tower co-ord nate system In addit on to the structural stiffnesses, centripetal stiffening of the rotor is a so mode led in the axis normal to the rotor disk (i e the axial direction) The rotor b ades are modelled in 4 degrees of freedom a lowing for flapwise and lead lag motions A number of e ements are used to model the blades The tower is modelled in 2 degrees of freedom allowing bending parallel to the incident wind again a number of e ements may be used to model the tower if required The induction generator is model ed as a damper on the low speed shaft.

The Global damping matrix is assembled in this worksheet with the values having been obtained from the *Aerana* aerodynamic analysis worksheet Terms are included for flap-wise and lead lag displacements and these have already been transformed into the global axis system Structural damp ng is NOT considered at this time

A prismoidal section is assumed for the calculation of the blade s structural properties. A tapering section is, however, employed for the element mass terms

Define the rotor parameters:

$R_h := 4.5$ Radius to root cut-out [m] $R := 20.5$ Rotor rad us [m]

$\beta_h := 0.0$ Blade twist at root cut-out $\beta_t := 0.02$ B ade twist at tip

$RPM := 27.7$ Revolutions per minute

$f_0 := \frac{RPM}{60}$ Rotor frequency [Hz], this may be expressed in rad/sec as - $f_0 = 0.462$

$\Omega := f_0 \cdot 2\pi$ i.e... $\Omega = 2.901$

Input Blade Data from Pre-processor Files:

The blade geometrical data is provided in the Aerana output file The Aerana analysis is car ied out for the airfoil section and ignores the root cut-out and any tip masses. These sections however are very significant structurally and therefore are be considered in the FEA analysis. The blade tip wi be modelled by an unloaded node while the root is modelled with the fo lowing number of nodes.

$root := 2$ Number of elements representing the blade root

Read in the *Aerana* data file $Prebu := READPRN("gaindamp.prn")$

Determine the number of elements in the blade $n := rows(Prebu) - root - 1$ i e $n = 7$

The number of nodes in the FEA model is therefore $nodes := n + 1$
see dia below

Define the ranging variable *ei* as the *element identity* $ei := 1..n$

Define the ranging variable *ni* as the *nodal identity* $ni := 1..nodes$

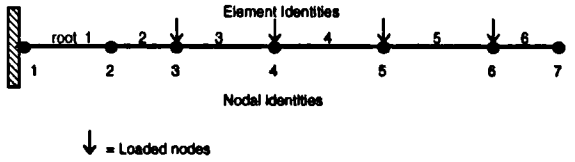

Typical FEA representation

$r_{ni} \quad if\left[ni=1,0,if\left[ni \le root+1,\frac{R_h(ni-1)}{root},if\left[ni=nodes,R,(Prebu^{<1>})_{ni-root-1}\right]\right]\right] \quad r_2 = 1.5$

$\beta_{ni} \quad if\left[ni \le root,0,if\left[ni=root+1,\beta_h,if\left[ni=nodes,\beta_t,(Prebu^{<3>})_{ni-root-1}\right]\right]\right]$

$g_{a_{ni}} \quad if\left[(ni<root+1) \cdot (ni=nodes),0,(Prebu^{<4>})_{ni-root-1}\right]$

$g_{t_{ni}} \quad if\left[(ni<root+1)+(ni=nodes),0,(Prebu^{<5>})_{ni-root-1}\right]$

$c_{a_{ni}} \quad if\left[(ni<root+1) \cdot (ni=nodes),0,(Prebu^{<6>})_{ni-root-1}\right]$

$c_{t_{ni}} \quad if\left[(ni<root+1)+(ni=nodes),0,(Prebu^{<7>})_{ni-root-1}\right]$

$\beta = \beta \cdot deg$

Review element data from Aerana file with root information included:

Rad us to blade node point $r^T = [0 \quad 1.5 \quad 4.5 \quad 6.5 \quad 10.5 \quad 14.5 \quad 18.5 \quad 20.5]$ [m]

Blade twist at node point $\beta^T = [0 \quad 0 \quad 0 \quad 13 \quad 4.85 \quad 2.02 \quad 0.14 \quad 0.02]$ deg

Effective blade pitch on each element $\beta_{ei} \quad \beta_{ei+1}$

$\beta^T = [0 \quad 0 \quad 13 \quad 4.85 \quad 2.02 \quad 0.14 \quad 0.02 \quad 0.02]$ deg

Axia and tangential gain factors $g_a^T = [0 \quad 0 \quad 0 \quad 181 \quad 303.8 \quad 550.5 \quad 480.4 \quad 0]$ [N/m sec^{-1}]

$g_t^T = [0 \quad 0 \quad 0 \quad 127.5 \quad 177.9 \quad 212.1 \quad 176.9 \quad 0]$

Axial and tangential damping factors $c_a^T = [0 \quad 0 \quad 0 \quad 147.1 \quad 245.7 \quad 226.5 \quad 175.3 \quad 0]$

$c_t^T = [0 \quad 0 \quad 0 \quad 18.77 \quad 17.3 \quad 8.738 \quad 3.731 \quad 0]$

element length $Le_{ei} \quad r_{ei+1} - r_{ei}$

Evaluate the node positions:

Calculate the length of each blade element. $Le^T = [1.5 \quad 3 \quad 2 \quad 4 \quad 4 \quad 4 \quad 2]$

radius vector $r_{n_{ni}} \quad if\left(ni=1,0,\sum_{n=1}^{ni-1} Le_n\right)$

Derive radius vector to each node $r_n^T = [0 \quad 1.5 \quad 4.5 \quad 6.5 \quad 10.5 \quad 14.5 \quad 18.5 \quad 20.5]$

Create a table showing the number of DOF at each node. $dofs_{ni} = 4$

start(dofs) $\left|\begin{array}{l} s_1 \leftarrow 1 \\ \text{for } i \in 2..last(dofs) \\ \quad s_i \leftarrow s_{i-1} + dofs_{i-1} \\ s \end{array}\right.$ $dof_n = stack(dofs^T, start(dofs)^T)$

$$dof_n = \begin{bmatrix} 4 & 4 & 4 & 4 & 4 & 4 & 4 & 4 \\ 1 & 5 & 9 & 13 & 17 & 21 & 25 & 29 \end{bmatrix}$$

Total number of DOFs in the global matrix $n_m \ge dof_n^{T<1>}$ $n_m = 32$

Topology table for the rotor blade elements and node points:

The element topology table is defined by $TOP_{blade}^{<ei>} \quad ei \quad ei \quad ei+1$

each column represents an element

$$TOP_{blade} = \begin{bmatrix} 1 & 2 & 3 & 4 & 5 & 6 & 7 \\ 1 & 2 & 3 & 4 & 5 & 6 & 7 \\ 2 & 3 & 4 & 5 & 6 & 7 & 8 \end{bmatrix}$$

<-- Element property reference

<-- element joins Node a

< to Node b

The nodal topology matrix is defined by $nTop_{blade}^{<ni>} \quad ni \quad ni$

Therefore the nodal topology table is:

$$nTop_{blade} = \begin{bmatrix} 1 & 2 & 3 & 4 & 5 & 6 & 7 & 8 \\ 1 & 2 & 3 & 4 & 5 & 6 & 7 & 8 \end{bmatrix}$$

<-- Node

<- Node property reference

Include the FEA algorithms from #fea mcd

Reference C:\usr\Appendix\#fea mcd

Input the structural data from the data file:

The structural data file gives mass and stiffness values at points along the rotor blade. These points do not necessar ly correspond with the FEA node points and therefore require processing. The Mass/Inertia of each element is calculated and a lumped mass matrix constructed The average stiffness of the points given along the beam are also evaluated and used in the stiffness matrix The stiffness matrix assumes a uniform d stribution at this time.

Read in the data file Structin READPRN(structin prn") dp length($Structin^{<1>}$)

Number of data points along blade dp 14

r_m $Structin^{<1>}$

m $Structin^{<2>}$

In order to evaluate the mass and stiffness values at the nodes it is desirable to linearly interpolate the values between the data points

r_s $Structin^{<3>}$

flap $Structin^{<4>}$

lag $Structin^{<5>}$

Interpolate the masses along the blade [kg/m] me(radius) linterp $(r_m, m, radius)$

Interpolate the stiffness [N mm²] in flapping Ely(radius) linterp $(r_s, flap, radius)$

" lead-lag Elz(radius) linterp $(r_s, lag, radius)$

Calculate the Lumped Mass element matrix for each element

This calculation assumes a linear mass distribution.

Calculate the mass of each e ement:

$$Me_{el} \int_0^{Le_{el}} me\left(r_{n_{el}} + x\right) dx$$

Me^T $1.251 \cdot 10^3$ 813.875 230 380 314 221.5 43]

Calculate the 1st moment on the element about the LHS node:

$$Z_{L_{el}} \int_0^{Le_{el}} me\left(r_{n_{el}} + x\right) x\, dx$$

Z_L^T 938.25 803.068 220.667 749.333 593.333 408.167 32]

Calculate the RHS reaction force for each element:

$$R_R \overrightarrow{-\frac{Z_L}{Le}}$$

R_R^T = 625.5 267.689 110.333 187.333 148.333 102.042 16

Calculate the moment on the element about the RHS node

$$Z_{R_{el}} \int_0^{Le_{el}} me\left(r_{n_{el}} + x\right)\left(Le_{el} - x\right) dx$$

Z_R^T = [938.25 $1.639 \cdot 10^3$ 239.333 770.667 662.667 477.833 54

Calculate the LHS reaction forces for each element:

$$R_L \overrightarrow{\frac{Z_R}{Le}}$$

R_L^T = 625.5 546.186 119.667 192.667 165.667 119.458 27

Check that total mass of element = sum of reactions

$\left(\overrightarrow{R_L + R_R}\right)^T$ = $1.251 \cdot 10^3$ 813.875 230 380 314 221.5 43

Me^T [$1.251 \cdot 10^3$ 813.875 230 380 314 221.5 43

Check the total mass $\Sigma R_L + \Sigma R_R = 3.253 \cdot 10^3$ $\Sigma Me = 3.253 \cdot 10^3$

check the blade mass A Me A Me_1 $2.002 \cdot 10^3$

Evaluate the blade mass, root moment and centre of gravity.

Enter the root radius [m]: R_{root} 1.5

Blade mass from root to tip [kg] $Blade_{mass} \int_{1.5}^{R} me(x)\, dx$ $Blade_{mass}$ $2.003 \cdot 10^3$

Blade bending moment due to gravity [N] $Blade_{mom}$ 9.81 $\int_{1.5}^{R} me(x)\, x\, dx$ $Blade_{mom}$ $1.455 \cdot 10^5$

Blade centre of gravity from root [m] CofG $\frac{Blade_{mom}}{Blade_{mass}}$ CofG = 72.68

Evaluate simplified rotational inertial terms for the elements:

Consider the element shown in the diagram below. If an angular rotation of 1 rad is applied to the node the element will take the deflected form illustrated. The small mass *dm* will thus be displaced through a distance *y* m. If an angular acceleration of 1 rad/sec² is applied to the node then, assuming a quasi static response, the mass *dm* will have an acceleration of y m/sec². The rotational inertia of the element about the node may therefore be calculated as the sum of moments of *dm* about the node.

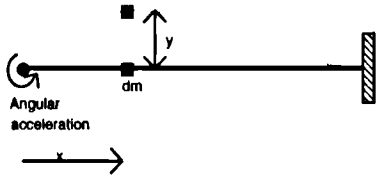

It is necessary first of all to consider the shape of the displaced element when subjected to a rotation of 1 radian at the node. From an analogy to the theory of structures we can see that this shape can be obtained by the superposition of two cantilevers as shown. The resultant shape is that of a propped cantilever.

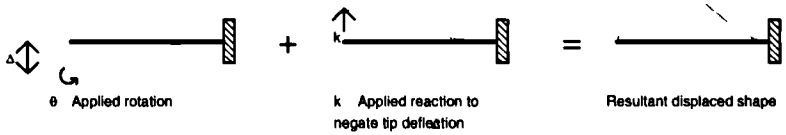

Consider the displacement of a cantilever subjected to a rotation of θ radians as shown above. The differential equation describing this shape is given as:

$$\frac{d^2}{dx^2}y = \theta \qquad \text{Integrating with respect to x yields.} \qquad \frac{d}{dx}y = \theta x + c$$

Where c is a constant of integration. Now when x=L then $\frac{d}{dx}y=0$ Therefore $c=\theta L$

Repeating the integration yields:

$$y=\theta L x - \frac{\theta x^2}{2} + c \qquad \text{Again, when x=L then y=0, therefore} \qquad c=-\frac{\theta L^2}{2}$$

The deflected shape is therefore given: $y=\theta L x - \frac{\theta x^2}{2} - \frac{\theta L^2}{2}$

The displacement at the tip (x=0) is therefore $y(0)=-\frac{\theta L^2}{2}$

Consider now the displaced shape of the cantilever subjected to a vertical reaction force as shown above. The differential equation describing this shape is given as:

$$\frac{d^2}{dx^2}y = k x \qquad \text{Integrating with respect to x yields} \qquad \frac{d}{dx}y = \frac{k x^2}{2} + c$$

Now when x = L then, $\frac{d}{dx}y=0$ Therefore $c=\frac{k L^2}{2}$

Repeating the integration yields:

$$y=\frac{k x^3}{6} - \frac{k L^2 x}{2} + c \qquad \text{Again, when x = L then y = 0, therefore} \qquad c=\frac{k L^3}{3}$$

The deflected shape is therefore given $y=\frac{k x^3}{6} - \frac{k L^2 x}{2} + \frac{k L^3}{3}$

The displacement at the tip (x=0) is therefore $y(0)=\frac{k L^3}{3}$

In order for both deflected shapes to have the same tip displacement then,

$$\frac{k L^3}{3} = \frac{\theta L^2}{2} \qquad \text{i.e.} \qquad k=\frac{3\theta}{2L}$$

By the principle of superposition the resultant displacement may be found as.

$$y=\theta L x - \frac{x^2}{2} - \frac{L^2}{2} + \theta \frac{x^3}{4L} - \frac{3 L x}{4} + \frac{L^2}{2}$$

Simplifying this yields $y=\frac{\theta x}{4L}(x-L)^2$

Now we want to know what the values of y are for a unit rotation of the propped cantilever. Differentiating the above with respect to x yields.

$$\frac{d}{dx}y=\frac{3\theta}{4L}(x-L)^2 + \frac{3}{2}\theta\frac{x}{L}(x-L) \qquad \text{Now at x = 0 then the required rotation is 1}$$

i.e.... $1=\frac{3}{4}\theta L$ Therefore rearranging to find θ $\theta=\frac{4}{L}$

Substituting this into the equation yields. $y(x,L)=\frac{x}{L^2}(x-L)^2$

The moments of inertia of the element about the nodes may be calculated. Taking moments about the LHS node for each element:

$$I_{L_{el}} \int_0^{Le_{el}} mc\, r_{n_{el}} + x\big)\, y\big(x, Le_{el}\big)\, x\, dx$$

$$I_L^T \quad 93\,825 \quad 187\,976 \quad 30\,667 \quad 201\,067 \quad 166\,267 \quad 119\,715 \quad 5\,733$$

For the RHS the terms in x above are replaced with $(Le_e - x)$. On evaluation this results in the same formula as that above, therefore the inertia about each node is the same i.e. ...

$$I_R = I_L$$

Define the leading diagonal of the element mass matrices:

$$M_{el}(R_L, I_L, R_R, I_R) := \begin{bmatrix} R_L & 0 & 0 & 0 & 0 & 0 & 0 & 0 \\ 0 & R_L & 0 & 0 & 0 & 0 & 0 & 0 \\ 0 & 0 & I_L & 0 & 0 & 0 & 0 & 0 \\ 0 & 0 & 0 & I_L & 0 & 0 & 0 & 0 \\ 0 & 0 & 0 & 0 & R_R & 0 & 0 & 0 \\ 0 & 0 & 0 & 0 & 0 & R_R & 0 & 0 \\ 0 & 0 & 0 & 0 & 0 & 0 & I_R & 0 \\ 0 & 0 & 0 & 0 & 0 & 0 & 0 & I_R \end{bmatrix}$$

Assemble the global Mass matrix:

First of all a vector of matrices will be formed called MT This is a list of 8x8 element matrices which are later used to assemble the global mass matrix

$$MT_{el} := M_{el}(R_{L_{el}}, I_{L_{el}}, R_{R_{el}}, I_{R_{el}})$$

Form a zero matrix $M := 0$

Assemble the global mass matrix

$$M := Ass_{global}(MT, TOP_{blade}, dof_n)$$

Calculate the elemental stiffness matrix:

The average stiffness at the data points is calculated and used in the Stiffness matrix

Average flapping

$$ave_y(r_1, r_2) := \frac{1}{r_2 - r_1} \int_{r_1}^{r_2} Ely(r)\,dr$$

Average Lead lag

$$ave_z(r_1, r_2) := \frac{1}{(r_2 - r_1)} \int_{r_1}^{r_2} Elz(r)\,dr$$

Therefore the average stiffnesses may be calculated for each element as follows

$$Ely_{el} := ave_y(r_{n_{el}}, r_{n_{el+1}})$$

$$Ely^T = \begin{matrix} 1.601 \cdot 10^9 & 2.645 \cdot 10^8 & 1 \cdot 10^8 & 3.467 \cdot 10^7 & 7.915 \cdot 10^6 & 1.641 \cdot 0^6 \end{matrix}$$

$$Elz_{el} := ave_z(r_{n_{el}}, r_{n_{el+1}})$$

$$Elz^T = \begin{matrix} 1.601 \cdot 10^9 & 3.085 \cdot 10^8 & 2.225 \cdot 10^8 & 8.897 \cdot 10^7 & 2.35 \cdot 10^7 & 1.586 \cdot 1(\end{matrix}$$

Define the local stiffness matrix for a 4DOF blade beam:

The stiffness matrix for a 4DOF beam element with bending about the 2 axes can be written as follows. For this case Ely is the flap-wise stiffness and Elz is the lead-lag stiffness L is the length of element.

$$k_e(Ely, Elz, L) := \begin{bmatrix} \frac{12\,Elz}{L^3} & 0 & 0 & \frac{6\,Elz}{L^2} & \frac{12\,Elz}{L^3} & 0 & 0 & \frac{6\,Elz}{L^2} \\ 0 & \frac{12\,Ely}{L^3} & \frac{6\,Ely}{L^2} & 0 & 0 & \frac{12\,Ely}{L^3} & \frac{6\,Ely}{L^2} & 0 \\ 0 & \frac{6\,Ely}{L^2} & \frac{4\,Ely}{L} & 0 & 0 & \frac{6\,Ely}{L^2} & \frac{2\,Ely}{L} & 0 \\ \frac{6\,Elz}{L^2} & 0 & 0 & \frac{4\,Elz}{L} & \frac{6\,Elz}{L^2} & 0 & 0 & \frac{2\,Elz}{L} \\ \frac{12\,Elz}{L^3} & 0 & 0 & \frac{6\,Elz}{L^2} & \frac{12\,Elz}{L^3} & 0 & 0 & \frac{6\,Elz}{L^2} \\ 0 & \frac{12\,Ely}{L^3} & \frac{6\,Ely}{L^2} & 0 & 0 & \frac{12\,Ely}{L^3} & \frac{6\,Ely}{L^2} & 0 \\ 0 & \frac{6\,Ely}{L^2} & \frac{2\,Ely}{L} & 0 & 0 & \frac{6\,Ely}{L^2} & \frac{4\,Ely}{L} & 0 \\ \frac{6\,Elz}{L^2} & 0 & 0 & \frac{2\,Elz}{L} & \frac{6\,Elz}{L^2} & 0 & 0 & \frac{4\,Elz}{L} \end{bmatrix}$$

The blade of the wind turbine has a pitch and twist associated with it β. The values of β at the node points has been calculated using Aerana and stored in a file Aerana The transformation of the blade element stiffnesses from the local flap and lead-lag axes to the global tower axes can be made via the following transformation matrix:

$$\phi_\beta(\beta) = \begin{bmatrix} \cos(\beta) & \sin(\beta) & 0 & 0 & 0 & 0 & 0 & 0 \\ \sin(\beta) & \cos(\beta) & 0 & 0 & 0 & 0 & 0 & 0 \\ 0 & 0 & \cos(\beta) & \sin(\beta) & 0 & 0 & 0 & 0 \\ 0 & 0 & -\sin(\beta) & \cos(\beta) & 0 & 0 & 0 & 0 \\ 0 & 0 & 0 & 0 & \cos(\beta) & \sin(\beta) & 0 & 0 \\ 0 & 0 & 0 & 0 & -\sin(\beta) & \cos(\beta) & 0 & 0 \\ 0 & 0 & 0 & 0 & 0 & 0 & \cos(\beta) & \sin(\beta) \\ 0 & 0 & 0 & 0 & 0 & 0 & -\sin(\beta) & \cos(\beta) \end{bmatrix}$$

The element stiffness matrix is now determined in the global co-ordinate system as follows:-

$$k_s(Ely\ Elz, L, \beta) \quad \phi_\beta(\beta)^T k_e(Ely, Elz, L)\, \phi_\beta(\beta)$$

Assemble the global structural stiffness matrix K_s:

Form a zero matrix $K_s \quad 0$

First of all assemble a vector of element matrices called KT. This is a list of 8x8 element matrices which are later used to assemble the global stiffness matrix.

The augmented array KT may thus be formed:-

$$KsT_{ei} \quad k_s\ Ely_{ei}, Elz_{ei}, Le_{ei}, \beta_{ei})$$

Now assemble the global stiffness matrix:

$$K_s \quad Ass_{global}\ KsT, TOP_{blade}, dof_n)$$

It is also desirable to obtain vectors of elemental stiffnesses and co-ordinate transformation matrices for use later in the backsubstitution section.

$$KeT_{ei} \quad k_e\ Ely_{ei}, Elz_{ei}, Le_{ei}) \qquad \phi T_{ei} \quad \phi_\beta\ \beta_{ei})$$

Centripetal stiffening matrix:

In addition to the structural stiffnesses there are also centripetal stiffnesses caused by the rotation of the blades. The centripetal stiffness in flapping can represented by the following matrix

Must also include lead lag stiffening later!

$$k_c(L, T) \begin{bmatrix} 0 & 0 & 0 & 0 & 0 & 0 & 0 & 0 \\ 0 & \frac{T}{L} & 0 & 0 & 0 & \frac{T}{L} & 0 & 0 \\ 0 & 0 & 0 & 0 & 0 & 0 & 0 & 0 \\ 0 & 0 & 0 & 0 & 0 & 0 & 0 & 0 \\ 0 & 0 & 0 & 0 & 0 & 0 & 0 & 0 \\ 0 & \frac{T}{L} & 0 & 0 & 0 & \frac{T}{L} & 0 & 0 \\ 0 & 0 & 0 & 0 & 0 & 0 & 0 & 0 \\ 0 & 0 & 0 & 0 & 0 & 0 & 0 & 0 \end{bmatrix}$$

Assemble the global centripetal stiffness matrix K_c:

First of all calculate the centrifugal force at each node [N].

The total mass at each node may be found from

$$Mass_{ei+1} \quad R_{R_{ei}} \qquad Mass_{ei} \quad Mass_{ei} \quad R_{L_{ei}}$$

The centrifugal force at each node is therefore $cf \quad Mass\ r_n\ \Omega^2$

$$cf^T = \begin{bmatrix} 0 & 1.479 \cdot 10^4 & 1.467 \cdot 10^4 & 1.657 \cdot 10^4 & 3.119 \cdot 10^4 & 3.267 \cdot 10^4 & 2.009 \cdot 10^4 & 2.76 \cdot 10^3 \end{bmatrix}$$

And the tension force [N] at each node may now be calculated - $Te_{ni} \quad \sum_{n=ni}^{nodes} cf_n$

$$Te^T = \begin{bmatrix} 1.327 \cdot 10^5 & 1.327 \cdot 10^5 & 1.179 \cdot 10^5 & 1.033 \cdot 10^5 & 8.671 \cdot 10^4 & 5.552 \cdot 10^4 & 2.285 \cdot 10^4 & 2.76 \cdot 10^3 \end{bmatrix}$$

Form a zero matrix $K_c \quad 0$

First of all assemble an augmented array called KT This is a list of 8x8 element matrices which are later used to assemble the global stiffness matrix.

The augmented array KT may thus be formed:-

$$KcT_{el} \quad k_c \; Le_{el}, Te_{el}$$

Now assemble the global centripetal stiffness matrix:

$$K_c \quad Ass_{global} \; KcT \; TOP_{blade} \; dof_n$$

Derive the total stiffness matrix:

The total stiffness matrix is the sum of the structural and centripetal stiffness matrices and is obtained by

$$K \quad K_s + K_c$$

Natural Frequency Analysis:

Deta is are available from Nedwind regarding the natural frequency of the blades when mounted to a rigid hub. It is desirable at this stage to ascertain the the calculated natural frequency in order to compare the model with the measured result.

A fixed hub stiffness and mass matrix may be formulated by deleting the first 4 rows and columns from the respective matrices.

$$K_{fxd} \quad submatrix(K_s, 5, n_m, 5, n_m) \qquad M_{fxd} \quad submatrix\ M, 5, n_m, 5, n_m$$

$$hub_{4, n_m} \quad 4 \quad 0$$

The Un-damped natural frequencies and relevant mode shapes of the blade may now be evaluated The equation of motion of the blade may be written.

$$M\, x'' + K\, x = 0$$

Rearranging this in the form $x'' + M^{-1} K\, x = 0$

and defining the matrix $Z_{fxd} \quad M_{fxd}^{-1} K_{fxd}$

the eigen values and vectors may be determined

Natural frequency [Hz] $\overrightarrow{\sqrt{eigenvals(Z_{fxd})}}$ Eigen vectors

$$f_{n\,fxd} \quad \frac{\overrightarrow{\sqrt{eigenvals(Z_{fxd})}}}{2\pi} \qquad \varepsilon_{n\,fxd} \quad stack\ hub, eigenvecs\ Z_{fxd}))$$

$f_{n\,fxd}^T =$ | 34.077 | 33.593 | 24 659 | 19.667 | 20 771 | 11 845 | 8 398 | 9 411 | 2 507 | 4 412 |

Consider now the lower frequency harmonics. We are interested in the in-plane (z) and out-of plane (y) displacements of the blade. The elements in the matrix relating to these may be determined by:-

In-plane modes $iz_{ni} \quad (ni \quad 1)\, dof_{n_{1\,ni}} + 1$

$iz^T = [\, 1 \;\; 5 \;\; 9 \;\; 13 \;\; 17 \;\; 21 \;\; 25 \;\; 29 \,]$

Out-of-plane $iy \quad \overrightarrow{-iz + 1}$

$iy^T = [\, 2 \;\; 6 \;\; 10 \;\; 14 \;\; 18 \;\; 22 \;\; 26 \;\; 30$

The normalised displacements of the nodes for the m^{th} mode can be obtained by the expression:

$$m \quad 1 \; n_m \quad 4$$

$$z_{ni,m} \quad \varepsilon_{n\,fxd}(iz_{ni}\ m) \qquad y_{ni+1,m} \quad \varepsilon_{n\,fxd}\ iy_{ni},m$$

Find the first mode flapping and Lead-lag modes:

Select mode to be plotted a 28

Frequency of the mode [Hz] $f_{n\,fxd_a} = 1.548$

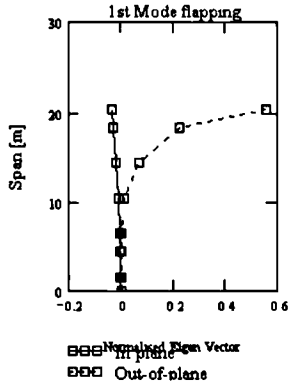

Select mode to be plotted a 26

Frequency of the mode [Hz] $f_{n\,fxd_a} = 2.507$

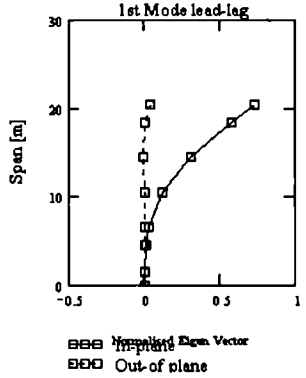

Determine the Damping matrix:

The aerodynamic damping factors for each element may be evaluated from the data given by Aerana The gain factors g_a and g_t give the damping with respect to the airflow perpendicu ar to the rotor plane. g_a is the flapping damping while g_t is the tangential Similarly the damping factors c_a and c_t give the damping with respect to the tangential airflow This effectively couples the flapping and lead-lag components.

N B. it is assumed that the damping is linear within the velocity range cons dered This is delt with in the study Aerana

The damping matrix will be developed using the methodology employed for the stiffness matrix For this however we shall be dealing with the nodes instead of the elements as Aerana evaluates the damping at each node and not over each element

Form a zero matrix C 0

Define the nodal damping matrix:

$$C_{node}(c_t, c_a, g_t, g_a) \begin{bmatrix} c_t & g_t & 0 & 0 \\ c_a & g_a & 0 & 0 \\ 0 & 0 & 0 & 0 \\ 0 & 0 & 0 & 0 \end{bmatrix}$$

In the same way as before, a vector of nodal matrices CT is assembled.

$$CT_{ni} \quad C_{node}(c_{t_{ni}}, c_{a_{ni}}, g_{t_{ni}}, g_{a_{ni}})$$

The damping matrix will be defined later in the worksheet as the tower and drive train have still to be defined.

Evaluation of the virtual linear transfer function:

The virtual transfer function is defined as the loading produced by a unit amplitude eddy hitting the blade The eddy is effectively the sinusoidal fluctuation of wind speed on the blade. This is solved in the frequency domain.

Define the matrix of gain factors for the unit wind loading, note these should include the cross terms for tangential effects caused by axial wind speed fluctuations.

The gain factors are again given for the nodes and not the elements The gain matrix may therefore be assembled as for the damping matrix First the single blade case will be derived and this then used to form the global matrix.

Form a zero matrix G 0

Define the nodal gain matrix·

$$G_{node\ g_t, g_a} \begin{matrix} 0 & g_t & 0 & 0 \\ 0 & g_a & 0 & 0 \\ 0 & 0 & 0 & 0 \\ 0 & 0 & 0 & 0 \end{matrix}$$

In the same way as before an augmented array GT is assembled of the nodal gain matrices.

$$GT_{ni} \quad G_{node\ g_{t_{ni}}\ g_{a_{ni}}}$$

The damping matrix w l be defined later in the worksheet as the tower and drive train have still to be defined.

Derive new transform matrices for the blades with a given angle in the azimuth plane:

A co-ordinate transformation is required to transform the blade co-ordinate system into the tower system to take account of the azimuth position of the blades Ordinarily this would be done by transforming the whole length of the blade into the global co-ordinate system This causes problems with this particular analysis as it would involve a pitching mode being added to the blades No data is available for pitching stiffnesses and so this wi l cause problems To overcome these t is proposed that only the blade root node be transposed into the global system The b ade root element therefore needs transforming in a rather unusual way to allow it to have 4DOF at one node and 6DOF at the other.

The following transformation procedure involves pre multiplying each nodal submatrix within the element matrix by the transformation matrix The new element matrix layout is as follows

Make original 4x4 node matrix into a 6x6 6x4 and 4x6 matrix by packing rows and columns with zero This is indicated by

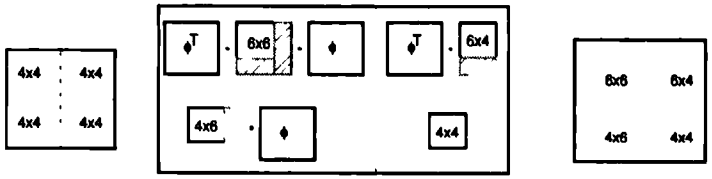

ϕ and ϕ^T are the transfer matrix and its transpose respectivly

The transformation matrix is defined by:

$$\phi_{azimuth(\varphi)} \begin{bmatrix} \sin(\varphi) & \cos(\varphi) & 0 & 0 & 0 & 0 \\ 0 & 0 & 1 & 0 & 0 & 0 \\ 0 & 0 & 0 & \sin(\varphi) & \cos(\varphi) & 0 \\ 0 & 0 & 0 & 0 & 0 & 1 \\ \cos(\varphi) & \sin(\varphi) & 0 & 0 & 0 & 0 \\ 0 & 0 & 0 & \cos(\varphi) & \sin(\varphi) & 0 \end{bmatrix}$$

The following routine manipulates the element matrix as described in the diagram:

$trans(M,\phi,\varphi) :=$

$M_{11} \leftarrow submatrix(M,1,4,1,4)$ — Split the element matrix into its nodal sub matrices

$M_{11_{6,6}} \leftarrow 0$

$M_{21} \leftarrow submatrix(M,5,8,1,4)$

$M_{21_{4,6}} \leftarrow 0$

$M_{12} \leftarrow submatrix(M,1,4,5,8)$

$M_{12_{6,4}} \leftarrow 0$

$M'_{22} \leftarrow submatrix(M,5,8,5,8)$ — Evaluate the transformed nodal sub matrices

$M'_{11} \leftarrow (\phi(\varphi))^{T} M_{11} \phi(\varphi)$

$M'_{21} \leftarrow M_{21} \phi(\varphi)$

$M'_{12} \leftarrow (\phi(\varphi))^{T} M_{12}$

$N_1 \leftarrow augment(M'_{11}, M'_{12})$ — Assemble the nodal sub matrices into the new element matrix

$N_2 \leftarrow augment(M'_{21}, M'_{22})$

$N \leftarrow stack(N_1, N_2)$

$Insert_{dof}(N,6)$

Define the new transformed stiffness matrices for the first root element of the blades:

Enter the number of blades and the rotor setting angle of the first blade:

$B := 3$ $\varphi := 0\,deg$

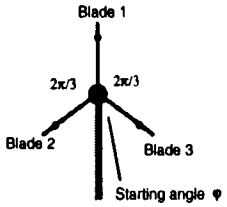

$node_{transform}(T,\varphi) :=$

$\theta \leftarrow \frac{2\pi}{B}$

$LAST \leftarrow last(T)$

for $i \in 1..B$

$tmp \leftarrow trans\left[T_1, \phi_{azimuth}, (\varphi + (i-1)\theta)\right]$

$T_{LAST+i} \leftarrow tmp$

T

$MT := node_{transform}(MT,\varphi)$

$KsT := node_{transform}(KsT,\varphi)$

$KeT := node_{transform}(KeT,\varphi)$

$KcT := node_{transform}(KcT,\varphi)$

The co-ordinate transformation vector ϕT also requires updating. The new transformations take the form of a 11x11 identity matrix. This is evaluated as follows

$add_{\phi}(T) :=$

$LAST \leftarrow last(T)$

for $i \in 1..B$

$T_{LAST+i} \leftarrow identity(11)$

T

$\phi T := add_{\phi}(\phi T)$

Input the Tower data:

It is uncommon for detailed tower properties to be given by turbine manufactures and the engineer is usually left with the job of estimating the structural stiffness For this part of the worksheet it is assumed that the tower has a linear variation in mass and stiffness These are evaluated from the diameter & steel thickness of a conical tower

The simple tower model is shown in the diagram below:-

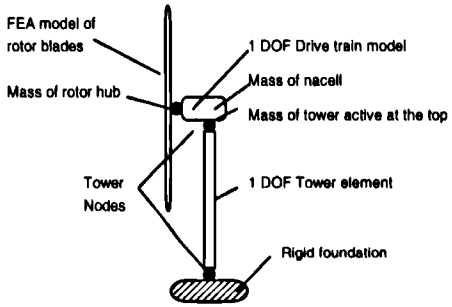

Simplified tower element

Height of tower [m]: $H_T := 35$

Rotor offset from tower centre [m] $Offset := 2.21$

Total mass of rotor blades [kg] $M_B := B \cdot (Me + Me_1)$ $M_B = 6.007 \cdot 10^3$

Mass of rotor hub [kg] $M_H := 4.6 \cdot 10^3$

Total mass of rotor [kg] $M_R := M_B + M_H$ $M_R = 1.061 \cdot 10^4$

Mass of nacelle [kg] $M_N := 21280$

Total mass at tower top (excluding the blade mass which is included in the blade elemental models) [kg] $M_{T\,top} := M_H + M_N$ $M_{T\,top} = 2.588 \cdot 10^4$

(***note*** : make sure that mass of hub is not included twice)

Import the tower mass and stiffness matrices from the tower pre-processor:

Import the augmented mass and stiffness matrices: $Tower_{mat} := READPRN("tower.prn")$

Split the matrices to determine the the separate mass and stiffness matrices

$M_T := submatrix(Tower_{mat}, 1, 12, 1, 12)$

$K_{eT} := submatrix(Tower_{mat}, 1, 12, 13, 24)$

$M_T := Insert_{dof}(M_T, 7)$

$K_{eT} := Insert_{dof}(K_{eT}, 7)$

Input Gearbox and Generator data:

The generator is modelled as a damper on the low speed shaft.

Damping from generator

Turbine rated capacity [watts] $P_r := 6 \cdot 10^5$

Torque [N m] $Torque := \frac{P_r}{\Omega}$ $Torque = 2.068 \cdot 10^5$

Slip at rated power $slip := 0.8\%$

∴ slip speed [rad/sec] $slip_{speed} := slip \cdot \Omega$ $slip_{speed} = 0.023$

Coefficient of damping $C_h := \frac{Torque}{slip_{speed}}$ $C_h = 8.913 \cdot 10^6$

Stiffness of drive train:

This value may be placed at zero for an induction generator unless another figure is available $k_h := 0$

Inertia of drive train:

Gearbox ratio $G_R := 50.0$

Inertia of items on high speed shaft [kg m²] $J_{hss} := 12$ (generator inertia)

Inertia of items on low speed shaft [kg m²] $J_{lss} := 50000$ (transmission inertia)

. the total inertia on the drive train [kg m²]

$M_h := J_{lss} + G_R^2 \cdot J_{hss}$ $M_h = 8 \cdot 10^4$

Define the Tower and Drive train element matrices:

To prevent any possible conditioning problems the drive train inertia's and damping are incorporated in the tower top node.

Mass...

The modified tower mass matrix allowing for the nacelle mass is found by:

$M_{T_{1,1}} := M_{T_{1,1}} + M_{T\,top} + M_B$

$M_{T_{2,2}} := M_{T_{2,2}} + M_{T\,top}$

$M_{T_{3,3}} := M_{T_{3,3}} + M_{T\,top}$

$M_{T_{7,7}} := M_{T_{7,7}} + M_h$

Stiffness...

There are three stiffness matrices for the blades These are the structural stiffness Ks, the centripetal stiffness Kc and the elemental stiffness. To maintain a common approach to the calculations (common topology table) it is necessary to derive a zero element matrix for the centripetal stiffness on the tower.

$K_{cT_{13,13}} := 0$

$K_{eT_{6,6}} := K_{eT_{6,6}} + k_h$ $K_{eT_{6,7}} := K_{eT_{6,7}} - k_h$

$K_{eT_{7,6}} := K_{eT_{7,6}} - k_h$ $K_{eT_{7,7}} := K_{eT_{7,7}} + k_h$

Blade co-ordinate transform ϕ_β ...

There is no transform associated with the tower element $\phi_T := identity(13)$

Damping:

The damping matrix again applies to a nodal position and not an element To maintain a common approach we shall again give the drive train damping as a nodal matrix as opposed to an elemental This should be added to the tower top node in the augmented damping matrix CT.

$$C_{T\,top} := \begin{bmatrix} 0 & 0 & 0 & 0 & 0 & 0 & 0 \\ 0 & 0 & 0 & 0 & 0 & 0 & 0 \\ 0 & 0 & 0 & 0 & 0 & 0 & 0 \\ 0 & 0 & 0 & 0 & 0 & 0 & 0 \\ 0 & 0 & 0 & 0 & 0 & 0 & 0 \\ 0 & 0 & 0 & 0 & 0 & C_h & -C_h \\ 0 & 0 & 0 & 0 & 0 & -C_h & C_h \end{bmatrix}$$

There is a zero damping matrix for the tower base node. It is necessary to define this node for the calculations. $C_{T\,base_{6,6}} := 0$

Aerodynamic gain:

There is no aerodynamic gain associated with the tower node so a zero gain matrix is defined. $G_{T\,base_{6,6}} := 0$ $G_{T\,top_{7,7}} := 0$

Augment these matrices to the property matrices, MT CT KsT & KcT, derived earlier for the blades.

$add_{prop}(M, T)$ $LAST \leftarrow last(T)$

$T_{LAST,1} \leftarrow M$

T

$MT \quad add_{prop}\, M_T, MT$ $\quad CT \quad add_{prop}\, C_{T\,base}, CT$ $\quad GT \quad add_{prop}\, G_{T\,base}, GT$

$KsT \quad add_{prop}\, K_{eT}, KsT$ $\quad CT \quad add_{prop}\, C_{T\,top}, CT$ $\quad GT \quad add_{prop}\, G_{T\,top}, GT$

$KcT \quad add_{prop}\, K_{cT}, KcT$ $\quad \phi T \quad add_{prop}\, \phi_T\, \phi T$

$KeT \quad add_{prop}\, K_{eT}, KeT$

Assemble the complete Mass, damping and stiffness matrices for the rotor and tower.

This section creates the global matrices for the analysis of the whole turbine structure.

Define topology table for the element properties:

Total number of nodes in the FEA representation: $n_n \quad B\,(nodes \quad 1) + 2 \qquad n_n = 23$

Total number of elements in the FEA representation: $n_{el} \quad B\,(nodes \quad 1) + 1 \qquad n_{el} = 22$

Define the ranging variable ei as the element identity $\quad ei \quad 1 \quad n_{el}$

Define the ranging variable ni as the nodal identity $\quad ni \quad 1 \quad n_n$

Define the ranging variable bi as the blade identity $\quad bi \quad 1 \quad B$

Create a table showing the number of DOF at each node $\quad dofs \quad 0 \qquad dofs_{ni} \quad 4$

Correct the last two nodes to allow for the 6DOF tower nodes. $\quad dofs_{n_n - 1} \quad 6 \qquad dofs_{n_n} \quad 7$

Create the table showing No of DOFs per node and the starting DOF for each node:

$dof_n \quad stack\left(dofs^T, start(dofs)^T\right)$

$$dof_n = \begin{bmatrix} 4 & 4 & 4 & 4 & 4 & 4 & 4 & 4 & 4 & 4 & 4 & 4 & 4 & 4 & 4 & 4 & 4 & 4 & 4 & 4 & 6 & 7 \\ 1 & 5 & 9 & 13 & 17 & 21 & 25 & 29 & 33 & 37 & 41 & 45 & 49 & 53 & 57 & 61 & 65 & 69 & 73 & 77 & 81 & 85 & 91 \end{bmatrix}$$

Calculate the total number of DOFs in the global matrices: $\quad n_m \quad \Sigma\, dof_n^{T\,\langle 1\rangle} \qquad n_m = 97$

Define the topology matrix:

```
Top = | for i ∈ 1 .. nodes - 2
      |   tmp_i ← i
      | v ← tmp + 1
      | w ← tmp
      | x ← tmp + 1
      | for j ∈ 1 .. B - 1
      |   | v ← stack(v, tmp + 1)
      |   | w ← stack(w, tmp + j·(nodes - 1))
      |   | x ← stack(x, tmp + 1 + j·(nodes - 1))
      | V ← stack(stack(v^T, w^T), x^T)
```

Augment the blade root and tower elements to this

$$Blade_{roots}^{\langle bi\rangle} \begin{bmatrix} (nodes - 1) \cdot bi \\ 23 \\ (nodes - 1)\,(bi - 1) - 1 \end{bmatrix} \quad Top \quad augment\,(Top, Blade_{roots})$$

Change the tower element to have the correct orientation

$$Tower_{el} \begin{bmatrix} last(KsT) \\ n_n \\ n_n - 1 \end{bmatrix} \quad Top \quad augment\,(Top, Tower_{el})$$

The new topology table is:-

1---2---3---- Element number --------->

Element--> property id

$$\text{Node 1 --> } Top = \begin{bmatrix} 2 & 3 & 4 & 5 & 6 & 7 & 2 & 3 & 4 & 5 & 6 & 7 & 2 & 3 & 4 & 5 & 6 & 7 & 8 & 9 & 10 & 11 \\ 1 & 2 & 3 & 4 & 5 & 6 & 8 & 9 & 10 & 11 & 12 & 13 & 15 & 16 & 17 & 18 & 19 & 20 & 23 & 23 & 23 & 23 \\ 2 & 3 & 4 & 5 & 6 & 7 & 9 & 10 & 11 & 12 & 13 & 14 & 16 & 17 & 18 & 19 & 20 & 21 & 1 & 8 & 15 & 22 \end{bmatrix}$$

Node 2 -->

Two important elements to consider are the tower and the blade root elements. These have the following element references.

$BladeRoot \quad 1 \qquad Tower \quad cols(Top) \qquad Tower \quad 22$

(N.B.... the blade root element is taken as the first proper blade element, i.e the first 8x8 DOF element, not the special co-ordinate transformation element.)

Define the topology table for the nodal properties:

Define the first row of the rotor topology matrix. This is a list of all the node numbers.

$nTop_{ni} \quad ni$

Define the second row of the topology table This give the nodal property number for each node

$nPid$ for $i \in 1 \ldots nodes - 1$
$tmp_i \leftarrow i + 1$
$V \quad tmp^T$
for $i \in 1 \ldots nodes - 1$
$temp_i \leftarrow i - 1$
for $j \in 1 \ldots B - 1$
$V \leftarrow augment(V, temp^T)$
V

Augment the tower top property table to this

$nPid_{tower} \quad (nodes + 1 \quad nodes + 2)$ $nPid \quad augment(nPid, nPid_{tower})$

Stack the node numbers and the node property numbers:

$nTop \quad stack(nTop^T, nPid)$

The new topology table is

Node -->

nTop	1	2	3	4	5	6	7	8	9	10	11	12	13	14	15	16	17	18	19	20	21	22	23
	2	3	4	5	6	7	8	2	3	4	5	6	7	8	2	3	4	5	6	7	8	9	10

Nodal property identity -->

Assemble the global matrices:

Assemble the mass matrix: $M \quad Ass_{global}(MT, Top, dof_n)$

Assemble the structural stiffness matrix: $K_s \quad Ass_{global}(KsT, Top, dof_n)$

Assemble the centripetal stiffness matrix: $K_c \quad Ass_{global}(KcT, Top, dof_n)$

The total stiffness matrix is the sum of the structural and centripetal matrices:

$K \quad K_s + K_c$

Assemble the damping matrix: $C \quad nAss_{global}(CT, nTop, dof_n)$

Assemble the gain matrix: $G \quad nAss_{global}(GT, nTop, dof_n)$

<u>Evaluation of the dynamic response to virtual wind speed:</u>

Consider the unit virtual wind speed applied to the blade axially at each node in turn on each blade. Enter the node points for loading on the first blade, the program will calculate the remaining node points on the other blades.

Form a zero matrix with each column being a separate virtual loading vector:

Number of loading vectors per blade $n_v \quad 4$ $p \quad 1 \ldots n_v$

Apply virtual wind to nodes: $V_{b\,node_p}$

3
4
5
6

Form the zero matrix $V_{rows(K)\,n_v B} \quad 0$

Evaluate the node numbers for all the blades $q \quad 1 \ldots B$

V_{node} | for $p \in 1 \ldots n_v$
for $q \in 1 \ldots B$
$V_{p\,(q-1)\cdot n_v} \leftarrow V_{b\,node_p} + (q-1)(nodes - 1)$
V

Form the virtual loading vectors: $q \quad 1 \ldots last(V_{node})$

$V_{\left[dof_n\left(2, V_{node_q}\right)+1\,,\,q\right]} \quad 1$

Evaluation of the complex transfer function:

The motion equation for the above blade may be expressed as:

$M x'' + C x' + K x = G V$ Where G V g ves the virtual force due to the unit wind speed

Assum ng the response of the blades is sinusoidal then the solution to the differential equation takes the form.

$x = X e^{i \omega t}$

Therefore $x = i \omega X e^{i \omega t}$

$x = -\omega^2 X e^{i \omega t}$

Substituting these into the motion equat ons and simpl fying yields

$M \omega^2 + C i \omega + K X = G V$ i e.... [Z] . [X] = [G] . [V]

So the displacement vector X is found by rearranging th s:

$X = M \omega^2 \quad C i \omega \quad K^{-1} G V$

Before calculating this it is necessary to restrain the tower foundation node The following subprograms are developed to facilitate the manipulation of the global matrices to al ow the restraint and the release of any DOF in any node.

Restrain the tower foundation node in all DOFs:

The new global matrices have a .fxd subscript to distinguish them.

The tower base node is given as. $n_{T\,base} \quad n_n \quad 1$ $n_{T\,base} = 22$

Define a vector containing the DOFs to be restrained

Number of DOFs restrained $p \quad 1 \quad dof_{n_{1,n_{T\,base}}}$

$Tbase_{dof_p} \quad dof_{n_{2,n_{T\,base}}} \quad 1 \quad p$ $Tbase_{dof} =$

Form new .fxd matrices

M_{fxd} restrain M, $Tbase_{dof}$

C_{fxd} restrain C, $Tbase_{dof}$

K_{fxd} restrain K, $Tbase_{dof}$ $K_{s\,fxd}$ restrain K_s, $Tbase_{dof}$

G_{fxd} restrain G, $Tbase_{dof}$)

V_{fxd} Fix V, $Tbase_{dof}$ <-- N B. V is an augmented vector of virtual loads.

Evaluate the complex transfer function:

Put $Z(\omega) \quad M_{fxd} \omega^2 + C_{fxd} i \omega + K_{fxd}$ i e... [Z] [X] [G] [V]

Now the complex transfer function is defined by:

$H(\omega) \quad Z(\omega)^{-1}$ i.e.... [X] = [H] [G] [V]

The forces induced on the structure due to the virtual wind speeds is obtained by [F] [Ks] [X] where Ks is the structural stiffness However for the matrix solution used above a restraint was added for the tower foundation, these DOFs should be added back so that the tower base reaction forces may be calculated.

$X_{fxd}(\omega) \quad H(\omega) G_{fxd} V_{fxd}$

Adding back the restrained DOFs. $X(\omega) \quad Release\ X_{fxd}(\omega), Tbase_{dof}$

These are evaluated for each frequency ω taken from the Turbana output, the frequencies considered are:- (N.B. 7.5 secs/frequency on a 25MHz 486DX)

$\omega \quad READPRN("freq prn") \qquad k \quad 1 \quad last(\omega)$

Evaluate the displacement matrices for frequencies ω. $x_k \quad X \omega_k$

$x^T =$ [redacted]

{97,12} {97,12} {97,12} {97,12} {97,12} {9 12}

Calculate the elemental forces and moments:

These are calculated by back substituting the nodal displacements into the elemental stiffness matrix. We must also take account of the co-ordinate transformations in the blades. The formulation follows the formula

$F = K \phi x$ Where;
F Force in the element
K=element stiffness
ϕ twist angle in the blade, (zero for the tower)
x augmented displacement vectors calculated above

The generator has been included as a damping element and the following formula is used to derive the force on it:

$F = C \omega x$ Where;

Define the elements for which results should be calculated:

NB IT'S ASSUMED IN FURTHER PROGRAMS THAT THE FIRST TERM BE FOR THE TOWER ELEMENT, AND THE SECOND FOR THE BLADE ROOT ELEMENT!

THE USER MAY DEFINE OTHER ELEMENTS AFTER THIS SELECTION

In order to evaluate this we must first of all derive functions to parse the correct displacements The following function parses the nodal displacement matrix x_k for the element el.

$$\text{parse}_{el}(X\ el) \left| \begin{array}{l} \text{first}_{node} \leftarrow \text{submatrix}\left(X, \text{dof}_{n\ 2\ Top_{2\ el}}, \text{dof}_{n\ 2\ Top_{el}}, \text{dof}_{n\ 1, Top_{2\ el}}, 1, 1, \text{cols}(X)\right) \\ \text{last}_{node} \leftarrow \text{submatrix}\left(X, \text{dof}_{n\ 2, Top_{3\ el}}, \text{dof}_{n\ 2, Top_{3\ el}}, \text{dof}_{n\ (1, Top_{3, el})}, 1, 1, \text{cols}(X)\right) \\ \text{stack}\left(\text{first}_{node}, \text{last}_{node}\right) \end{array} \right.$$

Evaluate the displacement vectors for the tower element Augment the vectors for each frequency.

$$\text{disp}_{T_k} = \text{parse}_{el}\left(x_k, \text{Tower}\right)$$

Evaluate the elemental stiffness, transformation and damping matrices·

$$\text{stiff}_T = \text{KeT}_{\left(Top_{1, Tower}\right)} \qquad \phi_T = \phi T_{\left(Top_{1, Tower}\right)}$$

Elemental damping matrix is $c_h = C_{T.top}$ $c_{h_{13,13}} = 0$

Calculate the force on the tower element. This is usually accomplished by taking the product of the element stiffness and the displacement. However as the generator has been modelled as a damper on the low speed shaft then the torque is best determined by taking the product of the element damping and the the velocity.

$$F_{T_k} = \text{stiff}_T \cdot \phi_T \cdot \text{disp}_{T_k} \qquad \text{RotorQ}_k = c_h \cdot \text{disp}_{T_k} \cdot \omega_k$$

Now replace the 6th and 7th rows of the F matrix with the 6th and 7th rows of the RotorQ matrix:

$$F_{T_k} \left| \begin{array}{l} F_{tmp} \leftarrow F_{T_k}^{T} \\ R_{tmp} \leftarrow \text{RotorQ}_k^{T} \\ F_{tmp}^{\langle 6 \rangle} \leftarrow R_{tmp}^{\langle 6 \rangle} \\ F_{tmp}^{\langle 7 \rangle} \leftarrow R_{tmp}^{\langle 7 \rangle} \\ F_{tmp}^{T} \end{array} \right.$$

Evaluate the displacement vectors for the blade root element. Augment the vectors for each frequency.

$$\text{disp}_{BR_k} = \text{parse}_{el}\left(x_k, \text{BladeRoot}\right)$$

Evaluate the elemental stiffness, transformation and damping matrices:

$$\text{stiff}_{BR} = \text{KeT}_{\left(Top_{1, BladeRoot}\right)} \qquad \phi_{BR} = \phi T_{\left(Top_{1, BladeRoot}\right)}$$

Calculate the force on the blade root element.

$$F_{BR_k} = \text{stiff}_{BR} \cdot \phi_{BR} \cdot \text{disp}_{BR_k}$$

Calculate any other blade elements which are required:

Number of elements required: $\text{Res}_{el} = 3$ $ri = 1$ Res_{el} res_{ri}

22
1
7

Evaluate the displacement vectors for the blade root element. Augment the vectors for each frequency.

$$disp_{ri\,k} \quad parse_{el}\ x_k\ res_{ri}$$

Evaluate the elemental stiffness, transformation and damping matrices:

$$stiff_{ri} \quad KeT_{\left(Top_{1\,res_{ri}}\right)} \qquad \phi_{ri} \quad \phi T_{Top_{1,res_{ri}}}\Big)$$

Calculate the force on the blade root element:

$$F_{ri\,k} \quad stiff_{ri}\,\phi_{ri}\,disp_{ri\,k}$$

Stack the Tower, Blade Root and other element forces: $F \quad stack\ F_T{}^T, F_{BR}{}^T$

(OR >) $F \quad stack\left(stack\left(F_T{}^T, F_{BR}{}^T\right), F\right)$

Save the Force matrices WRITEPRN("Force prn") F

View the virtual response at any prescribed element and under any load case:

The above Force matrix F is expressed as a 3 dimensional matrix This is a matrix where each row represents an element each column represents a frequency and each cell contains a matrix of forces for each DOF of the element. Each column represents a different loading case while each row represents a particular DOF

F

{13,12}	{13,12}	{13,12}	{13,12}	{13,12}	{13,12}	
{8 12}	{8 12}	{8 12}	{8 12}	{8 12}	{8 12}	
13 12}	{13 12}	{13,12}	{13 12}	{13 12}	{13 12}	
{8 12}	{8 12}	{8 12}	{8 12}	{8,12}	{8 12}	
{8 12}	{8 12}	{8,12}	{8,12}	{8 12}	{8,12}	

For all subsequent calculations it is desirable to rearrange this matrix into a 3 dimensional vector Results shall be obtained for any specified LOAD CASE, this is entered later Each element of the vector represents an element expressed in terms of a matrix Each row of the matrix represents a frequency while each column represents a force in each DOF The following subprogram calculates this.

combine(M, Lc)

```
for i ∈ 1 .. rows(M)
    tmp ← M_{i 1}^{<Lc>T}
    for j ∈ 2 .. cols(M)
        tmp ← stack(tmp, M_{i j}^{<Lc>T})
    N_i ← tmp
N
```

Select the element and load case that you wish to view. el 1 Lc 1

This represents the element res_{el} 22 in the model

Calculate the force vector

Force combine(F, Lc)

Define plot of force wrt frequency for the element and load case chosen:

plot $Force_{el}$

View the element reaction forces to the loading $\overrightarrow{\left|\left(plot^T\right)^1\right|} =$

$$\begin{bmatrix}
1.16411453\cdot10^{10}\\
127.55729454\\
183.89332992\\
2.42259326\cdot10^{10}\\
1.12871662\cdot10^{3}\\
827.17730574\\
827.17730574\\
1.16411453\cdot10^{-10}\\
127.55729454\\
183.89332992\\
2.42183687\cdot10^{-10}\\
7.56736876\cdot10^{3}\\
5.29343101\cdot10^{3}
\end{bmatrix}$$

Calculate the natural frequencies:

$$f_n \quad \frac{\overrightarrow{\sqrt{genvals\ K_{s\,fxd}, M_{fxd}}}}{2\pi}$$

Calculate the eigen vectors

$$\varepsilon_{n\,fxd} \quad genvecs\left(K_{s\,fxd}\ M_{fxd}\right)$$

$$\varepsilon_n \quad Release\ \varepsilon_{n\,fxd}, Tbase_{dof}\Big)$$

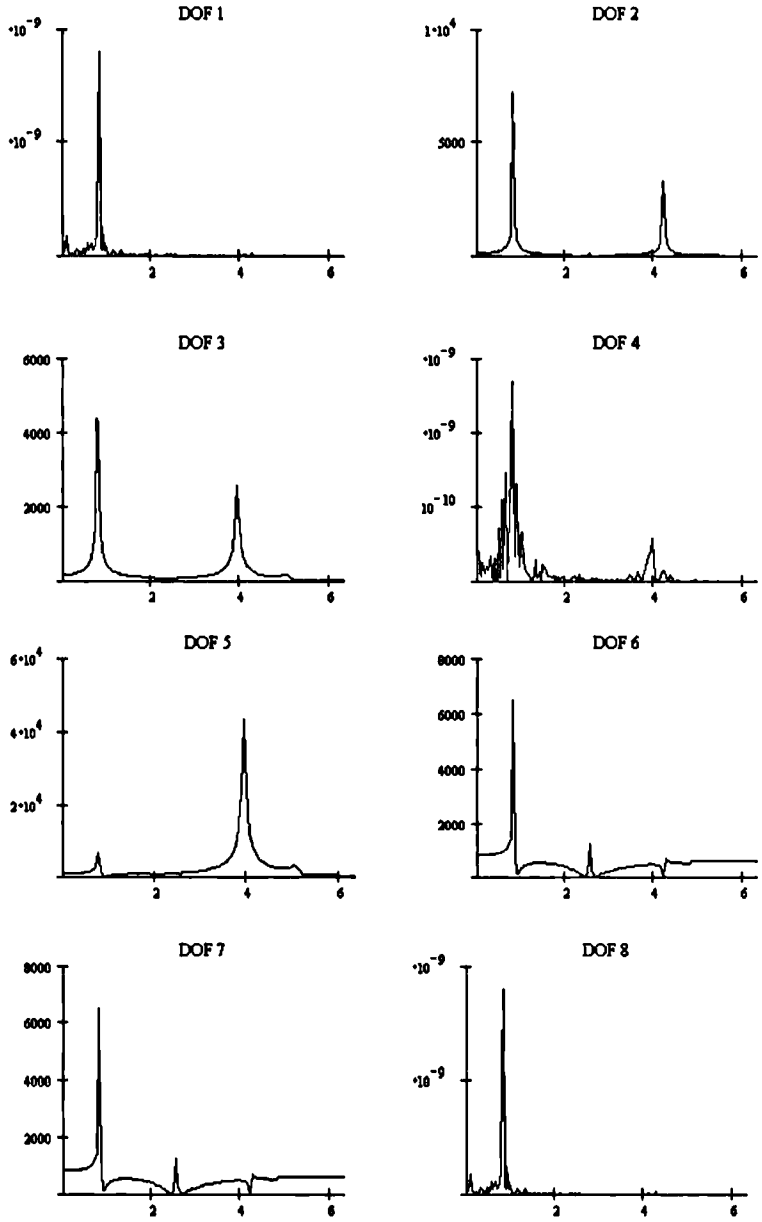
DOF 1
DOF 2
DOF 3
DOF 4
DOF 5
DOF 6
DOF 7
DOF 8
DOF 9
DOF 10
DOF 11
DOF 12
DOF 13

Plot the deflected shape:

The routines from #fea.mcd are used to plot the displaced shape of the structure. In order to plot these it is also necessary to define coordinates of the pre-deflected structure. The displaced nodal coordinates are then evaluated by summing the displacements and the original coordinates. (NB. The deflected shapes in each blade or tower member are draw in the local member axes Although in the diagram they look to be in the global axis this is indicative only.)

The following subprogram evaluates the pre-deflected coordinates of each node. It gives a matrix where each column represents a node and the rows give the x, y and z coordinates respectively.

$$
\begin{aligned}
x_o - \;& i \leftarrow 1 \\
& \text{for } b \in 1..B \\
& \quad \text{for } p \in 1..nodes-1 \\
& \quad\quad x_i \leftarrow H_T + r_{p+1}\cos\left[\phi + \frac{2\cdot\pi}{B}(b-1)\right] \\
& \quad\quad y_i \leftarrow r_{p+1}\sin\left[\phi + \frac{2\cdot\pi}{B}(b-1)\right] \\
& \quad\quad z_i \leftarrow Offset \\
& \quad\quad i \leftarrow i+1 \\
& x_i \leftarrow 0 \\
& y_i \leftarrow 0 \\
& z_i \leftarrow 0 \\
& i \leftarrow i+1 \\
& x_i \leftarrow H_T \\
& y_i \leftarrow 0 \\
& z_i \leftarrow 0 \\
& \text{stack}\left(\text{stack}\left(x^T, y^T\right), z^T\right)
\end{aligned}
$$

$x_o =$

36.5	39.5	41.5	45.5	49.5	53.5	55.5	34.25	32.75	31.75	<-- node number
0	0	0	0	0	0	0	1.299	3.897	5.629	<-- x co-ordinate
2.21	2.21	2.21	2.21	2.21	2.21	2.21	2.21	2.21	2.21	<-- y co-ordinate
										<-- z co-ordinate

Before this can be plotted it is necessary to evaluate the displacements in terms of elements in the form given below.

node at end 1 of element -->
node at end 2 of element -->
etc...

$$
\begin{bmatrix}
x_1 & y_1 & z_1 \\
x_2 & y_2 & z_2 \\
x_2 & y_2 & z_2 \\
x_3 & y_3 & z_3 \\
x_3 & y_3 & z_3 \\
x_4 & y_4 & z_4
\end{bmatrix}
$$

<-- element 1
<-- element 2
<-- element 3

The following subprogram is used to accomplish this:

$$
\begin{aligned}
x_{el} \quad & p \leftarrow 1 \\
& \text{for } ei \in 1..cols(Top) \\
& \quad \text{for } i \in 2..3 \\
& \quad\quad node \leftarrow Top_{i,ei} \\
& \quad\quad co_{p,1} \leftarrow x_{o_{1,node}} \\
& \quad\quad co_{p,2} \leftarrow x_{o_{2,node}} \\
& \quad\quad co_{p,3} \leftarrow x_{o_{3,node}} \\
& \quad\quad p \leftarrow p+1 \\
& co
\end{aligned}
$$

The displacement vectors calculated for the blades work in the blade local co ordinate axis system, it is necessary to change these to the rotational azimuth system. The following routine lists the azimuth angles of the nodes.

$$
\begin{aligned}
\phi_{plot} = \;& j \leftarrow 1 \\
& \text{for } b \in 1..B \\
& \quad \text{while } j \le b\,(nodes-1) \\
& \quad\quad \phi_{plot_{1,j}} \leftarrow j \\
& \quad\quad \phi_{plot_{2,j}} \leftarrow \phi + (b-1)\frac{2\cdot\pi}{B} \\
& \quad\quad j \leftarrow j+1 \\
& \text{for } i \in 1..2 \\
& \quad \phi_{plot_{1,j}} \leftarrow j \\
& \quad \phi_{plot_{2,j}} \leftarrow 0 \\
& \quad j \leftarrow j+1 \\
& \phi_{plot}
\end{aligned}
$$

ϕ_{plot}

5	6	7	8	9	10	11
0	0	0	2.094	2.094	2.094	2.094

Enter frequency case to be plotted:

Plot the deflected shape under the load case Lc 1

Enter the frequency to be plotted: freq 88

This relates to a frequency of $\frac{\omega_{freq}}{2\pi}$ 2 786 Hz OR natural frequency: $f_{n_{freq}} = 1.529$

Evaluate the coordinates of the displaced nodes or mode shapes and magnify these to: mag 5

ω =

0	3.358
1	3.406
2	3 454
3	3 502
4	3 549
5	3 597
6	3 645
7	3 693
8	3 74
9	3 788
10	3 836
11	3 884
12	3 931
13	3 979
14	4 027

DISABLE AS REQUIRED

Displacement --> δ magnify$\left[\delta_{xyz}\left[x_{freq}\right)^{<Lc>}, Top, dof_n, \phi_{plot}\right], mag\right] + x_{el}$

Mode shape --> δ magnify$\left(\delta_{xyz}\,\varepsilon_n^{<freq>}, Top, dof_n, \phi_{plot}\right)\ mag\right) + x_{el}$

Find the limits for the plot: lim PlotLimit(δ)

Transform this into the Mathcad DRAW format: δplot line2draw(δ)

Define the rang ng variable s for the plot: s 1 rows(δplot)

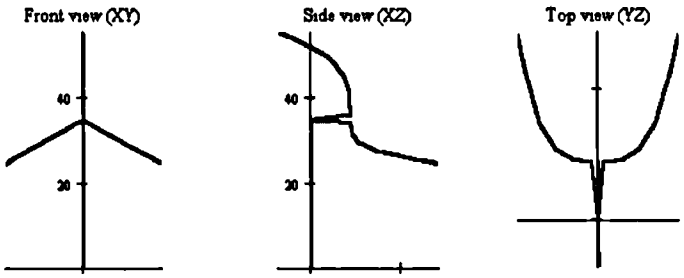

Appendix D

Loadana Listing

Loadana

ORIGIN=0

Calculation of PSDs and spectral moments for turbulent wind loading on a wind turbine

Andrew Halfpenny

Load the transfer function matrix and Turbulent loading matrices from *linana* & *turbana* respectively:

G_{blade} READPRN("blade.prn") G_{rotor} READPRN("rotor.prn") G_{yaw} READPRN("yaw.prn")

F READPRN("force.prn")

Load the frequencies ω READPRN("freq.prn") k 0 last(ω) last(ω) = 162

Transform frequency units to Hz

$G_{blade_k} \leftarrow G_{blade_k} \frac{2\pi}{1000^2}$ $G_{yaw_k} \leftarrow G_{yaw_k} \frac{2\pi}{1000^2}$ $G_{rotor_k} \leftarrow G_{rotor_k} \frac{2\pi}{1000^2}$ $\omega \leftarrow \frac{\omega}{2\pi}$

Number of blades B 3

Load the aerodynamic gain and damping coefficients from aerana This data is used to calculate the loading on a rigid blade This is handy to know so that natural frequencies etc can be noted from the PSD plots

data READPRN("gaindamp.prn") $g_a \leftarrow data^{\langle 3 \rangle}$ $g_t \leftarrow data^{\langle 4 \rangle}$ $r \leftarrow data^{\langle 0 \rangle}$

Get the PSDs for one blade The data above is saved for all blades and of this only the first is required The smaller matrices are obtained by taking sub matrices of the total matrix.

$G_{1\,blade_k}$ submatrix G_{blade_k} 0,3 0 3

Calculate the PSDs for the blade root moment and shear forces

Distance to root at which moment is to be calculated R_h 1.5 $r_h \leftarrow diag(\overrightarrow{r - R_h})$

Flapwise shear and moments:

$psd_{bsy_k} \quad g_a^T G_{1\,blade_k} g_a$ $psd_{bmy_k} \quad \left| \Sigma \left(g_a \right)^T r_h G_{1\,blade_k} r_h g_a \right|$

Edgewise shear and moments:

$psd_{bsz_k} \quad \Sigma \; g_t^T G_{1\,blade_k} g_t$ $psd_{bmz_k} \quad g_t^T r_h G_{1\,blade_k} r_h g_t$

Calculate the yaw/tilt moments: $p_a \quad \overrightarrow{g_a r}$

$psd_{mx_k} \quad \Sigma \left(p_a^T G_{yaw_k} p_a \right)$

View the loading spectra: Rotor frequency rpm] rpm 27.7 P $\frac{rpm}{60}$

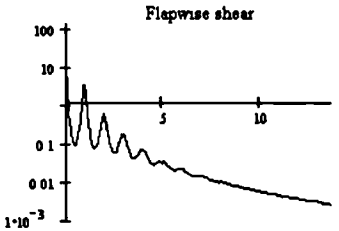

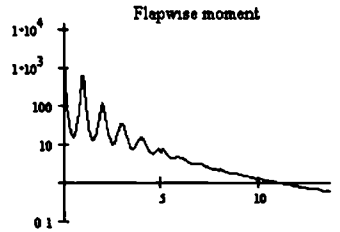

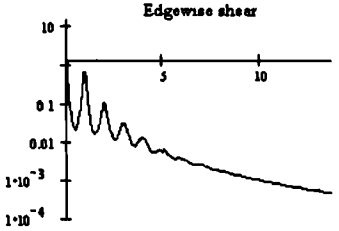

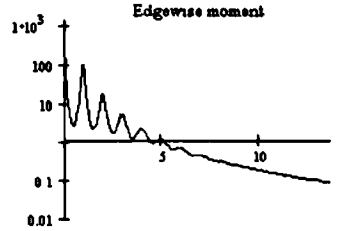

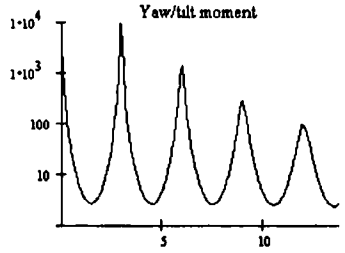

Calculate the tower overturning shear and moments and the rotor torsion.

The above vectors ga and gt are the gains for one blade. It is necessary to stack these to model the B number of blades n the turbine. The following routine processes this

stackit(g) v← g
for ι∈ 1 B 1 g_a stackit g_a g_t stackit g_t
v← stack(v g)
v r diag(stackit(r))

Calculate the PSDs for the foundation reaction assuming that the blades are rigid·

Tower base shear para el to the wind i e the rotor thrust psd_{sy_k} $g_a^T G_{blade_k} g_a$

The tower base moment is obtained by taking the rotor thrust multiplied by the tower height.

Tower height H 35

Overturning moment on the tower base· psd_{my} $psd_{sy} H^2$

Calculate the rotor torque: psd_{mz_k} $\sum g_t^T r G_{blade_k} r g_t$

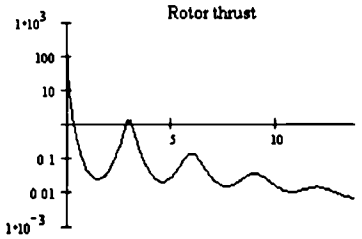

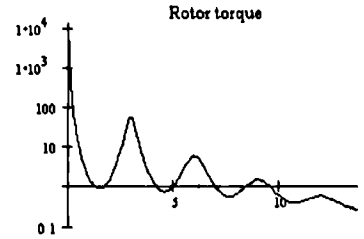

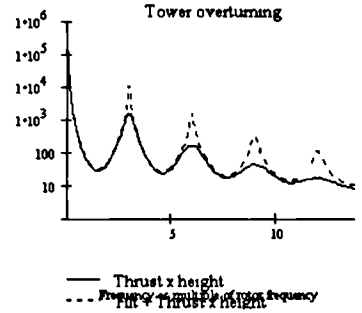

Elastic Model:

Calculate the elemental loading in any element:

The f l owing routines calculate the PSDs and spectral moments for the loading on any element Statistica properties are then evaluated

Define the ranging variable for the element identities ei 0 rows(F) 1

The PSD of element loading can be found using $PSD = F\,G_{blade}\,F^{T}$ Th s results in a square matrix with the autopower terms listed down the leading diagonal and cross power terms in the other cells. We are only interested in the autopower terms for these calculations and so the fo low ng subprogram has been defined tc extract the leading diagonal from the square matrices.

```
ldiag(M) | for i ∈ 0 rows(M) 1
         |   v_i ← M_i,i
         | v
```

The autopower spectra of element forces is therefore calculated us ng the following equation, where k is the ranging variable for frequency and ei is the ranging vanab e for the element

$$PSDa_{ei,k} \quad ldiag\left(F_{ei,k}\,G_{blade_k}\,F_{ei,k}^{T}\right)$$

The above equation resu ts in a 3 dimensional matrix This is a matrix where each row represents an element each column represents a frequency and each cell contains a vector of forces for each DOF of the element

PSDa

(13 1)	(13 1)	(13 1)	(13,1)	13 1)	(13,1)	(13,1)	<-- Tower element
(8 1)	(8 1)	(8 1)	(8 1)	(8,1)	(8 1)	(8,1)	<-- Blade root element
(13 1)	(13 1)	(13 1)	(13 1)	(13 1)	(13 1)	(13 1)	<-- el 3 (optioanl ...)
8 1)	(8 1)	(8 1)	(8 1)	8 1)	(8 1)	(8 1)	
(8 1)	(8 1)	(8 1)	(8 1)	(8 1)	(8 1)	(8,1)	

Gravity effect on blade edgewise loading.

Th s may be approximated in the mode by evaluating the mean squared moment on the blade root due to gravity This is then entered in the PSD by d viding the value by the frequency interval.

Enter blade root moment due to blade mass acting at the centre of gravity [kN m] $blade_{mom} \quad 1.455 \cdot 10^{2}$
(NB th s is g ven in linana if no other value is availab e)

Determine the mean squared moment $ms \quad \frac{blade_{mom}^{2}}{\sqrt{2}} \quad ms = 1.059 \cdot 10^{4} \quad \sqrt{ms} = 102.884$

Find the item in the vector at which the rotational period occurs. Rotor frequency [Hz] P = 0 462

```
find_item(V, n) | i ← 1
                | while i < last(V)
                |   break if V_i > n
                |   i ← i 1
                | i 1 V_i 1
                | i V_i
```

v find_item(ω, P)

v
16 0.446
17 0.478

The user should now decide where and over what frequency interval the mean squared value should be distributed. THE FOLLOWING EQUATIONS W LL PROBABLY NEED CHANG NG FOR EACH TURB NE!

$$\Delta\omega \quad \frac{\omega_{18}}{2} \quad \frac{\omega_{17}}{2} \quad \frac{\omega_{15}}{2} \quad \frac{\omega_{16}}{2} \qquad \Delta\omega = 0.048$$

Insert this in element number : ei 1 (NB. this should always be a blade root element)

$$tmp_7 \quad 0 \qquad tmp_3 \quad \frac{ms}{\Delta\omega}$$

$$PSDa_{el,16} \quad PSDa_{el,16} + \frac{tmp}{2} \qquad PSDa_{el\ 17} \quad PSDa_{el\ 17} + \frac{tmp}{2}$$

For a l subsequent calculations it is des rable to rearrange this matrix into 3 dimensional vector Each element of the vector represents an element expressed in terms of a matrix Each row of the matrix represents a frequency while each column represents a force in each DOF. The following subprogram calculates this.

```
combine(M) | for i ∈ 0 rows(M) 1
           |   tmp ← M_i^T
           |   for j ∈ 1 cols(M) 1
           |     tmp ← stack tmp M_j^T
           |   N_i ← tmp
           | N
```

Calculate the PSD force vector

PSD combine(PSDa)

PSD
(163,13)
(163,8)
(163 13)
(163,8)
(163,8)

Save the PSD file to disk:

WRITEPRN("psd prn") PSD

Calculate the tower top yaw and tilt moments using the super element concept:

Apply the super blade yaw matrix to the first blade of the model

Make other b ades zero

G_{yaw_k} | size ← cols G_{blade_k} 1 | $new_{size,size} \leftarrow 0$ | size ← cols G_{yaw_k} 1 | for $i \in 0$ size | for $j \in 0$ size | $new_{i,j} \leftarrow (G_{yaw_k})_{i,j}$ | new

G_{rotor_k} | size ← cols G_{blade_k} 1 | $new_{size,size} \leftarrow 0$ | size ← cols G_{rotor_k} 1 | for $i \in 0$ size | for $j \in 0$ size | $new_{i,j} \leftarrow (G_{rotor_k})_{i,j}$ | new

Calculate the yaw moment:

$PSDa_{yaw_k} \quad \text{ldiag}\ F_{1\,k}\ G_{yaw_k}\ F_{1\,k}^{T}$

$PSD_{yaw} \quad \text{combine}\ PSDa_{yaw}^{T}{}_{0}$

Calculate the rotor thrust and torque·

$PSDa_{rotor_k} \quad \text{ldiag}\ F_{1\,k}\ G_{rotor_k}\ F_{1\,k}^{T}$

$PSD_{rotor} \quad \text{combine}\ PSDa_{rotor}^{T}{}_{0}$

Calculate the tower and blade root forces for comparison with the rigid case and with the measured data:

B ade root shear and moments

$FLAP_{shear_k} \quad PSD_{1\,k\,0}$ $\qquad$ $FLAP_{mom_k} \quad PSD_{1\,k\,2}$

$EDGE_{shear_k} \quad PSD_{1\,k\,1}$ $\qquad$ $EDGE_{mom_k} \quad PSD_{1\,k\,3}$

Tower moments:

$THRUST_k \quad PSD_0)_{k,2}$

$TILT_k \quad PSD_{yaw})_{k\,2}$ $\qquad$ $TORQUE_k \quad PSD_{0\,k,5}$

$YAW_k \quad PSD_{yaw})_{k,2}$ $\qquad$ $TOWFROT_k \quad PSD_{0\,k\,11}$

View the spectra:

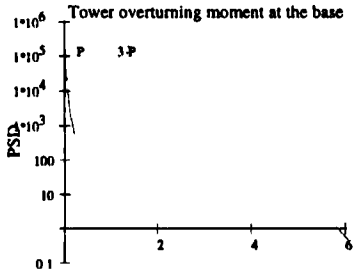

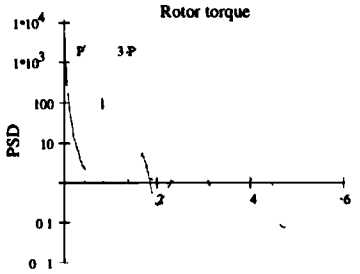

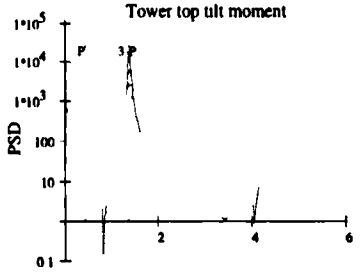

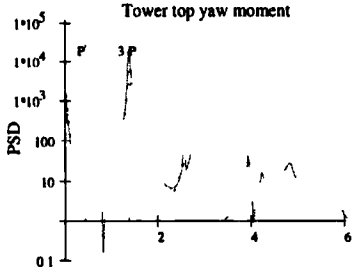

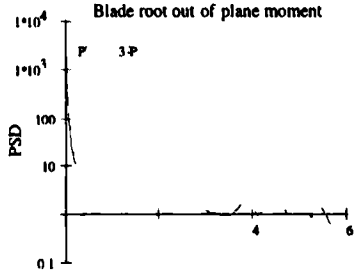

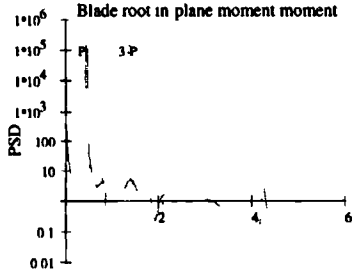

Import the measured data for comparison:

Include the spectral analysis tools: Reference C \usr\Appendix\#fft.mcd

Load data file: dataIN READPRN("data10.prn") data submatrix(dataIN 0 N 1,0 8)

time data<0> $wind_t$ data<1> $flap_t$ data<3> $edge_t$ data<4>

$tilt_t$ data<5> $torque_t$ data<6> yaw_t data< > $towerOT_t$ data<8>

Find the mean of the data and zero mean the time histories.

μ_{wind} mean $wind_t$ $\mu_{wind} = 10.142$ $wind_t$ $wind_t - \mu_{wind}$

μ_{flap} mean $flap_t$ $\mu_{flap} = 138.736$ $flap_t$ $flap_t - \mu_{flap}$

μ_{edge} mean $edge_t$ $\mu_{edge} = 2.862 \cdot 10^{3}$ $edge_t$ $edge_t - \mu_{edge}$

μ_{tilt} mean $tilt_t$ $\mu_{tilt} = 33.827$ $tilt_t$ $tilt_t - \mu_{tilt}$

μ_{torque} mean$(torque_t)$ $\mu_{torque} = 41.105$ $torque_t$ $torque_t - \mu_{torque}$

μ_{yaw} mean yaw_t $\mu_{yaw} = 82.562$ yaw_t $yaw_t - \mu_{yaw}$

$\mu_{towerOT}$ mean $towerOT_t$ $\mu_{towerOT} = 1.421 \cdot 10^{3}$ $towerOT_t$ $towerOT_t - \mu_{towerOT}$

Determine the sampling frequency [Hz]: $samp \leftarrow \frac{1}{time_1 - time_0}$ $samp = 25$

Calculated the PSDs of the blade and tower forces:

flap $psd_s(flap_t, samp)^{<1>}$ edge $psd_s(edge_t, samp)^{<1>}$ tilt $psd_s(tilt_t, samp)^{<1>}$

torque $psd_s(torque_t, samp)^{<1>}$ yaw $psd_s(yaw_t, samp)^{<1>}$ towerOT $psd_s(towerOT_t, samp)^{<1>}$

Determine the frequency: freq $psd_s(flap_t, samp)^{<0>}$ n 1..3..last(freq)

k 1..last(ω)

View the spectral results:

Tower overturning moment at the base

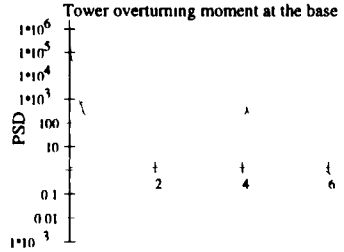

Rotor torque

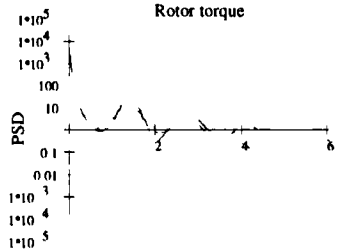

Tower top tilt moment

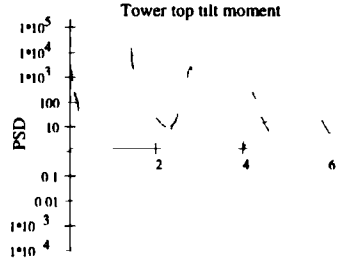

Tower top yaw moment

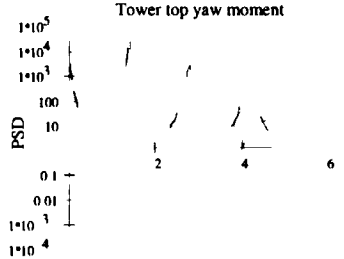

Blade root out of plane moment

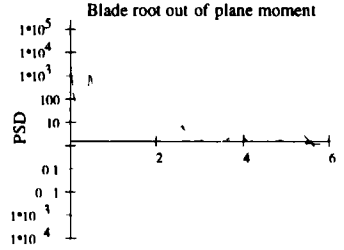

Blade root in plane moment moment

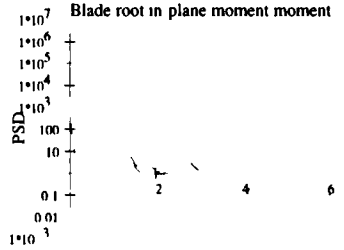

Calculate the spectral moments and statistics for the tower element.

In this section we shall calculate the spectral moments and statistics for each loading case in turn and compare them

Determine the cut-off frequency. max(ω) 6.366 max(freq) 12.5 f_n 6

Tower thrust:

m_{tsy} mom psd$_{sy}$, ω, f_n, 4) m_{THRUST} mom THRUST, ω f_n, 4)

$$m_{tsy} = \begin{bmatrix} 5.564 \\ 1.107 \\ 2.284 \\ 7.191 \\ 27.916 \end{bmatrix} \qquad m_{THRUST} = \begin{bmatrix} 18 \\ 17.417 \\ 39.533 \\ 134.047 \\ 534.978 \end{bmatrix}$$

s_{tsy} stats m_{tsy}) s_{THRUST} stats m_{THRUST})

$$s_{tsy} = \begin{bmatrix} 2.359 \\ 5.028 \\ 1.561 \\ 0.286 \\ 0.183 \end{bmatrix} \qquad s_{THRUST} = \begin{bmatrix} 4.243 \\ 1.033 \\ 0.675 \\ 0.272 \\ 0.403 \end{bmatrix}$$

Tower overturning.

m_{ot} mom psd$_{ot}$, ω, f_n, 4) $m_{TOWEROT}$ mom TOWEROT, ω, f_n, 4 $m_{towerOT}$ mom tow

$$m_{ot} = \begin{bmatrix} 7.863 \cdot 10^3 \\ 3.155 \cdot 10^3 \\ 7.261 \cdot 10^3 \\ 2.323 \cdot 10^4 \\ 9.095 \cdot 10^4 \end{bmatrix} \qquad m_{TOWEROT} = \begin{bmatrix} 2.026 \cdot 10^4 \\ 1.394 \cdot 10^4 \\ 2.002 \cdot 10^4 \\ 5.043 \cdot 10^4 \\ 1.815 \cdot 10^5 \end{bmatrix} \qquad m_{towerOT} = \begin{bmatrix} 1.68 \cdot 10^4 \\ 7.548 \cdot 10^3 \\ 1.242 \cdot 10^4 \\ 3.226 \cdot 10^4 \\ 1.191 \cdot 10^5 \end{bmatrix}$$

s_{ot} stats m_{ot} $s_{TOWEROT}$ stats $m_{TOWEROT}$ $s_{towerOT}$ stats $m_{towerOT}$)

$$s_{ot} = \begin{matrix} 88\,673 \\ 2\,492 \\ 1\,041 \\ 0\,283 \\ 0\,272 \end{matrix} \qquad s_{TOWEROT} = \begin{bmatrix} 142\,335 \\ 1\,453 \\ 1\,006 \\ 0\,332 \\ 0\,33 \end{bmatrix} \qquad s_{towerOT} = \begin{bmatrix} 129\,619 \\ 2\,226 \\ 1.163 \\ 0\,323 \\ 0\,278 \end{bmatrix}$$

$\overrightarrow{s_{TOWEROT}\ s_{towerOT}}$ / $s_{towerOT}$

$$\begin{matrix} 9\,81 \\ 34\,705 \\ 13\,508 \\ 2\,865 \\ 18\,93 \end{matrix} \%$$

Rotor torque.

m_{tmz} mom psd_{mz} ω f_n 4 m_{TORQUE} mom TORQUE, ω, f_n 4 m_{torque} mom torque, freq, f_n 4)

$$m_{tmz} = \begin{matrix} 196\,346 \\ 41\,1 \\ 86\,12 \\ 272\,582 \\ 1\,062 \cdot 10^3 \end{matrix} \qquad m_{TORQUE} = \begin{bmatrix} 209\,307 \\ 56\,297 \\ 94\,145 \\ 208\,353 \\ 551\,237 \end{bmatrix} \qquad m_{torque} = \begin{bmatrix} 289\,958 \\ 43\,179 \\ 90\,225 \\ 253\,811 \\ 758\,198 \end{bmatrix}$$

s_{tmz} stats m_{tmz} s_{TORQUE} stats m_{TORQUE} s_{torque} stats m_{torque})

$$s_{tmz} = \begin{matrix} 14\,012 \\ 4\,777 \\ 1\,51 \\ 0\,285 \\ 0\,189 \end{matrix} \qquad s_{TORQUE} = \begin{bmatrix} 14\,467 \\ 3\,718 \\ 1\,491 \\ 0\,413 \\ 0\,277 \end{bmatrix} \qquad s_{torque} = \begin{bmatrix} 17\,028 \\ 6\,715 \\ 1\,793 \\ 0\,345 \\ 0\,192 \end{bmatrix}$$

$\overrightarrow{s_{TORQUE}\ s_{torque}}$ / s_{torque}

$$\begin{bmatrix} 15\,038 \\ 44\,636 \\ 16\,826 \\ 19\,8 \\ 44\,035 \end{bmatrix} \%$$

Tower yaw/tilt:

m_{tmx} mom psd_{mx}, ω, f_n, 4) m_{TILT} mom TILT ω f_n 4 m_{yaw} mom(yaw freq, f_n, 4

$$m_{tmx} = \begin{bmatrix} 1\,046 \cdot 10^3 \\ 1\,8 \cdot 10^3 \\ 4\,464 \cdot 10^3 \\ 1\,442 \cdot 10^4 \\ 5\,675 \cdot 10^4 \end{bmatrix} \qquad m_{TILT} = \begin{bmatrix} 1\,563 \cdot 10^3 \\ 2\,267 \cdot 10^3 \\ 4\,001 \cdot 10^3 \\ 9\,517 \cdot 10^3 \\ 3\,245 \cdot 10^4 \end{bmatrix} \qquad m_{yaw} = \begin{bmatrix} 2\,042 \cdot 10^3 \\ 1\,168 \cdot 10^3 \\ 2\,117 \cdot 10^3 \\ 4\,869 \cdot 10^3 \\ 1\,401 \cdot 10^4 \end{bmatrix}$$

s_{tmx} stats m_{tmx} s_{TILT} stats m_{TILT} s_{yaw} stats m_{yaw}

$$s_{tmx} = \begin{bmatrix} 32\,348 \\ 0\,581 \\ 0\,484 \\ 0\,28 \\ 0\,579 \end{bmatrix} \qquad s_{TILT} = \begin{bmatrix} 39\,531 \\ 0\,689 \\ 0\,625 \\ 0\,351 \\ 0\,562 \end{bmatrix} \qquad s_{yaw} = \begin{matrix} 45\,188 \\ 1\,748 \\ 0\,982 \\ 0\,389 \\ 0\,396 \end{matrix}$$

$\overrightarrow{s_{TILT}\ s_{yaw}}$ / s_{yaw}

$$\begin{matrix} 12\,519 \\ 60\,559 \\ 36\,361 \\ 9\,673 \\ 41\,936 \end{matrix} \%$$

Blade root flapwise shear:

$m_{bsy} := mom\ psd_{bsy}, \omega, f_n, 4$

$$m_{bsy} = \begin{matrix} 1\ 07 \\ 0\ 487 \\ 0\ 818 \\ 2.383 \\ 9\ 12 \end{matrix}$$

$m_{FLAPshear} := mom\ FLAP_{shear}, \omega, f_n, 4$

$$m_{FLAPshear} = \begin{matrix} 1\ 302 \\ 2.79 \\ 6\ 971 \\ 17\ 723 \\ 45\ 434 \end{matrix}$$

$s_{bsy} := stats\ m_{bsy}$

$$s_{bsy} = \begin{matrix} 1\ 034 \\ 2\ 195 \\ 1\ 144 \\ 0\ 3 \\ 0\ 262 \end{matrix}$$

$s_{FLAPshear} := stats\ m_{FLAPshear}$

$$s_{FLAPshear} = \begin{matrix} 1\ 141 \\ 0\ 467 \\ 0\ 432 \\ 0\ 392 \\ 0\ 906 \end{matrix}$$

Blade root flapwise moment:

$m_{bmy} := mom\ psd_{bmy}, \omega, f_n, 4$

$$m_{bmy} = \begin{matrix} 173\ 843 \\ 89\ 939 \\ 160\ 512 \\ 482\ 292 \\ 1.872 \cdot 10^{3} \end{matrix}$$

$m_{FLAPmom} := mom(FLAP_{mom}, \omega, f_n, 4$

$$m_{FLAPmom} = \begin{matrix} 217\ 224 \\ 227\ 177 \\ 537\ 133 \\ 1\ 798 \cdot 10^{3} \\ 7\ 406 \cdot 10^{3} \end{matrix}$$

$m_{flap} := mom(flap, freq, f_n, 4$

$$m_{flap} = \begin{matrix} 1\ 092 \cdot 10^{3} \\ 862\ 62 \\ 1\ 386 \cdot 10^{3} \\ 3\ 698 \cdot 10^{3} \\ 1\ 396 \cdot 10^{4} \end{matrix}$$

$s_{bmy} := stats\ m_{bmy}$

$$s_{bmy} = \begin{matrix} 13.185 \\ 1\ 933 \\ 1\ 041 \\ 0\ 293 \\ 0\ 281 \end{matrix}$$

$s_{FLAPmom} := stats\ m_{FLAPmom}$

$$s_{FLAPmom} = \begin{matrix} 14\ 739 \\ 0\ 956 \\ 0\ 636 \\ 0\ 269 \\ 0\ 423 \end{matrix}$$

$s_{flap} := stats(m_{flap}$

$$s_{flap} = \begin{matrix} 33\ 043 \\ 1\ 266 \\ 0\ 888 \\ 0\ 315 \\ 0\ 355 \end{matrix}$$

$\overrightarrow{s_{FLAPmom}\ s_{flap}}$

s_{flap}

$$\begin{matrix} 55\ 396 \\ 24\ 456 \\ 28\ 349 \\ 14\ 545 \\ 19\ 265 \end{matrix} \%$$

Blade root edgewise shear force.

$m_{bsz} \quad mom\ psd_{bsz}\ \omega\ f_n, 4 \qquad m_{EDGEshear} \quad mom\ EDGE_{shear}, \omega, f_n, 4$

$$m_{bsz} = \begin{bmatrix} 0\,22 \\ 0\,09 \\ 0\,144 \\ 0\,408 \\ 1\,541 \end{bmatrix} \qquad m_{EDGEshear} = \begin{bmatrix} 1\,628 \\ 1.858 \\ 5\,323 \\ 20\,548 \\ 90\,959 \end{bmatrix}$$

$s_{bsz} \quad stats\ m_{bsz} \qquad s_{EDGEshear} \quad stats\ m_{EDGEshear})$

$$s_{bsz} = \begin{bmatrix} 0\,469 \\ 2\,437 \\ 1\,237 \\ 0\,306 \\ 0\,247 \end{bmatrix} \qquad s_{EDGEshear} = \begin{bmatrix} 1\,276 \\ 0\,876 \\ 0\,553 \\ 0\,242 \\ 0\,437 \end{bmatrix}$$

Blade root edgewise moment.

$m_{bmz} \quad mom\ psd_{bmz}\ \omega, f_n, 4 \qquad m_{EDGEmom} \quad mom\ EDGE_{mom}, \omega, f_n\ 4 \qquad m_{edge} \quad mom(edge, freq, f_n, 4$

$$m_{bmz} = \begin{bmatrix} 30\,203 \\ 14\,479 \\ 24\,874 \\ 73\,287 \\ 282\,043 \end{bmatrix} \qquad m_{EDGEmom} = \begin{bmatrix} 5\,528 \cdot 10^3 \\ 2\,975 \cdot 10^3 \\ 2\,467 \cdot 10^3 \\ 3\,938 \cdot 10^3 \\ 9\,035 \cdot 10^3 \end{bmatrix} \qquad m_{edge} = \begin{bmatrix} 5\,641 \cdot 10^3 \\ 2\,906 \cdot 10^3 \\ 2.223 \cdot 10^3 \\ 3\,795 \cdot 10^3 \\ 1.104 \cdot 10^4 \end{bmatrix}$$

$s_{bmz} \quad stats\ m_{bmz} \qquad s_{EDGEmom} \quad stats\ m_{EDGEmom}) \qquad s_{edge} \quad stats\ m_{edge})$

$$s_{bmz} = \begin{bmatrix} 5\,496 \\ 2\,086 \\ 1\,102 \\ 0\,297 \\ 0\,269 \end{bmatrix} \qquad s_{EDGEmom} = \begin{bmatrix} 74\,35 \\ 1\,858 \\ 1\,497 \\ 0\,523 \\ 0\,349 \end{bmatrix} \qquad s_{edge} = \begin{bmatrix} 75.104 \\ 1\,941 \\ 1\,593 \\ 0\,449 \\ 0.282 \end{bmatrix}$$

$$\overrightarrow{s_{EDGEmom} \quad s_{edge}} = \begin{bmatrix} 1\,003 \\ 4\,255 \\ 6\,022 \\ 16\,455 \\ 23\,918 \end{bmatrix} \%$$

Appendix E

Rotormat & Hydrana Listings

Rotormat & Hydrana

Dynamic Motion Analysis of a Moving Turbine Rotor

For the TURBANA Development Model

Andrew Halfpenny

ORIGIN 1

This worksheet ca culates the rigid body forces on a three bladed rotor as it is moved through the air The motion is g ven by displacements, velocities and accelerations in 6 degrees of freedom These motions are expressed in matrix format and the resultant force obtained using the equilibrium formula given below

$$M\,s'' + c\,s' + k\,s = F(t)$$

Where
- s(t) displacement as a function of time
- k Stiffness matrix
- c Damping matrix
- M Mass/inertia matrix

The Mass, Damping and Stiffness matrices are given in terms of gain factors These include Aerodynamic terms which are calculated in the Aerana program, and inertial terms which are calculated from the structural properties

Define the rotor parameters:

$B := 3$	Number of blades (MUST BE NO LESS THAN 3!)		
$R_h := 4.5$	Radius to root cut-out [m]	$R := 21.5$	Rotor radius [m]
$\beta_h := 0.0$	Blade twist at root cut out	$\beta_t := 0.0$	Blade twist at tip
$RPM := 27$	Revolutions per minute	$R_{root} := 1.3$	Root radius [m]:
$f_o := \frac{RPM}{60}$	Rotor frequency [Hz], this may be expressed in rad/sec as -	$f_o = 0.45$	
		$\Omega := f_o 2\pi$	i.e.. $\Omega = 2.827$

Input Blade Data from Pre-processor Files:

Read in the *Gaindamp* data file $Prebu := READPRN("gaindamp.prn")$

Determine the number of elements in the blade $n := rows(Prebu)$ i.e. $n = 4$

The number of nodes in the FE model is therefore $nodes := n + 1$
see dia below

Define the ranging variable *el* as the *element identity* $el := 1..n$

Define the ranging variable *ni* as the *nodal identity* $ni := 1..nodes$

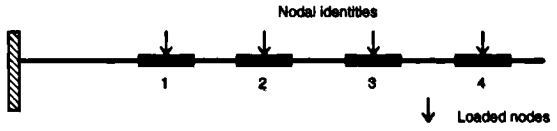

Typical FE representation

Input gain factors:

$r := Prebu^{\langle 1 \rangle}$ $\beta := Prebu^{\langle 3 \rangle}$ $g_a := Prebu^{\langle 4 \rangle}$ $g_t := Prebu^{\langle 5 \rangle}$

$c_a := Prebu^{\langle 6 \rangle}$ $c_t := Prebu^{\langle 7 \rangle}$ $\beta_a := Prebu^{\langle 8 \rangle}$ $\beta_t := Prebu^{\langle 9 \rangle}$

Modify β values for radian measure: $\beta := \beta \cdot deg$

Review element data from Aerana file with root information included:

Radius to blade node point $r^T = [6.625 \quad 10.88 \quad 15.13 \quad 19.38]$ [m]

Blade twist at node point $\beta^T = [9.538 \quad 3.637 \quad 1.35 \quad 0.212]$ deg

Axial and tangential gain factors $g_a^T = [165.6 \quad 172.4 \quad 80.26 \quad 276.8]$ [N/m sec^{-1}]

$g_t^T = [29.61 \quad 34.18 \quad 11.74 \quad 168.5]$

Axial and tangential damping factors $c_a^T = [224.4 \quad 281.1 \quad 329.1 \quad 259.9]$

$c_t^T = [81.59 \quad 97.28 \quad 88.14 \quad 28.18]$

Axial and tangential damping factors relating to blade pitching $\beta_a^T = [46.513 \quad 63.53 \quad 67.213 \quad 55.467] \frac{1}{deg}$

$\beta_t^T = [17.134 \quad 18.989 \quad 17.082 \quad 8.943] \frac{1}{deg}$

Aerodynamic element length $\Delta r \quad r_2 \quad r_1 \qquad \Delta r = 4.255$

Input the structural information from the data file: Structin READPRN("structin.prn")

Input radii $r_m \quad Structin_1^{\langle 1 \rangle}$ Input mass $m \quad Structin_1^{\langle 2 \rangle}$

Now these blade masses are given at a number of points along the blade and we therefore need to evaluate the effective masses on the nodes in question. We can do this as follows:

Interpolate the masses along the blade [kg/m] $me(radius) \quad linterp(r_m, m, radius)$

Determine a mass element vector to evaluate the masses for each element. An additional hub mass is also derived at r = 0.

$r_{n_{ni}} \quad if(ni=1, 0, if(ni=nodes, R, r_{ni-1}))$ $r_n^T = [0 \quad 6.625 \quad 10.88 \quad 15.13 \quad 21.5]$

Calculate the length of each element

$Le_{ei} \quad r_{n_{ei+1}} - r_{n_{ei}}$ $Le^T = [6.625 \quad 4.255 \quad 4.25 \quad 6.37]$

Calculate the Lumped Mass element matrix for each element

This calculation assumes a linear mass distribution.

Calculate the mass of each element:

$$Me_{ei} \int_0^{Le_{ei}} me\left(r_{n_{ei}} + x\right) dx$$

$Me^T = [4.787 \cdot 10^3 \quad 333.362 \quad 237.127 \quad 162.155]$

Calculate the 1st moment on the element about the LHS node

$$Z_{L_{ei}} \int_0^{Le_{ei}} me\left(r_{n_{ei}} + x\right) x\, dx$$

$Z_L^T = [3.856 \cdot 10^3 \quad 674.262 \quad 471.653 \quad 395.513]$

Calculate the RHS reaction force for each element

$$R_R \quad \frac{Z_L}{Le}$$

$R_R^T = [582.047 \quad 158.463 \quad 110.977 \quad 62.09]$

Calculate the moment on the element about the RHS node:

$$Z_{R_{ei}} \int_0^{Le_{ei}} me\left(r_{n_{ei}} + x\right)\left(Le_{ei} - x\right) dx$$

$Z_R^T = [2.786 \cdot 10^4 \quad 744.195 \quad 536.098 \quad 637.414]$

Calculate the LHS reaction forces for each element

$$R_L \quad \frac{Z_R}{Le}$$

$R_L^T = [4.205 \cdot 10^3 \quad 174.899 \quad 126.141 \quad 100.065]$

Check that total mass of element = sum of reactions

$\left(\overrightarrow{R_L + R_R}\right)^T = [4.787 \cdot 10^3 \quad 333.362 \quad 237.118 \quad 162.155]$

$Me^T = [4.787 \cdot 10^3 \quad 333.362 \quad 237.127 \quad 162.155]$

Check the total mass $\Sigma R_L + \Sigma R_R = 5\,519 \cdot 10^3$ $\Sigma Me = 5\,519 \cdot 10^3$

check the blade mass A ΣMe Me_1 A = 732 644

Evaluate the blade mass, root moment and centre of gravity.

Blade mass from root to tip [kg] $Blade_{mass} \int_{R_{root}}^{R} me(x)\,dx$ $Blade_{mass} = 1\,367 \cdot 10^3$

B ade bending moment due to gravity [N] $Blade_{mom}$ 9 81 $\int_{R_{root}}^{R} me(x)\,x\,dx$ $Blade_{mom} = 1\,094 \cdot 10^5$

Blade centre of grav ty from root [m] $CofG \frac{Blade_{mom}}{9\,81\ Blade_{mass}}$ CofG = 8.157

Calculate the total mass at each node.

$Mass_{ei+1}$ $R_{R_{ei}}$ $Mass_{ei}$ $Mass_{ei} + R_{L_{ei}}$ Check this ΣMass $5\,519 \cdot 10^3$

Calculate the force due to gravity at each node. g 9 81 m 0 m_{ei} $Mass_{ei+1}$

γ g m γ^T $7\,426 \cdot 10^3$ $2\,792 \cdot 10^3$ $2\,07 \cdot 10^3$ 609 103

Define the Mass, Damping and Stiffness matrices:

$$M(i) \begin{bmatrix} m_i & 0 & 0 & 0 & 0 & 0 \\ 0 & m_i & 0 & 0 & 0 & 0 \\ 0 & 0 & m_i & 0 & 0 & 0 \\ 0 & 0 & 0 & \frac{1}{2} m_i r_i^2 & 0 & 0 \\ 0 & 0 & 0 & 0 & \frac{1}{2} m_i r^2 & 0 \\ 0 & 0 & 0 & 0 & 0 & \frac{1}{2} m_i r_i^2 \end{bmatrix}$$

$$C(i, m, g_a, g_t, c_a, c_t) = \begin{bmatrix} \frac{1}{2} c_{t_i} & 0 & 0 & \frac{1}{2} g_{t_i} r_i & 0 & 0 \\ 0 & \frac{1}{2} c_{t_i} & 0 & 0 & \frac{1}{2} g_{t_i} r_i & 0 \\ 0 & 0 & g_{a_i} & 0 & 0 & c_{a_i} r_i \\ \frac{1}{2} c_{a_i} r_i & 0 & 0 & \frac{1}{2} g_{a_i} (r_i)^2 & -m_i (r_i)^2 \Omega & 0 \\ 0 & -\frac{1}{2} c_{a_i} r_i & 0 & -m_i (r_i)^2 \Omega & \frac{1}{2} g_{a_i} (r_i)^2 & 0 \\ 0 & 0 & -g_{t_i} r_i & 0 & 0 & c_{t_i} (r_i)^2 \end{bmatrix}$$

$$K(i) \begin{bmatrix} 0 & 0 & 0 & 0 & \frac{1}{2} \beta_{t_i} & 0 \\ 0 & 0 & 0 & \frac{1}{2} \beta_{t_i} & 0 & 0 \\ 0 & 0 & 0 & 0 & 0 & 0 \\ 0 & 0 & 0 & 0 & \frac{1}{2} \beta_{a_i} r_i & 0 \\ 0 & 0 & 0 & \frac{1}{2} \beta_{a_i} r_i & 0 & 0 \\ 0 & 0 & 0 & 0 & 0 & 0 \end{bmatrix}$$

Define a time domain transfer function to compare loads.

Sum each matrix for each blade elements contribution

mass B $\sum_{n=1}^{4} M(n)$ stiff B $\sum_{n=1}^{4} K\,n)$

damp m, g_a, g_t, c_a, c_t B $\sum_{n=1}^{4} C\,n, m\ g_a\ g_t, c_a, c_t$

Investigate the likely forces which result from each effect:

Stiffness forces:

Stiffness forces only occur with yaw and tilt rotations They result in a longitudinal force and a moment A rotation about the yaw (x) axis results in a force and moment along the sway (y) axis, and visa versa.

Yaw rotation $\text{stiff}\begin{bmatrix}0\\0\\0\\1\ \text{deg}\\0\\0\end{bmatrix}\begin{bmatrix}0\\0\ 093\\0\\0\\4\ 637\\0\end{bmatrix}$ *kN

Tilt rotation $\text{stiff}\begin{bmatrix}0 & 0\ 093\\0 & 0\\0 & 0\\0 & 4\ 637\\1\ \text{deg} & 0\\0 & 0\end{bmatrix}$ *kN

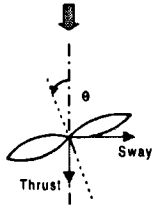

The yawing turbine has an induced sway loading as shown (This is opposed by the reaction hence the -ve sign.) The advancing blade (pointing vertically upwards) witnesses a larger incident wind speed and therefore sees larger axial and tangential loading Hence the rotor wants to move laterally in the sway d rection and also the top of the rotor wants to tilt over in the +ve tilt direction.

The loading is similar to that found by Sinclair and Jackson and is of the same order though approximately 4 5 times less than that given by Sinclair This is not so suprising though as the un-yawed thrust is approximately 4 5 times larger with Sinclair's formula (CD being given as 1.924 by Sinclair as opposed to 0 409 by theoretical calculation for this particular turbine.)

Damping.

Create a zero vector to replace zeroed gain factors: O_{ci} 0

Check the gyroscopic contribution:
Gyroscopic moments only occur when considering yaw and tilt motions.

Yaw: $\text{damp}(m, O, O\ O\ O)\begin{bmatrix}0\\0\\0\\1\ \text{deg}\\0\\0\end{bmatrix} = \begin{bmatrix}0\\0\\0\\0\\20\ 511\\0\end{bmatrix}$ kN

Tilt. $\text{damp}\ m, O, O, O, O)\begin{bmatrix}0 & 0\\0 & 0\\0 & 0\\0 & 0\\1\ \text{deg} & 0\\0 & 0\end{bmatrix} - \begin{bmatrix}0\\0\\0\\0\\20\ 511\\0\end{bmatrix}$ *k

Check the aerodynamic contribution·

Heave: $\text{damp}\left(O, g_a, g_t, c_a, c_t\right)\begin{bmatrix}1\\0\\0\\0\\0\\0\end{bmatrix} = \begin{bmatrix}0\ 443\\0\\0\\21\ 842\\0\\0\end{bmatrix}$ *kN

Sway· $\text{damp}\left(O, g_a, g_t, c_a, c_t\right)\begin{bmatrix}0 & 0\\1 & 0\ 443\\0 & 0\\0 & 0\\0 & 21\ 842\\0 & 0\end{bmatrix}$ kN

Surge $\text{damp}\ O, g_a, g_t, c_a, c_t)\begin{bmatrix}0\\0\\1\\0\\0\\0\end{bmatrix}\begin{bmatrix}0\\0\\2\ 085\\0\\0\\9\ 802\end{bmatrix}$ *kN

Yaw: $\text{damp}\ O, g_a, g_t, c_a, c_t\begin{bmatrix}0\\0\\0\\1\ \text{deg}\\0\\0\end{bmatrix}\begin{bmatrix}0\ 086\\0\\0\\3\ 927\\0\\0\end{bmatrix}$ *kN

Tilt· $\text{damp}\ O\ g_a, g_t, c_a, c_t\begin{bmatrix}0 & 0\\0 & 0\ 086\\0 & 0\\0 & 0\\1\ \text{deg} & 3\ 927\\0 & 0\end{bmatrix}$ *kN

Roll: $\text{damp}\ O, g_a, g_t, c_a, c_t\begin{bmatrix}0\\0\\0\\0\\0\\1\ \text{deg}\end{bmatrix}\begin{bmatrix}0\\0\\0\ 762\\0\\0\\2\ 401\end{bmatrix}$ *kN

Inertial terms.

Heave $\text{mass} \begin{pmatrix} 1 & 3.944 \\ 0 & 0 \\ 0 & 0 \\ 0 & 0 \\ 0 & 0 \\ 0 & 0 \end{pmatrix} \cdot kN$

Sway $\text{mass} \begin{bmatrix} 0 & 0 \\ 1 & 3.944 \\ 0 & 0 \\ 0 & 0 \\ 0 & 0 \\ 0 & 0 \end{bmatrix} \cdot kN$

Surge $\text{mass} \begin{pmatrix} 0 & 0 \\ 0 & 0 \\ 1 & 3.944 \\ 0 & 0 \\ 0 & 0 \\ 0 & 0 \end{pmatrix} \cdot kN$

Yaw $\text{mass} \begin{pmatrix} 0 & 0 \\ 0 & 0 \\ 0 & 0 \\ 1\ \text{deg} & 3.627 \\ 0 & 0 \\ 0 & 0 \end{pmatrix} \cdot kN$

Tilt $\text{mass} \begin{bmatrix} 0 & 0 \\ 0 & 0 \\ 0 & 0 \\ 0 & 0 \\ 1\ \text{deg} & 3.627 \\ 0 & 0 \end{bmatrix} \cdot kN$

Roll $\text{mass} \begin{pmatrix} 0 & 0 \\ 0 & 0 \\ 0 & 0 \\ 0 & 0 \\ 0 & 0 \\ 1\ \text{deg} & 3.627 \end{pmatrix} \cdot kN$

Calculate the time domain transfer function H(ω): $H(\omega) := B \quad \omega^2 M + i \ \omega C + K$

First we must redefine the damping matrix to include all effects

$\text{damp} \quad \text{damp}(m, g_a, g_t, c_a, c_t)$

The transfer function is given as follows:

$Z_R(\omega) \quad \omega^2 \cdot \text{mass} \quad i \ \omega \cdot \text{damp} + \text{stiff}$

Calculate the rotor cross-power force matrix:

$SR(\omega) \quad Z_R(\omega) \cdot S_{ij}(\omega) \cdot Z_R(\omega)^T$

$S_{ij}(\omega) \begin{pmatrix} 1 & 1 & 1 & 1 & 1 & 1 \\ 1 & 1 & 1 & 1 & 1 & 1 \\ 1 & 1 & 1 & 1 & 1 & 1 \\ 1 & 1 & 1 & 1 & 1 & 1 \\ 1 & 1 & 1 & 1 & 1 & 1 \\ 1 & 1 & 1 & 1 & 1 & 1 \end{pmatrix}$

We need to extract the leading diagonal from a matrix

$\text{ldiag}(M) \quad \left| \begin{array}{l} \text{for } k \in 1 \ldots \text{rows}(M) \\ \quad V_k \leftarrow M_{k,k} \\ V \end{array} \right.$

$\text{Res}(\omega) \quad \text{ldiag}(SR(\omega))$

$\text{Res}(1) \begin{bmatrix} 3.051 \cdot 10^{7} \\ 1.148 \cdot 10^{8} \\ 2.11 \cdot 10^{9} \\ 9.481 \cdot 10^{11} \\ 1.169 \cdot 10^{12} \\ 5.951 \cdot 10^{10} \end{bmatrix}$

Try the same thing again using cross power matrices instead of summing them first in the time domain:

Define transfer function for the kth blade element.

$$z(\omega,k) \quad B \quad \omega^2 M\,k) + i\ \omega C\,k\ m\ g_a\ g_t\ c_a, c_t \quad K(k))$$

Define cross power of responses between each e ement.

$$SR_{ij}(\omega,i,j) \quad z(\omega,i)\ S_{ij}(\omega)\ \ z(\omega,j)^T$$

Define cross power matrix.

$$SR(\omega) \quad \begin{bmatrix} SR_{ij}(\omega,1,1) & SR_{ij}(\omega,1,2) & SR_{ij}(\omega,1,3) & SR_{ij}(\omega,1,4) \\ SR_{ij}(\omega,2,1) & SR_{ij}(\omega,2,2) & SR_{ij}(\omega,2,3) & SR_{ij}(\omega,2\ 4) \\ SR_{ij}(\omega\ 3,1) & SR_{ij}(\omega,3,2) & SR_{ij}(\omega,3,3) & SR_{ij}(\omega,3,4) \\ SR_{ij}(\omega\ 4,1) & SR_{ij}(\omega,4,2) & SR_{ij}(\omega,4,3) & SR_{ij}(\omega,4,4) \end{bmatrix}$$

$$S(\omega) \quad \text{ldiag} \sum_{i=1}^{4} \sum_{j=1}^{4} SR(\omega)_{i,j}$$

$$S(1) \quad \begin{matrix} 3.051\cdot10^{7} \\ 1.148\cdot10^{8} \\ 2.11\cdot10^{9} \\ 9.481\cdot10^{11} \\ 1.169\cdot10^{12} \\ 5.951\cdot10^{10} \end{matrix} \qquad Res(1) - \begin{matrix} 3.051\cdot10^{7} \\ 1.148\cdot10^{8} \\ 2.11\cdot10^{9} \\ 9.481\cdot10^{11} \\ 1.169\cdot10^{12} \\ 5.951\cdot10^{10} \end{matrix}$$

These are the same. This is good because it allows a much faster calculation using a single 6 DOF matrix for the rotor blades.

Derive expression for the motion damping of a turbine situated on top of the rigid tower:

The expression given above is fine but it is more often than not the motion spectra will be given at the centroid of the platform. For this reason we need to include the tower height in the calculations

Hub height above centroid $L \quad 35$

$$\phi \quad \begin{bmatrix} 1 & 0 & 0 & 0 & 0 & 0 \\ 0 & 1 & 0 & 0 & 0 & L \\ 0 & 0 & 1 & 0 & L & 0 \\ 0 & 0 & 0 & 1 & 0 & 0 \\ 0 & 0 & 0 & 0 & 1 & 0 \\ 0 & 0 & 0 & 0 & 0 & 1 \end{bmatrix}$$

Define the element matrix for the turbine and tower attached to a platform node:

Define a procedure for combining 4 dimensional matrices into 2.

combine(G) $M \leftarrow G_{1,1}$

for $k \in 2 \ldots rows(G)$

$M \leftarrow stack(M, G_{k,1})$

for $j \in 2 \ldots cols(G)$

$tmp \leftarrow G_{1,j}$

for $k \in 2 \ldots rows(G)$

$tmp \leftarrow stack(tmp, G_{k,j})$

$M \leftarrow augment(M, tmp)$

M

Evaluate the element matrix for the rotor and tower.

$$Z(\omega) \quad combine\begin{bmatrix} Z_R(\omega) & Z_R(\omega)\,\phi \\ \phi^T Z_R(\omega) & \phi^T Z_R(\omega)\,\phi \end{bmatrix}$$

Check the transformation matrix.

We can check that the transformation matrix works by putting in pure translations and rotations at the top and bottom of the tower and comparing them. All pure translations and yaw should agree, while roll and tilt agree for unit angular displacement plus a translation of L at the tower top.

$$V = \begin{bmatrix} 0 \\ 0 \\ 0 \\ 0 \\ 0 \\ 0 \\ 0 \\ 0 \\ 0 \\ 0 \\ 0 \\ 1 \end{bmatrix} \qquad Z(1)\,V = \begin{bmatrix} 0 \\ 1.38\cdot10^{5} + 1.55\cdot10^{4}\,i \\ 4.368\cdot10^{4}\,i \\ 0 \\ -7.645\cdot10^{5}\,i \\ -2.078\cdot10^{5} + 1.376\cdot10^{5}\,i \\ 0 \\ 1.38\cdot10^{5} + 1.55\cdot10^{4}\,i \\ 4.368\cdot10^{4}\,i \\ 0 \\ 2.293\cdot10^{6}\,i \\ 5.039\cdot10^{6} + 6.8\cdot10^{5}\,i \end{bmatrix} \qquad U = \begin{bmatrix} 0 \\ L \\ 0 \\ 0 \\ 0 \\ 1 \\ 0 \\ 0 \\ 0 \\ 0 \\ 0 \\ 0 \end{bmatrix} \qquad Z(1)\,U = \begin{bmatrix} 0 \\ -1.38\cdot10^{5} + 1.55\cdot10^{4}\,i \\ 4.368\cdot10^{4}\,i \\ 0 \\ -7.645\cdot10^{5}\,i \\ -2.078\cdot10^{5} + 1.376\cdot10^{5}\,i \\ 0 \\ -1.38\cdot10^{5} + 1.55\cdot10^{4}\,i \\ 4.368\cdot10^{4}\,i \\ 0 \\ -2.293\cdot10^{6}\,i \\ -5.039\cdot10^{6} + 6.8\cdot10^{5}\,i \end{bmatrix}$$

Check--> $Z(1)\,U = Z(1)\,V \quad 1$

Calculate the response of a turbine rotor to a PSD of surge on a Tensioned Buoyant Platform (TBP):

Calcu ate the JONSWAP spectrum of surface elevation for the Rough Field in the North Sea. The data for the 1:50 year mean JONSWAP spectrum is given as follows

Modal frequency [Hz] $f_m \quad 0.0754$ expressed in rad an units; $\omega_m \quad 2\pi f_m \qquad \omega_m = 0.474$

Scale parameter $\alpha \quad 0.0081$

Peak enhancement parameter $\gamma \quad 3.3$

The JONSWAP parameters may therefore be determined from the following formulae:

$$\sigma_A \quad 0.07 \qquad \sigma_B \quad 0.09$$

$$\sigma(f) \quad \text{if}\left(f < f_m, \sigma_A, \sigma_B\right) \qquad \sigma(\omega) \quad \text{if}\left(\omega \le \omega_m, \sigma_A, \sigma_B\right)$$

$$a_f(f) \quad e^{\frac{-(f-f_m)^2}{2\cdot\sigma(f)^2 f_m^2}} \qquad a(\omega) \quad e^{\frac{-(\omega-\omega_m)^2}{2\cdot\sigma(\omega)^2\cdot\omega_m^2}}$$

The JONSWAP spectra, expressed in radian measure is determined as follows

$$S_{Wf}(f) \quad \alpha \frac{g^2}{(2\pi)^4 f^5} \exp\left[\frac{5}{4}\left(\frac{f_m}{f}\right)^4\right] \gamma^{a_f(f)} \qquad S_W(\omega) \quad \alpha \frac{g^2}{\omega^5} \exp\left[\frac{5}{4}\left(\frac{\omega_m}{\omega}\right)^4\right] \gamma^{a(\omega)}$$

Define range of frequencies in Hz and rad/sec: $fi \quad 1 \ldots 151$

Frequency [Hz] $f_{fi} \quad 0.05 + \frac{1}{1000}(fi - 1)$ Frequency [rad/sec] $\omega \quad f \cdot 2\pi$

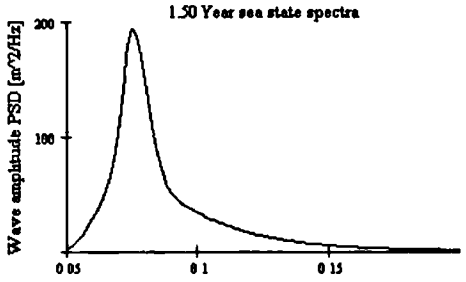

Define an alternative Pierson Moskowitz sea state spectrum:

Significant wave height [m] $H_s := 3.81$ Zero cross ng wave period $T_z := \begin{matrix} 9.1 \\ 1.408 \end{matrix}$

Calculate the Pierson Moskowitz spectra in radian measure

$$S_{\eta\eta f}(f) := \frac{H_s^2 T_z}{8\pi^2} f T_z^{\,5} e^{-\frac{1}{1.25}(f T_z)^4} \qquad S_{\eta\eta}(\omega) := \frac{H_s^2 T_z}{16\pi^3} \frac{\omega}{2\pi} T_z^{\,5} e^{-\frac{1}{1.25}\left(\frac{\omega}{2\pi} T_z\right)^4}$$

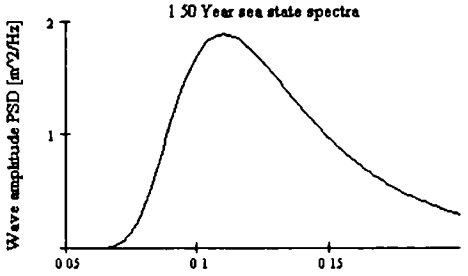

Perform calculations using JONSWAP or Pierson Moskowitz?

$S_W(\omega) \quad S_{\eta\eta}(\omega)$

Calculate the Surge RAO from Joel's paper:

Input scaled data for 4 column TBP from paper: di := 1 .. 16

$period_{di}$	$RAO_{surge_{di}}$
5	0 4
6	1 3
7	2 7
8	3 1
9	2 7
10	1 3
11	0 4
12	2 1
13	3 6
14	4 8
15	6 0
16	6 9
17	7 8
18	8 6
19	9 2
20	9 8

Interpolate this data to establish RAO with respect to frequency in rad/sec.

vs := cspline(period, RAO_{surge})

$T(\omega) := interp\left(vs, period, RAO_{surge}, \frac{2\pi}{\omega}\right)$

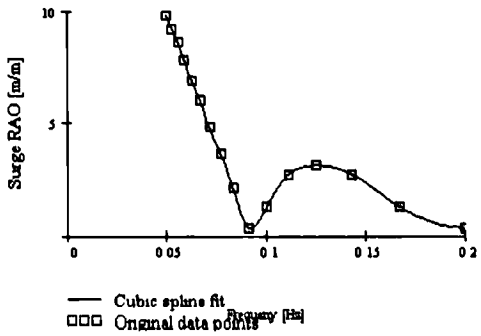

Calculate the Surge RAO from Joel's paper.

Input scaled data for 6 column TBP from paper: d6i 1 13

We shall need to redefine the frequency as we cannot extrapolate this curve like the last one. f6i 1 76

$period6_{di}$ $RAO6_{surge_{di}}$

Interpolate this data to estab ish RAO with respect to frequency in rad/sec.

$period6_{di}$	$RAO6_{surge_{di}}$
8	1 5
9	0 1
10	1 4
11	2 9
12	4 2
13	5 4
14	6 3
15	7 2
16	7 9
17	8 7
18	9 2
19	9 9
20	10 4

$vs \quad cspline(period6, RAO6_{surge})$

$T6(\omega) \quad interp\left(vs, period6, RAO6_{surge}, \frac{2\pi}{\omega}\right)$

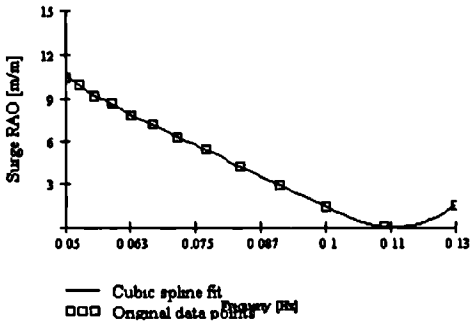

Derive surge response PSD:

$S_T(\omega) \quad (T(\omega))^2 S_W(\omega) \qquad S6_T(\omega) \quad (T6(\omega))^2 S_W(\omega)$

Plot the response spectrum:

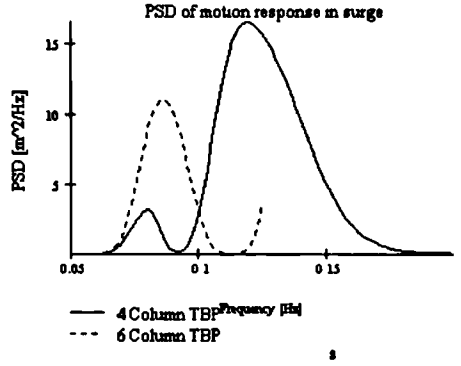

Calculate the tower base loading due to the surge loading:

We shall assume that only surge motions are appl ed to the platform base The rol , tilt and heave modes are negligible at the platform as the tethers can be assumed to be infinitely stiff In yaw surge and sway however, this assumption is invalid. No stiffness properties are given in these modes and so they are assumed infinitely stiff for the purpose of this calculation.

$$V(\omega) \quad \begin{bmatrix} 0 & 0 \\ 0 & 0 \\ 0 & 0 \\ 0 & 0 \\ 0 & 0 \\ 0 & 0 \\ 0 & 0 \\ 0 & 0 \\ S_T(\omega) & S6_T(\omega) \\ S_T(\omega) & S6_T(\omega) \\ 0 & 0 \\ 0 & 0 \end{bmatrix}$$

<== Change this matrix to analyse sway loads

$TL_{fi} \quad \left(\overrightarrow{Z\ \omega_{fi}}^2 V\ \omega_{fi}\right)$

$TL6_{f6i} \quad \left(\overrightarrow{Z\ \omega_{f6i}}^2 V\ \omega_{f6i}\right)$

force -
- $f \leftarrow TL^{\langle 1 \rangle T}$
- for $i \in 2..last(TL)$
- $f \leftarrow stack\left(f\ TL_i^{\langle 1 \rangle T}\right)$
- $\overrightarrow{f\ 2\pi}$

force6
- $f \leftarrow TL6_i^{\langle 2 \rangle T}$
- for $i \in 2..last(TL6)$
- $f \leftarrow stack\ f\ TL6_i^{\langle 2 \rangle T}$
- $\overrightarrow{f\ 2\pi}$

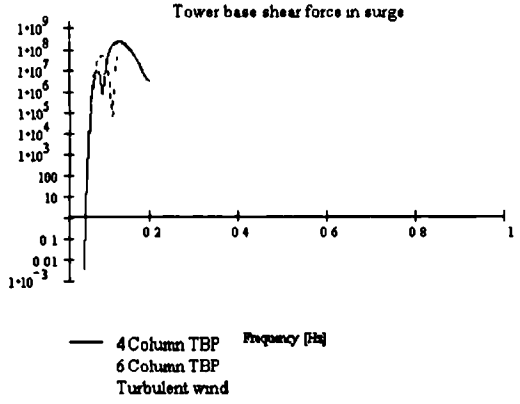

s

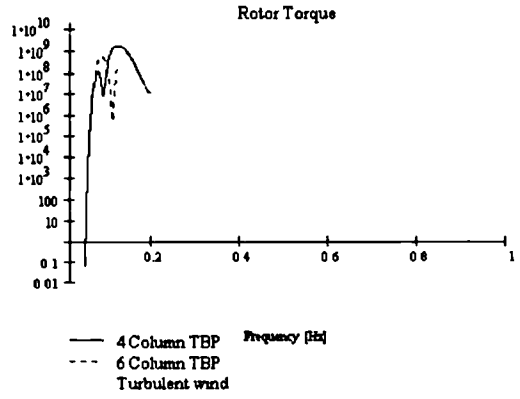

Compare spectral moments.

Define a routine to calculate the spectral moments:

$$\text{mom}(v, f, f_n, pwr) = \left|\begin{array}{l} ct \leftarrow 1 \\ \text{for } i \in 1 \ldots \text{last}(v) \\ \quad \text{if } |f_i| < f_n \\ \quad\quad g_{ct} \leftarrow f_i \\ \quad\quad u_{ct} \leftarrow v_i \\ \quad\quad ct \leftarrow ct + 1 \\ ct \leftarrow ct - 1 \\ \delta f_1 \leftarrow |g_1 - g_2| \\ \text{for } i \in 2 \ldots ct - 1 \\ \quad \delta f_i \leftarrow \left|\frac{g_{i+1} - g_{i-1}}{2}\right| \\ \delta f_{ct} \leftarrow |g_{ct} - g_{ct-1}| \\ \text{for } i \in 1 \ldots pwr + 1 \\ \quad m_i \leftarrow \sum \overrightarrow{u \cdot (|g|)^{i-1} \cdot \delta f} \\ m \end{array}\right.$$

Filter only frequencies within the cut off range

Evaluate the various δf values for the ordinates

Evaluate vector of the ith spectral moments

Determine the statistics from the spectral moments

Standard deviation $\sigma(m) \quad \sqrt{m_1}$

Expected number of zero up-crossings $E0(m) \quad \sqrt{\frac{m_1}{m_1}}$

Expected number of peaks $EP(m) \quad \sqrt{\frac{m_3}{m_1}}$

Irregularity factor $\gamma(m) \quad \frac{E0(m)}{EP(m)}$

Other interesting statistics:

Mean period $T_m(m) \quad \frac{m_1}{m_2}$

Mean period of zero up-crossing $T0(m) \quad \sqrt{\frac{m_1}{m_3}}$

Mean period between peaks $TP(m) \quad \sqrt{\frac{m_3}{m_5}}$

Form a vector of the interesting statistics:

$$stats(m) \quad \begin{bmatrix} \sigma(m) \\ T_m(m) \\ T0(m) \\ TP(m) \\ \gamma(m) \end{bmatrix}$$

Standard deviation
Mean period
Mean period between zero up-crossings
Mean period between peaks
Irregularity factor

Calculate the spectral moments for the tower base shear force.

moment mom(force<9>, f, 0 2, 4) moment6 mom(force6<9>, f, 0 2, 4) windmom mom(thrust, ft, 6, 4

$$moment = \begin{bmatrix} 6\,363 \cdot 10^{6} \\ 8\,486 \cdot 10^{5} \\ 1\,153 \cdot 10^{5} \\ 1\,597 \cdot 10^{4} \\ 2\,252 \cdot 10^{3} \end{bmatrix} \quad moment6 = \begin{bmatrix} 7\,415 \cdot 10^{5} \\ 6\,909 \cdot 10^{4} \\ 6\,576 \cdot 10^{3} \\ 640\,543 \\ 63\,94 \end{bmatrix} \quad windmom = \begin{bmatrix} 1.596 \cdot 10^{7} \\ 1\,579 \cdot 10^{7} \\ 3\,517 \cdot 10^{7} \\ 1.177 \cdot 10^{8} \\ 4\,669 \cdot 10^{8} \end{bmatrix}$$

$$stats(moment) = \begin{bmatrix} 2\,522 \cdot 10^{3} \\ 7\,499 \\ 7\,427 \\ 7\,156 \\ 0\,964 \end{bmatrix} \quad stats(moment6) = \begin{bmatrix} 861\,106 \\ 10\,732 \\ 10\,619 \\ 10\,141 \\ 0\,955 \end{bmatrix} \quad stats(windmom) = \begin{bmatrix} 3\,996 \cdot 10^{3} \\ 1\,011 \\ 0\,674 \\ 0\,274 \\ 0\,407 \end{bmatrix}$$

Calculate the spectral moments for the rotor torque:

moment mom(force<6>, f, 0 2, 4) moment6 mom(force6<6>, f 0 2 4) windmom mom(torque, ft 6, 4

$$moment = \begin{bmatrix} 4\,106 \cdot 10^{7} \\ 5\,327 \cdot 10^{6} \\ 7\,049 \cdot 10^{5} \\ 9\,506 \cdot 10^{4} \\ 1\,306 \cdot 10^{4} \end{bmatrix} \quad moment6 = \begin{bmatrix} 7\,46 \cdot 10^{6} \\ 6\,802 \cdot 10^{5} \\ 6\,32 \cdot 10^{4} \\ 5\,994 \cdot 10^{3} \\ 581\,481 \end{bmatrix} \quad windmom \begin{bmatrix} 1\,39 \cdot 10^{8} \\ 3\,817 \cdot 10^{7} \\ 6\,368 \cdot 10^{7} \\ 1\,433 \cdot 10^{8} \\ 3\,953 \cdot 10^{8} \end{bmatrix}$$

$$stats(moment) = \begin{bmatrix} 6\,408 \cdot 10^{3} \\ 7.709 \\ 7\,632 \\ 7\,347 \\ 0\,963 \end{bmatrix} \quad stats(moment6) \begin{bmatrix} 2\,731 \cdot 10^{3} \\ 10\,967 \\ 10\,865 \\ 10\,425 \\ 0\,96 \end{bmatrix} \quad stats(windmom) = \begin{bmatrix} 1\,179 \cdot 10^{4} \\ 3\,643 \\ 1\,478 \\ 0\,401 \\ 0\,272 \end{bmatrix}$$

Damping expressed as a percentage of critical in surge.

Enter damping coefficient from rotor in [N m/s] $Rotor_{damping} \quad 2085$

Enter mass of platforms in [kg] $Mass_{platform} \quad 47700000$ $Mass6_{platform} \quad 74360000$

Assume added mass = physical $Mass_{platform} \quad Mass_{platform}\,2$ $Mass6_{platform} \quad Mass6_{platform}$

$Mass_{platform} = 9\,54 \cdot 10^{7}$ $Mass6_{platform} \quad 1\,487 \cdot 10^{8}$

Enter natural surge period in [sec] $Per_{platform} \quad 93\,7$ $Per6_{platform} \quad 60\,8$

Calculate the stiffness in [N/m] $K_{platform} \quad \frac{4\,\pi^2\,Mass_{platform}}{Per_{platform}^2}$ $K_{platform} = 4\,29 \cdot 10^{5}$

$K6_{platform} \quad \frac{4\,\pi^2\,Mass6_{platform}}{Per_{platform}^2}$ $K6_{platform} \quad 6\,687 \cdot 10^{5}$

Determine the damping as a percentage of critical·

$2\sqrt{K_{platform}\,Mass_{platform}} = 1.279\cdot10^{7}$

$\dfrac{Rotor_{damping}}{2\sqrt{K_{platform}\,Mass_{platform}}} = 0.016\,\%$

$2\sqrt{K6_{platform}\,Mass6_{platform}} = 1.995\cdot10^{7}$

$\dfrac{Rotor_{damping}}{2\sqrt{K6_{platform}\,Mass6_{platform}}} = 0.01\,\%$

Calculate the spectra with a flexible tower:

At these frequencies the tower behaves quasi-statically and therefore there will be little dynamic amplification

Appendix F

Calculation of Normalised Equivalent

Fatigue Damage

Vibration Fatigue Analysis

For the TURBANA Development Model

Andrew Halfpenny

Standard deviation	σ 1 831			
Mean period	T 9 276			
Mean zero up crossing	T0 3 777			
Mean peak period	Tp 0 786	Expected number of peaks	Ep $\frac{1}{Tp}$	

Calculate spectral moments from the statistics:

$m_0 \quad \sigma^2 \qquad m_1 \quad \frac{m_0}{T} \qquad m_2 \quad \frac{m_0}{T0^2} \qquad m_3 \quad 0 \qquad m_4 \quad \frac{m_2}{Tp^2}$

$$m = \begin{matrix} 3.353 \\ 0\ 361 \\ 0.235 \\ 0 \\ 0\ 38 \end{matrix}$$

Enter spectral moments directly if you prefer:

Material SN data in FATIMAS format and Dirlik format:

SRI1 1868 b1 0 0958

Calculate the Dirlik equivalents:

$k1 \quad SRI1^{\frac{1}{b1}}$ $\qquad k1 = 1\ 406 \cdot 10^{34}$

$m1 \quad \frac{1}{b1}$ $\qquad m1 \quad 10\ 438$

Calculate probability density function of cycle stress ranges with Dirlik:

$\gamma \quad \frac{m_2}{\sqrt{m_0 m_4}} \qquad x_m \quad \frac{m_1}{m_0}\sqrt{\frac{m_2}{m_4}}$

$Z(S) \quad \frac{S}{2\sqrt{m_0}} \qquad D_1 \quad \frac{2\left(x_m - \gamma^2\right)}{1+\gamma^2} \qquad R \quad \frac{\gamma - x_m - D_1^2}{1 - \gamma - D_1 + D_1^2}$

$D_2 \quad \frac{1 - \gamma - D_1 + D_1^2}{1 - R} \qquad D_3 \quad 1 - D_1 - D_2 \qquad Q \quad \frac{1\ 25\ \gamma - D_3}{D_1} - D_2 R$

$$p(S) \quad \frac{\frac{D_1}{Q} e^{\frac{Z(S)}{Q}} + D_2 Z(S) e^{\frac{Z(S)^2}{2R^2}} + D_3 Z(S) e^{\frac{Z(S)^2}{2}}}{2\sqrt{m_0}}$$

Calculate eqiuvalent stress S:

$$S \quad \int_0^{14\sigma} S^{m1} p(S) dS$$

Calculate normalised equivalent Stress S_{eq}:

$$S_{eq} \quad \left(\int_0^{14 \cdot \sigma} S^{m1} p(S) dS \right)^{\frac{1}{m1}}$$

Calculate the material & normalised equivalent fatigue life:

$Life \quad \frac{k1}{Ep} S^{-} \qquad Life = 3\ 423 \cdot 10^{42}$

$Life_{eq} \quad \frac{k1}{Ep} S_{eq} \qquad Life_{eq} = 7\ 192 \cdot 10^{34}$